THERMO-MECHANICAL AND DURABILITY PROPERTIES OF CEMENT MORTAR INTEGRATED WITH NANO-SILICA PARTICLES

Thesis

Submitted in partial fulfillment of the requirements for the degree of

DOCTOR OF PHILOSOPHY

by

SNEHAL K

(177CV012)

DEPARTMENT OF CIVIL ENGINEERING

NATIONAL INSTITUTE OF TECHNOLOGY KARNATAKA,

SURATHKAL, MANGALORE-575 025

JULY, 2022

THERMO-MECHANICAL AND DURABILITY PROPERTIES OF CEMENT MORTAR INTEGRATED WITH NANO-SILICA PARTICLES

Thesis

Submitted in partial fulfillment of the requirements for the

degree of

DOCTOR OF PHILOSOPHY

By

SNEHAL K

(177CV012)

Under the guidance of

Dr. BIBHUTI BHUSAN DAS

Associate Professor

DEPARTMENT OF CIVIL ENGINEERING

NATIONAL INSTITUTE OF TECHNOLOGY KARNATAKA,

SURATHKAL, MANGALORE -575 025

JULY, 2022

DECLARATION

by the PhD Research Scholar

I hereby declare that the Research Thesis entitled **"Thermo-Mechanical and Durability Properties of Cement Mortar Integrated with Nano-Silica Particles"** which is being submitted to the **National Institute of Technology Karnataka, Surathkal** in partial fulfillment of the requirements for the award of the Degree of **Doctor of Philosophy** in **CIVIL ENGINEERING** is a bonafide report of the research work carried out by me. The material contained in this Research thesis has not been submitted to any University or Institution for the award of any degree.

Place: NITK, SURATHKAL

Date: 18/07/2022

SNEHAL K

177CV012

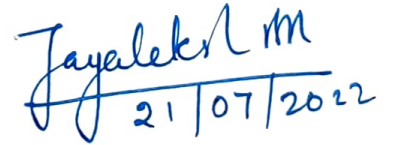Research Scholar

Department of Civil Engineering

CERTIFICATE

This is to certify that the Research thesis entitled **"Thermo-Mechanical and Durability Properties of Cement Mortar Integrated with Nano-Silica Particles"** submitted by **SNEHAL K (177CV012)** as the record of research work carried out by her is accepted as Research Thesis submission in partial fulfilment of the requirements for the award of degree of **Doctor of Philosophy**.

Dr. BIBHUTI BHUSAN DAS

Department of Civil Engineering

Research Supervisor

21/07/2022

Dr. B. R. Jayalekshmi

Department of Civil Engineering

Chairman - DRPC

Chairman (DRPC)
Department of Civil Engineering
National Institute of Technology Karnataka, Surathkal
Mangalore - 575 025, Karnataka, INDIA

Dedicated to

My Beloved Parents

and

Teachers

ABSTRACT

Evolution of infrastructure investments is important for the alleviation of poverty in emerging countries like India. Consequently, time frame execution of construction projects plays a vital role. This can be achieved through the application of superior pozzolanic material such as nano-silica in cementitious composites. However, there are certain number of problems associated with the inclusion of nano-silica such as workability issue, high heat of hydration, shrinkage and the associated cost. Hence, it is more appropriate to use supplementary cementitious materials (SCMs) in conjunction with nano-silica to produce high performance sustainable cementitious composite mixes. On the other side, the scientific and industrial communities are heavily investing on conservation of energy. Therefore, there is a need to increase the energy efficiency of the building constituents by cutting down the thermal loading. In this regard, various classes of phase change materials (PCMs) act as heat absorbing/transfer medium (latent heat storage system). However, major detriment of PCMs in cementitious composites are its physical and chemical interference with hydration products leading to loss in structural integrity. Therefore, there is a need to incorporate a highly reactive material like nano-silica along with PCM resulting in thermally efficient and sustainable construction material.

In this perspective, present study was carried out to understand the influence of nano-silica on hydration properties of binary, ternary and quaternary blended cementitious composites containing micro to nano sized admixtures including fly ash (FA), ultrafine fly ash (UFFA) and colloidal nano-silica (CNS). Study also demonstrated the influence of integrating phase change materials (PCMs) on thermo-mechanical properties of nano-silica admixed cementitious composites. In the initial stage of study dosage of nano-silica (0.5% to 3.5% at 0.5% interval) was replaced with ordinary Portland cement in correspondence to obtain the optimum compressive strength of cement mortar. Further, optimised cementitious mix was designed through particle packing theory by adding suitable proportion of FA and UFFA. In the later part of the experimental investigation, nano-silica modified mix was added with the desired proportion of PCMs to identify the thermal efficiency of the cementitious composite.

Hydration, mineralogical and microstructural studies of cementitious composites were carried out through advanced characterization techniques such as, thermogravimetric analysis (TGA), X-ray diffraction (XRD) and scanning electron microscopy empowered with energy dispersive X-ray spectroscopy (SEM-EDX), respectively. Thermal properties of PCM integrated cementitious composites were determined by means of differential scanning calorimetry (DSC). The experimental test results revealed that the optimum dosage of CNS in binary blended cementitious composites was found to be 3%. However, slump flow test indicated the intensified demand for water absorption and reduced workability with increase in level of CNS content. The presence of nano-silica in cementitious system amplified the hydration and pozzolanic activity, thereby promoting densified microstructure. It is to be noted that quaternary blended mix also showed promising results with respect to hydration, microstructure, mechanical and durability properties. Experimental results of PCMs integrated cementitious composites showed improved thermal efficiency as well as reduced the chemical shrinkage, but adversely affected the mechanical, hydration, and durability properties. It was found that cementitious mortar comprising of both nano-silica and PCMs have compensated the drawbacks of one another. Composite mix (having both nano-silica and PCMs) showed superior strength gain at early age, better durability resistance, low chemical shrinkage, and superior thermal performance.

At this point of time, it is understood from the experimental investigation that it is possible to attain sustainable cementitious composites by blending fly ash or/and ultrafine fly ash along with highly reactive nano-silica. This experimental study also gives an understanding that PCMs and nano-silica can be combined in cementitious composites to a suitable proportion to give the best performance with respect to the compressive strength development, minimization of shrinkage, hydration, and microstructure development. In addition, a PCM admixed cementitious composite can be proportioned to store a suitable amount of heat energy.

ACKNOWLEDMENTS

TABLE OF CONTENTS

<div align="center">Contents   Pg. No</div>

LIST OF FIGURES

LIST OF TABLES

NOMENCLATURE

The following is a general list of abbreviations used throughout the chapters.

AFm	Alumina ferric oxide mono-sulfate
AFt	Alumina ferric oxide tri-sulfate (Ettringite)
Al_2O_3	Aluminium oxide
ASTM	American Society for Testing and Materials
bwob	By weight of binder content
C_3A	Tri-calcium aluminate
C_4AF	Tetra-calcium alumino ferrite
CC	Calcium carbonate
C_2S	Di-calcium silicate
C_3S	Tri-calcium silicate
$CaCO_3$	Calcium carbonate
CH	Calcium hydroxide
CNS	Colloidal nano-silica
C-S-H	Calcium silicate hydrate
DTG	Differential thermogravimetry
DSC	Differential scanning calorimetry
EDS	Energy dispersive spectroscopy
FA	Fly ash
Fe_2O_3	Ferrous oxide
Fs	Freidel's salt
GGBFS	Ground granulated blast furnace slag
Gy	Gypsum
H_2SO_4	Sulfuric acid
IS	Indian Standard
NaCl	Sodium chloride
Na_2SO_4	Sodium sulfate
NEW	Non-evaporable water

oct	n-octadecane
OPC	Ordinary Portland cement
PCMs	Phase change materials
PRD	Pozzolanic reaction degree
RCPT	Rapid chloride ion penetration test
SAI	Strength activity index
SCC	Self-compacting concrete
SCMs	Secondary cementitious materials
SDM	Selective dissolution method
SEM	Scanning electron microscope
TGA	Thermogravimetric analysis
TiO_2	Titanium dioxide
UFFA	Ultra-fine fly ash
UHPC	Ultra high performance concrete
w/b	Water binder ratio
WH	water related to hydration product excluding calcium hydroxide content
XRD	X-ray diffraction

CHAPTER-1

INTRODUCTION

1.1   GENERAL

Concrete is a composite material, which consists of a binding material known as cement. Ordinary Portland cement (OPC) is favourably and widely consumed for the production of concrete. However, with the consumption of each ton of OPC, there is an equal amount of CO_2 released to the atmosphere (Augustine et al., 2009; Huntzinger and Eatmon, 2009; Turner and Collins, 2013). With increasing level of industrialization and rapid urbanization, huge amount of industrial wastes or by-products are generated, which become challenging for disposal. It is observed that researchers have successfully utilized these industrial by-products in concrete (Sensale, 2006; Giner et al., 2011; Bagheri et al., 2012; Sahoo et al., 2017). The most prominent ones in this regard are fly ash, ground granulated blast furnace slag (GGBFS), silica fume, rice husk ash etc., popularly known as secondary cementitious materials (SCMs). From the available literature it is observed that when SCMs are used in conjunction with OPC it contributes to the engineering properties of cementitious composites by means of its pozzolanic activity (Sensale, 2006; Giner et al., 2011; Bagheri et al., 2012; Sahoo et al., 2017). For instance, fly ash, an industrial by-product from coal based thermal power plant is extensively used pozzolanic ingredient for cement-based materials (Saha, 2018). Another widely used SCM in construction industry is GGBFS produced from pig-iron industries (Zhou et al., 2012). Silica fume, an ultrafine pozzolanic material from silicon industry with average particle size ranging from 0.1 μm to 1 μm, is identified as the supreme pozzolanic material (Giner et al., 2011; Diab et al., 2012). In addition to silica fume, it is observed that researchers have used classified/processed ultrafine particles from industrial by-products such as fly ash and GGBFS (Obla et al., 2003; Dai et al., 2019). However, most of these SCMs initially behave only as filler and remain inert in the hydration process leading to lower early compressive strength in concrete (Copeland et al., 2001; Obla et al., 2003; Das et al., 2012; Sahoo et al., 2017).

Moving ahead from micron sized SCMs over the past decades of development, use of nano-additives in the field of construction has opened up new avenues in the cementitious systems (Sobolev et al., 2006; Khitab and Arshad, 2014). Amongst a number of nano-additives, nano-silica is finding pronounced interest by the researchers owing to its superior and hasty pozzolanic reactivity (Givi et al., 2010; Zhang and Li, 2011; Supit et al., 2013; Shaikh et al., 2014). It is reported that implementation of nanotechnology in cementitious composites by introducing nano-silica significantly improved the properties and performance of cement composites (Han et al., 2017). Incorporation of nano-silica in cement composites showed superior pozzolanic reactivity as compared to that of silica fume, fly ash, GGBFS and etc., on account of its higher surface to volume ratio (Qing et al., 2007; Biricik and Sarier, 2014). Nano sized silica particles are also capable of filling the voids between the particles of C-S-H gel resulting in greater densification of micro-structure followed by improved mechanical and durability properties of concrete (Givi et al., 2010; Zhang and Li, 2011; Zhang et al., 2012). Hence, the problem of lower initial strength gain was mitigated and "high performance concrete" could be effectively produced with a greater service life (Sobolev 2009; Said et al 2012).

However, literature says that particle size and quantity of nano-silica has an impact on drying shrinkage (Litifi et al., 2011; Sattawa et al., 2017), workability (Berra et al., 2012: Chithra et al., 2016) and heat of hydration (Wang et al., 2016; Isfani et al., 2016). In this perspective, it is very much necessary to use SCMs in cement composites with the relevant choice of size and type of SCMs to produce a sustainable concrete. With the advancement in concrete technology from a single binder base to binary, ternary and quaternary blends, the selection of right combination of material plays vital role in enhancing the performance of concrete (Nehdi, 2001). Choosing suitable combinations of replacement materials by adopting trial and error technique becomes a tedious job. Furthermore, performance of concrete is directly influenced by the type of ingredients and their packing characteristics (Cai, 2017). Thus, knowledge of particle packing concept and its influence on cementitious system is necessary to enable a mixture designer to select apt proportion of replacement materials from a pool of SCMs (Sentil and Santhanam, 2003).

The particle packing of concrete is measured in terms of its packing density. It can be defined as ratio of the solid volume of the particle to total volume occupied by the particles (Sentil and Santhanam 2003). For achieving the optimal particle packing of cementitious matrix with multiple ingredients, modified Andreasen and Andersen model is found to be one of the appropriate and best-known packing models (Dinger and Funk 1997). It is reported that blended cement mortar designed using modified Andreasen and Andersen model showed optimistic properties like improved hydration, compressive strength, filler effect and dense microstructure (Borges et al., 2016; Cai, 2017 ; Li et al., 2018).

Although nano-silica admixed concrete functioned well in early strength gain by means of its accelerated hydration rate and reduced setting time, it is reported that self-desiccation of nano-silica in concrete promotes autogenous shrinkage (Bjornstrom et al., 2004; Sobolev et al., 2009).

From other point of view, thermal efficiency in buildings is of the concern in a diverse climatic conditions and a tropical country like India. Increasing energy efficiency of the building by reducing the thermal loading can be accomplished by employing potential latent heat storage material in building components (Kiviste and Lindberg, 2014). Phase change materials (PCMs) are one such smart material, which possess a potential to store latent heat. PCMs has a capacity to engross and relieve heat energy when the material changes from one phase to another such as solid to liquid and vice versa (Kanimozhi et al., 2017). PCMs can be of organic (paraffin wax and non-paraffin), in-organic (salt hydrates and metallic) and eutectic (suitable mixture of organic and in-organic) type (Ling and Poon 2014; Sahu et al 2017). Most commonly used PCMs in concrete are organic PCMs such as paraffin wax, n-octadecane, poly ethylene glycol etc. Application of PCMs in building components (walls, ceiling and floors) improves the comfort level of habitants owing to its ability to maintaining the preferred level of temperature for a longer duration. This makes the implementation of PCMs in structural elements as one of the supreme technologies in developing energy efficient buildings (Stritih et al., 2003).

The integration of PCMs in cementitious system functions as both heating and cooling arrangement for a building by its repeated phase change cycles (Zhang et al.,

2013). In general, the integration of PCMs into cementitious system can be done by either direct addition during mixing of concrete or by impregnation into the concrete through light weight aggregates or by mixing micro-encapsulated PCMs during concrete preparation (Sahu et al., 2017). It is reported that direct addition of PCMs in cementitious composites is an easy and economical practice of integrating PCMs into concrete (Lee et al., 2015, Cellat et al., 2017). Effective usage of PCMs in cementitious system reduces the thermal loading as well as it reduces the thermal stresses driven by the cement hydration reaction (Fernandes et al., 2014). However, one of the disadvantages reported by the researchers is the leakage issue of PCM, which may alter the properties of cementitious matrix (Ling and Poon, 2014). Literature also states that some PCMs are unstable in alkaline condition (Fernandes et al., 2014). Hawes et al (1993) stated that PCMs react with the hydration products such as calcium hydroxide and undergo hydrogen bonding with silica hydrates losing its functionality as a thermal efficient material. Choi et al. (2014) reported that presence of PCM in cement mortar showed lesser hydration. It is also stated that PCMs provided favourable properties of latent heat by eliminating micro cracks and volume changes that arise due to thermal stresses in massive concrete structures (Pisello et al., 2016). The experimental study by Norvell et al., (2013) reports that incorporation of PCMs in concrete amplified the water demand and hindered the hydration process inducing significant obstruction in strength gain. Further, it is also reported that issues on mechanical performance of PCMs admixed cementitious products is attributed to its physical and chemical interference on hydration products (Jayalath et al., 2016; Hunger et al., 2009). Aforementioned factors possibly hindered its practical applicability in cementitious products.

At this point of time, it was understood that utilization of SCMs in conjunction with nano-silica is essential to counter balance the negative effects of SCMs (low initial compressive strength) and nano-silica (drying shrinkage, workability and high heat of hydration) to obtain a high performance and sustainable material. This investigation was also framed to identify the addition of phase change materials on the engineering properties of nano-silica admixed cementitious composite. Mechanical, hydration, thermal, microstructure, and durability properties of various designed and optimised

cementitious mixes were determined and advanced characterization studies were also carried out.

1.2   NEED FOR PRESENT WORK

In an emerging country like India, infrastructure growth is very much essential at this point of time. For the faster growth of a nation's economy, execution of construction projects within a specified time frame is the need of the hour. For some of the key infrastructure projects there is a requirement of high compressive strength, early removal of the formworks and a sustainable life cycle. For achievement of high early and later compressive strength, it is essential to include nano-silica particles in cementitious composites. However, small particle size of nano-silica induces certain weaknesses in cementitious system such as low workability, shrinkage (autogenous and drying), high heat of hydration and non-economical. Hence, the present need is to use SCMs in conjunction with nano-silica as a multi-blended (binary, ternary and quaternary) cementitious composite. In order to counter balance the drawbacks of SCMs (low initial strength, delayed setting time etc.) and nano-silica to obtain high performance sustainable cementitious composites. Optimized blended cementitious composites can be achieved by adopting the concept of particle packing theory (modified Andreasen and Andersen model).

In other perspective, global energy demand is increasing swiftly along with the rapid growth in economy, urbanization and industrialization. Reduction of energy consumption is the focal point on achieving toward energy efficient sustainable buildings. It can be made possible by blending thermally efficient smart material such as phase change materials (PCMs). PCMs has certain number of advantages mostly in controlling the peak temperature during initial days of hydration by absorbing energy there by reducing the rise in heat within the cementitious matrix. However, incorporation of PCMs greatly effects the mechanical performance of cementitious composites owing to its leakage issue. It is understood that incorporation of nano-silica in cementitious composites benefits in early strength with enhanced engineering and microstructure properties. However, inclusion of highly pozzolanic nano-silica in cementitious material induces shrinkage there by developing a larger number of cracks in concrete because of the faster rate of hydration reaction. Hence, it is

believed that amalgamation of these two materials (nano particles and PCMs) can mitigate the problems of one another thus resulting in high performance and thermally efficient sustainable infrastructure.

1.3 SCOPE OF THE STUDY

The thesis aims to determine the best performing blended cementitious composite by proportioning micron size (fly ash), sub-micron size (ultrafine fly ash) and nano-size (nano-silica) particles. In addition, this study also investigates the possibility of developing a heat storage material by adding phase change materials in the nano-silica admixed mortar. For achieving the former, particle packing theory based on modified Andreasen and Andersen model was adopted in this study for suitable proportioning of blended cementitious composite. For Binary blended CNS mixes proportioning was done at the replacement level of 0.5% to 3.5% with respect to OPC and the optimum dosage of 20 nm size CNS in cementitious mortar was checked with respect to the 28 days compressive strength measurement.

Further, three different percentage levels of fly ash were chosen i.e., 15% (minimum content), 25% (moderate content) and 35% (maximum content). Same percentage replacement levels were also chosen for UFFA, FA + UFFA, FA+CNS, UFFA+CNS, and FA+UFFA+ CNS mixes in order to maintain the homogeneity in this experimental program. The optimized proportion of each raw material in the mix were determined using "EMMA" software tool which works on the principle of modified Andreasen and Andersen particle packing model. Optimized particle packing curve for particular blended mortar mixtures with respect to ideal curve was obtained by continuously modifying the material proportions till the actual gradation curve of the particular mix reaches the optimal fit with that of target curve (ideal curve).

Early age properties of the mixes were characterized through the measurement of setting time, flow diameter and surface temperature. Compressive strength and density of these mixes were measured at different curing periods of 3, 7, 28 and 56 days. Advanced characterization studies such as thermogravimetric analysis (TGA), X-ray diffraction (XRD) and scanning electron microscopy with energy dispersive X-ray spectroscopy (SEM-EDS) were employed to characterize the hydration and microstructure studies. Other important studies such as pozzolanic reactivity (strength

activity index and selective dissolution method), rapid chloride ion permeability, permeable porosity, drying shrinkage and aggressive exposure (acid, alkali and chloride) were also carried out to define the durability characteristics. The results were discussed and various correlations were developed between several important parameters.

However, in case of PCM based cementitious mixes particle packing concept was not adopted. Here, three different PCMs (paraffin, sodium carbonate and n-octadecane) at 1, 3 and 5 weight percentage of OPC was added without replacing any of the ingredients. On the basis of compressive strength measurement at the age of 28 days, the best performing PCM mixes that attains the desired compressive strength were considered for further studies. These best performing PCM mixes were proportioned by adding 3% nano-silica in a replacement to OPC. Early age, mechanical, microstructure and durability properties on the best performing mixes were evaluated in a similar fashion as explained above. In addition, to determine the latent heat capacity of the PCM admixed cementitious mixes, differential scanning calorimetric study was carried out.

1.4 THESIS STRUCTURE

The thesis consists of six Chapters. Chapter one, provides the brief description of general introduction and need of the study. Chapter two, gives the comprehensive review of related literatures, followed by critical review and objectives of present research work. Chapter three, presents the detailed information of the materials used, mix design and methodology adopted for sample preparation and various testing in present study. Fourth Chapter contains the experimental results and discussion on the early age, hydration, mechanical, durability and microstructure properties of nano-silica blended cementitious composites. The test results on the influence of integration of phase change materials on early age hydration and microstructure properties of nano-silica admixed cementitious mortar along with durability properties are presented in Chapter five. Conclusions, which includes the major findings of experimental study and scope for future work are given in chapter six.

A broad frame work of this research is presented in a flow chart (Figure 1.1).
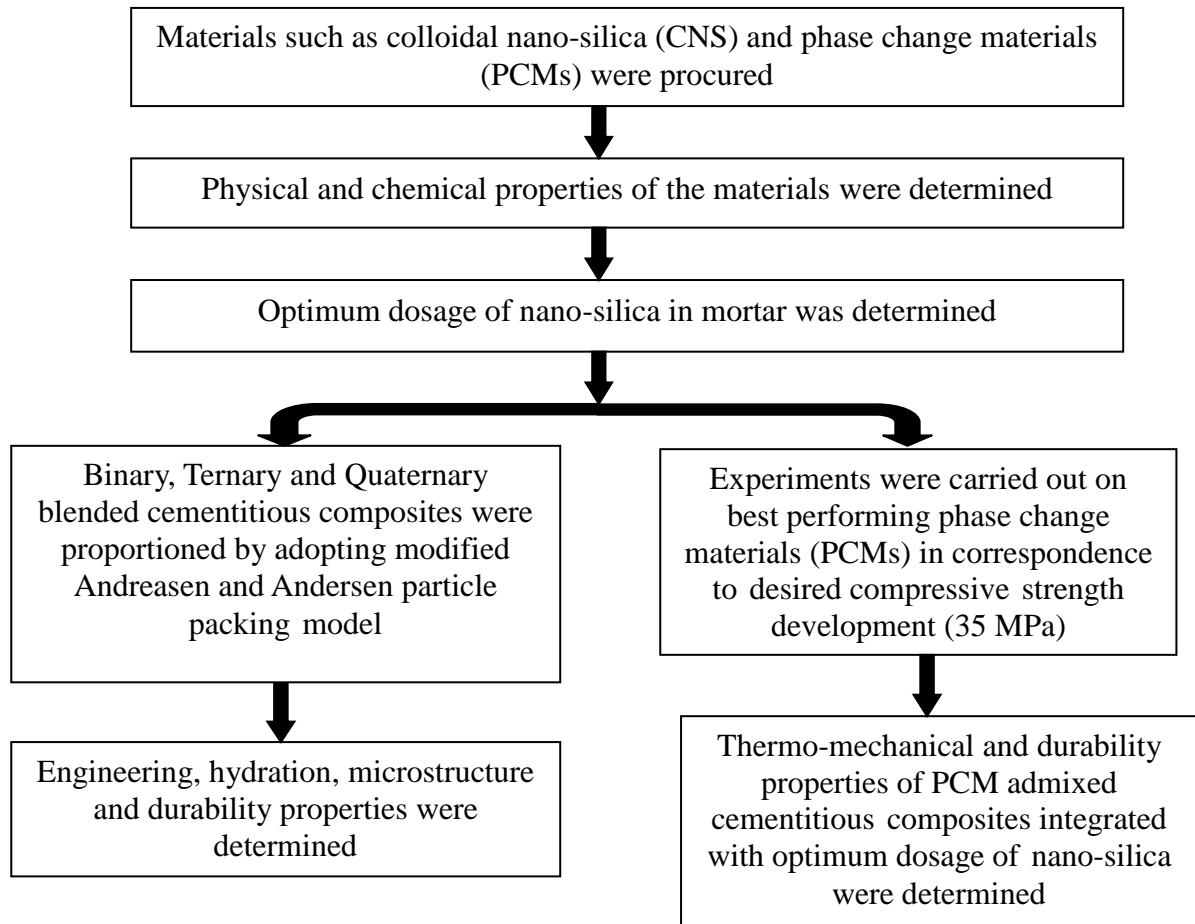
Figure 1.1: Flowchart of the experimental investigation

CHAPTER 2

REVIEW OF LITERATURE

2.1 GENERAL

This Chapter delivers a comprehensive review on relevant literature of secondary cementitious materials, nanotechnology, nano-silica and its influence on cementitious composites. This Chapter also provides the brief review of particle packing theory and the application of Andresen and Andersen model in the design of multi-blended cementitious composites. Further, the influence of latent heat storage material i.e. phase change materials on cementitious composites was reviewed. Finally, critical review of literature and research objectives were summarized.

2.2 SECONDARY CEMENTITIOUS MATERIALS (SCMs)

At present scenario, secondary cementitious materials (SCMs) have become a portion of cement and concrete. Use of supplementary cementitious materials (SCMs) or pozzolanic materials as partial replacement to OPC is turned out to be a sustainable solution for construction industry. Most predominantly expended SCMs are industrial by-products such as fly ash, ground granulated blast furnace slag (GGBFS), silica fume and etc. A brief review of literature on the influence of these SCMs in cementitious composite are presented in the following sections.

2.2.1 Fly ash (FA)

Fly ash, a by-product from thermal power plant is an extensively studied and used SCM in cementitious composites. Fly ash particles are spherical and generally cenospheres, whose average particle size lies closer to cement particles (Li, 2004; Goodarzi, 2006; Sahoo et al., 2017). ASTM C 618 categorizes fly ash as class C and class F in correspondence to its oxide composition. It is reported that class F fly ash are pozzolanic and considered to be as more significant for its use in cementitious composites as it possess lower level of calcium (Li, 2004; Goodarzi, 2006; Das and Pandey, 2011). Siliceous and aluminicious component of fly ash particles are responsible for directing porous calcium hydroxide (CH) into denser calcium silicate

hydrates. Fly ash particles contributed in long term strength and durability properties of cementitious composites (Goodarzi, 2006; Sahoo et al., 2017). Pore filling ability of fly ash particles also adds in refining the pore structure of cementitious composites and benefitted in providing better resistance to the ingression of chemical ions (Sahoo et al., 2017). Several researchers reported that utilization of fly ash as a partial replacement to OPC significantly improved the flow property owing to the ball bearing action of spherical particles (Li, 2004). Fly ash blended cementitious composites also minimizes the amount of heat liberated during the process of hydration. It is also reported that when its rate of replacement to cement exceeds the standard value of 20-30%, there found to be a reduction in its performance depending on the quality of fly ash (Rashad, 2014). In addition, fly ash extends the setting time of cementitious composites and performs poor in terms of early strength gain (Wescott et al., 2010).

2.2.2 Ground granulated blast furnace slag (GGBFS)

Another widely used secondary cementitious material in construction industry is GGBFS, produced from iron blast furnace (Zhang et al., 2012). Several researchers work on slag based cement composites reported that GGBFS, which possess particle size of approximately 40 µm effectually replaced OPC by 30-65% (ASTM C989-93). The existence of GGBFS in cement composites exhibited extra positive properties such as less water permeability, better workability, and higher resistance to sulphate/chloride ingression, resistance to corrosion in reinforced concretes and also assisted in long term strength gain (Wescott et al., 2010). However, it is reported that blending of GGBFS in cementitious composites also proliferates the setting time and leads to the lower early strength gain compared to that of 100% OPC based cementitious composites (Zhou et al., 2012).

2.2.3 Silica fume (SF)

Silica fume, an ultrafine pozzolanic material from silicon industry with average particle size ranging from 0.1 µm to 1 µm was identified as the supreme pozzolanic material (Giner et al., 2011; Diab et al., 2012). Literature states that silica fume concrete has tremendous advantages as compared to other mineral admixtures such as it reduces permeability and bleeding, reduces porosity, enhances durability, and mechanical

performance (Giner et al., 2011; Bagheri et al., 2012; Diab et al., 2012). Diab et al., (2012) reported that silica fume accelerates the calcium silicate hydrate formation and acts as nucleation site in cement matrix. In addition, it also improves the structure of interfacial transition zone (ITZ) there by enhancing the strength and reducing the susceptibility for water absorption. Silica fume is also considered as one of the key ingredients in the production of high strength and high performance concrete with the effective replacement level of 5%-10% by mass of cement (Kosmatka et al., 2003). It was reported that silica fume admixed cementitious system did not show much effect on setting time and initial strength as like other SCMs such as fly ash and GGBFS (Kosmatka et al., 2003; Biricik and Sarier, 2014). However, silica fume presence in cement composites are said to be more prone to plastic shrinkage (Biricik and Sarier, 2014).

2.2.4 Ultra-fine fly ash (UFFA)

It has been recognized by the research fraternity that reactivity of FA can be improved by reducing its particle size (Obla et al., 2003; Li and Wu, 2005). On this view point, UFFA particles were synthesized by processing class F fly ash (20-30 μm) into finer particles, whose average particle size (<7 μm) is closer to that of silica fume (Obla et al., 2003; Subramaniam et al., 2005). In addition to increase in specific surface area of UFFA, it also reduced the degree of crystallinity and anion polymerization of silicates and aluminates (Duan et al., 2018). It is reported that UFFA concrete performs similar to silica fume admixed concrete in correspondence to strength and durability, however, slight higher fraction (9.3%) of replacement was preferred in comparison to that of silica fume (8%) (Obla et al., 2003; Subramaniam et al., 2005). Literature says that intervention of UFFA in cementitious composites could improve the interfacial transition zone (ITZ) structure (Supit et al., 2013; Duan et al., 2018). Comparative study on UFFA and silica fume by Lin (2020) reported that performance of UFFA was better in terms of workability, permeability and mechanical properties, where in, silica fume reduced the workability and increased the demand for water. It was also reported that UFFA has not been contributed to thermal cracking as like silica fume (Ruybal, 2007).

2.3 NANOTECHNOLOGY

The branch of material science dealing with nano particles that has one of its dimensions in nanometers or 10^{-9} is termed as 'nanotechnology' (Gopalakrishnan, 2011). A particle with dimensions in the range of 100 nm to 1 nm is defined as 'nanoparticle'. Nanotechnology is a looming field of technology that brought revolution in the world for past few decades. Making use of intensively small active particles of size less than 100 nm leads to the extraordinary behaviour in the properties of materials. Materials functioning at ever-smaller dimensions drastically changed the physical, chemical, mechanical, and optical properties of materials in an unusual way and behavd exclusively superior by exploiting the properties of nano facet structures (Kithab and Arshad, 2014).

Richard P Feynman on 1960, an American physicist started the journey of nanotechnology with his remarkable lecture saying "There's Plenty of Room at the Bottom" at California Institute of Technology (Toumey, 2008; Maynard et al., 2010). The term 'Nanotechnology' was pioneered by Norio Taniguchi, later on Dexler presented 'Nanotechnology', as a science capable of producing nano-scale dimensions with precision ranging from 100 nm to 0.1 nm (Taniguchi, 1974)

2.4 NANO PARTICLES IN CEMENTITIOUS COMPOSITES

Singh et al (2016) stated that nano-science appliance in the area of civil engineering and construction is finding its relevance progressively, by means of incorporating nano particles in cementitious matrix. This led to the significant development in properties of cementitious composites and benefited in arriving at its sustainable life cycle. ''Nano-technology in construction materials'', a report from RILEM Technical Committee 197-NCM was the first document that emphasized the prospective of nanotechnology in terms of the development of construction and building materials (Bartos et al., 2002). Over the world survey of nanotechnology, construction industry is located at 8th position out of ten relevancies (Singh et al., 2013). The first is the health sectors followed by chemicals, information and communication, environmental application, energy, transportation, consumer goods, construction, house hold products, defence, aerospace, personal care, textiles and food industry. Concrete is a

heterogeneous and predominantly used construction material. Heterogeneity of particle size for multi-scale constituents in concrete ranging from nano to macro scale is presented in Figure 2.1 (Sobolev et al, 2005). The Figure states that particle size and surface area of concrete materials are inter connected, i.e. finer the particle size of nano-silica (< than100 nm) larger is the surface area (> than 10000 m^2/kg).
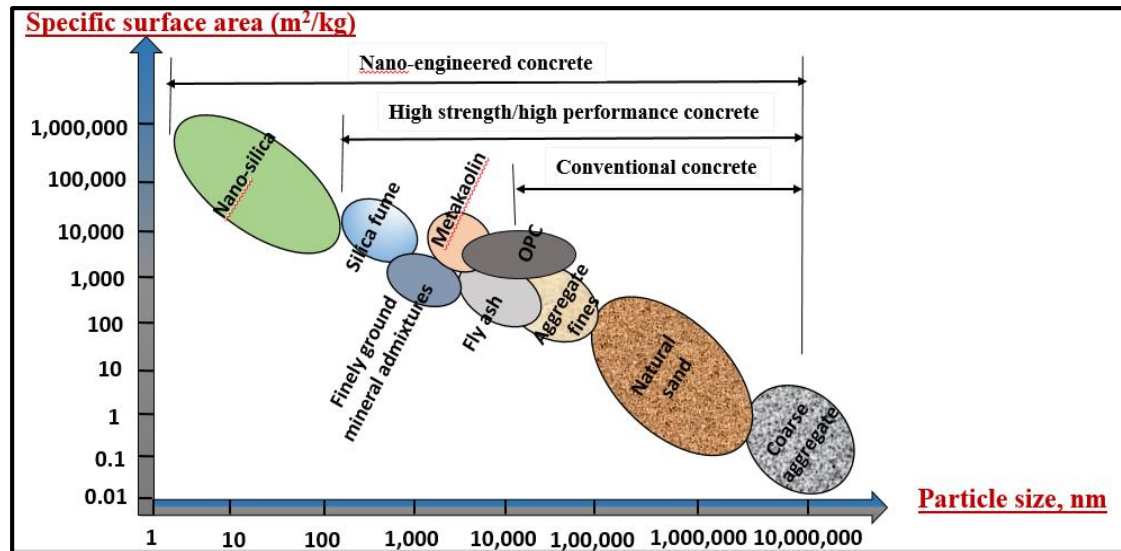
Figure 2.1: Particle size and specific surface area related to concrete materials

According to latest explorations, concrete made by utilizing nano constituents whose dimensions are less than 500 nano metres size was defined as "nano concrete" (Sanchez and Sobolev, 2010; Balaguru and chong, 2008 and Aitcin et al., 2000). Norhasri et al., (2017) discussed in one of their review paper that nano concrete with nano particle additives performed brilliantly in comparison to that of conventional concrete by improving the packing structure or bulk property and strength capacity. In addition, it is capable to execute an excellent filler effect by refining the pore structure, interfacial transition zones, and also controls the cement matrix structure at nano-scale. Richardson, (2008) discussed in his article that the core hydration product i.e. calcium silicate hydrate (C-S-H) arises at the nano level. This nanostructured phase describes the properties of cementitious composites at macro scale that are liable to strength plus durability of concrete (Belaguru and chong, 2008). Figure 2.2 represents the physical scale of concrete constituents.
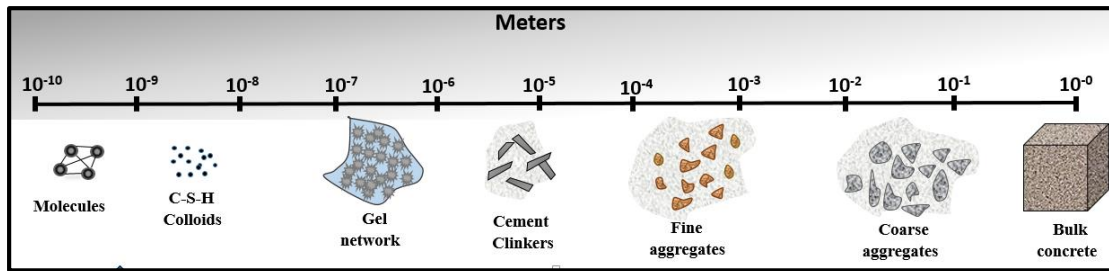
Figure 2.2: Magnitude of concrete components

The study conducted by Zhao et al., (2014) on nano-mechanical behaviour of a green ultra-high performance concrete reported that skill of nano particles built up a combined effect in concrete i.e., efficient and massive C-S-H structure additional to amazing filler property.

Hou et al., (2013) carried out a study to determine the effect of colloidal nano-silica addition on hydration of cement and its gel property. Authors have concluded from their study that the pozzolanic reactivity of nano based concrete is highly developed compared to that of pozzolanic material such as silica fume in concrete. Further, authors also reported that nano based concrete accelerated the hydration rate especially at the early age.

Safiuddin et al., (2014) presented a review study on the potential use of nano materials in concrete. Authors have reported that most of the researchers work on nano engineered concrete with the incorporation of nano particles like nano-silica and nano-TiO$_2$ showed enriched mechanical and durability properties of cementitious composite. Nano particles also reduced the bleeding and segregation in cementitious composites.

Birgisson et al., (2010) studied the influence of nano-modified concrete in transportation infrastructure. Authors reported the chief intention of exploiting the nanotechnology in concrete, such as1) achieve excellent mechanical and durability properties thus producing the ultra-high performance cementitious composites, 2) attaining of sustainable concrete structures by reducing the unfavourable effect on environment accordingly minimizing the utilization of energy in the process of cement manufacturing by improving safety, 3) accomplishment of smart concrete material by incorporating nano based self-sensing and powered materials, 4) development of innovative concrete with nano based production of cement and concrete and 5)

obtaining the essential multiscale models with highly developed depiction and modelling of concrete from nano to macro scale.

Shekari and Razzaghi, (2011) studied the influence of addition of nano particles in concrete with 15-18 nm size range such as nano-TiO_2, nano-Al_2O_3, nano- Fe_2O_4 and nano-ZnO_2. Authors concluded stating that addition of nano particles successfully achieved the elevated mechanical performance as well as durability of concrete at its hardened stage.

The study conducted by Singh et al., (2013) reported that fundamental structure of cementitious material can be modified by the incorporation of nano particles. Three key beneficial uses of nano particles in cement matrices are reported as, a) highly durable and ultra-high strength concrete can be created especially for distinctive appliances b) minimizing the quantity of cement utilization in the production of mortar and concrete without compromising in strength and in that way reduces the atmospheric impact as well as the cost on construction materials. c) nano particles addition helps in attaining fast-track construction with lesser period of curing.

The significant research were carried out in regard to the potential utilization of nano particles in cementitious composites. Majority of the studies were focused on the nanoparticles such as nano-silica, nano-TiO_2, and carbon nano tube (CNTs). While, few studies on other nano particle inclusion in cementitious composites such as nano-Al_2O_3, nano-Fe_2O_3, nano clay and nano-$CaCO_3$ were also been carried out. In the midst of several nano additives, nano-silica was found to have pronounced attention by the researcher community as it momentously benefits in mechanical and durability properties of cementitious composites owing to its dual actions such as superior reactivity and nano-filler effect (Givi et al., 2010; Zhang and Li, 2011; Supit et al., 2013; Shaikh et al., 2014). Following sections provides the comprehensive review on nano-silica and its influence on cementitious composites. Table 2.1 presents the summary of nanoparticles and its benefits in cementitious composites.

Table 2.1: Summary of nanoparticles and its benefits in cementitious composites

Nanoparticles (Authors)	Findings from literature
Nano-silica (Hou et al.,2013; Singh et al., 2013)	Faster rate of hydration, high early strength, enriched mechanical and durability properties, reduce bleeding and segregation
Nano-TiO$_2$ Shekari and Razzaghi., 2013; Safiuddin et al., 2014)	Self-cleaning, pollution reduction, rapid hydration, enriched mechanical and durability properties
CNT (Safiuddin et al., 2013)	Improved the tensile, flexural, compressive and bond strength
Nano-CaCO$_3$ (Kawashima et al., 2013)	Improved mechanical strength as well as modulus of elasticity
Nano-Fe$_2$O$_3$ (Shekari and Razzaghi., 2013)	Improved strength, self-sensing and modified electrical resistivity
Nano-clay (Hosseini et al., 2012)	Improved the tensile, flexural, compressive strength and durability

2.5   NANO-SILICA: PROPERTIES

The main constituent present in nano-silica is silicon dioxide (SiO_2) with a value of 99.5%. Table 2.2 states the chemical composition of silicon dioxide. Silicon dioxide nano particles appear white in colour. The physical and thermal characteristics of nano-silica are presented in Table 2.3 and Table 2.4, respectively.

Table 2.2: Chemical composition of nano-silica (Source: AZoNano., 2013)

Element	Content (%)
Silicon	46.83
Oxygen	53.33

Table 2.3: Physical characteristics of nano-silica (Source: Prasada Rao & Navaneethamma, 2016)

Properties	Metric
Active Nano content (% wt/wt)	30-32
PH	9-10
Specific gravity	1.20-1.22
Texture	White milky liquid
Dispersion	Water

Table 2.4: Thermal properties of nano-silica (Source: AZoNano., 2013)

Properties	Metric
Melting Point	1600°C
Boling Point	2230°C

2.6 MECHANISM ACTION OF NANO-SILICA IN CEMENTITIOUS COMPOSITES

Nano-silica presence in cementitious composites undergoes two stage mechanism such as, i) chemical effect: hydration, nucleation and pozzalonic reaction ii) physical effect: filler ability (Dunster, 2009). The schematic representation of nano-silica mechanism in cementitious composites is presented in Figure 2.3 (Lazaro et al., 2014)
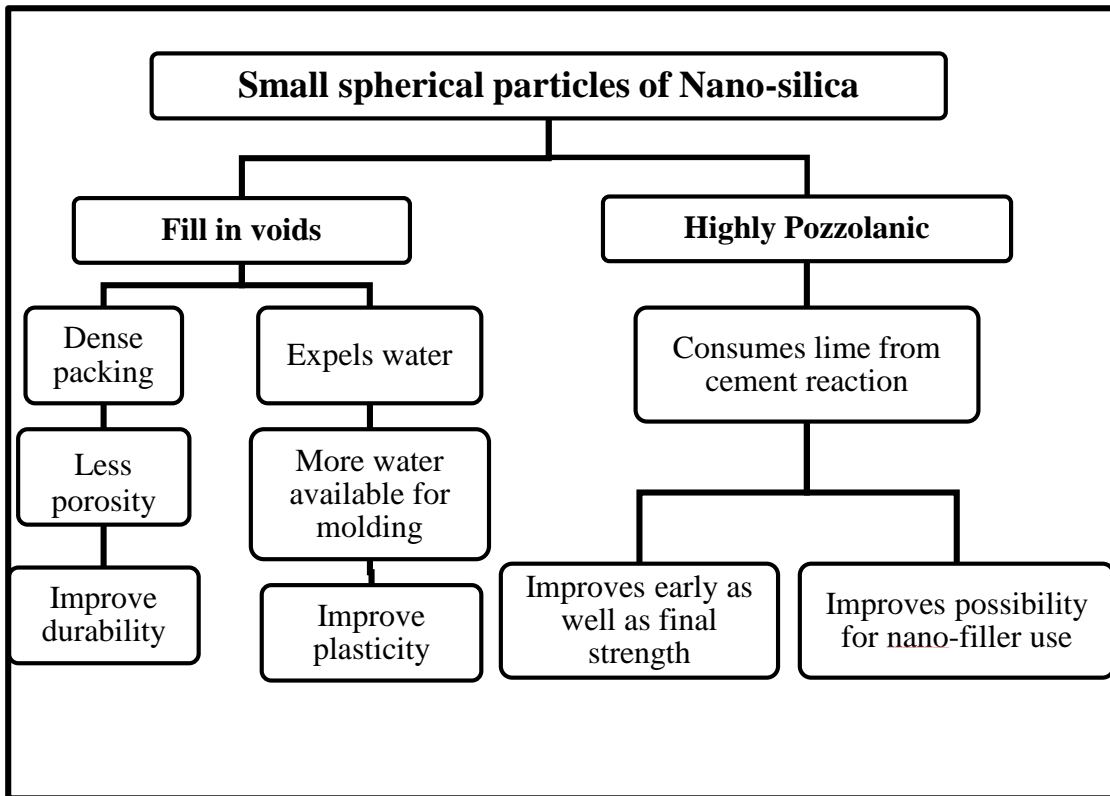
Figure 2.3: Schematic representation of nano-silica mechanism in cementitious composites (source: Lazaro et al., 2014)

2.6.1 Nucleation reaction

Jo et al., (2007) studied the influence of nano-silica particles on the properties of cement mortar. Authors reported that occurrence of nano-silica particles in cementitious media leads to the faster disbanding of tri calcium silicate and thereby leads to C-S-H formation. It is also stated that this action works in reverse manner to the particle size.

Thomson et al., (2009) studied the nucleation seeding effect of cement hydration mechanism and their results evidenced that presence of nano-silica made the cement hydration self-catalytic and keyed up the development of C-S-H gel. Authors also reported that assorted forms of reactive silica accelerated the hydration rate in a new way by C-S-H seeding effect. This is ascribed to the reaction between C-S-H and calcium ion released during the dissolution process of cement.

Quercia and Brouwers, (2010) carried out a research on application of nano-silica in concrete. The study reported that the major principle involved behind nucleation reaction is high surface area of nano-silica.

Raki et al., (2010) reviewed the importance of nano-science and technology in cementitious composites and identified that nanoparticles and nano tubes have scope in altering the hydrated structure of cement as well as aids in development of strength. Authors also stated that pre-hydrated silicates of nano-silica is the one of the major factor that improved the hydration process.

Land et al., (2012) studied the influence of nano-silica on the hydration properties on cementitious composites. It was stated that nucleation seeding effect of nano-silica gives the remarkable acceleration in cement hydration. This action significantly modified the structure of hydrated cementitious composites at micro to nano scale by, thereby enhanced the performance of cementitious composites.

Singh et al., (2013) conducted a study to optimize the amount of nano-silica particles in cementitious composites. Authors reported that $H_2SiO_4^{2-}$ formed with the incorporation of nano-silica comes in contact with calcium ions to form extra C-S-H. In addition, the extra C-S-H formation is not only restricted on surface of cement grains, as like in C_3S may also occurs in pore spaces. This nucleation reaction is presented in the Figure 2.4.

Figure 2.4: Nucleation reaction, formation of extra C-S-H seeds (Source: Singh et al., 2013)

Yu et al., (2014) conducted an investigation on nano-silica admixed ultra-high performance concrete (UHPC). It was reported that dosage of nano-silica plays a significant role in the development of cement hydration process and microstructure of

UHPC. Researchers also noticed that due to the higher viscosity of cement matrices in presence of nano-silica increased the porosity. Hence it has been concluded that inclusion of optimum dosage (5%) of nano-silica well balanced the pessimistic effect of entrapped air by its optimistic effect of nucleation. Summary of this section can be found in the Table 2.5

Table 2.5: Summary of literature of nucleation reaction of nano-silica in cementitious composites

Authors	Findings from literature
Quercia and Brouwers, 2010	• High surface area of nano-silica acted as the nucleation site for the production of C-S-H gel.
Raki et al., (2010) ; Land et al., (2012)	• Nucleation seeding is one of the major factor that modified the hydration process by utilizing it as pre-hydrated silicates. • Modified the structure of hydrated cementitious system in micro as well as in nano scale by the advancement in C-S-H gel formation
Jo et al., (2007)	• Faster disbanding of tri calcium silicate and conversion to C-S-H
Yu et al., (2014)	• The inclusion of optimum dosage (5%) of nano-silica well balanced the pessimistic effect of entrapped air by its optimistic effect of nucleation.

2.6.2 Pozzolanic reaction

Calcium hydroxide ($Ca(OH)_2$) is one of the by-product formed during cement hydration, which is a crystalline phase and has no significant role in strength (Singh et al., 2013; Sonebi et al., 2015).While, in the later period of cement hydration maximum concentration of calcium hydroxide will be attained (Sebok et al., 2001). Calcium hydroxide can be consumed by the utilization of pozzolanic materials (FA, GGBFS, SF etc.) in cementitious composites. It has been reported that nano-silica addition to cement concrete mix react hastily with $Ca(OH)_2$ and helps in the formation of additional C-S-H. This phenomenon drastically reduced the content of free lime by reducing its growth (Sonebi et al., 2015). Equation 2.1, 2.2 and 2.3 demonstrates the pozzolanic

reactivity in cementitious composites with the addition of nano-silica (Singh et al., 2013)

$$\text{Nano-silica} + H_2O \rightarrow H_2SiO_4^{2-} \qquad\qquad (2.1)$$

$$Ca(OH)_2 + H_2O \rightarrow Ca^{2+} + OH^- \qquad\qquad (2.2)$$

$$H_2SiO_4^{2-} + Ca^{2+} \rightarrow C–S–H \text{ (Additional C–S–H)} \qquad\qquad (2.3)$$
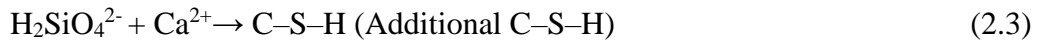
Bjornstrom et al., (2004) conducted a study related to the enhanced property of colloidal nano-silica on the useful formation of C-S-H in cement paste. The study showed that the nano-silica has a greater ability to react with calcium hydroxide crystals arranged in the crucial zone of interfacial transition zone. Occurrence of nano-silica significantly helped in improving the bond strength of hardened cement paste.

Givi et al., (2010) carried out an experimental investigation to assess the size effect of nano-silica particles in concrete. Higher pozzolanic reactivity was noticed for nano-silica with particle size of 15 nm than that of 80 nm that resulted in amplified early age strength of the concrete.

Hou et al., (2013) assessed the tailoring effects of cement matrix in the presence of nano-silica. It was stated that amplification of C-S-H gel owing to the significant pozzolanic reaction between nano-silica content and calcium hydroxide enhanced the strength and durability of cementitious composites. The study also revealed that CH adsorption on nano-silica particles, pozzolanic activity was found to be rapid and ended in the boundary of 7 days of hydration.

Hou et al., (2014) studied the effectiveness on pozzolanic reactivity for cement based materials integrated with nano-silica. It was reported that smaller the size of nano-silica higher is the pozzolanic reactivity with quicker reduction of CH content.

Summary of literature on pozzolanic reaction of nano-silica in cementitious composites is presented in Table 2.6.

Table 2.6: Summary of literature on the pozzolanic reaction of nano-silica in cementitious composites

Authors	Findings from literature
Bjornstrom et al (2004)	• Study showed the advancement in pozzolanic reactivity compared to that of silica fume • Nano-silica has a greater ability to react with $Ca(OH)_2$ crystals arranged in the crucial zone of concrete (i,e. interfacial transition zone)
Givi et al (2010); Hou et al., (2014)	• Smaller the size of nano-silica higher is the pozzolanic reactivity with quicker reduction of CH content
Hou et al (2013);	• CH adsorption on nano-silica particles intensified the pozzolanic activity and ended in the boundary of 7 days of hydration

2.6.3 Hydration reaction and microstructure

Bjornstrom et al., (2004) assessed the formation of functional C-S-H in cementitious composite admixed with colloidal nano-silica. Hydration effect was studied using diffuse reflectance FTIR. Authors identified that 5 nm size colloidal nano-silica accelerated the Ca^{2+} ion interaction in the formation of C-S-H network, that ensued the primary stage of hydration for around 4-12 hrs. It was also observed that addition of colloidal nano-silica enhanced the C_3S dissolution.

Jo et al., (2007) evaluated the cement mortar characteristic with the addition of nano-silica particles and observed that rate of evolution of heat during hydration process is associated to the fineness of the cementitious materials. Researchers reported that quantity of heat developed by 10% wt of nano-silica, 10% wt of silica fume and OPC without admixture were 245.5 J/g, 235.7 J/g and 231.1 J/g, respectively in 72hrs of hydration time.

Hou et al., (2013) studied the role of colloidal nano-silica (CNS, 10 nm) and silica fume in altering cement hydration and gel property. From semi- adiabatic calorimetry results authors reported that CNS enhanced the hydration peak temperature and reaction rate

of cementitious system to a greater extent compared to that of silica fume. Further, SEM analysis showed the dense hydrated morphology for nano-silica mixes.

Biricik et al., (2014) conducted a relative characteristic study on cement mortar with the addition of nano-silica, silica fume and fly ash. Authors have noticed that particles of nano-silica chiefly supported the C_3S and C_2S hydration activity through its nucleating effect compared to that of silica fume and fly ash particles. It was also reported that plenty of broken Si–O– and Si– bonds on surface of nano-silica behaved as a dynamic spots for pozzolanic activity.

Yu et al., (2014) determined the outcome of utilizing nano-silica with lower amount of binding material on hydration and microstructure properties for ultra-high performance concrete (UHPC). The study revealed that degree of cement hydration of mix incorporated with 5% nano-silica was increased by about 66.7%.

Land et al., (2015) considered the influence of nano-silica in controlling the hydration of cement. Study concluded that the key reasons behind the C-S-H seeding action was size effect of nano particles as well as its chemical composition. It has also been reported that nano-silica particles acted as a distinctive accelerator for cement hardening characteristic.

Singh et al., (2015) adopted non-evaporable water (NEW) method to determine the degree of hydration (DOH) for cement paste admixed with nano-silica and silica fume. It was observed that formation of hydration products during the period of pre-induction for nano-silica admixed cement paste is due to the development of extra hydration sites from nano-silica particles.

Wang et al., (2016a) carried out advanced studies such as SEM, XRD, and TGA to characterize the microstructure in regard to the activity of nano-silica at different ages. The SEM study showed numerous needle and bar like structures in early age further dense matrix was observed with the increase in curing period. X-ray diffraction study reported that as the age proceeds the diffraction peak intensity of CH drastically reduced. The CSH peak was found to initiate at 12 hrs and one day itself. TG-DSC study demonstrated that after three day the endothermic peak of CH was tend to get diluted.

Ma and Zhu, (2017) conducted an experimental investigation on concrete with nano-silica and basalt fibres. It was found that cement hydration in concrete with the dosage of 1.2% nano-silica significantly enhanced the amount of ettringite crystals and flocculent of CSH gel. Authors also noticed that increase in nano-silica dosage to 1.8% reduced the free water available for hydration of cement as well as the formation of ettringite crystals and flocculent C-S-H gel.

Summary of literature on the influence of nano-silica in the hydration reaction of cementitious composites is presented in Table 2.7.

Table 2.7: Summary of literature on the hydration reaction of nano-silica in cementitious composites

Authors	Findings from literature
Bjornstrom et al., (2004)	• 5 nm size colloidal nano-silica accelerated the Ca^{2+} ion integration in C-S-H network formation at initial hydration stages around 4-12hrs.
Jo et al., (2007); He and Shi., (2008); Wang et al., (2016)	• Quantity of heat developed for 10% wt of nano-silica was higher (245.5 J/g) compared to that of silica fume (235.7 J/g) in 72hrs of hydration time • Paste with nano-silica showed dense-compacted hydration products with lowered crystals of $Ca(OH)_2$ and fewer ettringite crystals
Biricik et al., (2014)	• Nano-silica particles chiefly supported the C_3S and C_2S hydration activity through its nucleating effect
Hou et al., (2013); Yu et al., (2014)	• Accelerating effect of hydration degree was not that powerful when nano-silica dosage exceeds 3% the cement content • Colloidal nano silica enhanced the hydration peak temperature and reaction rate to a greater extent
Singh et al., (2015)	• Formation of hydration products during the period of pre-induction allowed extra sites for hydration

2.6.4 Pore-filling effect

Concrete products are made up of porous media, these pores are responsible for the harmful effects on the life of cementitious composites (Kim et al., 2014). Pores in cement paste are divided into 4 types: a) innocuous pores (the diameter < 20 nm), b) less harmful pore (20–50 nm), c) detrimental pores (50–200 nm), and d) much-detrimental pores (>200 nm, Yang et al 1990).

Du et al., (2014) investigated the influence of nano-silica at two levels i.e. 0.3% and 0.9% on the durability properties of concrete. They found that dense microstructure of concrete with the incorporation of nano-silica reduced the permeability in the crucial zones such as ITZ. It was also stated that nano-silica addition to cement composites blocked the outlet for harmful agents due to the physic-chemical performance of nano-silica.

Experimental study conducted by Yu et al., (2014) on nano-silica admixed ultra-high performance concrete showed the decrease in initial porosity with the addition of nano-silica. Authors also reported that addition of nano-silica improved the degree of hydration with the bonus production of C-S-H phase that aided in filling up the pores. It was concluded that lowest porosity can be achieve by incorporating optimal amount of nano-silica.

Wang et al., (2016b) conducted mercury intrusion porous meter (MIP) test for cement paste with and without 3% nano-silica. They found that total porosity decreased by 2.21%, 5.51%, 2.95%, and 5.4% at 1, 3, 7 and 28 days, respectively in the presence of nano-silica. Authors reported that it was attributed to filler action of tiny nano-silica particles in filling the pores between unhydrated particles of cement.

Mohammed et al., (2018) evaluated the properties of high volume fly ash (HVFA) roller compacted concrete pavement by the inclusion of crumb rubber and nano-silica by means of non-destructive techniques. Authors found 1% as optimum dosage of nano-silica. It was justified that as the content of nano-silica increased reduction in reliability of RCC pavements with HVFA was observed as it imbibes the water used for mixing leading to the pores in between aggregates and ultimately effects the strength.

Summary of literature on pozzolanic reaction of nano-silica in cementitious composites is presented in Table 2.8.

Table 2.8: Summary of literature on pore-filling effect of nano-silica in cementitious composites

Authors	Findings from literature
Du et al (2014)	• Bigger sized large capillary pores were refined due to the dual performance of nano-silica as a nano-filler and the pozzolanic activator.
Yu et al (2014)	• Degree of hydration with the bonus production of C-S-H phase and that also filled the pores.
Wang et al (2016)	• Nano-silica acted as filler between un-hydrated particles and significantly reduces the total porosity

2.7 INFLUENCE OF NANO-SILICA ON VARIOUS ENGINEERING PROPERTIES OF CEMENTITIOUS COMPOSITES

2.7.1 Fresh properties

Literature reports that incorporation of extremely small sized mineral particles with high surface to volume ratio into cementitious mixes amplified the need for mixing water and chemical admixtures (Neville, 2008; Aitcin, 1998).

Jo et al., (2007) conducted an investigation on nano-silica based cement composite. The study reported that when nanoparticles are dispersed uniformly in cement composites the cohesiveness of the fresh mix increased and this necessitated the need for larger amount of superplastisizer.

Senff et al., (2009) assessed the function of nano-silica on rheological and fresh properties of cement paste and mortar. The study revealed that incorporation of nano-silica into cementitious mixture lowered the spread diameter by about 19.6%.

Ltifi et al., (2011) noticed rapid drop in the flow time with the increment of nano-silica content in cement mortar. Researchers also observed that percentage of nano-silica inclusion directly increased the water demand for mixture.

Berra et al., (2012) found that reduction in workability of mix with nano-silica was attributed to the immediate interaction of nano-silica sol with liquid part of cementitious mix leading to the gel formation. Authors have concluded undesirable influence of nano-silica on workability of mix can be reduced by delayed addition of mixing water aliquots without varying the w/b ratio or adding superplastisizer.

Kong et al., (2013) conducted a study to determine the effect of nano-silica agglomerates on fresh properties of cement pastes. It was noticed from their study that agglomerates in nano-silica has a unique ability to absorb water molecules in the mix. It was concluded that rheology of paste depends on the way how nano-silica particles behaves as a filler, incorporation of precipitated nano-silica to cement paste with large agglomerates showed better rheological performance than fumed nano-silica.

Yu et al., (2014) observed from their experimental study that slump flow linearly decreased with the increased amount of nano-silica. Authors have reported that the reason behind the slump loss was increased water demand leading to decrease in available lubricating water between interconnected pores. Further, authors have stated that increase in plastic viscosity of concrete also affected the workability in great extent.

Chaitra et al., (2016) found from their study that the resulted higher water demand in nano-silica mix was ascribed to the engrossing of water molecules by nano-silica particles owing to its higher surface area and reactivity. Researchers have made a modification in dosage of superplasticizer in order to sustain a constant workability as that of reference concrete mix.

Table 2.9 presents the summary of literature on the influence of nano-silica on fresh properties of cementitious system.

Table 2.9: Summary of literature on fresh properties of nano-silica admixed cementitious composites

Authors	Findings from literature
Senff et al., (2009); Ltifi (2011)	• Rapid drop in the flow and flow time with the increment of nano-silica content.
Berra et al (2012)	• Nano-silica sol immediately interacts with liquid part of cementitious mix leading to high water retention capacity through gel formation.
Kong et al., (2013);Yu et al (2014); Chaitra et al., (2016)	• Reduced the lubricating water in between the pores interconnected lead to increased yield stress and plastic viscosity of concrete that affected the workability in great extent.

2.7.2 Mechanical properties

Nazari et al., (2010) studied the physical, mechanical, thermal and microstructure of nano-silica modified concrete, their experiments were carried out by making use of different dosages of nano-silica with 15 nm size. The results signified that with the incorporation of nano-silica it was able to enhance the flexural strength. However authors also noticed that addition of nano-silica content more than 4 wt% caused inappropriate dispersion and reduced the flexural strength value.

Zhang et al (2012) reported that 3 and 7 days compressive strength increased substantially (30% and 25%) for high volume slag concrete with nano-silica inclusion (dosage 0.5%-2%). It was also reported by the authors that reduction in the size of nano particles significantly enhanced the early strength of the slag mortar.

Quercia et al., (2012) examined the influence of two forms of nano-silica (fumed powder silica and precipitated silica in colloidal suspension) in cementitious composites. Study revealed that addition of two forms of nano-silica enhanced the

compressive and split tensile strength of self-compacting concrete. However, authors have concluded that among the two forms of nano-silica, precipitated silica in colloidal suspension form was found to be more efficient.

Hou et al., (2013) assessed the impact of colloidal nano-silica on fresh and mechanical properties of fly ash blended cement mortar. Authors have observed from their investigation that colloidal nano-silica addition to 40% fly ash cement mortar showed more prominent enhancement in early strength compared to that of silica fume addition. It was reported by the authors that presence of 5% colloidal nano-silica in fly ash blended cement mortar mix improved the 3 and 7 days strength by 16% and 45%, respectively.

Yu et al., (2014) reported that flexural and compressive strength of UHPC at the age of 3, 7 and 28 days showed parabolic variation with respect to the dosage of nano-silica. Authors have concluded that 3.74 wt% of nano-silica was found to be the optimized dosage for the betterment of mechanical properties.

Singh et al., (2015) carried out an experimental investigations on mechanical properties of nano-silica modified cement mortar. It was evaluated from the study that mechanical performance of cement mortar enhanced with the inclusion of nano-silica in both powdered and colloidal form compared to that of silica-fume added mortar. Authors have observed that powdered nano-silica has great potential in accelerating the mechanical performance of cement mortar.

Chaitra et al (2016) evaluated the mechanical performance of cementitious composites admixed with colloidal nano-silica. Authors have observed from their study that inclusion of 2% colloidal nano-silica in cement mortar with 40% copper slag as a partial substitute to fine aggregates amplified the compressive strength compared to that of control mix. It was also concluded that existence of nano-silica in high performance concrete influenced greatly on early development of compressive strength. Furthermore, authors reported that strength enhancement at later ages was attributed to its filler effect than its pozzolanic action.

Wang et al., (2016a) scrutinized the impact of 0%, 1%, 3% and 5% nano-silica particles on the mechanical properties. Authors have noticed that for 3% dosage of nano-silica compressive strength was improved by 33.2%, 29.1%, 18.5% and flexural strength by 30.4%, 22.2%, and 6.7% at 3 days, 7 days, and 28 days, respectively. Eventually from the investigation authors have concluded that nano-silica had a significant influence at the age of 3 days followed by 7 days and 28 days.

Ma and Zhu, (2017) carried out an experimental study on concrete admixed with nano-silica and basalt fibers for compressive, tensile and microstructure properties. They observed that 1.2% of nano-silica content produced optimum quantity of CSH gel and ettringite crystals making the concrete compact resulting in high compressive strength and split tensile strength.

Summary of literature on the influence of nano-silica on mechanical properties of cementitious system is presented in Table 2.10

Table 2.10: Summary of literature on mechanical properties of nano-silica admixed cementitious composites

Authors	Findings from literature
Zhang et al., (2012)	• Researchers have reported that 3 and 7 days compressive strength substantially increased with nano-silica inclusion
Berra et al., (2012)	• Among the two forms of nano-silica colloidal nano-silica was found to me more efficient for compressive strength.
Nazari et al., (2010); Yu et al (2012)	• Flexural and compressive strength of UHPC at the age of 3, 7 and 28 days showed parabolic variation with respect to the dosage of nano-silica
Quercia et al., (2012); Chithra et al., (2016); Ma and Zhu, (2017)	• Appropriate addition of nano-silica significantly improved the compressive strength and split tensile strength

2.7.3 Thermal properties

It is stated in the literature that thermal properties of concrete is considered as one of the imperative facet in its durability point of view (Ballim et al., 2009). Literature says thermal conductivity, thermal diffusivity, specific heat and coefficient of thermal expansion are the chief thermal properties observed in concretes (Marshall 1972).

Jittabut et al., (2015) measured the physical and thermal conductivity properties of cement paste incorporated with nano-silica. Authors have studied the thermal properties by determining the thermal coefficient using surface probe (ISOMET2114) a direct gauging instrument. It was observed from their experimental results that incorporation of nano-silica particles with 12 nm, 50 nm and 150 nm size reduced the thermal conductivity of cement paste by 21%, 15% and 15%, respecively.

Lim and Mondal, (2015) evaluated the influence of nano-silica on the improvement in thermal stability of cementitious composites. Authors examined the effect of nano-silica on deprivation of cement paste (by decreasing the calcium hydroxide content) at assorted heating and cooling system. Researchers had exposed cement paste to heat up to 500 °C with two cooling system. Authors have noticed that specimens composing of nano-silica that are exposed to elevated temperature were able to retain beyond atmospheric temperature for a prolonged period of time without rigorous cracks.

Sikora et al., (2017) studied the mechanical and thermal properties of cement mortars admixed with nano-silica particles at varied dosages of 0, 1 and 3 wt%. Authors revealed that incorporation of WG as fine aggregates in place of river sand reduced the thermal conductivity and sorptivity coefficient without hampering the mechanical properties. Authors also reported that 3% addition of nano-silica particles resulted in still more reduction in thermal conductivity and sorptivity coefficient.

Biricik and Sarier, (2014) did a relative characteristic study on incorporating 10 wt% of nano-silica, silica fume and fly ash particles in cement mortar. They used thermogravimetric-differential thermo-gravimeter (TG-DTG) analysis technique to understand the reaction taking place in cement mortar when exposed to elevated temperature from room temperature to 1000°C. Their results demonstrated that at the age of 7 days mass percentage of CH and calcium carbonate of mortar with 10 wt%

nano-silica was resulted to be as least value of 9.9% and 17.4%, respectively compared to other two supplementary materials.

Table 2.11 presents the summary of literature on the thermal properties of nano silica admixed cementitious system

Table 2.11: Summary of literature on thermal properties of nano-silica admixed cementitious composites

Authors	Findings from literature
Jittabutt et al., (2015)	• Cement paste admixed with nano-silica found to be an outstanding energy saving insulating material especially when it is utilized in wall
Lim and Mondal (2015)	• Specimens exposed to elevated temperature were retained beyond atmospheric temperature for a prolonged time
Sikora et al., (2017)	• 3% addition of nano-silica particles resulted in still more reduction in thermal conductivity

2.7.4 Durability properties

2.7.4.1 Leaching effect

Gaitero et al., (2008) concluded from calcium leaching studies that the combined effects of nano-silica such as reduced amount of pore (slows down degradation rate by ingression of harmful solution), pozzolanic reactivity and enhanced silicate chain length lead to the controlled calcium leaching.

Singh et al., (2012b) prepared nano sized silica particles of ~50 nm size by sol gel process to incorporate in cement paste and aimed to study its effect on resistance to calcium leaching in cement paste and compared with that of silica fume admixed cement paste. Authors have observed that addition of nano-silica particles enhanced the decomposition of calcium hydroxide (CH) by pozzolanic reactivity thereby aided to the reduction of calcium leaching than that of silica fume.

2.7.4.2 Shrinkage effect

Sadrmomtazi et al., (2010) assessed the shrinkage behaviour of nano-silica admixed rice husk self-compacting concrete (SCC). It was observed by the researchers that nano-silica admixed concrete reduced the shrinkage strain compared to that of plain SCC. It was also reported that for rice husk based SCC shrinkage strain found to be in similar to control mix. But, presence of nano-silica in rice husk based SCC minimized the rate of shrinkage. Consequently, it was concluded that nano-silica showed positive impact on drying shrinkage of the SCC by overcoming the unfavourable effect of rice hush ash on concrete shrinkage.

Sonebi et al., (2015) conducted a study to assess the effect on rheological and shrinkage properties of cement mortar modified with nano-silica particles. Authors have noticed the potential decrement in plastic shrinkage with the increase in nano-silica content. It was reported that this was attributed to the filler effect and amplified rate of hydration by nano-silica particles thereby lead to the controlled volume changes.

Haruehansapong et al., (2017) did a comparative study on nano-silica, silica fume and plain cement mortar for drying shrinkage. Researchers had noticed greater shrinkage in nano-silica and silica fume admixed cement mortar. Authors also stated that nano-silica cement mortar due to its accelerated hydration rate had a higher rate of autogenous shrinkage and related chemical shrinkage. It was concluded that particle size of nano-silica along with its amount of addition had greater impact on drying shrinkage i.e. smaller the particle size higher is the rate of drying shrinkage and crack numbers.

2.7.4.3 Water permeability

Ji et al., (2005) carried out a preliminary study on nano-silica based concrete for water permeability and the test results showed 14.6 cm depth of water penetration for normal concrete and 8.1 cm for nano-silica admixed concrete. Based on this experimental result authors had concluded that nano-silica based concrete showed better resistance to water permeability than that of normal concrete.

Quercia et al., (2012) studied the use of nano-silica in concrete and found that presence of nano-silica in concrete drastically reduced the total permeability of concrete. This

was due to its nano filler and anti-leaching effect in adjacent to its accelerated hydration effect.

Haruehansapong et al., (2017) noticed that due to the smaller size and momentous packing ability, nano-silica particles supported in blocking the pore connectivity as well as channels for water molecules. This reduced the rate of water permeability for nano-silica based mortar to a greater extent than control and silica fume mortar.

2.7.4.4 Water absorption and sorptivity

Ehsani et al., (2016) studied the impact of nano-silica on water absorption of fly ash (FA) based cement paste and concrete along with its mechanical properties. Authors reported that mix with 5% nano-silica and without FA showed minimal water absorption, correspondingly mix with 3% nano-silica + 15% FA and 5% nano-silica + 25% FA also showed reduced rate of water absorption due to bulk microstructure.

Chaitra et al., (2016) reported that dual property of nano-silica in concrete that is void filling effect and increased rate of hydration lead to the densified matrix that lowered the water absorption and sorptivity values of concrete.

2.7.4.5 Rapid chloride ion permeability test (RCPT)

Chaitra et al., (2016) concluded from their rapid chloride penetration test (RCPT) results that high performance nano-silica concrete incorporated with 2% nano-silica content showed low values of charge passed at the age of 7 and 28 days. This was due to the increase in packing density of concrete by the addition of small sized nano-silica particles.

Said et al., (2012) carried out a rapid chloride ion penetration test for nano-silica admixed concrete and found that even a small addition of nano-silica reduced the amount of charge passing as well as depth of chloride ingression. Authors have reported that this was due to the refinement of pore structure in cement matrix owing to the presence of finer nano-silica particles.

Table 2.12 presents the summary of literature on the durability properties of nano silica admixed cementitious system.

Table 2.12: Summary of literature on durability properties of nano-silica admixed cementitious composites

Authors	Findings from literature
Gaitero et al., (2008); Singh et al., (2012b)	• Nano-silica admixed cement paste lead to the controlled calcium leaching.
Haruehansapong et al (2015)	• Reduction in the particle size of nano-silica increased the rate of drying shrinkage and crack numbers.
Sadrmomtazi et al., (2010)	• Nano-silica showed a positive impact on drying shrinkage of the SCC by overcoming the unfavourable effect of rice hush ash on concrete shrinkage
Sonebi et al (2015)	• Potential decrement in the plastic shrinkage with increase in nano-silica content that was attributed to the densified matrix, which controlled the volume changes
Ji et al., (2005) ; Quercia et al., (2012); Chithra et al (2016) Haruehansapong et al (2017)	• Nano-silica based concrete has better resistance to water permeability • lowered the water absorption and sorptivity values of concrete
Said et al., (2012); Chithra et al (2016)	• Nano-silica addition had a remarkable reduction in chloride penetration.

2.8   PARTICLE PACKING THEORY

Particle packing is of the interest for research fraternity in the production of concrete, mortar, ceramics etc. Literature says that dense packing of concrete with aggregate phase is one of the effective ways to curtail the use of binder quantity. That helps in developing an ecological and economical benefited concrete, in addition to that it also favours in reducing the level of shrinkage and creep (Neville, 1995; Bleeck, 2011).The traditional method of concrete mix proportioning involves volumetric packing, that is by means of an ideal gradation curve of aggregate proportions (Neville 1995; Kumar and Santhanam, 2003; Bleeck, 2011; Fennis and Walgreen, 2012). But, the

characteristic of particle packing also depends on the finer particle ingredients of concrete such as cement and other cementitious particles. The amount of solid particles per unit volume expresses the degree of particle packing (Kumar and Santhanam, 2003). The definition of packing density is given as the solid volume of particles to the total volume occupied by the particles, mathematically expressed as unit volume minus porosity (Kumar and Santhanam, 2003). The improvement of particle packing density depends on the void filling capacity of larger particles by smaller particles and void spaces between the small particles by further finer particles and so on (typically represented in Figure 2.5).
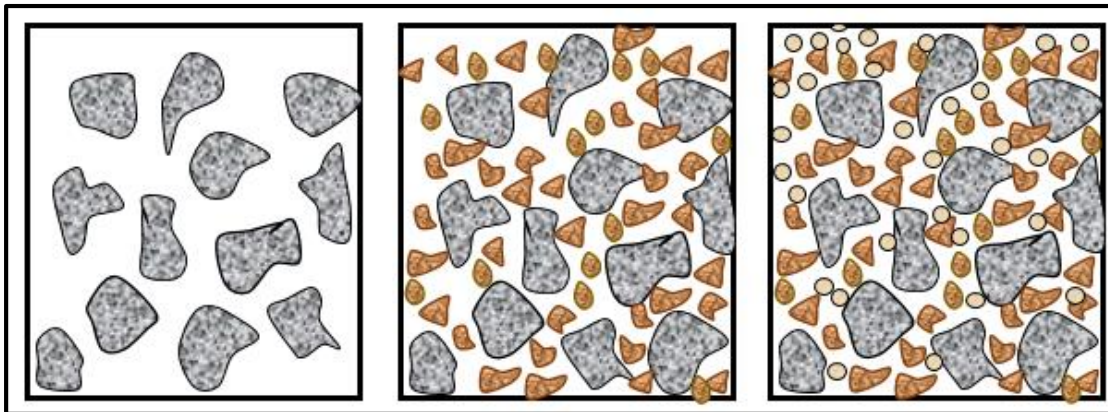
Figure 2.5: Typical representation of particle packing definition

2.8.1   History

The studies on particle packing theory is not new, it was initiated in early 20th century by Feret in 1892 (Feret 1892), who stated that content voids in matrix is inversely proportional to the strength achieved and the degree of packing is the function of grading curve. He signified that minimal voids in matrix is responsible in achieving maximum strength.

The study followed by Fuller and Thompson in 1907 (Fuller and Thomson 1907) presented the importance of particle size distribution of aggregates and concrete properties on the line of particle packing theory. They concluded that continuous grading of concrete composite mixture could help to enhance the concrete properties. The proposed gradation curve for maximum density known as fuller's curve (Fullers equation is described in Table 2.13, Equation 2.8). The study related to particle packing

of aggregates conducted by Suenson in 1911 demonstrated the triangular packing diagrams of aggregates (Suenson 1911). The basic investigation on packing theory for sphere shaped particles was started by Furnas in 1931 (Furnas 1931) by assuming that cavity between bigger particles will be filled by smaller particles.

In 1930, Andreasen and Andersen (Andersen and Johansen 1993) improved the fuller curve and proposed Andreasen equation (Equation 2.10) which emphasizes that the void ratio is mainly depends on the distribution modulus "q". It has been suggested that q factor could be varied in the range of 0.21 to 0.37 (Feret 1892; Andersen and Johansen 1993). Both the models presumed the minimum size of the particles as zero, i.e. particle is of infinite fineness (Cai 2017) with which it may not be able to practically satisfy the ideal distribution of particles. Later in 1980, Dinger and Funk (Dinger and Funk 1994) considering the minimum particle size in the distribution modified Andreasen and Andersen equation (Table 2.13, Equation 2.11).

It has been noticed that the widespread research was carried out by Powers in 1968 (Powers 1968) by hosting the importance of void ratio diagram on the basis of particle packing theory and developed a suitable model for concrete and mortar mixtures. However, the attention towards particle size optimization is amplified few decades ago in particularly with the emerging trends in concrete like high strength, high performance, high dense, self-compacting concrete etc. The concept of particle packing is beneficial in contrast to the conventional mix design as it is mainly developed on the basis of physical mechanism. Particle packing models are derived on the concept of theory of particle packing. The applicability of packing theories is chiefly affected by following factors: (a) particle gradation; (b) methods of compaction (c) shape and size of particles (d) wall effects (It is the disturbance in packing density due to the presence of isolated coarse particle in the matrix of fine aggregate, Figure 2.6a) and (5) loosening effects (it is the disturbance in packing density due to the presence of larger sized small particle which cannot fit in the void spaces of coarse aggregate, Figure 2.6b) (Mohammed et al 2013).
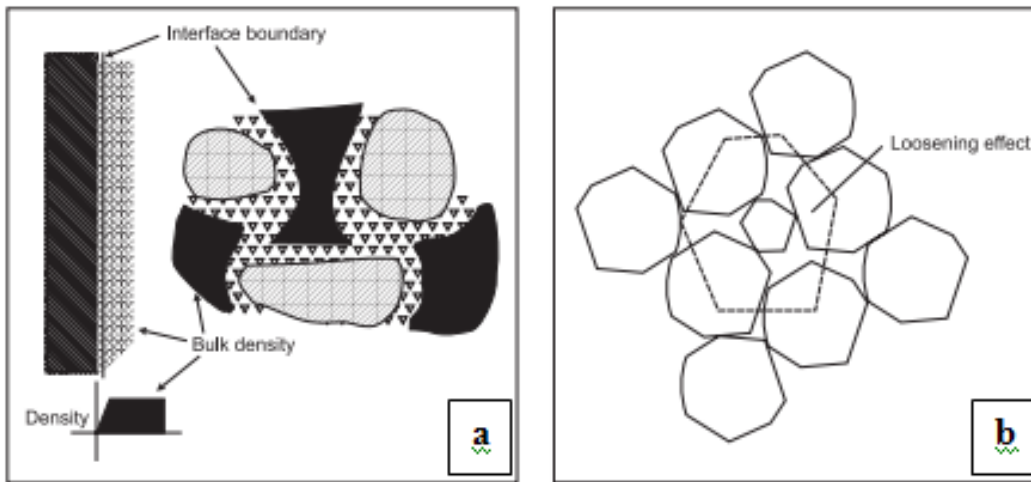
Figure 2.6: a) The wall effect (after Johansen) and b) The Lossening effect (after De Larrard)

It is found that there are several particle packing models were established by the researchers in order to achieve optimal filling: Furnas (Furnas 1931), Aim (Andersen and Johansen 1991), Toufar (Andersen and Johansen 1991), Stovall (Stovall and De Larrard 1986), Dewar (Dewar 1999), De Larrard (De Larrard 1998), Fuller Thomson (Fuller and Thomson 1907), Rosin Rammler (Kumar and Santhanam 2003) and Andressen models (Andersen and Johansen 1991). However, application of Andreasen and Andersen and modified Andreasen and Andersen model for the particle packing of multiple ingredients of cementitious matrix found to be largely being accepted by the researchers and considered as one of the beat known packing model.

2.8.2 Types of particle packing models

In the past 100 years numerous models on particle packing theory were suggested by researchers. In general particle packing can be classified into two entities i.e. discrete model and continuous model. The broad classification of developed particle packing under these categories is presented in Figure 2.7 and Table 2.13. Among all the developed particle packing models Andreasen and Andersen/modified Andreasen and Andersen particle packing model is found to be largely accepted by the researchers and considered as one of the best known particle packing model for designing a multi blended cementitious composite mixes.
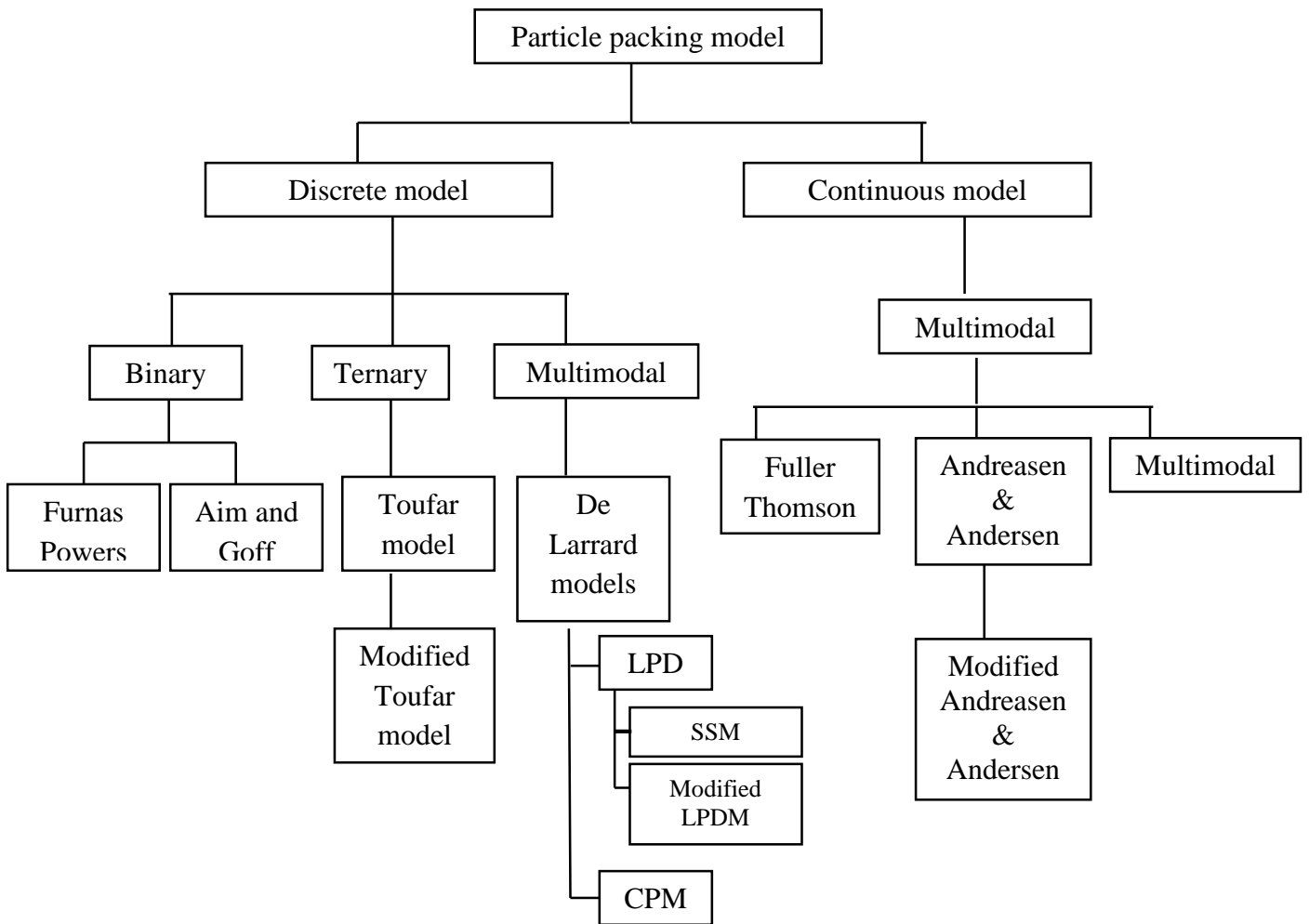
Figure 2.7: Broad classification of particle packing models

Table 2.13: Classification of developed particle packing under these categories

Particle packing model (PPM)				Theory
Primary classification	**Secondary classification**	**Ternary classification**	**Quaternary classification**	
Discrete model	Binary	Furnas Powers (Furnas 1931 ; Powers 1968)	-	* Considered for ideal packing of two materials. i.e. fine and coarse particles. * d_1 & d_2- diameter; y_1 & y_2- volume fraction and φ_1 & φ_2 –packing density of fine and coarse particles respectively. * Two conditions considered: 1) $y_1 >> y_2$- fine grain dominant $\varphi t = \dfrac{1}{y2 + \frac{y1}{\varphi 1}}$ $\qquad$ (2.4) 2) $y_2 >> y_1$- coarse grain dominant $\varphi t = \dfrac{\varphi 2}{1 - y1} = \dfrac{\varphi 2}{y2}$ $\qquad$ (2.5) * Furnas model is valid only if $d_1 << d_2$, if not it also depends on d_1/d_2 ratio. * Power proposed an equation to get lesser ratio of void for two size system. i.e. d_{max}/d_{min} $\qquad$ (2.6) Where, dmax- diameter of maximum size particle; dmin- diameter of minimum size particle.

		Aim and Goff (Andersen and Johansen 1991)	-	* Proposed a simple geometrical model to deal with the wall effect (Figure 2.8a) of binary mix and suggested a correction factor in order to avoid excess porosity in the first layer of spherical grains in contact with a plane and smooth wall. * $(d_{max} /d_{min})^{n}$ (2.7) Where, n- degree of an "ideal" curve equation
		Toufar model (Andersen and Johansen 1991)	-	Assumption: In this model spaces between large particles cannot be able to fill by smaller particles only.
	Ternary	Modified Toufar model (Stovall and De Larrard 1986)	-	* The Toufar model is altered by Goltermann et al (1997) and proposed a well-known model "modified Toufar model". * In accordance with their work procedure, packing degree of each component is computed and termed as eigen factor (φ_1 and φ_2) * Modified Toufar model fitted better with experimental values compared to the Aim and Toufar model for binary system (Andersen and Johansen 1991). * Further ternary particle packing also measured and theoretical diagram of packing is produced with respect modified Toufar model to create the packing density contours

			LPDM (Linear packing density model)	*Necessary input to be considered in this model are: density of packing, and equivalent diameters of each ingredients.
Multi-modal		De Larrard model (De Larrard 1998)	LPDM (Linear packing density model)	*This model is proposed by Stovall et.al (Stovall and De Larrard 1986), stating that with the information of size of particle and particle size distribution (PSD) packing density could be calculated. * This model performed well in designing the superplasticised cementitious materials
			SSM (Solid suspension model)	* The model proposed with some alterations to LPDM by De Larrard and Sedran and named as solid suspension model (SSM). * It is an excellent means to validate the high packing density of cementitious materials * An important concept is that this model considered the dissimilarity between real packing density (ϕ) and practical packing density (β) * It was reported that for a given mix it could be able to attain the maximum packing density by maintaining the original shape of each particle as well as by positioning one after the other in a mix. *This model would be appropriate in case of concentrated suspensions to predict the plastic viscosity

			Modified LPDM	*The LPDM concept was extended with the calculation of Eigen packing density and PSD for various blends of all set of size 'i'. *This modification was termed as Modified LPDM model.
			CPM (compressible packing model)	* The model is recommended by De Larrard. * This model is independent of LPDM/ SSM, rather depends on compaction index 'K'. *where, packing density is calculated similar to LPDM; while, for different compaction indices the virtual Eigen packing density varies.
Continuous model	Multi-modal	Fuller Thomson (Fuller and Thomson 1907)	-	* For obtaining the maximum density, Fuller and Thomson recommended the ideal gradation curves (Fuller's ideal curve). * The Fullers equation that is given as: $CPFT= (d/D)^n \ 100$ (2.8) Where, CPFT = Cumulative percentage finer than; n = 0.45-0.5; d = Particle size; D = larger particle size. * Further this expression is modified for concrete mix proportioning and is represented as: $CPFT=T_n \ (d_i/d_0)^n$ (2.9) Where, n = degree of an ideal curve. T_n = constant, dependent aggregate size (max) and the exponent n.

		Andreasen and Andersen (Andersen and Johansen 1991)	**Modified Andreasen and Andersen**	*Andreasen proposed an equation for ideal packing considering the particle size distribution via continuous approach. The equation is well known as Andreasen expression, say: $CPFT = (d/D)^q\,100$ (2.10) *Funk and Dinger brought modification to Andreasen equation considering the minimum particle size diameter. This model is popularly known as modified Andreasen model and the equation is given as: $CPFT = \{[(d-d_0)]/[(D-d_0)]\}^q\,100$ (2.11) Where, CPFT = cumulative percent finer than, d = particle size, do = particle size distribution of smaller particles, D = the maximum particle size, and q = distribution exponent.
		Rosin-Rammler (Kumar and Santhanam 2003)	-	* Rosin-Rammler equation considers the characteristic diameters $(D^{'})$ of the various ingredients gradation curve used for concrete. *Rosin-Rammler equation is given as: $R\,(D) = \exp(-D/D^{'})^n$ (2.12) Where, R (D) = % Residue fraction; D= diameter, n= 1.04 – 4 (constant).

2.8.3 Andreasen and Andersen / modified Andreasen and Andersen model

On the way to improve Fullers equation Andreasen and Andersen carried out a research on particle packing considering the concept of particle size distribution by means of continuous approach and proposed an equation for ideal packing in 1930. The equation is well known as "Andreasen equation" (Equation 2.10). Though Andreasen equation method is more into theoretical means, it partially signifies the practical concept of particle packing. The Andreasen and Andersen's research and proposed Andreasen equation emphasizes that the void ratio is mainly depends on the distribution modulus "q" and was suggested to use q factor in the between 0.33-0.5 (Hunger and Brouwers, 2009). Kennedy et al., (1994) used 0.45 as q factor for asphalt concrete mix design to attain better densified packing. It was reported by Hummel (1959) that higher packing density was achieved by considering q value as 0.4. However, Andreasen equation assumed that the fine particles are infinitely small i.e. $D_{min}=0$, which cannot be accept in practical point of view (Kumar and Santhanam, 2003).

Funk and Dinger specified that in any realistic particle size distribution Dmin cannot be infinitely small it must have some limited lower size value (Dinger and Funk, 1994). Hence, on this baseline Funk and Dinger in 1994 (Dinger and Funk, 1994) modified the Andreasen's equation considering the minimum particle size (D_{min}) as a finite factor and proposed an equation known as "modified Andreasen model" (Equation 2.11).

On the other hand it has been reported that distribution modulus (q) in Andreasen and Andersen model/ modified Andreasen and Andersen model equation varies depending on the need for workability, i.e. higher the value of q factor lower is the degree of workability (refer to Table 2.4). It means that higher is the amount of coarse material larger is the q value and if amount of fine materials are more than lower is the q value (Kumar and Santhanam, 2003). The amount of fine particles in mixture has the ability to control the water demand and capacity to hold water, in which the exponent q acts as an indicator for volume of finer fraction that could be placed in mixture. This provides a platform for opting the reasonable amount of water and water reducing agents (Kumar and Santhanam, 2003). The selection of distribution modulus should be done carefully so that it should not be too high or too low in order to avoid the adverse effect on the concrete/ mortar mixture. Higher value of q exponent may create

segregation effect and lower the value of q exponent may lead to obvious viscosity. It have been reported that in general the distribution modulus q for recent developed concrete mixtures varies between about 0.21 to 0.37 (presented in Table 2.14). For producing high performance and conventional concretes the q value in the range 0.25 to 0.3 may be considered by keeping the slump constraint in view. Further for self-compacting concretes, value of q may be considered as lesser than 0.23 (Kumar and Santhanam, 2003).

Table 2.14: Relative values of compaction factor and 'q' [Source: EMMA manual & table 20 and 22 in SP 23 Handbook]

Degree of workability	q	Compaction factor
Very Low	0.37	0.8
Low	0.32	0.85
Medium	0.27	0.9
High	0.22	0.95

The user friendly software, which works on the principle of Andreasen and Andersen model/modified Andreasen and Andersen model is "LISA (Language Independent Size distribution Analyser)" and is presently called as "EMMA (Elkem Materials Mixture Analyzer)" software. This software was designed to quantify the proportions of materials in multi-blended cementitious mixes. EMMA software is also designed for calculating the CO_2 content for optimized concrete mixture and hence, supports in minimizing the carbon footprint.

The steps involved in mix proportioning of concrete/mortar with multiple ingredients by EMMA software is represented in a flow chart (Figure 2.8).

One can create a customized library of particle size distributions (PSD) for different choosed materials for the mix

i.e through material library icon, which includes material name, density,CO_2 content if required, PSD in microns-the software will calculate D50, mean value of material grading)

Save the matrial -follow the step for the n materials

Then the gradation for any combination of ingredients considered can be determined

i.e through preparing a recipe using the new recipe icon, where the materials required for the mix are dragged from the material library

Mix name is entered

After that the quantity of the individual materials has been entered along with quatity of water, the distribution is presented in numbers as well as in a graphical representation

Use preview plot to monitor fitting to the target curve

Next select the calculation model, i.e. Andreasen and Andersen or modified Andreasen and Andersen model

Enter the maximum and minimum particle size accordingly and approriate 'q' value to the type of mix to be designed

This graph is compared to the Andreasen and Andersen or modified Andreasen and Andersen model

view graph

Optimization of mix can be done by adjusting the PSD for better fit to the Andreasen and Andersen or modified Andreasen and Andersen curve for better particle packing of the mix

Save the recepi

Figure 2.8: Flow chart representing the steps involved in mix proportioning of concrete/mortar with multiple ingredients by EMMA software

2.8.4 Application of Andreasen and Andersen model and modified Andreasen and Andersen particle packing model in design of cementitious composites

Study carried out by Kumar and Santhanam, (2003) to validate the usage of modified Andreasen and Andersen particle packing model to design mortar mixture. Authors have reported that the modified mortar design mix with incorporation of crushed sand, quartz powder and micro silica fitted better with ideal curve compared to the reference mix designed in accordance with IS 4031 – 1996 without any additives. Authors stated that it was attributed to the modification of the reference mix by additives with particle size of missing zones and there by representing the better particle packing. Authors

concluded stating that modified mix performed well with respect to 3, 7 and 28 days compressive strength i.e. approximately 28 - 30 % increase in strength for all the curing ages has been accomplished.

The comparative study was conducted by Gopinath et al., (2011) to optimize the mix deigns for normal and high performance concrete using ACI and BIS mix design methods. Further, EMMA particle packing software was used to modify the mixes. Authors have stated that the designed M30 mixes by ACI and BIS methods were optimized by fitting the actual gradation curve of the mix with modified Andreasen and Andersen curve (ideal curve) by keeping w/c ratio constant. Authors concluded stating that designed mixes modified by the method of particle packing projected closer compressive strength to that of designed mixes.

Li et al., (2018) conducted a study on ultra-high performance concretes (UHPCs) using basalt coarse aggregates (BA). Authors have applied the modified Andreasen and Andersen model with the constant distribution modulus value (q=0.2) for designing the mix in order to consider optimal proportion of powder content (i.e. cement, micro silica and lime powder). Authors have altered the powder content from 900 kg/m^3 to 650 kg/m^3 and used the basalt aggregates of maximum size ranging from 3 mm-16 mm. It was found by the researchers that on implementing particle packing theory it was able to reduce the fine contents and also achieved the maximum strength.

The study was conducted by Brouwers and Radix, (2005) to assess the role of particle size distribution in self-compacting concrete. Researchers have utilized slag blended cement, combinations of three sands, gravel and superplasticizer for their experimentations. Authors were aimed to reduce the quantity of paste (cement, limestone powder and water) as much as possible with certain amount of solid contents (sand and gravel). Fuller curve, Andreasen and Andersen curve and modified Andreasen and Andersen curve was used by the researchers to validate the mix designs. It was reported that the actual gradation curve of all the mixes fitted well with the ideal curve of modified Andreasen and Andersen model (with q=0.25) compared to that of other two models.

The experimental investigation was carried out by Borges et al., (2016) on the fabrication of geo-polymer concrete. Authors had employed Andreasen particle packing model to improve the geo-polymer formulations. Authors have considered three q factors i.e. 0.21, 0.235 and 0.26 with the solution to solid rate (s/s) of 1.3, 1.4 and 1.5. Further, two aggregate type i.e. glass and quartz were considered in their investigation. It was reported that lower value of q factor showed better workability irrespective of the aggregate type. Authors have concluded by stating that Andreasen method may be considered as suitable technique to alter the rheological properties for developing various mixes of geo-polymers.

Table 2.15 presents summary of literature on the application of Andreasen and Andersen model and modified Andreasen and Andersen particle packing model in design of cementitious composites

Table 2.15: Summary of literature on application of Andreasen and Andersen model and modified Andreasen and Andersen particle packing model in design of cementitious composites

Authors	Findings from literature
Kumar and Santhanam (2003)	• Modified mix designed using particle packing model performed well with respect to 3, 7 and 28days compressive strength i.e. strength increased approximately by 28 - 30 % increase.
Li et al (2018)	• Implementing particle packing theory it was able to reduce the fine contents in ultra-high performance concrete.
Brouwers and Radix (2015)	• Economical concrete mixes can be developed by means of particle packing theory by meeting the standards and requirements in fresh state.
Chithra et al (2016)	• Andreasen and modified Andreasen particle packing model can be considered as a suitable technique to improve geopolymer formulations by altering the rheological properties of geo-polymer mixes

2.9 PHASE CHANGE MATERIALS (PCMs)

Phase changes materials (PCMs) are sensible and latent heat storage materials with the potential to store and release energy in the form of heat during the process of phase transition i.e. solid to liquid, liquid to gas or vice versa (Demirbas, 2006; Pasupathy et al., 2008; Fernandes et al., 2014; Jayalath et al., 2016). The ideal response of PCMs to temperature and heat variation is that, when the temperature rises to the phase transition point in its high enthalpy phase conversion occurs either solid to liquid (captures heat and reduces the level of heat in the system) or liquid to solid stage (releases the captured heat and reduces the level of cooling in the system) and therefore, acts as an absolute media for latent heat storage (Fernandes et al., 2014; Savija, 2018). Figure 2.9 gives the idyllic response of PCMs on temperature variation and phase transition i.e. solid to liquid and vice versa.
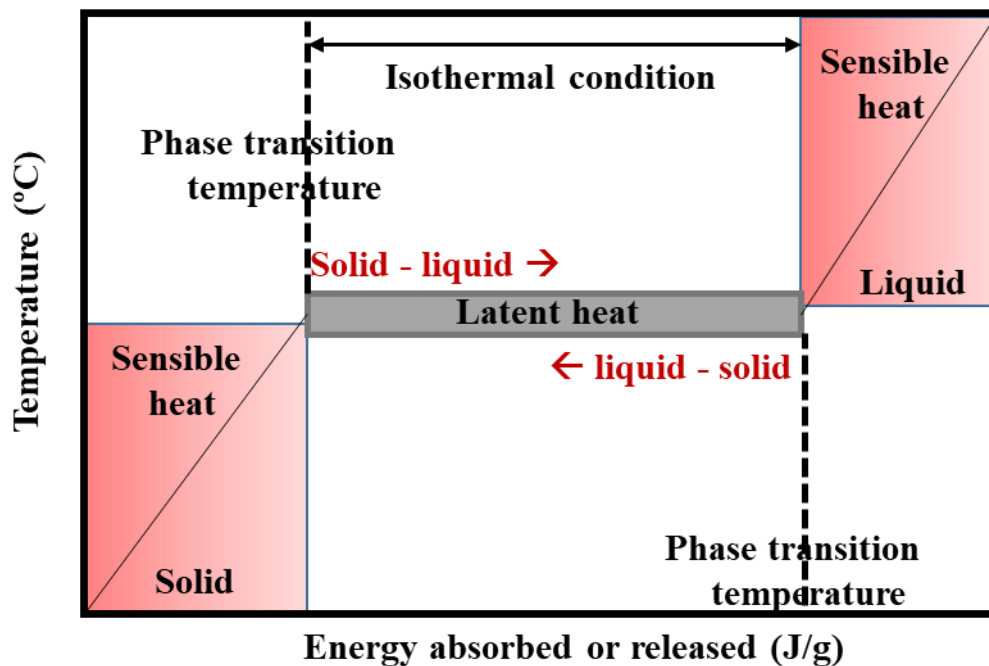
Figure 2.9: Idyllic representation of PCMs response to temperature variation, solid to liquid and vice-verse phase transition

2.9.1 Categories of Phase Change Materials (PCMs) and forms of PCM incorporation in to the cementitious composites

The PCMs are classified into three main classes. Detailed categorization of PCMs with its merits and demerits are presented in Table 2.16.

Selection of appropriate way to embed PCMs in cementitious material is very much essential to avoid its adverse effect on this materials. Inclusion of PCMs in concretes can be done by either of the ways mentioned in the following.

i) Direct addition of PCM: It is an easy practice of employing PCMs (Lee et al., 2015). However, major detriment is its leakage effect and alters the material matrix (Schossig et al., 2005).

ii) Pipes added with PCMs: This approach of incorporating PCMs can be able to resist physical and chemical damage endure during the stage of mixing, casting and loading.   In addition, pipe system avoids the PCM leakage and its negative influence on fresh and hardened concrete properties. But this approach is complicated and it shows lesser thermal influence due to limited spacing as well as partial melting of PCMs in pipes (Savija, 2018).

iii) Surface incorporation of PCMs via pores of concrete: In this method PCM in the melted form are allowed to engross into porous concrete and left for certain time to soak. The major drawback of this technique is PCM leakage (Farnam et al., 2015; Savija, 2018).

iv) Light weight aggregated impregnated with PCMs: this method adopts evacuation of light weight aggregates followed by immersing into liquid PCM and kept soaking in precise atmosphere for certain duration (Eddhahak-Ouni et al., 2014).

v) Micro-encapsulated PCMs with polymeric shell: is a recent technique where base PCM particles are encapsulated within a polymeric shell, which is capable to withstand the outside atmosphere and able to provide cyclic stability. It also possess high surface to volume ratio due to its micro sizes (Farnam et al 2015; Niall et al., 2016; Savija, 2018).

Table 2.16: Classification of PCMs (Fernandes et al 2014; Kalnaes et al 2015; Jayalath et al 2016; Cao et al 2017)

PCMs	Types	Examples	Remarks
Organic PCMs	Paraffin (C_nH_{2n+2})	Paraffin wax	**Merits**: chemically stable, no super cooling, recyclable, high heat of fusion.
	Non-paraffin (fatty acids, $CH_3(CH_2)_{2n}.COOH)$	Butyl stearate, lauric acid, capric acid, octadecane, glycerol etc.	**Demerits**: low thermal conductivity, volume change, flammable.
Inorganic PCMs	Salt hydrates ($A.nH_2O$; A-salts)	Sodium carbonate, $CaCl_2.6H_2O$, $NaCH_3COO.3H_2O$, NaCH3COO.3H2O, CaCl2.6H2O	**Merits**: low cost, non-flammable, high thermal conductivity, high heat of fusion.
	Metallic	Al, Mg, Zn etc.	**Demerits**: corrosive, super cooling
Eutectic PCMs	Organic-organic,	Ammonium alum-ammonium nitrate, capric acid-lauric acid, methyl stearate-methyl palmitate, myristic acid–palmitic acid etc.	**Merits**: properties can be tailored to match specific requirements, High volumetric thermal storage density and sharp melting point.
	Inorganic-inorganic	$NaCH_3COO.3H_2O$ +$NaBr.2H_2O$, $CaCl_2.6H_2O$+$CaBr_2.6H_2O$, $NaCH_3COO.3H_2O$ +$NaBr.2H_2O$.	**Demerits:** less data on thermo-physical properties for many combinations, high cost
	organic-inorganic	$LiCO_3$ +$NaCO_3$	

2.9.2 Effect of PCMs on thermal properties of cementitious composites

2.9.2.1 Thermal conductivity

The study conducted by Cao et al., (2017) on PCM based concrete revealed that rate of thermal conductivity reduced with the increase in concentration of microencapsulated PCM. It was reported that this statistics is mainly owing to the replacement of sand (thermal conductivity range: 1.8-2.5 W/m °C) by microencapsulated PCM (thermal conductivity: 0.2 W/m °C) and also due to amplified porosity of specimens. Researchers also noticed that samples with PCM in solid phase showed higher thermal conductivity than in liquid phase. This was attributed to the higher thermal conductivity of PCM in solid phase than liquid phase.

The experimental investigation carried out by Jayalath et al., (2016) specified that there is a drop in thermal conductivity with the increase in PCM content for both mortar and concrete specimens. This was ascribed to the replacement of sand, which contributes for higher thermal conductivity by PCM particles or may be due to the entrapped air.

The experimentation by Hunger et al., (2009) revealed that micro encapsulated PCM modified concrete resulted in declined thermal conductivity and stated that the reason could be due to increased air content.

The study on thermal conductivity of cementitious composites incorporated with microencapsulated PCM by Ricklefs et al., (2017) indicated that with the increase in microencapsulated PCM fraction, thermal conductivity declined linearly. It was described that this could be due to lower thermal conductivity of both the PCM core and shell compared to that of cement paste. It has also been stated by the authors that estimated value by Felske model (Fleske, 2004) agreed well with the experimental data and deviation was less than 4.5%.

Sakulicha and Bentz, (2012) reported that control mixes showed higher thermal conductivity compared to that of LWA impregnated PCM mixes. Among all the PCM mixes (paraffin wax, vegetable oil-based PCM, PEG400 & PEG600- 400 and 600

molecular mass polyethylene glycol) used in their investigation, pumice/vegetable oil based PCM indicated the lower most thermal conductivity i.e. 2.02 ±0.06 W/m K.

The experimental study carried out by Pisello et al., (2016) reported that micro-encapsulated PCM added concrete diminished the thermal conductivity and specified that this would be ascribed to the pore filling ability of micron sized PCMs. Authors have concluded that PCMs increased the capacity of thermal wave propagation and presented as a capable thermal-energy storage material for cement based material.

Zhang et al., (2013) conducted an experiment to measure the thermal conductivity of cement mortar board specimens assimilated with shape modified PCM composites (n-octadecane/expanded graphite). From experimental results authors clearly identified a linear drop in thermal conductivity i.e. of about 15.5% reduction for 2.5% PCM dosage. This has been justified to the fact that enhanced porosity resulted with the presence of PCM, which promoted the thermal insulation of mortar specimens.

2.9.2.2 Thermal energy storage

The research carried out by Cao et al., (2017) revealed that specific heat capacity of microencapsulated PCM modified concrete was approximately alike in solid and liquid phase of PCMs, even though the specific heat capacity of microencapsulated PCM is greater in solid phase (3050 J/kg ℃) than in its liquid phase (2740 J/kg ℃).

Hunger et al., (2009) measured the specific heat capacity by means of thermal analysis device with the temperature range of 19 °C to 28 °C while the device temperature maintained at 32 °C. The data recorded from the device i.e. sample temperature and heat flux, heat capacity was calculated using the following equation:

$$C_p = \frac{Aq}{m(\frac{dT}{dt})} \quad \text{and} \quad M_{th} = m\,C_p \qquad (2.12)$$

Where, C_p: heat capacity, M_{th}: thermal mass, A: sample heat exchange area, q: heat flux per square meter, m: sample mass, T: sample temperature and t: time. Experimental results signified the considerable increased rate of specific heat in proportional to the PCM quantity (temperature range of 24 – 26 °C) and found to be increased by 3.5 times for 5%

PCM content. It is also reported that even though the specific heat capacity increased significantly with the increment of PCM concentration, the maximum thermal mass was found to be observed roughly of 6800 J/K on 4% to 5% PCM content, which would possibly help to enhance the concrete thermal performance. The authors reported that about 12% energy saving can be made with 5% PCM content.

Sakulicha and Bentz, (2012) reported from their study that control mortar with the absence of PCM content exhibited the minor specific heat by mass. While, the mix containing pumice LWA impregnated with vegetable oil PCM showed utmost specific heat by mass in contrast to all other PCM mixes (paraffin wax; vegetable oil-based PCM; PEG400 & PEG600- 400 and 600 molecular mass polyethylene glycol).

The differential scanning calorimetry (DSC) results by Fernandes et al., (2014) indicated that latent heat capacity of micro-encapsulated PCM is in the range of 110-118 J/g, which is well within the manufacturers value i.e., 110 J/g. Authors have observed that endothermic peak temperature (within 21.9°C- 22.7°C) of microencapsulated PCM integrated cement paste performed relatively same as that of pure PCM irrespective of the PCM dosage. However, it has been reported by authors that latent heat capacity of cement paste significantly increased corresponding to the PCM concentration.

The experimental study by Jayalath et al., (2016) used paraffin based microencapsulated PCM to examine its influence on heat capacity. Authors have noticed that there is a significant rise in heat capacity with the increase in PCM content i.e. 55% PCM mixture exhibited three times higher latent heat capacity than 20% PCM mixture. On the other hand, authors have also observed that 55% PCM in cementitious composite increased the thermal mass of a mixture by 1.8 times to that of a mixture contains 20% PCM.

Ge et al., (2014) studied the thermal properties of PCM composites (graphite + euthetic carbonate + MgO) by means of TG-DSC curves. DSC curves represented the melting enthalpy of 348.5 J/g and 178.3 J/g for euthetic carbonate (LiNaCO$_3$) and composites, respectively. Authors stated that the reduction in melting enthalpy of composites could be imputed to the less amount of molten carbonate salts in composites. The TG-DSC results

of composite specimens subjected to twenty eight thermal cycles and that indicated the stability of the composite material with respect to its thermal efficiency. Authors also noticed that original shape of specimens were retained after 28 thermal cycles, which represents the state of physical stability of the composite.

Bentz and Turpin, (2007) utilized different PCMs (poly ethylene glycol –PEG -400, 600, 1000; octadecane and paraffin wax) to analyse the thermal property (via DSC) of cementitious composites. It was noticed that high-pitched transition (melting and solidification) rate in case of octadecane PCM compared to the other PCMs. While, for PEG and paraffin wax PCMs transition peaks were observed to be at 30-40 °C and 50-60 °C, respectively.

Table 2.17 presents summary of literature on the effect of PCMs on thermal properties of cementitious composites.

Table 2.17: Summary of literature on effect of PCMs on thermal properties of cementitious composites

Authors	Findings from literature
Zhang et al., (2013); Jayalath et al (2016); Cao et al (2017)	• Thermal conductivity drops with the increase in PCM content in both mortar and concrete specimens • This statistics is mainly owing to the replacement of sand (thermal conductivity range:1.8-2.5W/m °C) by PCM (thermal conductivity: 0.2 W/m °C) and also to amplified porosity of specimens
Hunger et al., (2009); Sakulicha and Bentz, (2012); Fernandese et al (2014)	• Increased the rate of specific heat and latent heat capacity in proportional to the PCM quantity. • 12% energy saving can be made with 5% PCM content.

2.9.3 Effect of PCMs on hydration properties of cementitious composites

The experiments carried out by Sakulicha and Bentz, (2012) examined the influence of incorporating light weight aggregates-LWA (expanded clay and a naturally porous Greek pumice) impregnated with four different types of PCMs (paraffin wax based, vegetable oil-based, PEG 400 and PEG 600) on cement hydration for mortar samples. Authors have observed from the study that vegetable oil based PCM impregnated in pumice showed little higher release in heat compared to that of other PCMs. However, the strength loss was observed to be higher than control in vegetable oil based PCM and paraffin based mixes. While, in case of LWA/PEG incorporated samples (P600, P400, G600 and G400; P-pumice and G-clay) almost 40% suppression of hydration peaks were observed irrespective of LWA type and the molecular weight of PEG

Eddhahak et al., (2014) observed that when mortar specimens was included with PCM (paraffin based) heat of hydration lowered and hydration kinetics found to be delayed compared to that of control mortar. Authors have observed that PCMs gets damaged during the mixing process and this resulted to deviation in hydration rate and that was ascribed to the seepage of paraffin wax distressing the hydration products.

The hydration study carried out by Jayalath et al., (2016) by means of isothermal calorimetry showed the delay in heat of hydration peak with the increase in replacement level of sand by microencapsulated PCM particles in comparison to control mortar. Authors reported that 20% and 50% sand replacement with PCM delayed the hydration peak by 1 hr and 2.5 hrs, respectively with respect to control mix. It has been reported that delay in appearance of maximum hydration peak could be owed to the high latent heat capacity of PCM.

Experimentation conducted by Bentz and Turpin, (2007) showed that PEG impregnated LWA in cement mortar hindered the cement hydration process. Hence, authors suggested that for its effective employment in fresh concrete, encapsulation through an inert material is essential. The semi-adiabatic temperature v/s time curves for different mixes (control mortar, PEG impregnated LWA mortar and PCM mortar with 27 grams of PEG) revealed

that PCM modified mixes (both PEG impregnated LWA mortar and PCM mortar with PEG) postponed the peak temperature by about 1 hr.

The study conducted by Hunger et al., (2009) reported that there is delayed hydration peak and reduction in peak height with the increase in PCM dosage. Authors have also reported that unpredictable higher rise in temperature was observed in case of 3% PCM mix than 1% mix and stated that this was attributed to the larger rate of damaged PCMs.

Table 2.18 presents summary of literature on the effect of PCMs on hydration properties of cementitious composites.

Table 2.18: Summary of literature on effect of PCMs on hydration properties of cementitious composites

Authors	Findings from literature
Sakulicha and Bentz (2012)	• 40% suppression of hydration peaks were observed
Eddhahak et al (2014)	• Mortar specimens with PCM (paraffin based) inclusion set out lower heat of hydration and delayed the hydration kinetics compared to that of control mortar
Jayalath et al (2016)	• Authors reported that 20% and 50% sand replacement with PCM delayed the hydration peak by 1 h and 2.5 h, respectively with respect to control mix

2.9.4 Effect of PCMs on fresh properties of cementitious composites

Snoeck and Belie, (2017) conducted a study on fresh property of cement mortar incorporated with different types of micro encapsulated PCMs (water dispersed form: Micronal DS 5039X, Powder form: Micronal DS 5040X, Micrathermeric D18, Micrathermeric D18, Micrathermeric D24, Micrathermeric D28). Study revealed that PCM dosage is inversely proportional to flow diameter. Researchers had also noticed that well

dispersed PCM showed lower workability, this was attributed to the reduction of water and also owing to its clogging effect.

Fenollera et al., (2013) examined the impact of micro-encapsulated PCMs (paraffin based) inclusion on flow property in self compacting concrete (SCC) and reported that there is a drop in flow diameter with the increase in PCM content. It has also been reported that SCC mix with 20% PCM did not accomplished the permissible range of flow leading to higher viscosity.

Yang et al., (2016) carried out an investigation on PCM (PX28) modified concrete by implementing two mix design methods i.e. by total replacement method and sand replacement method. It has been noted from their experimental data that increased PCM content reduced the flow-ability of concrete and reported that PCM replaced with respect to sand content lowered the flow more compared to that of total replacement.

Luscas et al., (2010) conducted an investigation on lime mortar integrated with PCMs and found that inclusion of greater percentage (20%) of PCMs lowered the workability. However, lower amount of PCM i.e. 5% and 10% showed good flow value. Therefore, authors have reported that quantity of PCM usage in mortar plays a key role in its lubricating action.

Table 2.19 presents summary of literature on the effect of PCMs on fresh properties of cementitious composites.

Table 2.19: Summary of literature on effect of PCMs on fresh properties of cementitious composites

Authors	Findings from literature
Yang et al (2016)	• Increased PCM content reduced the flow ability
Snoeck and Belie (2017)	• PCM dosage is inversely proportional to flow diameter

2.9.5   Effect of PCMs on density and porosity of cementitious composites

2.9.5.1 Density

The study by Hunger et al., (2009) emphasized that PCMs (Micronal DS 5008 X) greatly affected the density of concrete by decreasing the unit weight.

The study conducted by Pisello et al., (2016) reported that PCMs (organic paraffin based) presence in the concrete lowered the density value in comparison to that of no PCM concrete. Authors also stated that PCM added concrete may possibly act as light weight concrete.

The study on shape stabilized n-octadecane/expanded graphite composite PCM in cement mortar by Zhang et al., (2013) revealed that increase in composite PCM content in cement mortar samples linearly reduced its apparent density. However, it was also identified that cement mortar with 2.5% PCM reduced the density by only 9.5% to that of control mortar.

The experiments conducted by Fenollera et al., (2013) on PCM (0-20%) added concrete samples showed the consistent value of density and drastically lowered when 25% PCM was used. Authors reported that with reference to the preliminary stipulation of 2400 kg/m^3 as the range of concrete density, PCM admixed concrete up to 10% (density lower than 2300 kg/m^3) can be considered for its use in structural panels.

Yang et al., (2016) stated that PCMs are much lighter in weight compared to other ingredients of concrete with specific weight of about 0.694 g/m^3 that acted as a key in reducing the total unit weight/density of concrete.

2.9.5.2 Porosity

The experiments by Hunger et al., (2009) on porosity of self-compacting concrete (SCC) integrated with PCM resulted higher rate of porosity with increased dosage of PCM compared to that of control SCC. Authors stated that this may be attributed to the change in structural integrity and packing ability owing to the low specific gravity of PCM with respect to other ingredients of concrete.

The investigation by Luscas et al., (2010) on mortars integrated with PCMs (Micronal DS5008, BASF) showed higher porosity at 10 % PCM dosage compared to the reference mortar. It is reported by researchers that mean pore size was reduced in case of 10% PCM mortar with respect to the reference mortar and this was attributed to the contribution of PCM particles in filling up the larger pores. It was also stated that 20% PCM content in mortar tends to reduce the total porosity as compared to the reference mortar.

Table 2.20 presents summary of literature on the effect of PCMs on density and porosity of cementitious composites.

Table 2.20: Summary of literature on effect of PCMs on density and porosity of cementitious composites

Authors	Findings from literature
Hunger et al., (2009); Luscas et al (2010)	• PCMs greatly affected the density of concrete by decreasing the unit weight • Porosity increased with the increase in the dosage of PCM compared to the control
Pisello et al., (2016)	• PCM added concrete may possibly act as light weight concrete.

2.9.6 Effect of PCMs on mechanical properties of cementitious composites

2.9.6.1 Compressive strength

The investigation conducted by Jayalath et al., (2016) on mortar and concrete admixed with microencapsulated PCM showed reduced trend of compressive strength with increase in percentage of PCM. Authors have reported that two contrary factors that paid for the variation in compressive strength were, a) replacement of sand (hard particles) by microencapsulated PCMs (soft particles) and b) smaller particle size of microencapsulated PCM assisted in improving the compressive strength by the consequence of enhancing the nucleation sites for hydration. Authors have reported that strength loss occurred at 0% -

5% dosage of PCM was due to the less availability of nucleation sites. However, 10% - 20% PCM dosage mixes showed lower strength than control mix but were proved to have higher strength than 5% PCM dosage mixes. It was stated that it was attributed to the formation of sufficient nucleation site. It was also reported that at higher PCM dosage (35%-55%) "first factor" showed the dominant effect in reducing the strength.

The study conducted by Savija et al., (2018) reported that compressive strength reduced with the incorporation of PCMs and stated that optimum usage of PCM is very much necessary for its use as structural concrete.

Hunger et al., (2009) noticed the significant drop in the compressive strength of concrete with the increase in PCM content. Authors reported that each increase (1-5%) in percentage of PCM content reduced the concrete strength by 13%.

The study carried out by Falzone et al., (2016) also experienced the significant drop in strength. In order to compensate this critical effect of PCM mortar researchers have used quartz particles as supplement in their experimentation.

The experimental study carried out by Pisello et al., (2016) on 5% micro and macro incorporated paraffin based PCM showed lower compressive strength compared to the reference concrete. Authors observed that micro-encapsulated PCM concrete are more reliable than macro-encapsulate PCM concrete in terms of compressive strength. Authors reported that this could be due to the breakage and fracture of macro-PCMs.

The experimentation conducted by Zhang et al., (2013) reported that increased mass percentage of PCM reduced the compressive strength of cement mortar. However, researchers noticed a sudden drop in strength from 23.7 to 16.1 MPa with 0.5% PCM content and with further increase in PCM content gradual reduction in strength was observed.

The investigation carried out by Fenollera et al., (2013) reported that 5% PCM based concrete showed 7% drop in compressive strength compared to that of control mix and further increase in PCM content reduced the strength drastically. Authors conveyed by

their observation that drop in strength may be attributed to increased porosity, clustering and segregation of PCMs particles on top of the specimens during curing.

The experimental study by Qiao et al., (1955) reports that n-octadecane micro encapsulated PCM presence in cement mortar showed enhancement in strength for 5% PCM content than control mortar. While, for PCM mass fraction of 10% and 15% authors have observed marginal increase in compressive strength but further increase in PCM mass fraction to 20% and 25% compressive strength reduced to that of original mortar.

The study by Lecompte et al., (2015) noticed that mechanical strength of micro encapsulated PCM modified mortar/concrete reduced significantly. It was reported that the drop in strength was relied on two chief factors that were a) higher water demand (10% the mass) and b) rupture of capsules during compression, leading to the formation of voids.

2.9.6.2 Flexural strength

The experimental study by Luscas et al., (2010) reported that 10% PCM in lime mortar lowered the flexural strength due to the reason of enhanced porosity. It was also stated by the authors that 20% PCM content improved the flexural strength along with its compressive strength as a reflex of reduction in the porosity and pore size.

The investigation by Qiao et al., (1955) examined that 5% mass fraction of PCM showed highest flexural strength. Authors reported that further increase in mass fraction of PCM from 5% - 15% reduced the flexural strength gradually but it was observed to have higher flexural strength compared to that of control mortar. Further, higher PCM dosage from 20% - 25% has showed drastically reduced the flexural strength.

2.9.6.3 Modulus of elasticity

The study conducted by Yang et al., (2016) revealed that elastic modulus of concrete reduced with increase in the dosage of PCM with respect to the total replacement method of PCMs. Authors have reported that this was due to lower strength and stiffness of the soft PCMs. It was also reported that higher elastic modulus was seen at 23 °C curing condition

than that of 40 °C curing condition for the specimens prepared by both total replacement method and sand replacement method.

The experimental investigation conducted by Farnam et al., (2015) on mortar specimens integrated with PCMs (paraffin and methyl laurate) embedded light weight aggregate (LWA) revealed that LWA containing PCMs in mortar reduced the dynamic elastic modulus. Authors have identified that LWA containing paraffin oil PCMs mortar sustained the dynamic elastic modulus for about 95% of control mortar in contrast to that of methyl laurate PCMs.

Table 2.21 presents summary of literature on the effect of PCMs on mechanical properties of cementitious composites.

Table 2.21: Summary of literature on effect of PCMs on mechanical properties of cementitious composites

Authors	Findings from literature
Hunger et al (2009); Zhang et al (2013); Fenollera et al (2013)	• PCM content reduced the compressive strength drastically in a linear pattern.
Luscas et al (2010)	• PCM in lime mortar lowered the flexural strength
Yang et al (2016)	• Elastic modulus reduced with the increase in dosage of PCM

2.9.7 Effect of PCMs on shrinkage properties of cementitious composites

The experimental study conducted by Yang et al., (2016) in regard to the shrinkage effect of concrete incorporated with PCM in two ambient curing temperature i.e. 23 °C and 40 °C indicated that higher amount of PCM inclusion enhanced the rate of drying shrinkage irrespective of temperature condition. It was reported by the authors that this was attributed to the low stiffness and strength of PCM material with respect to other ingredients of concrete that hampered the resistance towards drying shrinkage. Authors reported that total replacement method reduced the cement content by increasing the water cement ratio that

deliberately increased the shrinkage rate in concrete. While, in case of sand replacement method drying shrinkage rate was observed to be lesser compared to the total replacement method as cement and water cement ratio were kept constant.

The study by Wei et al., (2017) investigated the response of PCM (MPCM24D) inclusion in cementitious matrix on drying shrinkage (as per ASTM C157) for two drying regimes (50% RH and 75% RH) where, the specimens were partially sealed up to 7 days. Researcher noticed that as per the anticipation the specimens in both the drying regime condition showed similar results on drying shrinkage and mass loss over the time of 7 days. It has been reported by the authors that quartz included paste mixture performed better in terms of shrinkage compared to that of PCM or plain mixtures and this was due to the stiff property of quartz material in contrary to the soft nature of PCM.

Table 2.22 presents summary of literature on the effect of PCMs on shrinkage properties of cementitious composites.

Table 2.22: Summary of literature on effect of PCMs on shrinkage properties of cementitious composites

Authors	Findings from literature
Yang et al., (2016)	• Higher amount of PCM inclusion enhanced the rate of drying shrinkage irrespective of temperature condition.
Wei et al., (2017)	• Shrinkage and mass loss was found to be greater in the drying regime condition of 50% RH than 75% RH

2.10   CRITICAL REVIEW

2.10.1 Influence of SCMs and nano-silica on cementitious composites

From the available literature it was observed that when pozzolanic materials/SCMs (fly ash, GGBFS, silica fume, rice husk ash, bagasse ash and etc.) were used in conjunction with OPC it contributes to the engineering properties of cementitious composites by means of its hydraulic and pozzolanic activity (Giner et al., 2011; Sahoo et al., 2017).

For an instance, several researchers reported that utilization of fly ash as a partial replacement to OPC significantly improved the workability, durability, chemical resistance and final strength of concrete (Li, 2004; Hou et al., 2013; Sahoo et al., 2017). The existence of another widely used SCM i.e. GGBFS in cement composites exhibited extra positive properties than conventional concrete like less water permeability, better workability, and higher resistance to sulphate/chloride ingression, resistance to corrosion in reinforced concretes and also aids to the long-term strength gain (Wescott et al.,2010). Literature states that silica fume concrete has tremendous advantages as compared to other mineral admixtures as it reduces permeability, bleeding, porosity and enhances durability and mechanical performance (Giner, 2004; Diab et al., 2012). Silica fume is also considered as one of the key ingredients in the production of high strength and high performance concrete with the effective replacement level of 5% - 10% by mass of cement (Kosmatka et al., 2003). In addition to silica fume, it was observed that researchers have utilized the classified/processed ultrafine particles from the industrial by-products such as fly ash and GGBFS in the production of cementitious composites. It is reported that inclusion of UFFA in cementitious composites improved the structure of interfacial transition zone (ITZ) owing to its increased surface activity (Feng et al., 2015) and setting time of cement paste was found to be increased (Obla et al., 2003).

However, most of these secondary cementitious materials initially behaved only as filler and remained inert in the hydration process that leads to the lower early compressive strength of cementitious composites (Das et al., 2012; Sobolev, 2009; Sahoo et al., 2017).

Over the past decades the use of nano-additives in cementitious composites has opened up new avenues. In the midst of several nano additives, nano-silica usage in cementitious composites has been reported extensively by the researchers owing to its superior and hasty pozzolanic reactivity as well as pore-filling ability at nano scale as compared to any other pozzolanic materials (Givi et al., 2010; Zhang et al., 2012; Supit et al., 2013). It was reported that implementation of nanotechnology in cementitious composites by introducing novel pozzolanic materials with extremely smaller particle size i.e. nano-silica

in cementitious composites mitigated the problem of lower early strength and found to be more competent in terms of filler, hydraulic and pozzolanic activity. Sobolev, (2009) stated that by the use of nano-silica it can be able to achieve at high performance concrete with a greater service life. However, literature also reports that use of nano-silica beyond 3-5 wt% (depending on its particle size) of OPC adversely effected the cementitious system such as high heat of hydration, slump loss and shrinkage, further nano-silica is non-economical (Litifi et al., 2011).

In this point of view it is more appropriate to use SCMs in conjunction with highly reactive nano-silica as multi-blended cementitious composites (binary, ternary and quaternary blends) to countervail the short comings of one another and hence, to obtain high performance sustainable cementitious composites.

2.10.2 Influence of particle packing theory in the design of cementitious composites

Several particle packing models were developed by the researchers to achieve the optimal packing of composites. However, application of Andreasen and modified Andreasen particle packing model was found to be the best choice and largely accepted by the researchers for designing the special concrete such as high performance, high strength, self-compacting and multi-blended mixes. On adopting Andreasen and modified Andreasen model it was able to achieve increased compressive strength in mortar (Kumar and Santhanam, 2007), high performance concrete (Gopinath et al., 2011) and ultra-high performance concrete (Li et al., 2018). Further, by implementing modified Andreasen particle packing model it was able to reduce the fine contents in ultra-high performance concrete (Li et al., 2018). Economical self-compacting concrete mixes with required fresh property was developed by adopting modified Andreasen particle packing model (Brouwers and Radix, 2005).

In view of that, for achieving the optimal particle packing of cementitious composites the appropriate and best-known particle packing model was found to be as modified Andreasen and Andersen model. The user-friendly software designed based on Andreasen and

Andersen/ modified Andreasen and Andersen model (EMMA software) made the mixture designer ease in designing the cement composite mixes with improved packing density.

2.10.3 Influence of PCMs and nano-silica on cementitious composites

Phase change materials (PCMs) are gaining more attention in achieving the sustainability and are being widely adopted as a green building material because of their exclusive ability to store latent heat of thermal energy. PCMs have a capacity to minimize the energy loads and to provide thermal comforts in building infrastructures by its iterative cycle of absorbing and releasing heat energy (Sakulich and Bentz, 2012; Zhang et al., 2013). The potential need for manipulating the heating and cooling effect in buildings is significantly increasing especially in temperature fluctuating and varied climatic regions like India. It is for this one of the significant reasons, PCMs are getting pronounced interest by the research fraternity in the development of a thermally effective PCM based construction material.

From the literatures it can be understood that inclusion of phase change materials in the cementitious composites enhances the thermal mass, latent and specific heat capacity and found to be increased with increase in PCM concentration (Bentz and Turpin, 2007; Sakulich and Bentz, 2012; Jayalath et al., 2016). It was reported that existence of PCM in cementitious composites reduce the heat of hydration and also the associated chemical shrinkage (Fernandes et al., 2014). PCMs offers favourable properties of latent heat by eliminating micro cracks and volume changes that arise due to thermal stresses in massive concrete structures (Pisello et al., 2017). However, one of the major disadvantages reported was the leakage issue of PCM, which may lead to alteration in the properties of cementitious matrix (Ling and Poon, 2013). It was also reported that some PCMs are unstable in alkaline conditions, some react with the hydration products (i.e.CH), and some PCMs undergo hydrogen bonding with silica hydrates, thereby losing its functionality as a thermally efficient material (Hawes et al., 1993). PCM doped cementitious composites drastically reduced the mechanical performance, density and increased the porosity of cementitious composites owing to the low density and physical/chemical interference of PCMs with cement hydration products (Sharma, 2013; Jayalath et al., 2016).

Aforementioned reasons possibly hindered its practical applicability in cementitious composites.

At this point of time it is very much essential to use highly reactive superior pozzolanic ingredient i.e. nano silica in conjunction with PCM based cementitious composite to alleviate the associated loss in structural integrity due to the presence of PCM. Further, the presence of PCM in nano-silica admixed cementitious composites may aid in mitigating the shrinkage and thermal issues raised by the highly reactive nano-silica particles.

2.11 RESEARCH OBJECTIVES

The objectives of this research project are

- To identify the optimum dosage of nano-silica particles for the compressive strength development of cementitious composites.
- To determine the influence of nano-silica particles on early age, hydration, durability and microstructure characteristics of cementitious composites integrated with nano-silica particles.
- To measure the engineering properties of optimized blended cementitious composites integrated with secondary cementitious materials (SCMs) and nano-silica particles.
- To identify the best performing phase change materials (PCMs) in correspondence to desired compressive strength development.
- To determine the thermo-mechanical and durability properties of PCM admixed cementitious composites integrated with optimum dosage of nano-silica.

CHAPTER-3

EXPERIMENTAL METHODOLOGY

3.1 GENERAL

This Chapter provides the detailed information about the materials and their properties used for the experimental work, mix design and experimental methodology followed to study the early age, hydration, mechanical, thermal, durability and microstructure properties of the cementitious composites.

3.2 RAW MATERIALS AND THEIR PROPERTIES

The physical, chemical and mineralogical characterization of ingredients used for the experimental study was determined in the laboratory in accordance with standard specifications.

3.2.1 Cement

Commercially available ordinary Portland cement (OPC) of 53 grade conforming to IS 12269:2013 was used for experimental investigations. The oxide composition and physical properties of OPC are presented in Table 3.1. The particle size distribution of OPC is presented in Figure 3.1.

3.2.2 Fly ash

Low calcium class F fly ash (FA) procured from Udupi thermal power plant, Dakshina Kannada, Karnataka, India conforming to IS 3812:2003 was used. The oxide composition and physical properties of FA are presented Table 3.1. The particle size distribution of fly ash particles used in the study is presented in Figure 3.1.

3.2.3 Ultra-fine fly ash

Ultra-fine fly ash (UFFA), is a processed form of Class F fly ash. The UFFA used in this study was obtained from Zigma International, Mumbai and has particles of spherical shape with an average size of 5 microns. The oxide composition and physical properties of FA are presented Table 3.1. The particle size distribution of ultra-fine fly ash particles used in the study is presented in Figure 3.1.

3.2.4 Nano-silica

A water-based and sodium-stabilized colloidal nano-silica (CNS) with an average particle size of 20 nm, obtained from sisco research laboratories, Mumbai was used. The basic properties provided by the manufacturers are listed in Table 3.1. The particle size distribution of CNS is presented in Figure 3.1.

Table 3.1: Oxide composition and physical properties of OPC, FA, UFFA and CNS

Oxide composition		OPC	FA	UFFA	CNS*
Oxide		OPC	FA	UFFA	CNS*
SiO_2		20.5	60.6	63	99.9
Al_2O_3		4.0	28.6	29.2	-
CaO		64.2	1.5	1.3	-
Fe_2O_3		4.96	3.9	3.2	-
K_2O		-	0.1	0.12	-
MgO		1.2	1.8	1.4	-
Na_2O		-	0.4	0.28	-
SO_3		1.8	1.2	1	-
LOI		2.11	1.6	1.5	-
Compressive Strength (MPa)	3 days	22.1	-	-	-
	7 days	36.5	-	-	-
	28 days	48	-	-	-
Physical Properties					
Specific gravity		3.15	2.2	2.2	2.2-2.4
Specific surface area (m^2/kg)		300	265	670	200,000
Initial setting time (min)		110	-	-	-
Final setting time (min)		170	-	-	-
Solid content (%)		-	-	-	40 (w/v)
Dispersion medium		-	-	-	water
pH		-	-	-	9

*provided by the manufacture

3.2.5 Phase change materials (PCMs)

The PCMs used in this study are paraffin wax (organic PCMs), n-octadecane (organic PCMs) and sodium carbonate hydrate (inorganic PCM). The physical properties of PCMs as per the manufactures report is shown in Table 3.2.

Table 3.2: Physical properties of PCMs used in the study

Type of PCM	Appearance	Density (g/cm^3)	Melting Point	Latent heat of fusion (J/g)
Paraffin wax	Waxy solid	0.9	53-58°C	200-220
n-octadecane	oil	0.78	26-29°C	289.4
Sodium carbonate hydrate	White powder	1.46	34°C	264

3.2.6 Fine aggregate

Fine aggregate used for the experimental work was locally available river sand passing through 4.75mm sieve, conforming to zone II as per IS 383:1970. The required tests for assessing the properties of sand was determined as per IS 2386:1963. The physical properties of fine aggregates tested are presented in Table 3.3. The particle size distribution curve for fine aggregate is presented in Figure 3.1.

Table 3.3: Physical properties of fine aggregate used for study

Sl. No	Property		Value
1	Specific gravity		2.56
2	Bulk density	Loose	1524 kg/m^3
		Compacted	1780 kg/m^3
3	% of voids		35.5 %
4	Moisture content		Nil
5	Water absorption		1%
6	Fineness modulus		3.14

3.2.7 Water

Potable water confirming to drinking water standards of IS: 10500 - 2012 was used for mortar mixing.

3.2.8 Super plasticizer

The poly carboxylate ether (PCE) based Master Glenium 51 super plasticizer from BASF confirming to IS 9103: 1999 was used in the present investigation. Table 3.4 presents the properties of superplasticizer given by the manufactures.

Table 3.4: Properties of super plasticizer

Property	Value
Colour	Light brown liquid
Relative density	1.08 ± 0.01 at 25ºC
pH	≥6
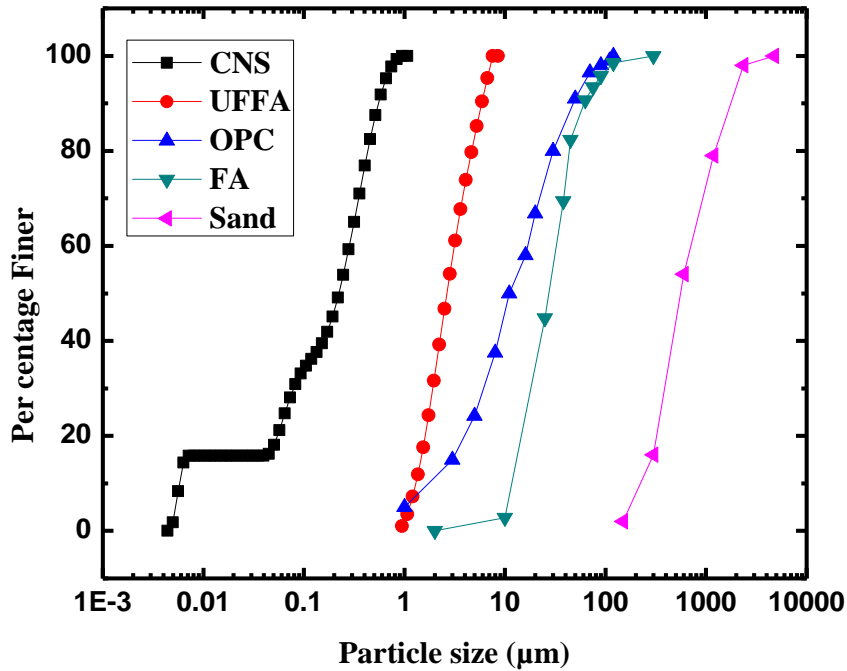
Figure 3.1: Particle-size distribution characteristics of the materials used in the study

3.3   MIX PROPORTIONS

3.3.1   Modified Andreasen and Andersen particle packing model

In this study modified Andreasen and Andersen particle packing model (Equation 2.5) was employed to design the mortar mixes of multiple blends (i.e. binary, ternary and quaternary blend). Twenty-six mortar mixes were prepared with different combination of OPC, FA, UFFA and CNS. The mix designations for different combinations of binary, ternary and quaternary mixes are presented in Table 3.5.

Table 3.5: Mix designations for binary, ternary and quaternary blended mixes

Blends	Different combination	General Designation	Percentage of replacement				
			OPC (%)	Total replacement (%)	FA (%)	UFFA (%)	CNS (%)
Control	OPC	C	100	0	-	-	-
Binary blend	OPC + CNS	CNS-0.5	99.5	0.5	-	-	0.5
		CNS-1	99	1	-	-	1
		CNS-1.5	98.5	1.5	-	-	1.5
		CNS-2	98	2	-	-	2
		CNS-2.5	97.5	2.5	-	-	2.5
		CNS-3	97	3	-	-	3
		CNS-3.5	96.5	3.5	-	-	3.5
	OPC+FA	F-15	85	15	15	-	-
		F-25	75	25	25	-	-
		F-35	65	35	35	-	-
	OPC+UFFA	U-15	85	15	-	15	-
		U-25	75	25	-	25	-
		U-35	65	35	-	35	-
Ternary blend	OPC+FA+UFFA	FU-15	85	15	10	5	-
		FU-25	75	25	15	10	-
		FU-35	65	35	20	15	-
	OPC+FA+CNS	FN-15	85	15	13	-	2
		FN-25	75	25	23	-	2
		FN-35	65	35	33	-	2
	OPC+UFFA+CNS	UN-15	85	15	-	13	2
		UN-25	75	25	-	23	2
		UN-35	65	35	-	34	1
Quaternary blend	OPC+FA+UFFA+CNS	FUN-15	85	15	9	4	2
		FUN-25	75	25	16	7	2
		FUN-35	65	35	20	14	1

The software "EMMA", which works on the principle of modified Andreasen and Andersen packing model was adopted to design the mortar mixes of multiple blends. The optimized proportion of each raw material in the mix were determined using "EMMA" software tool which works on the principle of modified Andreasen and Andersen particle packing model. Optimized particle packing curve for particular blended mortar mixtures with respect to ideal curve was obtained by continuously modifying the material proportions till the actual gradation curve of the particular mix reaches the optimal fit with that of ideal curve (Snehal and Das, 2022). A distribution coefficient (q) value of 0.30 suitable for medium workability was considered for all mortar mix proportions. The mixture proportions of multi blended mortar mixes and paste mixes (excluding sand content) designed using particle packing mix design tool "EMMA" are listed in the Table 3.6.

The blended mortar specimens were prepared with a fixed binder-sand ratio of 1:3 and water-binder (w/b) ratio of 0.5. Considering the quantity of water present in the CNS (60% liquid phase), addition of water content was adjusted accordingly for mixes comprising of CNS in order to maintain the constant w/b ratio.

Table 3.6: Mix recipe for various blended mixes used in present study

Mix designation	OPC (kg/m³)	FA (kg/m³)	UFFA (kg/m³)	CNS (kg/m³)	Sand (kg/m³)	Water (kg/m³)	W/C ratio	SP (% bwob)
CM/CP	568.35	-	-	-	1705.1	284.2	0.5	-
CNS-0.5M/P	565.51	-	-	2.84	1705.1	284.2	0.5	-
CNS-1M/P	562.67	-	-	5.68	1705.1	284.2	0.5	0.1
CNS-1.5M/P	559.82	-	-	8.53	1705.1	284.2	0.5	0.15
CNS-2M/P	556.98	-	-	11.37	1705.1	284.2	0.5	0.2
CNS-2.5M/P	554.14	-	-	14.21	1705.1	284.2	0.5	0.22
CNS-3M/P	551.30	-	-	17.05	1705.1	284.2	0.5	0.25
CNS-3.5M/P	548.46	-	-	19.89	1705.1	284.2	0.5	0.27
F-15M/P	483.1	85.25	-	-	1705.1	284.2	0.5	-
F-25M/P	426.35	142.09	-	-	1705.1	284.2	0.5	-
F-35M/P	369.4	198.92	-	-	1705.1	284.2	0.5	-
U-15M/P	483.1	-	85.25	-	1705.1	284.2	0.5	-
U-25M/P	426.35	-	142.09	-	1705.1	284.2	0.5	-
U-35M/P	369.4	-	198.92	-	1705.1	284.2	0.5	-
FN-15M/P	483.1	73.89	-	11.4	1705.1	284.2	0.5	-
FN-25M/P	426.35	130.72	-	11.4	1705.1	284.2	0.5	-
FN-35M/P	369.4	187.56	-	11.4	1705.1	284.2	0.5	-
UN-15M/P	483.1	-	73.89	11.4	1705.1	284.2	0.5	-
UN-25M/P	426.35	-	130.7	11.4	1705.1	284.2	0.5	-
UN-35M/P	369.4	-	193.2	5.7	1705.1	284.2	0.5	-
FUN-15M/P	483.1	51.15	22.7	11.4	1705.1	284.2	0.5	-
FUN-25M/P	426.35	90.94	39.8	11.4	1705.1	284.2	0.5	-
FUN-35M/P	369.4	113.67	79.6	5.7	1705.1	284.2	0.5	-

*bwob: by weight of binder materials * M stands for mortar mix * P stands for paste mix (excludes sand content)

3.3.2 Design of PCM admixed cementitious composite mixes

To study the performance of PCM admixed cementitious composites, total fourteen mixes were prepared, out of which one was control mix and considered as a reference mix. These fourteen mixes were prepared in two phases: at first stage, the desired PCM content was found in correspondence to designated compressive strength of 35 MPa. Nine mortar mixes were added with different PCMs such as paraffin (PF), n-octadecane (oct) and sodium carbonate hydrate (SC) at the rate of 1%, 3% and 5% by weight of binder. At second stage, mix proportion was carried out to check the performance of blended mortar integrated with optimized nano-silica and the desired PCM content. Three cementitious mortar mixes were designed by integrating the optimized nano-silica (3% by weight of binder) in conjunction with the desired PCM content (i.e. 1%, 3% and 5%, n-octadecane PCM). All the mortar mixes were prepared with constant binder-sand ratio of 1:3 and water-binder ratio of 0.5. The mix designation and proportions adopted in first and second stage of the study on PCM admixed cementitious composites are listed in the Table 3.7 and Table 3.8, respectively.

Table 3.7: Mix proportions for PCM added cementitious composites

Mixes	Mix Designation	OPC (%)	PCM (%)	Cement (kg/m³)	PCM (kg/m³)	Sand (Kg/m³)	Water (kg/m³)
Control	CM	100	-	568.35	0	1705.1	284.2
OPC + n-octadecane-1%	oct-1M	100	1	568.35	5.68	1705.1	284.2
OPC + n-octadecane-3%	oct-3 M	100	3	568.35	17.05	1705.1	284.2
OPC + n-octadecane-5%	oct-5 M	100	5	568.35	28.42	1705.1	284.2
OPC + sodium carbonate -1%	SC-1 M	100	1	568.35	5.68	1705.1	284.2
OPC + sodium carbonate 3%	SC-3 M	100	3	568.35	17.05	1705.1	284.2
OPC + sodium carbonate -5%	SC-5 M	100	5	568.35	28.42	1705.1	284.2
OPC + paraffin-1%	PF-1 M	100	1	568.35	5.68	1705.1	284.2
OPC + paraffin -3%	PF-3 M	100	3	568.35	17.05	1705.1	284.2
OPC + paraffin -5%	PF-5 M	100	5	568.35	28.42	1705.1	284.2

Table 3.8: Mix proportions for best performing PCM admixed cementitious composites integrated with optimized nano-silica

Mixes	Mix Designation	OPC (%)	CNS (%)	PCM (%)	Cement (kg/m³)	CNS (kg/m³)	PCM (kg/m³)	Sand (Kg/m³)	Water (kg/m³)
Control	CM/CP	100	-	-	568.35	0	0	1705.1	284.2
OPC + nano-silica -3%	CNS-3M/P	97	3	-	551.30	17.05	0	1705.1	284.2
OPC + n-octadecane-1%	oct-1 M/P	100	-	1	568.35	0	5.68	1705.1	284.2
OPC + n-octadecane-3%	oct-3 M/P	100	-	3	568.35	0	17.05	1705.1	284.2
OPC + n-octadecane-5%	oct-5 M/P	100	-	5	568.35	0	28.42	1705.1	284.2
OPC + 3% nano-silica + n-octadecane-1%	CNS/oct-1 M/P	97	3	1	551.30	17.05	5.68	1705.1	284.2
OPC + 3% nano-silica + n-octadecane-3%	CNS/oct-3 M/P	97	3	3	551.30	17.05	17.05	1705.1	284.2
OPC + 3% nano-silica + n-octadecane-5%	CNS/oct-5 M/P	97	3	5	551.30	17.05	28.42	1705.1	284.2
* M stands for mortar mix * P stands for paste mix (excludes sand content)									

3.4 SAMPLE PREPERATION AND TEST METHODS

3.4.1 Preparation of cementitious mortar specimens

The mixing of cementitious mortar composites were performed by means of an automatic mortar mixer designed in accordance with EN 196-1. Mixes of blended mortars were cast in cubical specimens of size 70.6 mm × 70.6 mm × 70.6 mm for compressive strength test, cylindrical mortar specimens of size 100 mm diameter and 50 mm height for rapid chloride ion penetration test and mortar prisms of size 25 mm × 25 mm × 285 mm for measurement of length change. Additional cubical specimens of size 70.6 mm × 70.6 mm × 70.6 mm were also cast to measure the permeable porosity of the mixes. Further, the compacted cube and cylindrical specimens were stored in a humid condition (27 ± 2 ºC temperature and 95% relative humidity) and were de-molded after 24 hours of storage. Subsequently, these samples were stored in a curing tank (water submerged condition) until the day of testing.

3.4.2 Preparation of cementitious paste specimens

Mixing of cementitious paste composites were performed by means of an automatic mixer designed in accordance with EN 196-3. Setting time, surface temperature variation during the period of setting, workability (flow diameter and flow value) and chemical shrinkage of all the mixes were measured. To be used in microstructural characterization, blended cement paste samples of each mixes were cast in cylindrical silicon mould (30 mm diameter and 20 mm height) for 24 hours at 27 ± 2 °C and then placed in a saturated water condition for certain curing ages. After the accomplishment of appropriate curing ages samples were subjected to solvent exchange technique using isopropanol for 24 hours in order to stop the hydration process (Zhang and Schere, 2011, Das et al., 2007). Then, samples were oven dried at 40-60 °C up to the attainment of constant weight and were preserved in a desiccator containing pellets of silica gel (to avoid any moisture contact) till the day of testing.

3.4.3 Testing methods adopted for cementitious composites

Table 3.9 and 3.10 presents the test methods adopted for cementitious mortar and paste composites, respectively.

Table 3.9: Test methods for cementitious mortar composites

Tests	As per	Remarks
Compressive Strength	IS 4031-Part 6:1988	Using compressive testing machine; - Measured at 3, 7, 28 and 56 days (blended cementitious composites) - Measured at 3, 7 and 28 days (PCM admixed cementitious composites)
Density	-	Using weighing balance; - Measured at 3, 7, 28 and 56 days (blended cementitious composites) - Measured at 3, 7 and 28 days (PCM admixed cementitious composites)
Drying shrinkage	ASTM C157 / C157M	Using length comparator; - Measured at 1, 3, 7, 14, 30, 60, 90, 120 and 180 days (blended cementitious composites and PCM admixed cementitious composites)
Pozzolanic activity test: Strength activity index (SAI)	ASTM C 311	Using compressive testing machine; - Measured at 7 and 28 days (blended cementitious composites)
Permeable porosity	Safiuddin and Hearn 2005; Das et al, 2010	Using Vacuum desiccator; - Measured at 3, 7, 28 and 56 days (blended cementitious composites) - Measured at 3, 7 and 28 days (PCM admixed cementitious composites)
Rapid chloride-ion penetration test (RCPT)	ASTM C 1202	Using RCPT equipment; - Measured at 7, 28 and 56 days (blended cementitious composites) - Measured at 7 and 28 days (PCM admixed cementitious composites)
Acid, alkali and chloride resistance	Strength loss/ Density loss : Sahoo et al, 2017 Length change : ASTM C157 / C157M	• Strength loss: Using compressive testing machine; • Density loss: Using weighing balance; - Measured at 30, 60, 90, 120 and 180 days (blended cementitious composites and PCM admixed cementitious composites) • Length change: Using length comparator; - Measured at 1, 3, 7, 14, 30, 60, 90, 120 and 180 days (blended cementitious composites and PCM admixed cementitious composites)

Table 3.10: Test methods for cementitious paste composites

Tests	As per	Remarks
Setting time	IS 4031-Part 5:1988	Using Vicat apparatus
Surface temperature	-	Using infrared thermometer (measured until 300min)
Workability	EN 1015-3; Sneff et al 2009	Mini flow table (15 strokes)
Chemical shrinkage	ASTM C 1608	Using dialometry method; • Measured at 1, 3, 7, 28 and 56 days (blended cementitious composites) • Measured at 1, 3, 7 and 28 days (PCM admixed cementitious composites)
Pozzolanic reaction test: Selective dissolution method (SDM)	Li et al, 1985	Using picric acid-methanol-water solution; • Measured at 7 and 28 days (blended cementitious composites)
Thermo gravimetric analysis (TGA)	-	Using TG/DTA analyser (EXSTAR 6000 TG/DTA 6300); • Measured at 7 and 28 days (blended cementitious composites) • Measured at 28 days (PCM admixed cementitious composites)
Differential scanning calorimetry (DSC)	-	Using Differential scanning calorimetry; - Measured at 28 days (PCM admixed cementitious composites)
X-Ray diffraction (XRD)	-	• Using Jeol-JPX 8P, XRD analyser; • Measured at 7 and 28 days (blended cementitious composites) • Measured at 28 days (PCM admixed cementitious composites)
Scanning electron microscopy-Energy dispersive X-Ray spectroscopy (SEM-EDX)	-	Using scanning electron microscope from Jeol (JSM-638OLA) associated by an EDS analyser; • Measured at 7 and 28 days (blended cementitious composites) • Measured at 28 days (PCM admixed cementitious composites)

3.4.3.1 Compressive strength

The compressive strength of blended mixes (at curing ages of 3, 7, 28 and 56 days) and PCM admixed mixes (at curing ages of 3, 7 and 28 days) were determined in accordance with IS 4031-Part 6:1988 at a loading rate of 35 N/mm^2/min. Three specimens of each mix for all the curing ages were considered and the average was noted as the compressive strength value of the corresponding mix.

3.4.3.2 Density

At the curing ages of 3, 7, 28 and 56 days for blended mortar mixes and 3, 7 and 28 days for PCM admixed mortar mixes, specimens were taken out from the curing tank, wiped in a cloth and kept in air for half an hour. Just before compressive strength testing, the samples were weighed and the ratio of sample weight to the total volume of sample was reported as the density (g/cc or kg/m^3) of the cementitious mortar specimens. Average of three specimens for each curing ages were taken and the same is considered as the density of the respective mix.

3.4.3.3 Drying shrinkage

Drying shrinkage of mortar specimens (25 mm × 25 mm × 285 mm) were measured in terms of length change using length comparator (ASTM C490 / C490M) in accordance with ASTM C157 / C157M. First, all the mortar specimens water cured for the duration of 28 days were checked for initial compactor reading at surface dry condition. Then, mortar specimens were exposed to the ambient drying condition (temperature: 27 ± 3 °C and relative humidity: 50 ± 5%) and then measured for the length comparator reading at the exposure period of 1, 3, 7, 14, 30, 60, 90, 120 and 180 days. Shrinkage strains of all the mortar specimens at various period of exposure were calculated using the Equation 3.1 (ASTM C 596):

$$\Delta L_x = \frac{L_x - L_o}{G} \times 10^4 \qquad\qquad (3.1)$$

where, ΔL, L_x and L_o represents the change in length at age "x" (micro strain), comparator reading at specified exposure age "x" and initial comparator reading, respectively. Further, G designates the gauge length value (250 mm).

3.4.3.4 Pozzolanic reactivity test: strength activity index (SAI)

The pozzolanic reactivity was also determined by means of strength activity index (SAI) in accordance with ASTM C 311 and as specified by ASTM C 618 standard. Cubical mortar samples (70.6 mm size) cured for 7 and 28 days were tested for compressive strength as specified in IS 4031-Part 6:1988 to determine the value of SAI. Three specimens were considered for each type and age of mixes and average strength was reported as compressive strength of corresponding mix. SAI of blended mortar mix is determined by calculating the percentage strength in relation to control mortar of respective curing age and the equation for SAI is given as,

$$SAI\ (\%) = \left[\frac{\sigma_i}{\sigma_c}\right] x100 \tag{3.2}$$

where, σ_i : refers to the compressive strength of blended cementitious mortar and σ_c : refers to the compressive strength of control mortar.

3.4.3.5 Permeable Porosity

The permeable porosity was determined by vacuum water absorption technique (Safiuddin and Hearn, 2005; Das et al., 2010). At the end of each curing period, the samples were initially oven dried for 24 hours at 105-110 °C and then weighed for dry weight of the sample after cooling to the room temperature in a desiccator. Further, dry samples were water saturated in vacuum desiccators (ASTM C 1202) for 24 hours. The saturated weight of sample after sponging the surface dampness was noted down. The permeable porosity was determined by considering the ratio of volume of voids (i.e. difference between dry and saturated weight) to total mortar volume. Permeable porosity was measured at the curing ages of 3, 7, 28 and 56 days for blended cementitious composites and at the curing ages of 3, 7 and 28 days for PCM admixed cementitious composites. Three specimens of

each mix for all the curing ages were considered and the average was recorded as the permeable porosity value of the corresponding mix.

3.4.3.6 Rapid chloride-ion penetration test (RCPT)

Rapid chloride-ion penetration test (RCPT) is a method used to figure out the durability of cementitious composites and the test was carried out for three identical cylinders as per ASTM C 1202. This test method monitors the amount of charges passing through the cylindrical specimens (100 mm dia and 50 mm thick) for a period of 6 hours.

In this study, RCPT test was conducted at the curing ages of 7, 28 and 56 days for all the blended mixes and 7 and 28 days for all PCM admixed cementitious mixes. Three specimens of each mix for all the curing ages were tested and the average value was taken into account.

3.4.3.7 Acid, alkali and chloride attack

Acid, alkali and chloride resistance test for control and best performing blended cementitious mortar mixes (CNS-3M, F-25M, U-25M, FU-25M, FN-25M, UN-25M, FUN-25M) and PCM admixed cementitious composite mortar (oct-1M, oct-3M, oct-5M, CNS/oct-1M, CNS/oct-3M and CNS/oct-5M) was performed by assessing density loss, strength loss and change in length, as durability performance indicators. Cubical mortar specimens (70.6 mm × 70.6 mm × 70.6 mm) water cured for 28 days were considered to measure the density and strength losses. Further, length change measurements was done for mortar prisms of the dimension 25 mm × 25 mm × 285 mm using length comparator devise (ASTM C490 / C490M).

After 28 days of water saturated curing, specimens were allowed to attain saturated dry condition. Subsequently, initial density, compressive strength and comparator reading of mortar specimens before chemical exposure were recorded using weighing balance, compressive strength testing machine (2000 kN capacity at loading rate of 35 N/mm^2/min) and length comparator device, respectively. Next, all the specimens (cubical and prism) were subjected for chemical exposure by immersing in 1% sulphuric acid solution (acid

environment, pH 0.3), 5% sodium sulphate solution (alkali environment, pH 12.0) and 5% sodium chloride solution (chloride environment, pH 7.0). Specimens were made to store in independent containers for a duration of 30, 60, 90 and 180 days to measure the density/strength losses and for the duration of 1, 3, 7, 14, 30, 60, 90 and 180 days to measure the change in length. The pH of each chemical solutions were periodically checked and maintained throughout the days of exposure.

After attaining a certain period of exposures specimens were removed out from chemical solution and allowed to achieve surface dry condition. Subsequently, density, compressive strength and length comparator reading of the exposed specimens were measured. Then, density loss and strength loss of particular mix, type and period of chemical exposure was calculated considering the initial density and compressive strength of 28 days water cured specimen using the Equations 3.3 and 3.4.

$$\rho_{loss}(\%) = \frac{\rho_i - \rho_F}{\rho_i} \times 100 \tag{3.3}$$

$$\sigma_{loss}(\%) = \frac{\sigma_i - \sigma_F}{\sigma_i} \times 100 \tag{3.4}$$

Where, ρ_i and σ_i represents the initial density and compressive strength of a mortar specimen at the curing age of 28 days; ρ_F and σ_F represents the density and compressive strength of a mortar specimen at specific type and duration of chemical exposure.

Further, length change for acidic and chloride conditions were measure in accordance with ASTM C157 / C157M and for sulfate condition measurement was done in compliance to ASTM C1012/1012M. Length change (shrinkage/expansion) in terms of micro strain for blended mortars were measured using the Equation 3.1. Average of three specimens for each mix, type and period of exposure were recorded as density loss, compressive strength loss and length change strain of particular mix at specified type and period of exposure.

3.4.3.8 Setting time and surface temperature

Initial setting time and final setting time test for all the cementitious composite paste mixes were conducted in accordance with IS 4031-Part 5: 1988.

The surface temperature of the mixes was measured for the duration of setting time at the interval of 10 minutes with the aid of infrared thermometer. Measurement of surface temperature was initiated from the mixing stage of composite paste mixes till 300 minutes of setting to understand the variation of surface temperature during the early age hydration phase of cementitious pastes.

3.4.3.9 Workability

The mini flow table test was carried out to measure the slump flow of cementitious composite paste in accordance with EN 1015-3 with 15 strokes (Sneff et al 2009). The average flow diameter of four perpendicular directions was measured and flow value was determined as a percentage of the actual base diameter of the mini slump cone.

3.4.3.10 Chemical shrinkage

Chemical shrinkage was determined by means of dilatometry method as specified in ASTM C 1608 standards. The drop in water level in a hydrating cement paste was considered as chemical shrinkage i.e. ml/100 gm. Chemical shrinkage of each sample was periodically recorded after 1, 3, 7, 14, 28 and 56 days. Photo of the test setup used for the dilatometer method of testing chemical shrinkage is presented in Figure 3.2.

Figure 3.2: Test setup used for the dilatometer method of testing chemical shrinkage

3.4.3.11 Pozzolanic reactivity test: selective dissolution method (SDM)

Pozzolanic reaction degree of blended cementitious composites was determined by means of selective dissolution method using picric acid-methanol-water solution. Similar procedure of picric acid-methanol-water solution technique as described by Li et al., (1985) in quantifying the pozzolanic reaction degree was adopted. However, for multi blended mix pozzolanic reaction degree was modified and given as:

$$pozzolanic\ reaction\ degree(\%) = [1 - \frac{S_s - \rho_c S_c}{\sum \rho_i S_i}]\ x\ 100 \tag{3.5}$$

$$\sum \rho_i S_i = \rho_F S_F + \rho_U S_U + \rho_N S_N \tag{3.6}$$

where, S_S is the residue per gram of blended sample, S_c, S_i, S_F, S_U and S_N are the residue per gram of ignited pure component of cement, pozzolanic particles, fly ash, ultrafine fly

ash and nano-silica, respectively. ρ_c, ρ_i, ρ_F, ρ_U and ρ_N are the percentage weight component of cement, pozzolanic particles, fly ash, ultrafine fly ash and nano-silica, respectively.

3.4.3.12 Thermo gravimetric analysis (TGA)

Thermogravimetric analysis was carried out by employing a TG/DTA analyser from Seiko (EXSTAR 6000 TG/DTA 6300). Hardened cementitious paste composite samples were grinded to powder, passed through 75 mm sieve and were characterized at temperature range of 50-900 ˚C in nitrogen purge atmosphere. Heating rate and purge rate was 10 ˚C/min and 20 ml/min, respectively.

From TG results, calcium hydroxide (CH) content for all blended cementitious composite mixes were determined at 7 and 28 days of curing and for all PCM admixed cementitious composite mixes it was calculated at the curing age of 28 days . Decomposition of CH was considered as weight loss between the temperature range of 400-500 ˚C (Jain and Neithalath 2009). Temperature boundaries were identified from derivative thermogravimetric curve (DTG) (Singh et al., 2012a; Singh et al., 2012b). On the basis of CH decomposition (Equation 3.4), the percentage of CH content was quantified using the Equation 3.5 (Singh et al., 2012a; Singh et al., 2012b).

$$Ca(OH)_2 \rightarrow CaO + H_2O \tag{3.7}$$

$$CH\% = (\%W_{CH}) \cdot \left(\frac{M_{CH}}{M_{H_2O}}\right) = \left(\%W_{CH} \times \frac{74}{18}\right) \tag{3.8}$$

Where, W_{CH} is the mass loss percentage at specified temperature of 400ºC and 500ºC respectively (CH decomposition temperature range), M_{CH} and M_{H_2O} represents the molecular weight of CH and H_2O i.e. 74 and 18, respectively.

Further, from the total weight loss percentage for temperature range of 35–600 ˚C, amount of water associated to CH content was subtracted and the resulted value is expressed as WH, i.e. the amount of water associated to hydration products excluding CH content (Soriano et al., 2013) and given by the Equation 3.6.

$$WH\% = W_T - W_{CH} \tag{3.9}$$

TG-DTG analysis was also carried out for cementitious mixes exposed to acid, alkali and chloride solutions. On the basis of obtained TGA results, compounds formed due to acid and alkali attack i.e. ($Ca_6Al_2(SO_4)_3(OH)_{12}.26H_2O$, Aft) and gypsum ($CaSO_4.2H_2O$, Gy) were quantified using the Equation 3.7 and 3.8 considering the mass loss at particular temperature boundaries of 50-120 °C and 120-150 °C, respectively. Further, Friedel's salt (Fs) formed during chloride exposure was quantified using the Equation 3.9 for the mass loss at the specified temperature range of 230-380 °C.

$$AFt\ (\%) = W_{AFt} \cdot \frac{M_{AFt}}{26M_H} \tag{3.10}$$

$$Gy\ (\%) = W_{Gy} \cdot \frac{M_{Gy}}{2M_H} \tag{3.11}$$

$$Fs\ (\%) = \frac{M_{Fs}}{6 \times M_H} \times W_{Fs} \tag{3.12}$$

Where, W_{AFt}, W_{Gy} and W_{Gy} describes the percentage mass loss linking to AFt, Gy and 6 molecular layer of water from Fs at the temperature ranges of 50-120 °C, 120-150°C and 230- 380 °C, respectively. M_{AFt}, M_{Gy}, M_{Fs} and M_H represents the molecular weight of AFt, Gy, Fs and H_2O i.e., 786.7 g/mol, 172.17 g/mol, 561.3 g/mol and 18.02 g/mol, respectively.

3.4.3.13 Differential scanning calorimetry (DSC)

Heat capacity of the PCM admixed cementitious composites were analysed by means of differential scanning calorimetry. Heating range of 5 ˚C to 50 ˚C in nitrogen purge environment with a purge rate of 10 ml/min and heating/cooling rate of 2 K min^{-1} was used.

3.4.3.14 X-ray diffraction (XRD)

The hardened cementitious paste composite samples at curing ages of 7 and 28 days (blended composites) and 28 days (PCM admixed composites) were grinded, passed through 75 mm IS sieve and was analyzed for mineralogical composition. XRD patterns of powdered samples were obtained by employing Jeol-JPX8P with Cu Kα radiation (40

kV/40 mA) at deflection angle ranging from 10˚ to 80˚ and at a scanning speed of 2˚/min. The obtained XRD patterns were then analyzed using X'Pert High Score Plus software

3.4.3.15 Scanning electron microscopy – energy dispersive x-ray spectroscopy (SEM-EDS)

From the stored samples as explained in Section 3.4.2, chunks from the core of the paste samples were collected and then gold sputtered for microstructural analysis with aid of scanning electron microscope (SEM). Images were obtained through scanning electron microscope (Jeol, JSM-638OLA) in secondary electron mode and elemental analysis was conducted through an EDS analyser to know the change in elemental composition within the boundary of image.

CHAPTER – 4

ENGINEERING AND MICROSTRUCTURE PROPERTIES OF NANO-SILICA BLENDED CEMENTITIOUS COMPOSITES

4.1 GENERAL

This Chapter deals with the results of the experimental investigation carried out to study the influence of binary, ternary and quaternary blended cementitious composites, which includes 10^{-6} to 10^{-9} m matrix sized SCMs i.e. fly ash (FA), ultrafine fly ash (UFFA) and nano-silica on early age, hydration, mechanical durability and microstructure properties of cementitious paste and mortar. Advanced characterization methods such as thermogravimetric analysis (TGA), x-ray diffraction studies (XRD) and scanning electron microscopy with energy dispersive x-ray spectroscopy (SEM-EDX) were employed. The optimised proportions of the blended cementitious composites are designed through modified Andreasen and Andersen particle packing model.

4.2 MODIFIED ANDREASEN AND ANDERSEN PARTICLE PACKING MODEL

The optimized particle packing curves for multi blended mortar mixes are presented in the Figures 4.1 - 4.3. The particle size distribution of binary, ternary and quaternary blended mixes were made to relate with the modified Andreasen and Andersen model curve i.e. ideal curve for the arrival of better packing density. It can be observed from the figures that actual gradation curve of all mixes found to be fit with ideal gradation curve with a q value of 0.3. This is to be noted that for attaining optimum particle packing it is essential to have q-value of less than 0.36 (EMMA user manual). The closest matching between gradation curve of recipe and ideal curve was obtained through altering material quantity inputs by trial and error. In this investigation, sand content was kept fixed for all blended mortar mixes.

The gradation curves were statistically fit and it was found that the exponential relation gives the best correlation. The obtained coefficient of determination for the blended mixes are presented in Table 4.1.

Table 4.1: Coefficient of determination of the fitted curves for the blended mixes

Blends	Specimen	Coefficient of determination "R^2"value
Binary Blends	CNS 0.5M	0.9465
	CNS 1M	0.9466
	CNS 1.5M	0.9468
	CNS 2M	0.9468
	CNS 2.5M	0.9469
	CNS 3M	0.9471
	CNS 3.5M	0.9470
	F-15M	0.9291
	F-25M	0.9293
	F-35M	0.9294
	U-15M	0.9295
	U-25M	0.9298
	U-35M	0.9301
Ternary Blends	FU-15M	0.9461
	FU-25M	0.9424
	FU-35M	0.9433
	FN-15M	0.9552
	FN-25M	0.9565
	FN-35M	0.9574
	UN-15M	0.9576
	UN-25 M	0.9595
	UN-35M	0.9618
Quaternary Blends	FUN-15M	0.9601
	FUN-25M	0.9712
	FUN-35M	0.9642

It can be seen from the Table 4.1 and Figures 4.1 to 4.3 that with the incorporation of blended admixtures possessing different particle size improvement in particle packing curves were noted. It can be noted that compared to the particle packing curve of binary blended mixes (Figure 4.1a - 4.1c), ternary blended mixes (Figure 4.2a - 4.2c) showed the better fit. However, quaternary blend intermixing of three varied sized admixture (micro to nano) i.e. FA, UFFA and CNS (Figure 4.3) represented the best fit amongst all the mixes (Table 4.1).
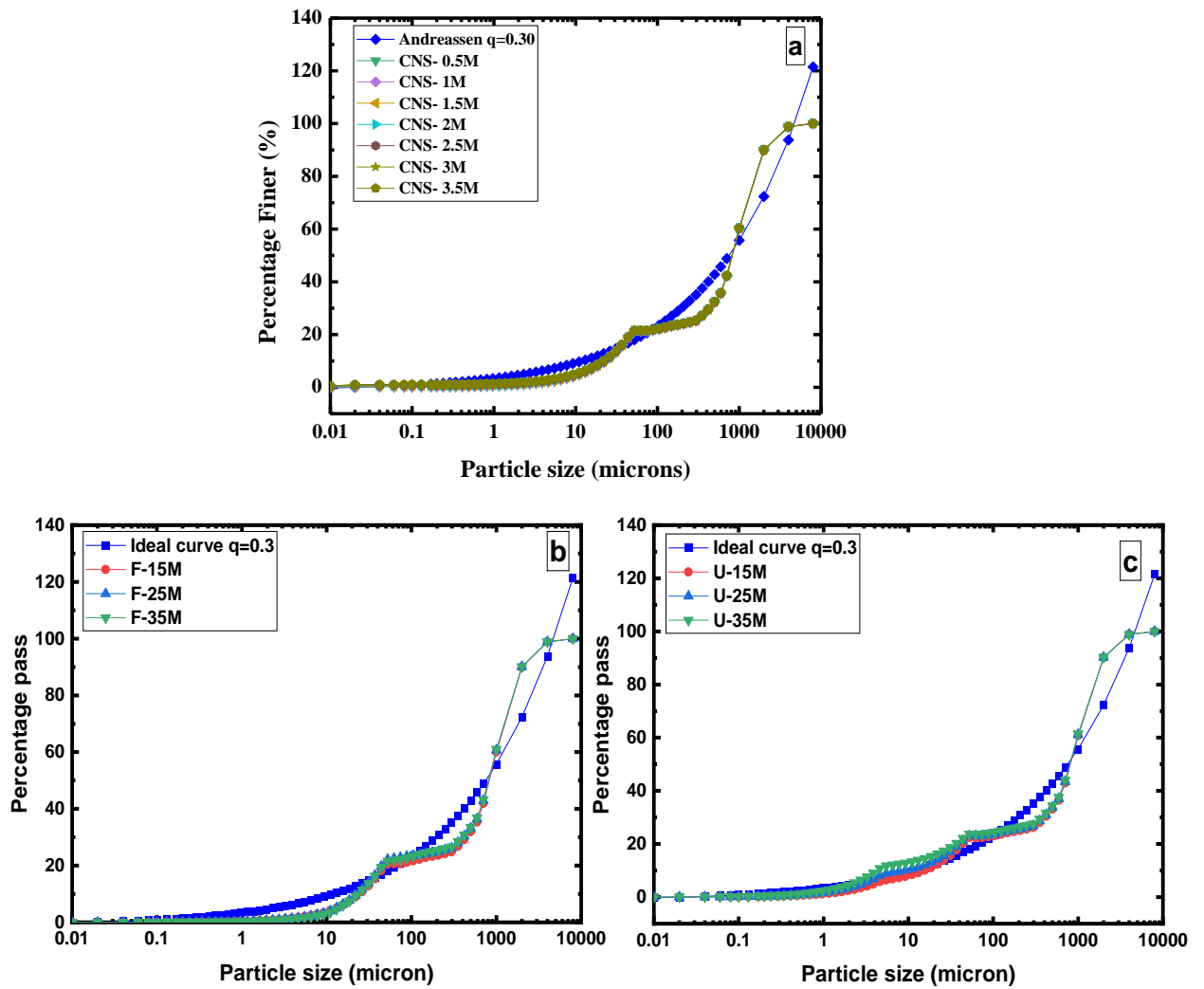
Figure 4.1: Optimized particle packing curve for binary blended mortar mixes using modified Andreasen and Andersen packing model a) CNS mortar mixes b) F mortar mixes and c) U mortar mixes
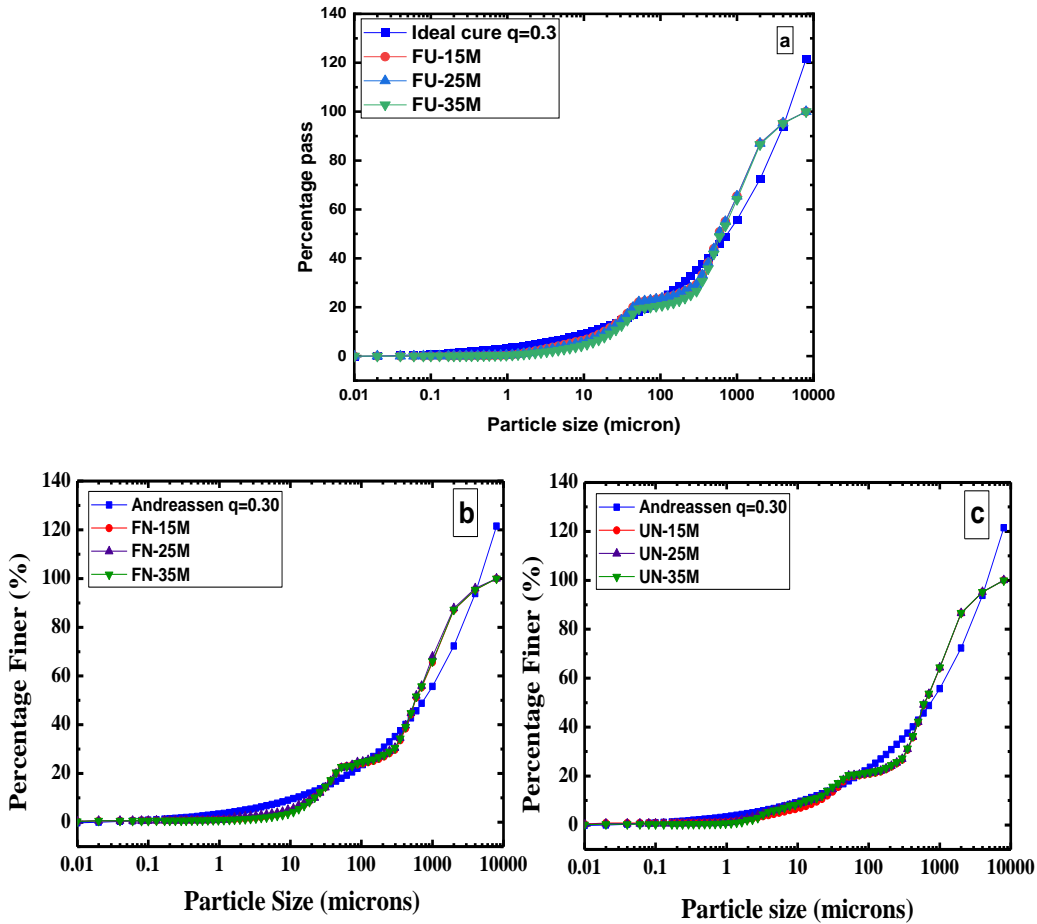
Figure 4.2: Optimized particle packing curve for ternary mixes using modified Andreasen and Andersen packing model a) FU mortar mixes b) FN mortar mixes c) UN mortar mixes
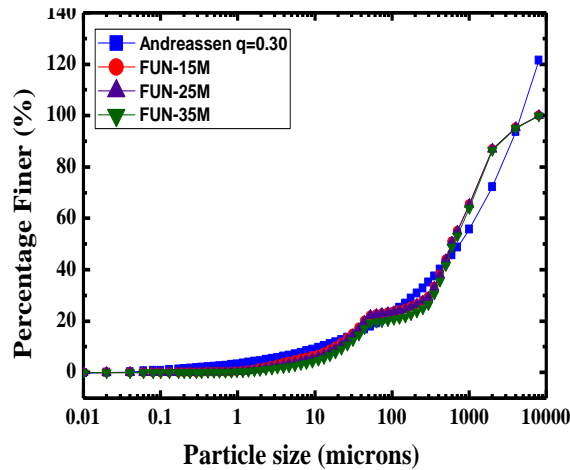
Figure 4.3: Optimized particle packing curve for quaternary blended FUN mixes using modified Andreasen and Andersen packing model

4.3 BLENDED CEMENTITIOUS MORTAR

4.3.1 Compressive strength

Compressive strength results of binary blended mortar mixes admixed with the combination of OPC and CNS or FA or UFFA at the curing ages of 3, 7, 28 and 56 days are plotted as histogram and presented in Figures 4.4a – 4.4c.
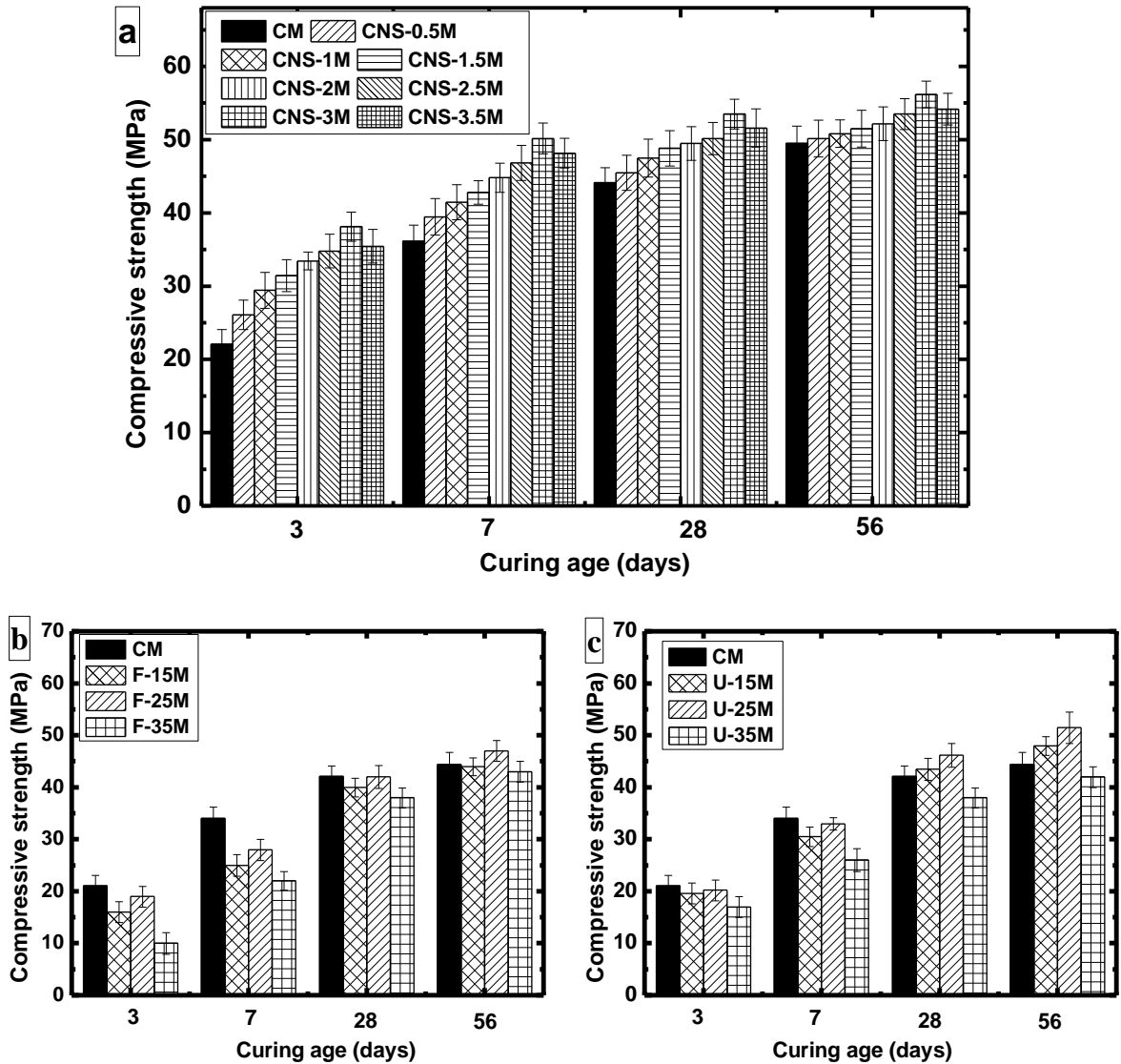
Figure 4.4: Compressive strength of binary blended cement mortar mixes a) CNS mixes b) F mixes c) U mixes

It can be observed from the Figure 4.4a that among all CNS binary blended mortar mixes CNS-3M mortar mix exhibited the highest compressive strength with respect to control mortar. The percentage of strength gain for CNS-3M mix was observed to be 73%, 39%, 21% and 14% at the curing age of 3, 7, 28 and 56 days, respectively in comparison with control mortar (CM). It can be understood from the graphical representation that influence of CNS on the development in compressive strength is more effective at the age of 3 days compared to 7, 28 and 56 days of curing age. This can be attributed to the implication of early age hydration process. Rapid improvement in early age strength could be due to the reason that, presence of nano sized silica particles may promote the early hydration reaction of cement particles acting as a nucleation site for C-S-H gel formation (Yu et al., 2014). In addition to that superior pozzolanic reactivity of nano-silica amplified the C-S-H gel formation by consuming $Ca(OH)_2$ crystals thereby promoting the improvement in compressive strength (Qing et al., 2007; Singh et al., 2012b; Hou et al., 2013; Yu et al., 2014).

On the other hand, beyond 3% replacement of CNS, it was observed that there is a noticeable drop in compressive strength at all the curing ages. The possible reason for the drop in compressive strength after certain level of CNS replacement may be due to the presence of excessive nano-silica, which suppressed the hydration process by engrossing the water necessary for hydration of cement particles in production of C-S-H gel (Hou et al., 2013). Further, the presence of excess nano-silica content may lead to silica leaching (Wang et al., 2016b) and also agglomerated particles generated a weak porous zone that hampered the compressive strength development (Quercia et al., 2012). The resulted increase in permeable porosity for 3.5% dosage of nano-silica mix can be seen in the Section 4.3.5.1. In addition, TGA results also reflected that as compared 3% CNS mix increase in CH% and decrease in WH% was decreased for 3.5% CNS mix (refer to Table 4.2).

It can be observed from the Figures 4.4 (b-c) that binary blended mortar mixes composed of FA and UFFA showed lower initial strength especially at the ages of 3 and 7 days. This

is mainly attributed to the initial filler effect of Pozzolans rather than involving in reactivity (Copeland et al., 2001; Sobolev, 2009; Das et al., 2012). It is important to note that for binary blended U mixes improvement in strength was noticed at 28 days of curing age and that found to be increased by 8% and 15% to that of control for U-15M and U-25M mixes, respectively at the age of 56 days. U-25 mix performed better in terms of compressive strength among binary blended U mixes. This improved strength in U mixes is mainly ascribed to the smaller particle size of UFFA (5-10 microns), which initiated early reactivity as compared to that of FA (50-60 microns) particles. However, F mixes found to be performed better at the age of 56 days and F-25 mix showed 2% increase in compressive strength with respect to control mix.

Figure 4.5 (a-c) represents the compressive strength plot for ternary blended cement mortar at the curing ages of 3, 7, 28, 56 days.
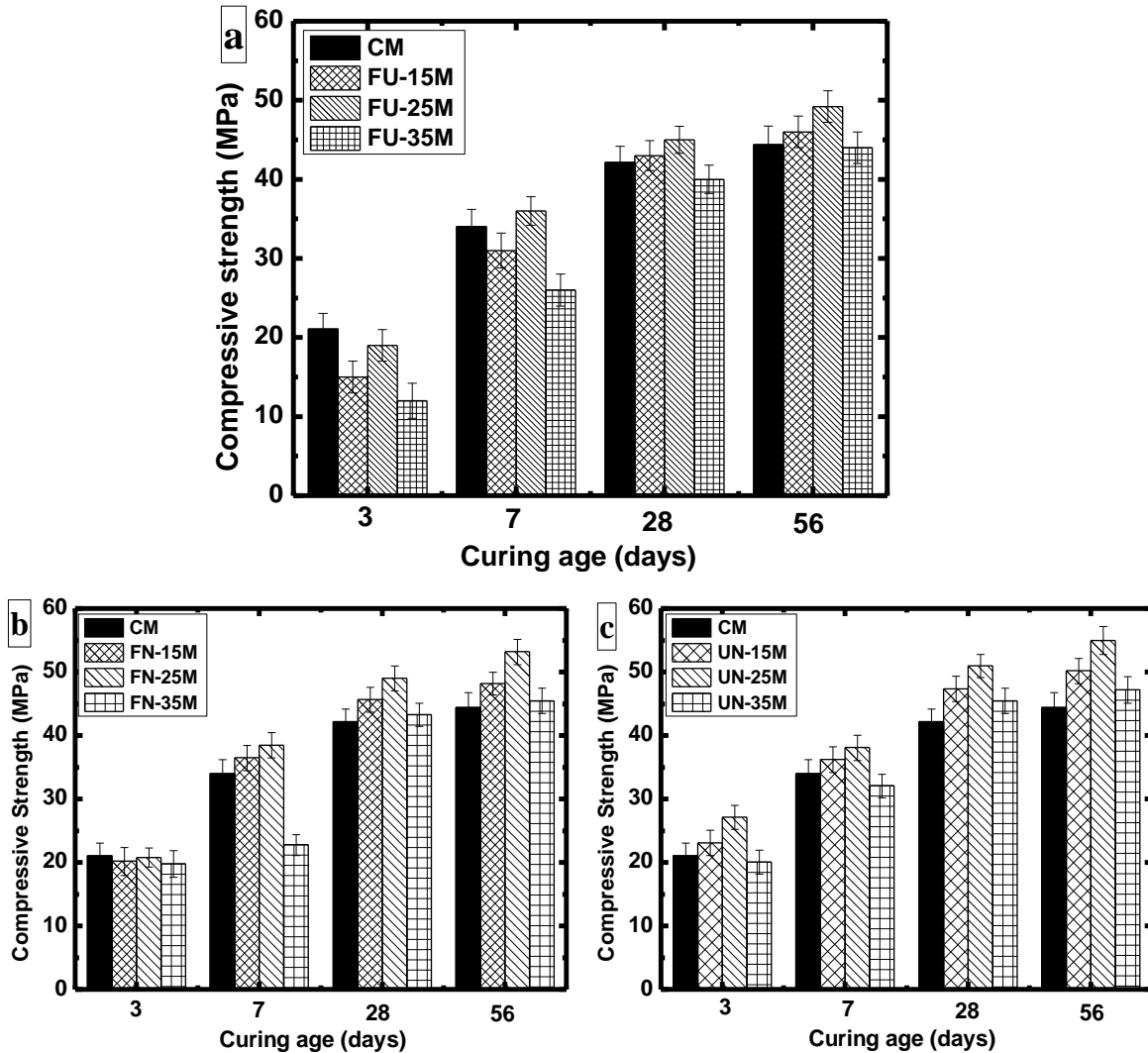
Figure 4.5: Compressive strength of ternary blended cement mortar mixes a) FU mixes b) FN mixes c) UN mixes

It can be observed from the Figure 4.5a that ternary blended FU mortar mixes exhibited lower early strength gain at the curing ages of 3 and 7 days as compared to that of control mortar (similar to binary blended F and U mixes). This delay in development of early strength may be attributed to the reason that FA and UFFA initially performed as a filler material rather than involving in pozzolanic reaction (Copeland et al., 2001; Sobolev, 2009; Das et al., 2012). Highest improvement in strength among FU mixes was noticed for FU-25M mix after 28 days of curing. This may be attributed to the better packing density/

filling effect of FA and UFFA combination. In addition to that smaller particle size of UFFA may possibly promoted the pozzolanic reactivity earlier than FA (Copeland et al., 2001). However, strength gain for FU-35M mixes was seen to be lower to that of control mix even after the curing age of 28 days, this may be due to the dilution effect that slowdowns the rate of hydration reaction (Narmuluk et al., 2011 2012; Hannesson et al., 2012).

It can be noted from the figure (Figure 4.5b – 4.5c) that presence of CNS particles in ternary blended mixes (FN and UN) improved the early as well as later age compressive strength. This might be attributed to the optimum particle packing of mortar mix along with the influence of CNS in terms of hydraulic and pozzolanic reaction. Nevertheless, UN mortar mixes displayed slightly higher compressive strength than control mortar even in 3 days of curing age. However, the strength gain in UN mortar mixes was observed to be better compared to that of FN mortar mixes.

Figure 4.6: Compressive strength of quaternary blended FA, UFFA and CNS cement mortar

Compressive strength results of quaternary blended cement mortar presented in Figure 4.6 illustrates that gain in compressive strength is found to be more than control mix. This may

be ascribed to better particle packing in addition to the pozzolanic reactivity of FA, UFFA and CNS in different scale. The reason could also be attributed to finer particles of UFFA add faster reactivity along with the presence of CNS and better pore filling effect at micro to nano scale (Supit, 2013)

4.3.2 Density

The influence of CNS, FA and UFFA on density of binary blended cementitious mortar is presented in the Figure 4.7a – 4.7c.
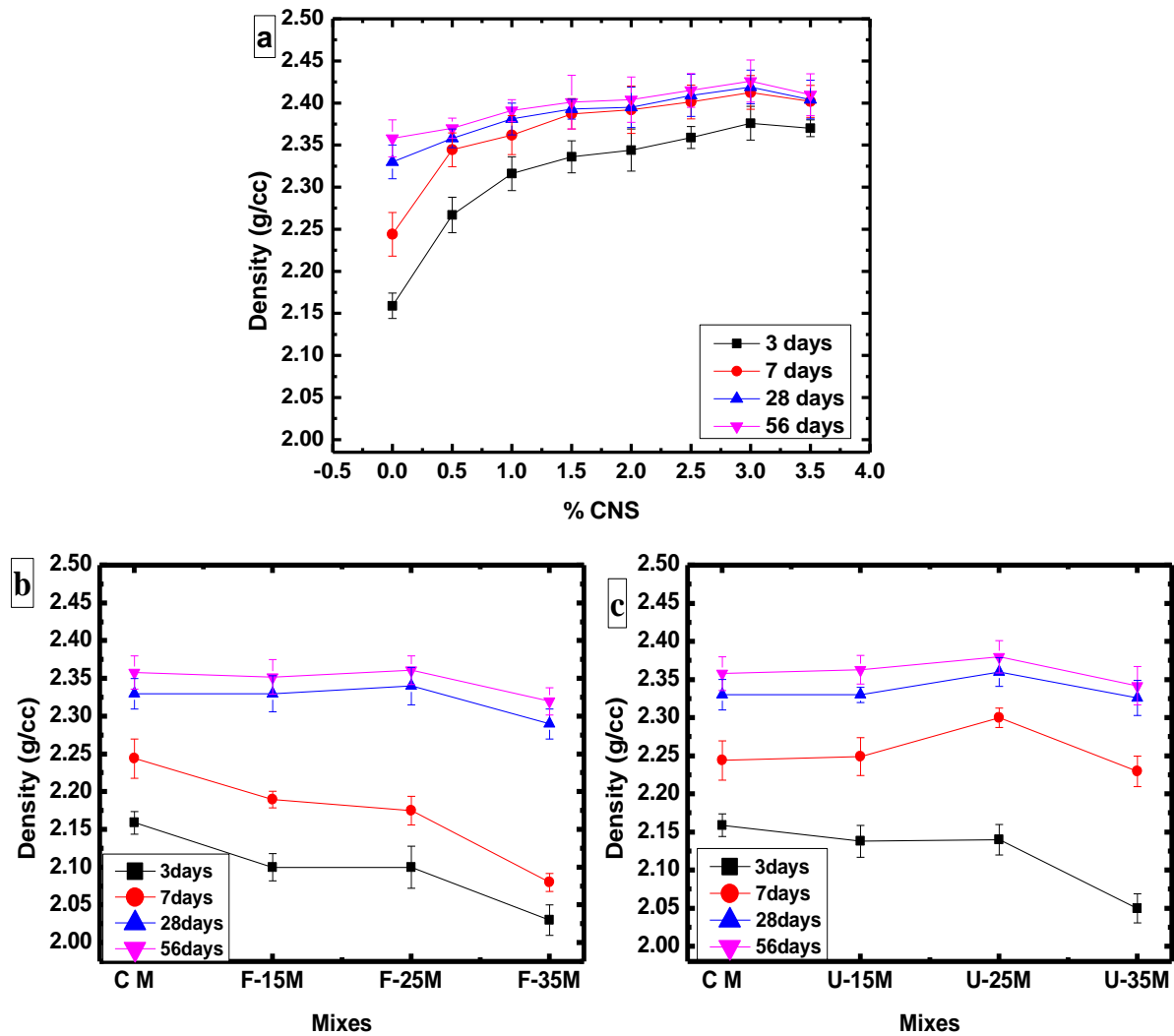
Figure 4.7: Density of binary blended cement mortar a) CNS mixes b) F mixes c) U mixes

It can be perceived from the Figure 4a that increase in the content of nano-silica improved the density of binary blended CNS mortar. It was found that rate of increase in density of binary blended CNS mortar is more significant at early ages (i.e. 3 days and 7 days) compared to that of later ages (i.e. 28 days and 56 days). The maximum density was achieved for 3% CNS admixed mortar i.e. 2.38, 2.41, 2.42 and 2.43 g/cc at the curing ages of 3, 7, 28 and 56 days, respectively. This may be attributed to the physical and chemical impact of nano-silica in cementitious system, which effactually enhanced the bulkiness of paste and tightened the transition zone between the paste and aggregate (Singh et al., 2015; Ehsani et al., 2017). Physically, nano-silica minimized the void content with the aid of nano filler action. Further, chemically, smaller particle size of nano-silica amplified the pozzolanic reaction by consuming $Ca(OH)_2$ to produce secondary stable C-S-H gel (Sanchez and Sobolev, 2010; Quercia et al., 2012) that promoted in densifying the microstructure of cementitious matrix. It can also be seen that after 3% CNS content there is no improvement in density rather drop in density was noticed. As mentioned in the section 4.3.1 excessive addition of nano-silica leads to the agglomeration of nano-silica particles and that produces weak porous zones by hindering the hydration process.

It can be seen from the Figure 4.7b that binary blended F mixes shows lower density as compared to control at the curing ages of 3 and 7 days, this is due to incomplete pozzolanic reaction of FA particles. While, binary blended U mortar mixes initially showed lower density at the age of 3 days and found to be increased at the later ages of 7, 28 and 56 days. This could be due to greater surface area of UFFA particles, which improved the reactivity speed in cementitious composites (Obla et al., 2003). F-25M and U-25M mixes showed highest density among binary blended F and U mixes, respectively. It is important to note that 35% replacement of cement by FA and UFFA showed lower performance in terms of density owing to the dilution effect.

The variation in density of ternary blended cement mortar admixed with the combination of FA, UFFA and CNS is graphically represented in Figure 4.8 (a-c).
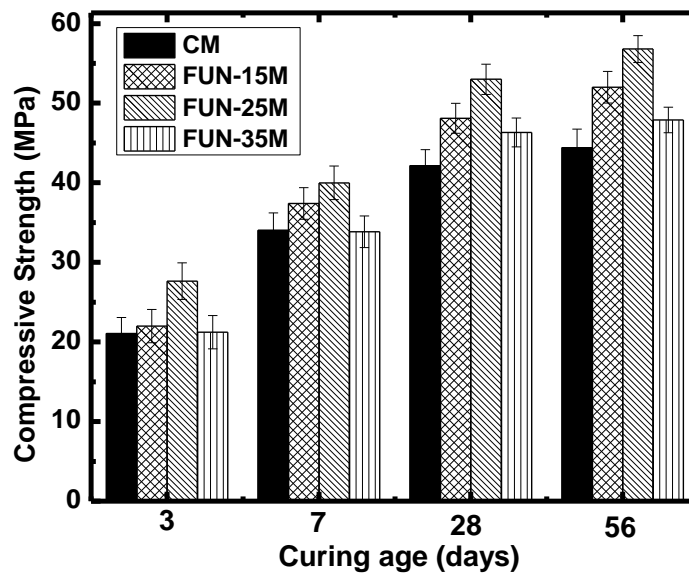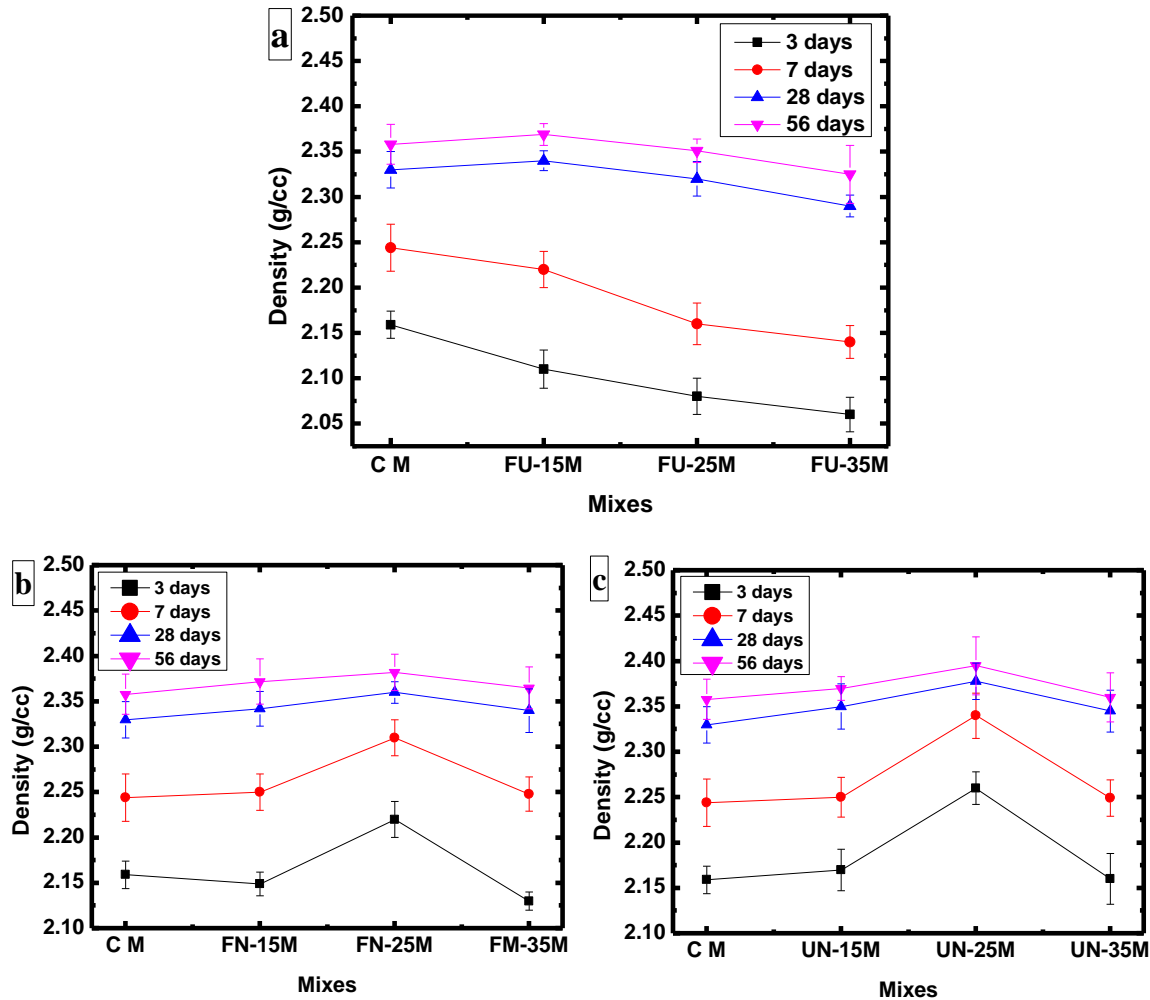
Figure 4.8: Density of ternary blended cement mortar a) FU mixes b) FN mixes c) UN mixes

It can be seen from the Figure 4.8a that the ternary blended FU mortar mixes initially showed lower density at the age of 3 and 7 days. However, FU mortar mix with total replacement of 15% and 25% displayed slight higher density with respect to control mortar at the later ages of 28 and 56 days. Further, it was also noticed that increase in total replacement of cement by 35% of FA+UFFA showed drop in density. This could be due to the fact that replacement of more reactive cement by comparatively less reactive FA and UFFA particles particularly at the early ages (Obla et al., 2003; Das et al., 2012).

The impact of CNS intervention in FA and UFFA based ternary blended mortar on density is shown in the Fig. 4.8 (b-c). It can be clearly observed that presence of CNS in FN (Figure 4.8b) and UN (Figure 4.8c) mortar mixes showed significant improvement in density at early as well as later ages compared to that of control mortar. The reason associated to this may be the presence of highly active CNS, which compensates the drawback of FA and UFFA particularly at early ages (Said et al., 2012; Zhang et al., 2012; Hou et al., 2013).
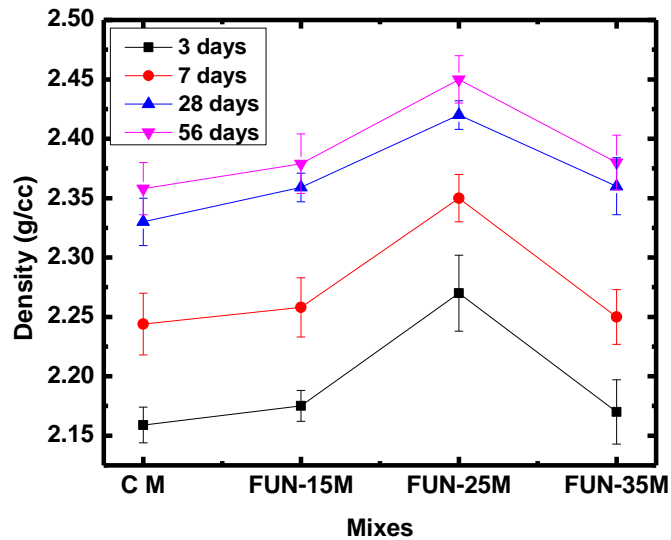
Figure 4.9: Density of quaternary blended FUN cement mortar mixes

Figure 4.9 shows the density plot for quaternary blended cement mortar with the mixture of FA, UFFA and CNS. It can be noted that quaternary blended mortar showed better density compared to ternary blends. This could be attributed to optimised particle packing by filling up the varied sized voids in cementitious system. The presence of multi-sized mineral admixture along with cement particles had tailored the solidity of cementitious mortar composites, especially presence of nano sized silica particles contributed in filling up the voids at nano-scale.

4.3.3 Drying Shrinkage

Variation in drying shrinkage (micro strain) for all the mixes at various exposure period are presented in Figures 4.10 to 4.13.
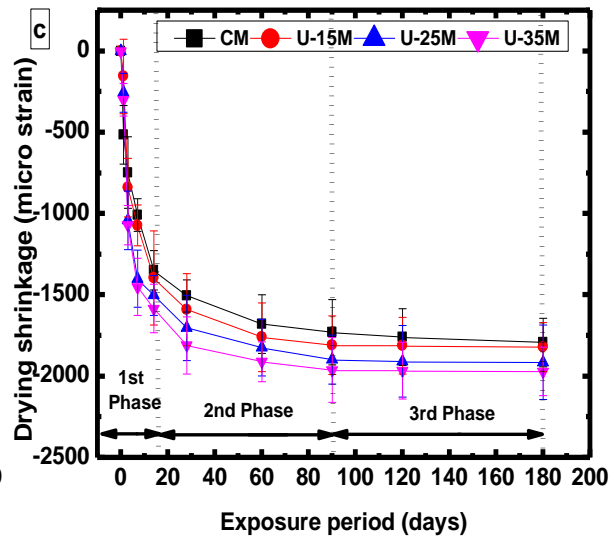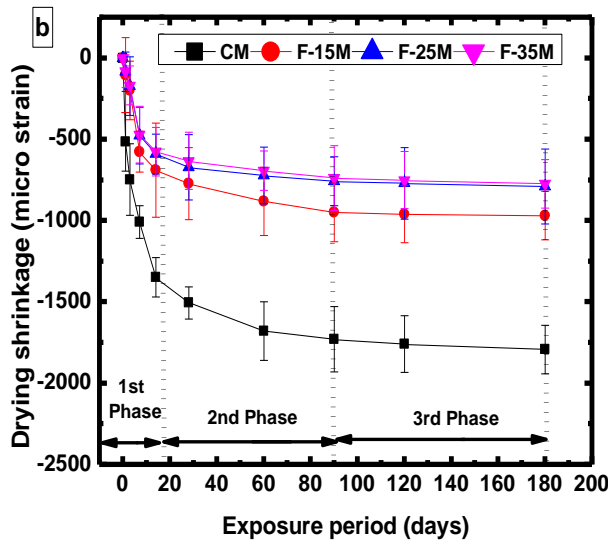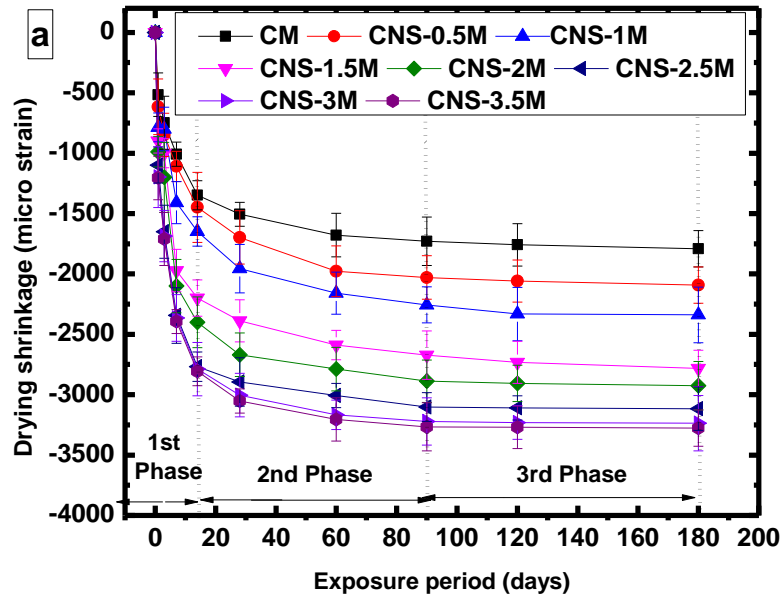
Figure 4.10: Drying shrinkage values for binary blended cementitious mortar a) CNS mixes b) F mixes c) U mixes

It can be observed from the figure that for all the mixes rate of increase in drying shrinkage was found to be higher in initial periods (1-14 days), then tends to reduce rapidly at the exposure period of 30 days and thereafter shrinkage curve gets stabilized. This initial increase in drying shrinkage was due to the additional impact of chemical and autogenous shrinkage related to the hydration activity caused by consumption of water being held in capillary pores (Hawlett, 1998). Drying shrinkage value for control mix at the exposure

106

period of 180 days was seen to be 1780 micro strain. This higher rate of drying shrinkage could be attributed to greater water/cement ratio. So, the excess amount of water present in capillary pores of hardened cementitious mortar dries out on evaporation causing drying shrinkage.

It can also be seen from the Figure 4.10a that binary blended CNS mixes increased the shrinkage strains with the increase in CNS content and found to be much higher to that of control mortar. At the exposure period of 180 days, drying shrinkage value for CNS-3M mix was found to be 3316 micro strain, highest among all the mixes. This could be attributed to the accelerated chemical reaction of nano-silica particles owing to the smaller particle size and higher surface area of nano-silica that amplified the availability of reactive atoms in the surface (Haruehansapong et al., 2017). This would increase heat of hydration, internal drying, thus accelerates autogenous and related chemical shrinkage within the cementitious system causing exacerbated drying shrinkage. Another fact is that larger surface area of nano-silica would absorb large amount of water available for hydration. Therefore, it would necessitate ingestion of external water to balance the hydration reaction, on the other hand the process of water absorption would be hindered due to the pore refinement by nano-silica (Haruehansapong et al., 2017). This would lead to the increase in negative capillary pressure at certain pore sizes, thus triggering drying shrinkage especially when difference in temperature and relative humidity between in and out of mortar surface is significant.

For F-mixes drying shrinkage was found to be much lower to that of control mix. Further, increase in the amount of FA content showed reduction in drying shrinkage (Figure 4.10b). Drying shrinkage value for F mixes were found to be in the range of 550 to 760 micro strain at the exposure period of 180 days. This lowered drying shrinkage in F mixes would be due to the following properties of fly ash: a) dilution effect and reduced initial hydration, which aids in minimizing the chemical and autogenous shrinkage that was provoked due to the cement hydration (Wongkeo et al. 2012) b) unreacted fly ash particles could act as micro-aggregates (filler) and aids in retaining the shrinkage to a certain level c) pozzolanic

activity of FA based cement mortar also benefits in better pore refinement, subsequently would reduce the rate of water loss and hence the drying shrinkage (Wang and Ma, 2018). In case of U mixes drying shrinkage results were seen to be in contrast to that of F mixes and seen to be larger to control. Presence of submicron sized UFFA particles in U mixes triggered the rate of drying shrinkage and found to be higher than that of control mix. Drying shrinkage values of U mixes were found be in the boundaries of 1790 to 1970 micro strain at the exposure period of 180 days (Figure 4.10c). This could be attributed to the faster reactivity of finer UFFA particles by providing additional nucleation sites for hydration, which thereby increases the rate of chemical and autogenous shrinkage by imbibing the available capillary pore water (Hewellet, 1998). It is also reported that fine pore structure of micro fine particles has an ability to hold more water owing to the effect of osmatic suction (Haruehansapong et al., 2017).
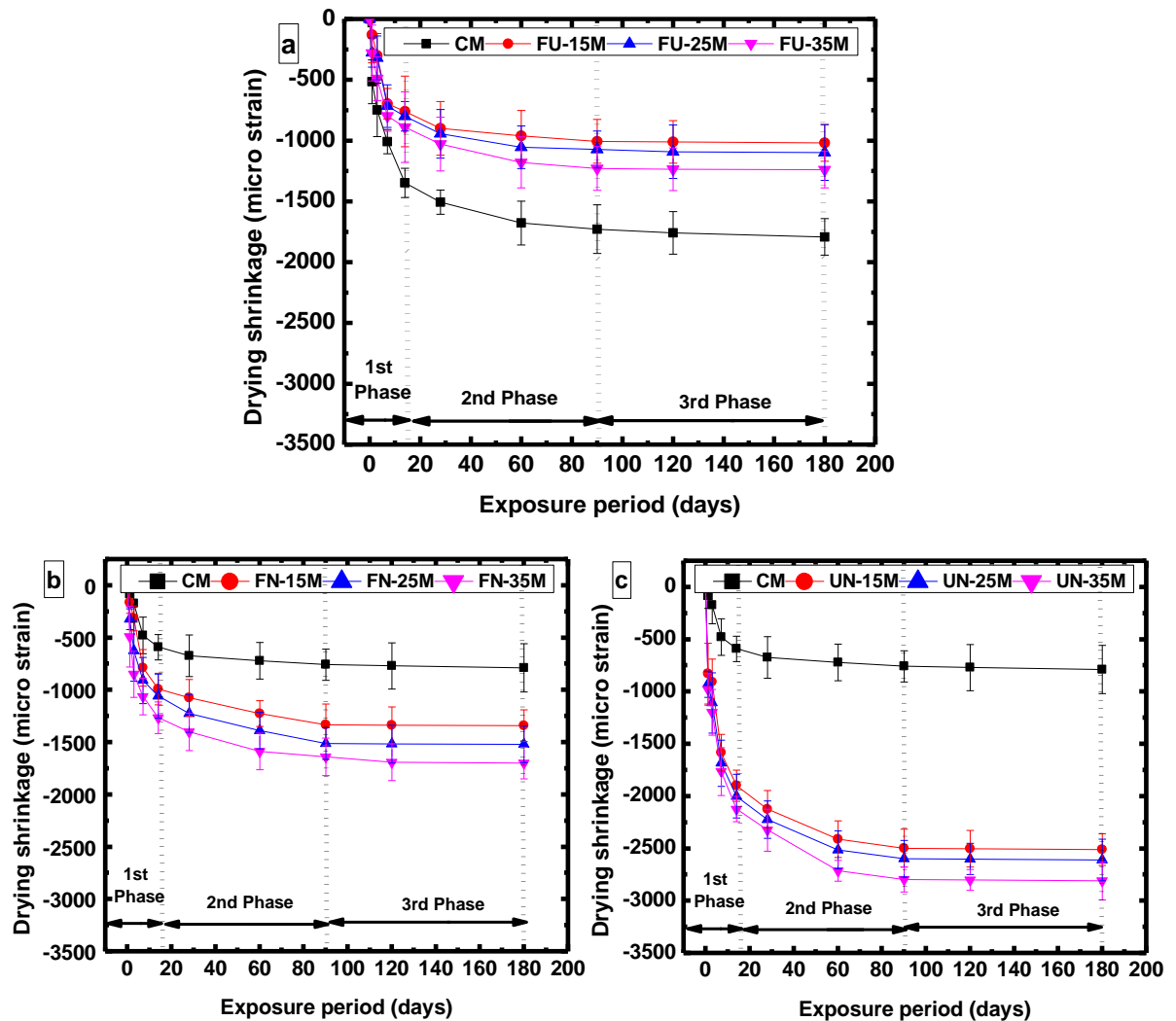
Figure 4.11: Drying shrinkage values for ternary blended cementitious mortar a)
FU mixes b) FN mixes c) UN mixes

It is to be noted from the Figure 4.11a that for FU mixes drying shrinkage was seen to be controlled and its drying shrinkage values were found to fall in between control and F-mixes. This could be due to the action of balanced reactivity of FA and UFFA in cementitious composites. Drying shrinkage values for FU blended mixes were found be in the boundaries of 1012 to 1219 micro strain at the exposure period of 180 days, which is 45% to 48% lower to that of U-mixes.

It can be noticed from the Figures 4.11b and 4.11c that when FA and UFFA were used in conjunction with nano-silica shrinkage strain was found to be intensified as compared to binary blended F and U mixes. This could be due to the presence of high reactive nano-silica particles. Shrinkage strain values for FN and UN mixes at the exposure period of 180 days were found to be in the range of 1340 to 1690 micro strains and 2509 to 2810 micro strain, respectively. However, shrinkage strains for FN mixes were seen to be lower to that of control mix owing to presence of fly ash particles.
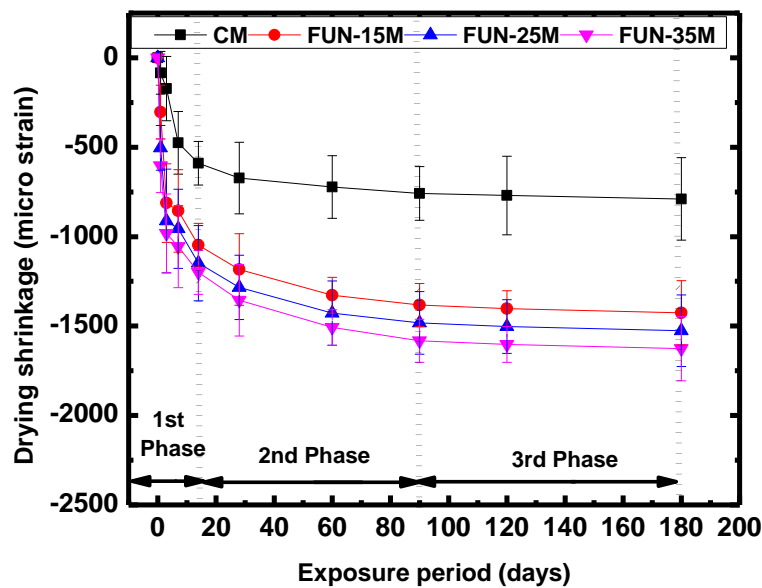
Figure 4.12: Drying shrinkage values for quaternary blended cementitious mortar

It can be observed from Figure 4.12 that similar to ternary blended FN mixes, when UFFA and CNS were used in combination with fly ash in the form of quaternary blends (FUN mixes) also showed tailored drying shrinkage and found to be lower to that of control mix. Drying shrinkage values of FUN-mixes were found to be reduced by 10%-20% with respect to control mix at the exposure period of 180 days. This could be due to the synergic effect of FA, UFFA and CNS that complemented in the modification of shrinkage. Therefore, combined usage of CNS, UFFA and FA could be more effective in comparison with the individual use of finer particles such as CNS and UFFA. Shrinkage strains could still be reduced for present mixes by reducing water/binder ratio, as this study adopted constant water/binder ratio (0.5) that is bit on the higher side.
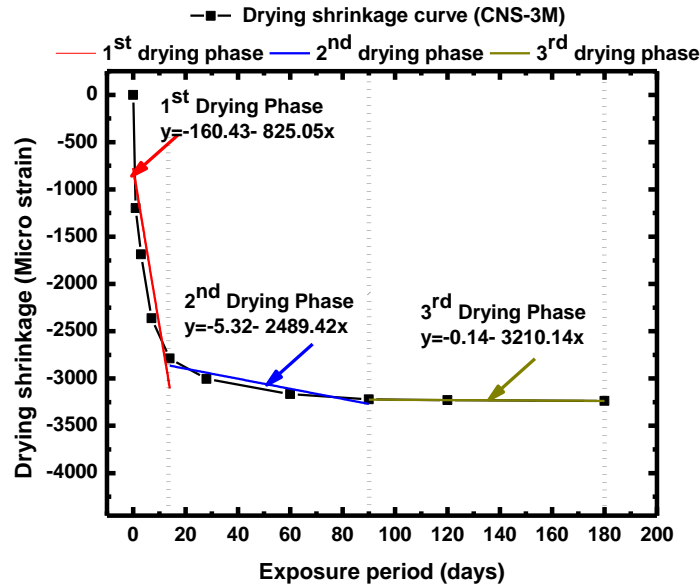
Figure 4.13: Distinctive plot representing the three phase system of drying curve

The general trend of drying shrinkage curve for all the mixes found to be of in a similar manner and a typical drying curve for CNS-3M mix is plotted in Figure 4.13. It can be observed from the figure that there exists a three-phase drying system in the cementitious composites unlike a two-phase drying system reported earlier (Scheffler and Plagge, 2017). First phase can be regarded to the linear weight loss that is directly proportional to time. In this phase moisture transport happens faster to the surface of the material than that it gets evaporated. However, it is to be noted that this phase shows limited drying with respect to the boundary conditions (i.e. climatic- temperature and humidity; transfer condition-air velocity and surface roughness).

Whereas, in the second phase of drying, mechanism seems to be converse i.e. moisture transport to the material surface gets slow down and the rate of evaporation of surface vapour tends to be higher. The third drying phase seems to be a stabilised system, the rate of moisture transport either to the material surface or from the surface to the environment tends to zero. This mechanism that has been explained above can be substantiated from the slope obtained for three different phases of drying curve that is plotted in Figure 4.13. The slope values for three phases of drying are -160.43 (1st phase), -5.32 (2nd phase) and -0.14 (3rd phase).

This signifies that initial 14 days of water curing is very crucial to control the primary phase of drying in practice for cementitious composites and thereby governs in sustaining the service life of a material (Kulakarni, 2011; Yang et al., 2017). Further, next 14 to 90 days movement of moisture from the cementitious composites reduces gradually, which seems to have not that significant impact on materials property (Shafiq and Cabrera, 2004; Das et al., 2014).

4.3.4 Pozzolanic activity test: strength activity index (SAI)

Strength activity index (SAI) of all the blended mixes corresponding to control mortar at the ages of 7 and 28 days are presented in Figure 4.14 to Figure 4.16.
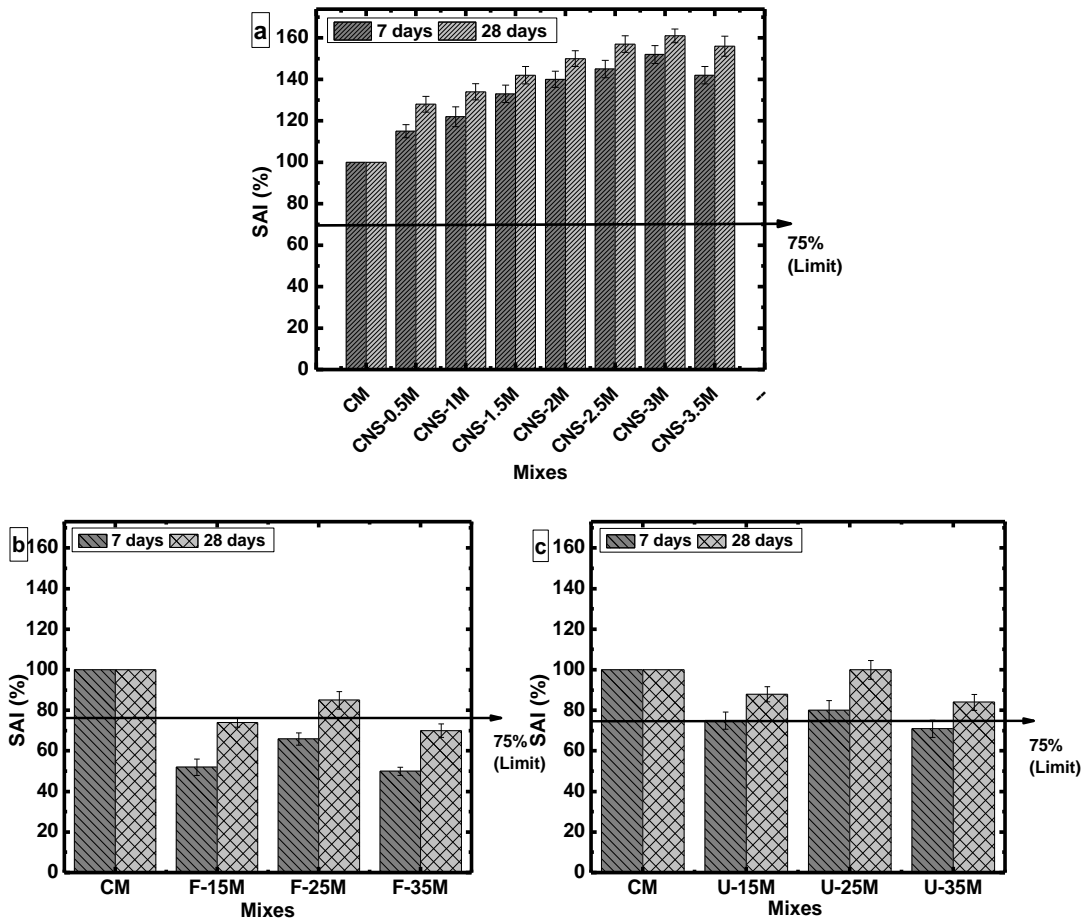
Figure 4.14: Strength activity index for binary blended cementitious mortar a) CNS-mixes b) F mixes c) U mixes

It can be seen from the Figures 4.14 that all binary blended mortar mixes except F mixes showed SAI greater than the limit i.e. 75% (as specified in ASTM C 618) even at the early age of 7 days. It can be noticed from Figure 4.14a that binary blended CNS-3M mortar mix showed superior SAI with a value of 152% and 161% at the ages of 7 days and 28 days, respectively among all blended mortar mixes. This may be attributed to extremely smaller particle size ($\leq$ 20 nm) with high specific surface area. Further, presence of higher percentage of reactive silica content (99.5%) in nano-silica accelerated the pozzolanic reactivity to greater extent, there led to the improved microstructure and strength of cementitious system owing to its rapid formation of secondary C-S-H (Yu et al., 2014).

It can be observed from Figure 4.14b that after 28 days of curing age F-25M mix also showed increase in SAI (>75%) signifying the slow improvement in pozzolanic activity. However, U mixes performed better compared to F mixes (Figure 4.14c) and U 25M mix showed the SAI values above the limiting value (75%) even at the curing age of 7 days. This could be due to the improved physical and chemical activity of UFFA particles.
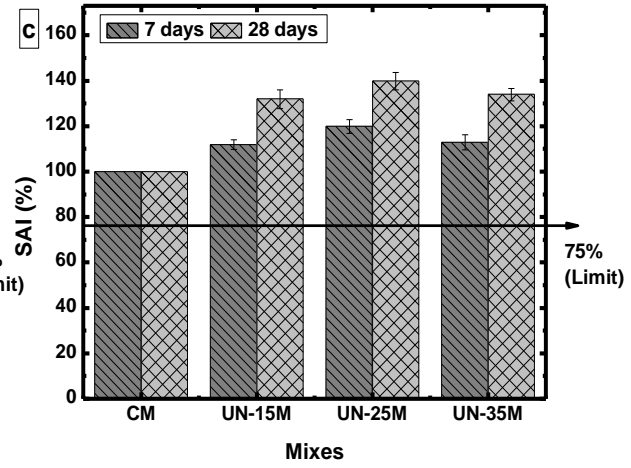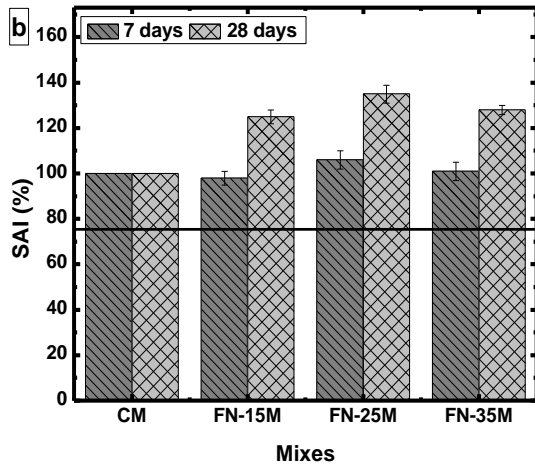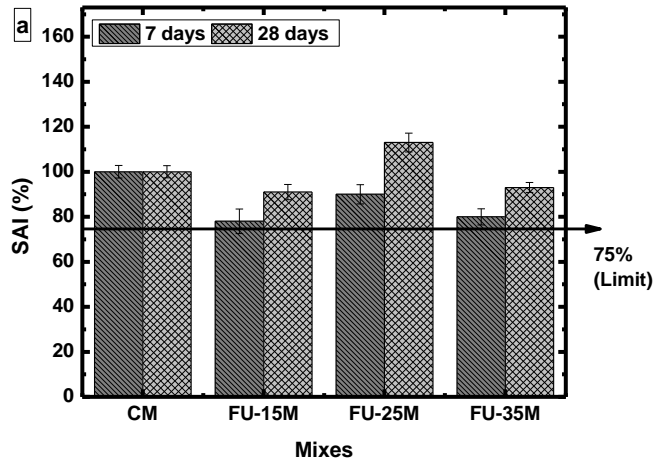
Figure 4.15: Strength activity index for ternary blended cementitious mortar a) FU-mixes b) FN mixes c) UN mixes
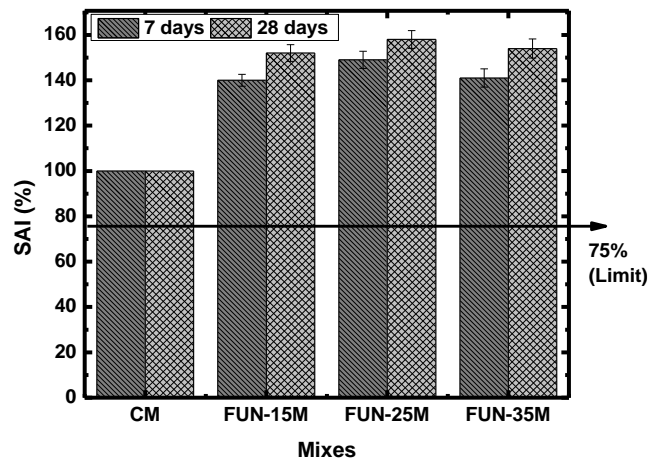
Figure 4.16: Strength activity index for quaternary blended cementitious mortar

114

It is important to note from the Figure 4.15 and Figure 4.16 that all ternary and quaternary blended mixes showed SAI value beyond the limiting value of 75%. This could be attributed to the synergetic act of multiple Pozzolans. Further, SAI was found to be intensified for ternary and quaternary blended mortar mixes consisting of nano-silica particles as compared to the mixes without nano-silica. SAI value of FN-25M, UN-25M and FUN-25M mixes at the age of 28 days were seen 138%, 142% and 158%. It was very much interesting to note that quaternary blended FUN-25M mix resulted in SAI closer to CNS-3M mix. This increase of SAI for quaternary blended mortar mixes would be benefitted due to particle packing effect prompted by multi-sized SCMs, pozzolanic activity induced by SCMs and enhanced microstructure of silicate based hydration products formed by pozzolanic activity.

4.3.5   Durability properties

4.3.5.1 Permeable porosity

Figure 4.17 (a-c) represents the variation in porosity of binary blended mortar mixes composed of CNS, FA and UFFA particles at the curing ages of 3, 7, 28 and 56 days.
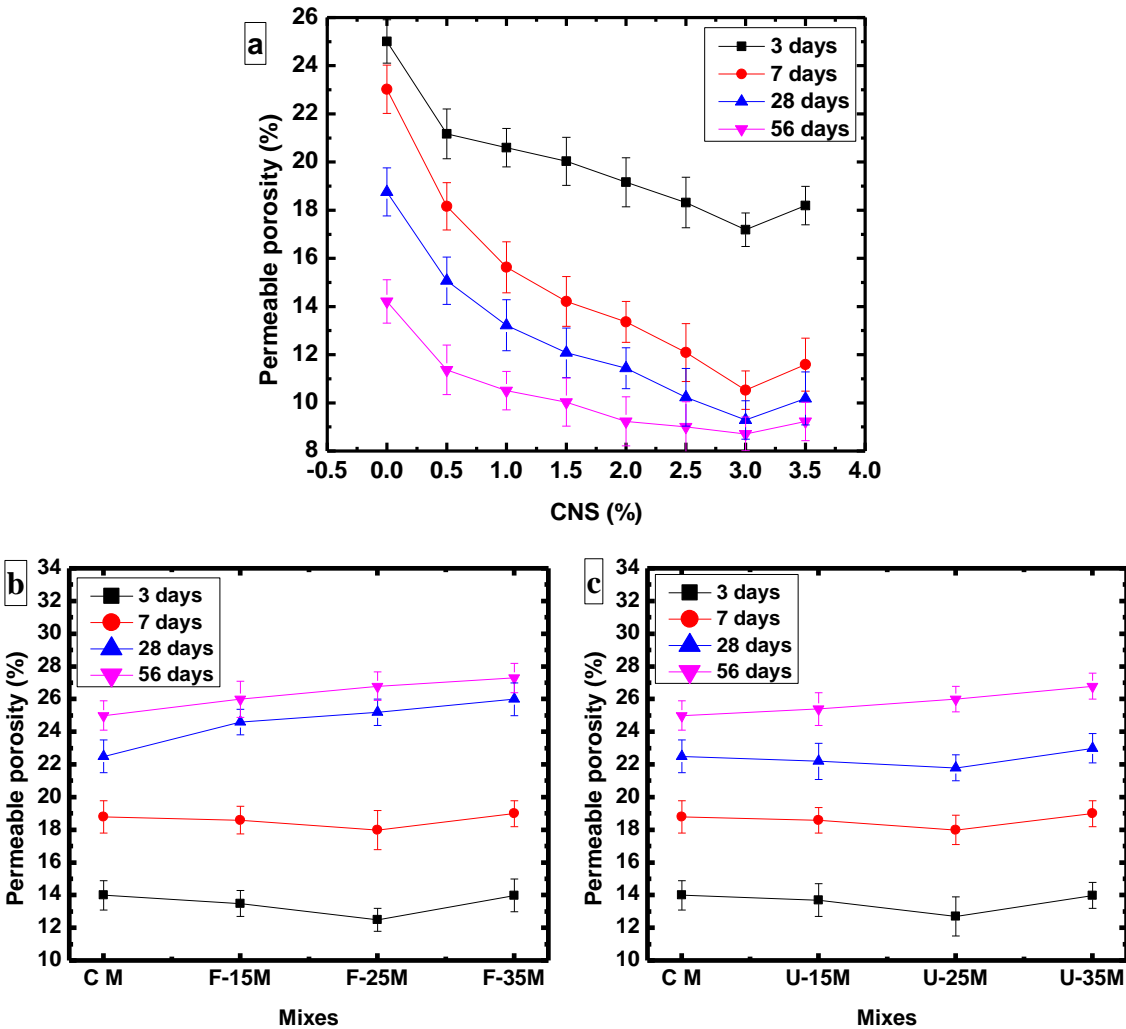
Figure 4.17: Influence of binary blended cement mortar mixes on percentage of porosity a) CNS mixes b) F mixes and c) U mixes

It can be observed from Figure 4.17a that the porosity percentage found to be decreased from 25% to 18.19%, 23% to 10.23%, 18.76% to 9.09% and 14.21% to 8.8% at the age of 3, 7, 28 and 56 days, respectively for CNS replacement from 0-3%. However, all the mixes showed lesser porosity compared to control mortar irrespective of curing age. The resulted lower porosity was mainly attribute to the densified microstructure associated to the pore filling effect by nano-silica particles as reported in density section for CNS blended mortar.

Binary blended F and U mortar mixes showed greater porosity (Figure 4.10b – 4.10c) compared to that of binary blend CNS mixes (Figure 4.10a). This variation of permeable porosity values may be due to low rate of pozzolanic and hydraulic reaction of mixes containing FA and UFFA linking to domination of dilution effect and low packing density.

Figure 4.18 (a-c) and Figure 4.19 illustrates the influence of ternary and quaternary blended cement mortar on permeable porosity percentage, respectively.
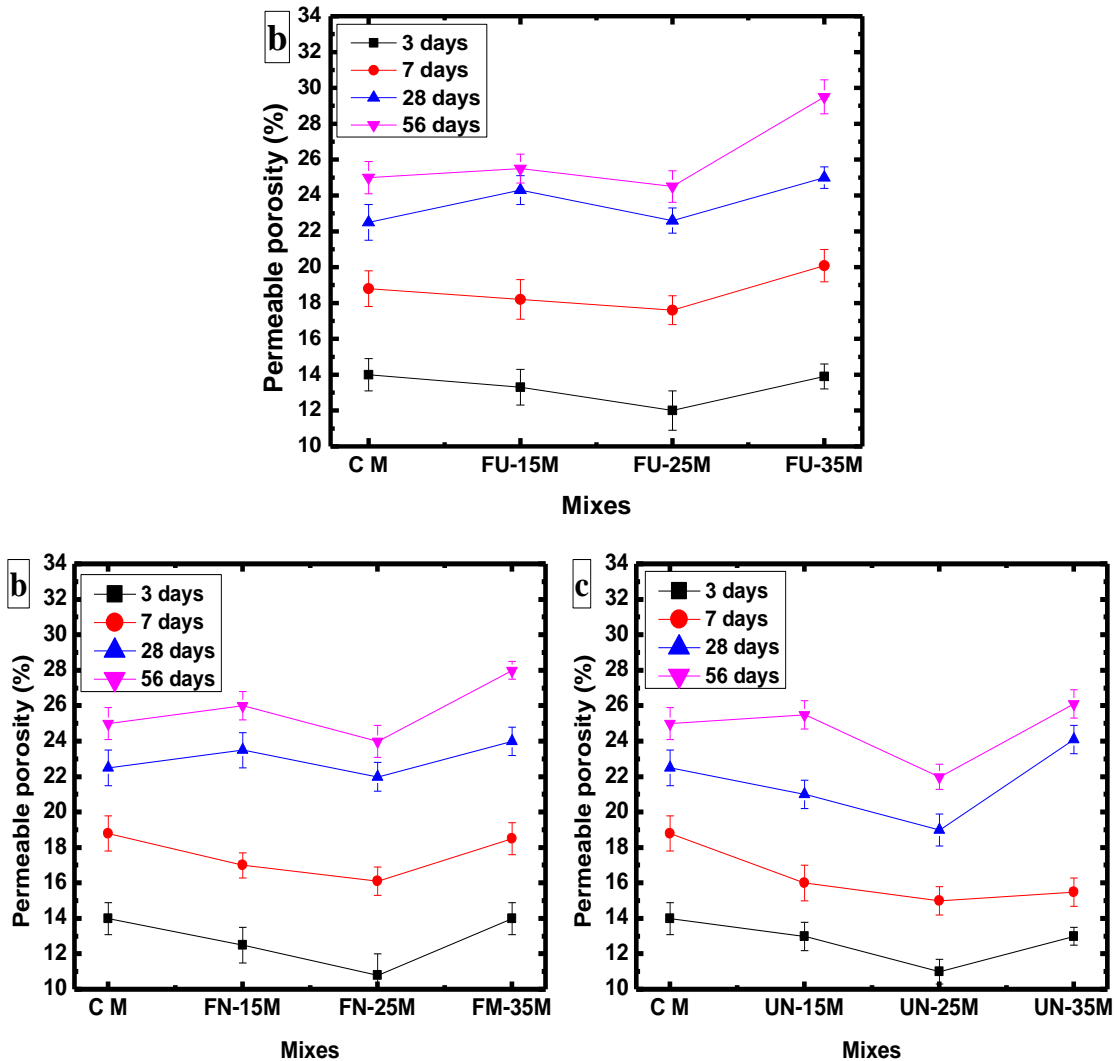
Figure 4.18: Influence of ternary blended cement mortar mixes on percentage of permeable porosity a) FU mixes b) FN mixes c) UN mixes

It can be observed from the results that in FU ternary blended cement mortar porosity tends to increase with the replacement percentage (Figure 4.18a). But, it was noticed that after the curing age of 28 days in FU-25M mortar mix there was a reduction in porosity compared to control. The porosity of FU-25M mix was found to be reduced by 9.27% and 12.56% with respect to control mortar at the ages of 28 and 56 days, respectively.

In case of ternary blended FN (Figure 4.18b) and UN (Figure 4.18c) mortar mixes permeable porosity was found to be drastically reduced especially for replacement level of 25% as compared to that of control mix and this was possible due to the intrusion of nano-silica particles. The porosity percent was observed to be slightly higher for FN-15M and FN-35M mixes compared to control at the early ages of 3 and 7 days and found to be reducing in later ages of 28 and 56 days. On the other hand, reduced permeable porosity for UN mixes was noticed at the early age of 3 days, the reducing trend in porosity was seen up to the replacement level of 25%, further at replacement level of 35% permeable porosity was found to be increase owing to the dilution effect.
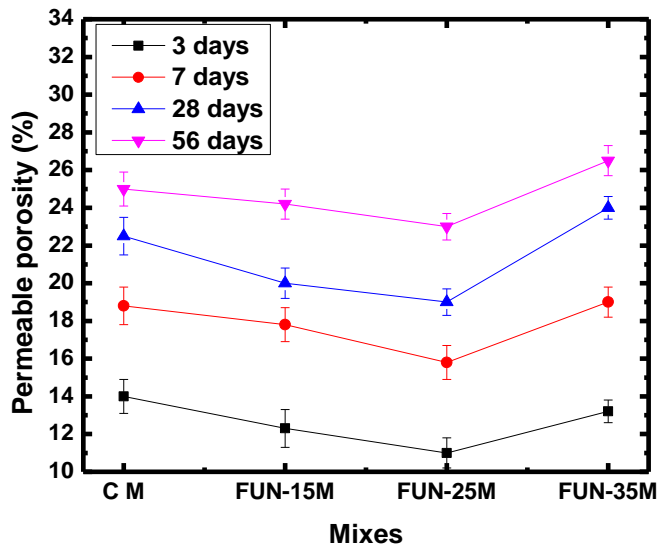
Figure 4.19: Influence of quaternary blended FUN cement mortar mixes on percentage of permeable porosity

The quaternary blended cement mortar showed better reduction in porosity compared to that of ternary blended mortar mixes (Figure 4.19). Among all quaternary blended mixes

FUN-25M performed the best in correspondence to porosity i.e. porosity percent was seen to be lowered by 9.39%, 12.54%, 19.51 % and 23.71% at the curing ages of 3, 7, 28 and 56 days, respectively. As reported earlier this may be owing to the betterment in pore structure due to finest packing ability along with its improved chemical reactivity.

4.3.5.2 Rapid chloride-ion penetration test (RCPT)

The results of RCPT for binary blended admixed mortar consisting of CNS, FA and UFFA contents at the age of 7, 28 and 56 days is presented in histogram as shown in Figure 4.20.
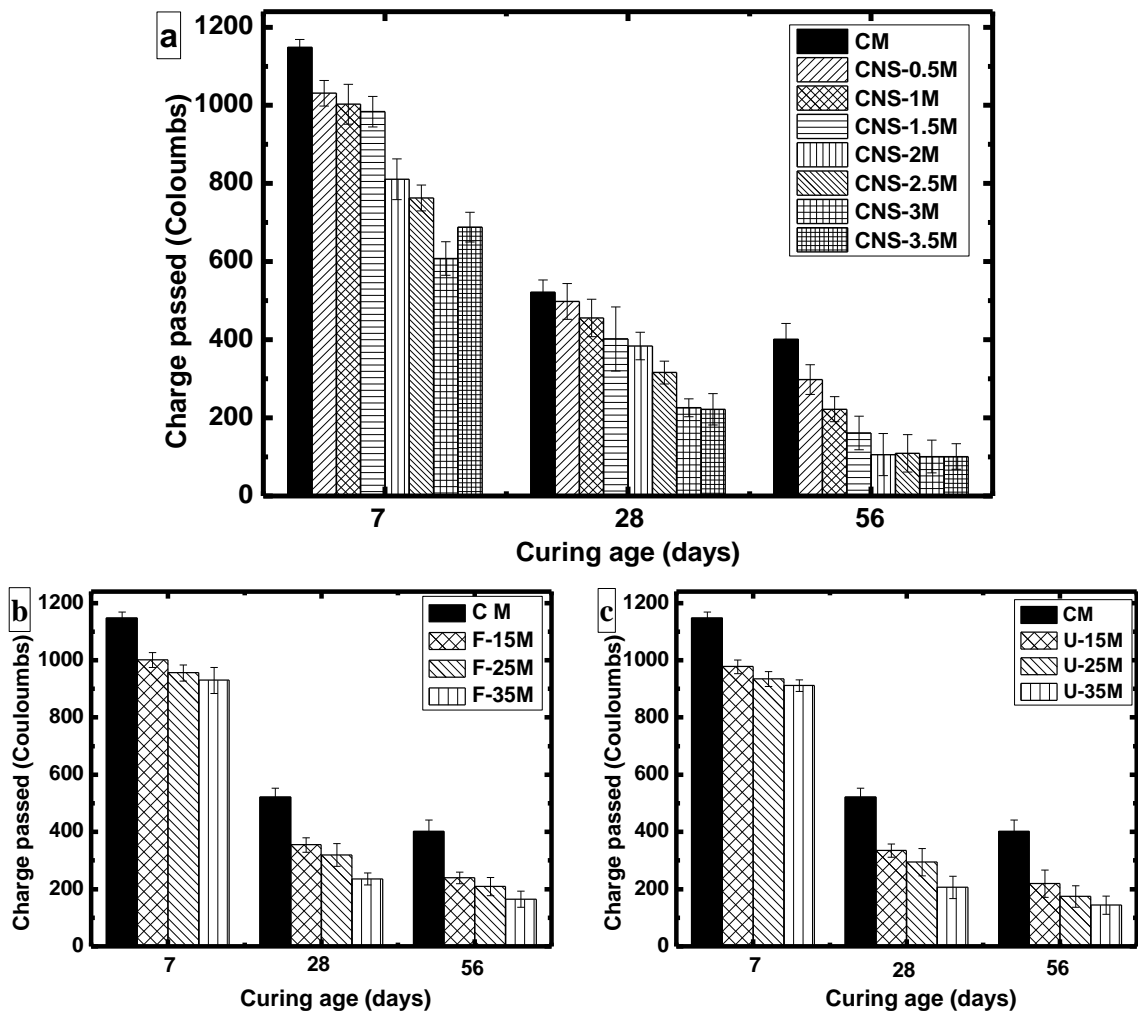
Figure 4.20: Variation of charge passed versus curing ages for binary blended mortar a) CNS mixes b) F mixes c) U mixes

It can be observed from the table that incorporation of nano-silica in mortar mixes significantly reduces the penetration of chloride ions (charge passing) compared to control mix. It can also be noticed that reduction in charge passing is more pronounced after curing age of 28 days. The reduction in charge passing was observed to be more prominent for 3% CNS admixed mortar and the values for CNS-3M were 206 coulombs and 101 coulombs at the age of 28 and 56 days, respectively.

It can noticed from the Figure 4.20 (b-c) that binary blended F and U mixes also showed lesser charge passed as compared to that of control. However, the intensity of reduction in change passed was much lower to that of binary blended CNS mixes. Percentage of reduction in charge passed for FA and UFFA admixed binary blended mixes were seen to be in the range of 18%-32% and 38%-50%, respectively.

Figure 4.21 (a-c) and Figure 4.22 reports the RCPT values of ternary and quaternary blended cement mortar at the age of 7, 28 and 56 days, respectively.
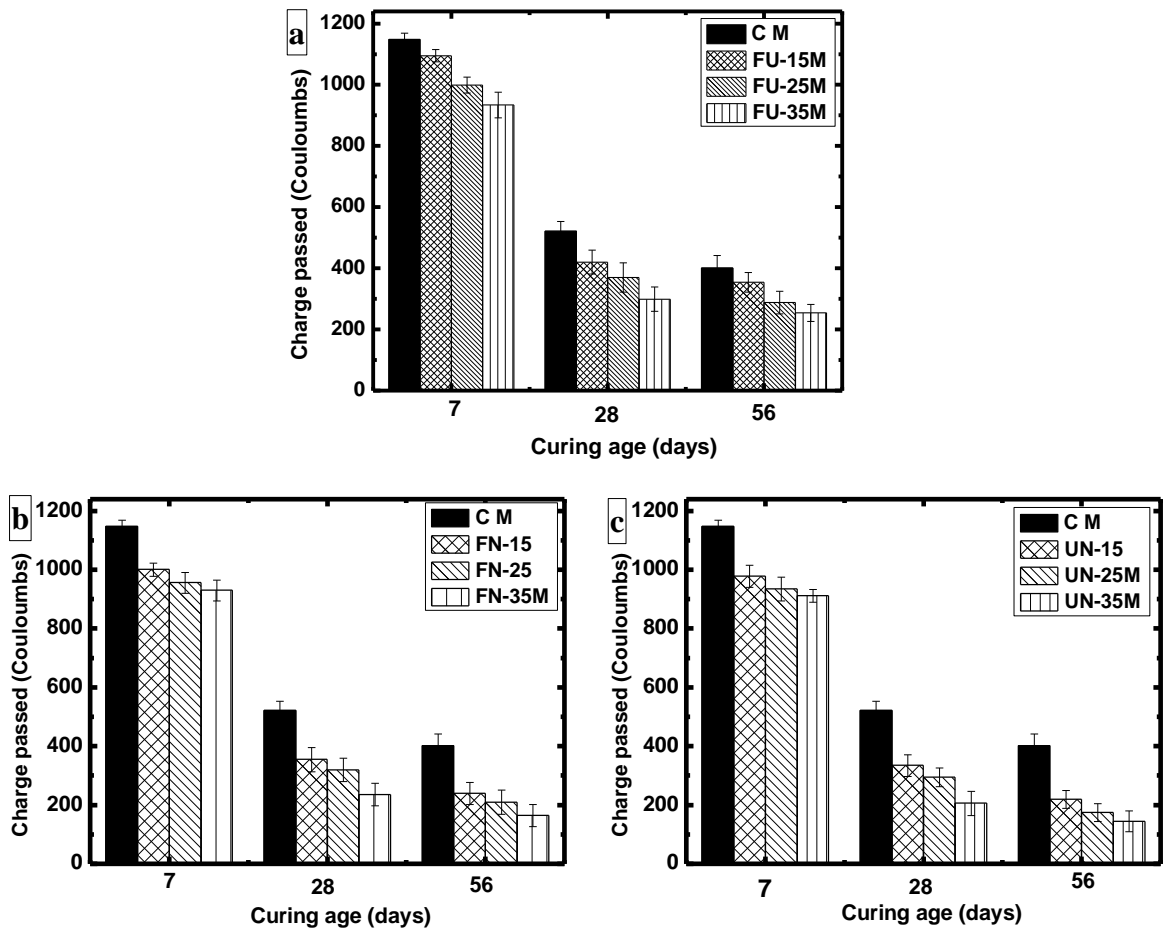
Figure 4.21: Variation of charge passed versus curing ages for ternary blended mortar a) FU mixes b) FN mixes c) UN mixes
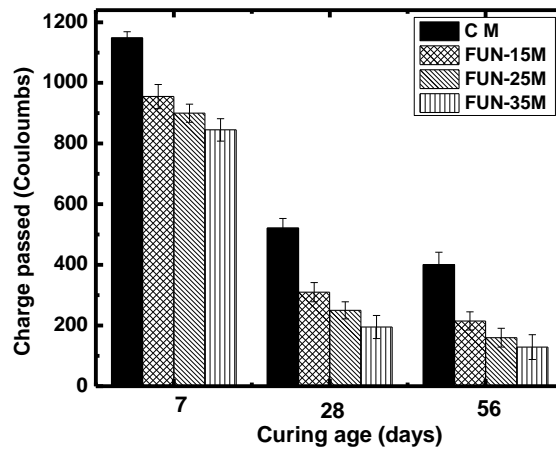
Figure 4.22: Variation of charge passed versus curing ages for quaternary blended FUN mortar mixes

It is clear from the Figure 4.21a that compared to control mortar, ternary blended cement mortar incorporated with both FA and UFFA particles reduced the rate charge passing through the mortar. Percentage reduction in charge passing for FU mortar mixes were found to be in the range of 47% - 61% at the end of 56 days with respect control mortar. Whereas, the percentage of reduction in charge passed for CNS intermixed ternary (FN, Figure 4.21b; UN, Figure 4.21c) and quaternary blended (FUN, Figure 4.22) mortar mixes were found to be in the range of 52%-68%, 58%-75% and 62%-78%, respectively at the age of 56 days with respect to control mortar. The substantial reduction of charge passed with the addition of nano-silica or pozzolanic materials may be attributed to the significant effect of secondary cementitious materials on pore solution chemistry that are affected by alkalis, level of replacement and age that greatly influences on RCPT results (Shi 2003).

4.3.5.3 Acid, alkali and chloride resistant test

4.3.5.3.1 Exposure to acid (H_2SO_4) solution

4.3.5.3.1.1 Density loss and strength loss

Figure 4.23 presents the resulted density loss and strength loss data for control and blended cementitious mortar cured for 28 days and exposed to 1% sulfuric acid (H_2SO_4) solution for the exposure periods of 30, 60, 90, 120 and 180 days.
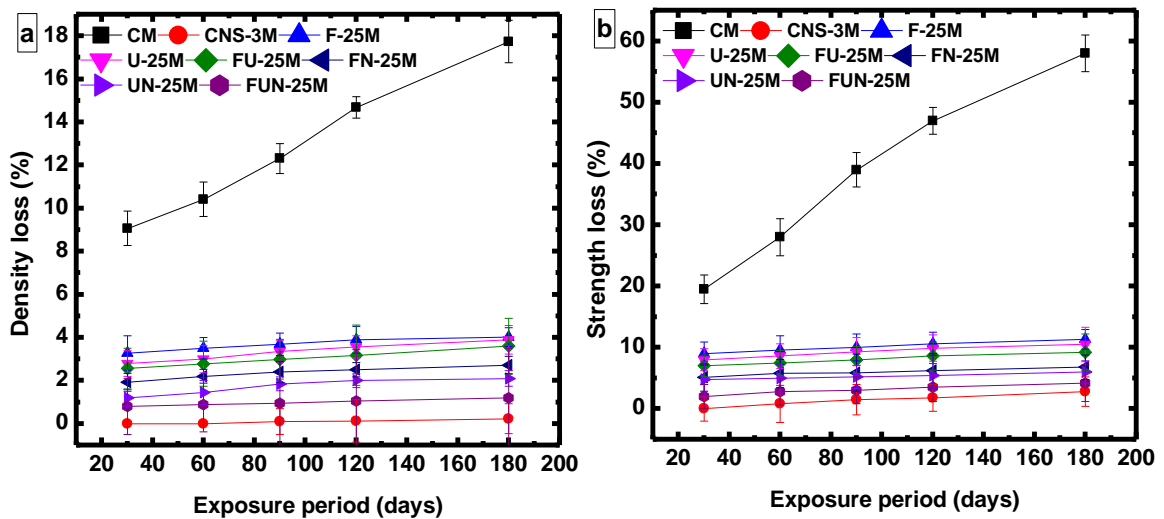
Figure 4.23: Variation in a) density loss and b) strength loss percentage of control and blended cementitious mortar exposed to sulfuric acid (H₂SO₄) for the period of 30, 60, 90, 120 and 180 days

It can be observed from the figure that amid all mixes control mix shows the highest deterioration. Deterioration due to sulfuric acid (H₂SO₄) exposure was found to be more intense due to the synergistic act of acid and sulfates (Turkel et al., 2007; Sahoo et al., 2017). It is to be noted that for exposure period of 180 days control mortar underwent an acute density and strength losses of 18% and 59%, respectively. Figure also illustrates that in case of sulfuric acid (H₂SO₄) exposure all the blended mortar mixes exhibited lower percentage of density and strength losses as compared to that of control mortar, irrespective of exposure period. In the midst of all the blended mixes, binary blended CNS-3M mortar mix showed lowest density loss (0.23% at 180 days) and strength loss (2.4% at 180 days). Quaternary blended FUN-25M was the next mix, which exhibited lower density loss (1.1% at 180 days) and strength loss (2.9% at 180 days).

Sulfuric acid (H₂SO₄) being a strong acid, which when diffuses into the cementitious composites pH of pore solution drops down drastically and hydration products starts to disintegrate (Turkel et al., 2007). This could be attributed to the threat caused by H₂SO₄ in dissolving the hydration products and formation of gypsum (Gy) and ettringite (AFt).

Secondary gypsum formed are highly soluble and unstable in nature, which leads to the loss in material binding ability and increase in porosity (Sahoo et al., 2017). Further, secondary ettringite (AFt) formed are voluminous compounds.

Chemical reactions occurring during the process of H_2SO_4 exposure on cementitious materials are given below (Izzat et al., 2013).

$$Ca(OH)_2 + H_2SO_4 \rightarrow CaSO_4.2H_2O \ (\text{gypsum}) \tag{4.1}$$

$$3CaO.2SiO_2.3H_2O + H_2SO_4 \rightarrow CaSO_4.2H_2O + Si(OH)_4 \tag{4.2}$$

$$3CaSO_4 + 3CaO.Al_2O_3.6H_2O + 25H_2O \rightarrow 3CaO.Al_2O_3.3CaSO_4.31H_2O \ (\text{ettringite}) \tag{4.3}$$
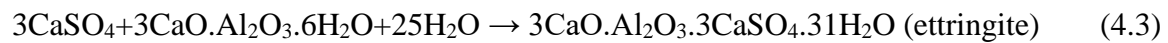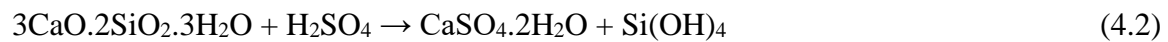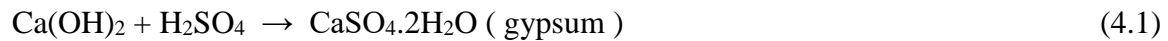
In order to understand the influence of H_2SO_4 on multi-blended cementitious composites thermogravimetric analysis (TG-DTG) was carried out. Figure 4.24 demonstrates TG and DTG plots for all the blended cementitious mixes exposed to H_2SO_4 solution for the period of 180 days.
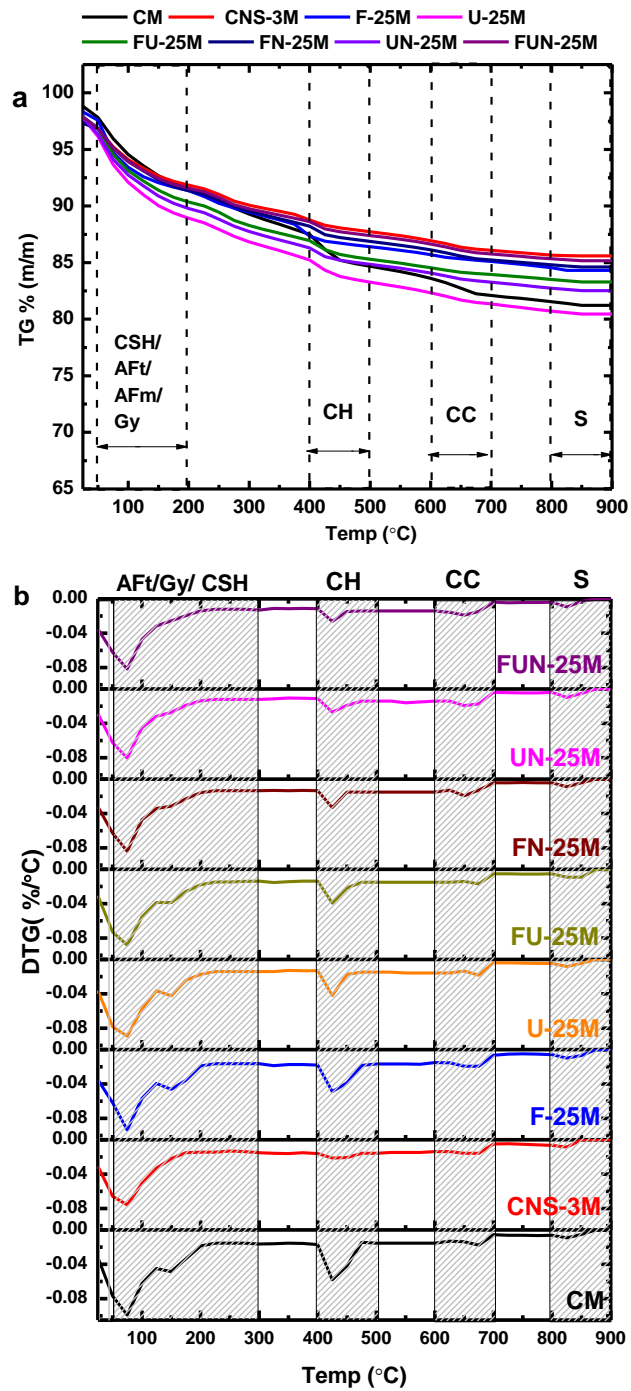
Figure 4.24: a) TG and b) DTG plots for control, binary, ternary and quaternary blended cementitious mixes exposed to H₂SO₄ solution for the duration of 180 days

It can be observed from the Fig. 4.24a that mass loss takes place at various temperature boundaries for cementitious mixes exposed to H_2SO_4. The mass loss occurred at a particular range of temperature is due to the decomposition of more than one compound. However, identification of endothermic peaks through differential thermogravimetric curve (DTG) gives clear indication of the presence of different compounds at specific temperature ranges (Figure 4.24b). Endothermic peaks at temperature boundaries of 25-50 °C, 150-300 °C, 400-500 °C and 600-700 °C signifying the loss of free water molecules, dehydration of chemically bound water from calcium silicate hydrates(CSH), dehydroxylation of calcium hydroxide (CH) and decarbonation of calcium carbonate (CC), respectively. Further, endothermic peaks at 50-120 °C and 120-150 °C indicates the dehydration of compounds such as ettringites (AFt) and gypsum (Gy), respectively that are more prominently seen in specimens subjected acid and alkali exposure (Chen et al., 2000). Existence of mass loss at temperature beyond 800 °C designates the decomposition of sulfates (S), specifically seen in specimens consisting of sulfate ions (Chen et al., 2000).

From the genesis of TGA results it can be understood that diffusion action of H_2SO_4 into cementitious system leads to the disbanding of Portlandite (CH) and forms gypsum an ettringite. To know the extent of deterioration of blended cementitious mortar exposed to H_2SO_4 solutions, amount of voluminous products formed due to H_2SO_4 exposure i.e. AFt and Gy were quantified on the basis of obtained TG mass losses at specific range of temperatures using the Equation 3.10 and Equation 3.11, respectively (Chen et al., 2000).

Figure 4.25 shows the quantified amount of AFt and Gy for all the mixes exposed to H_2SO_4 solution for the duration of 180 days.
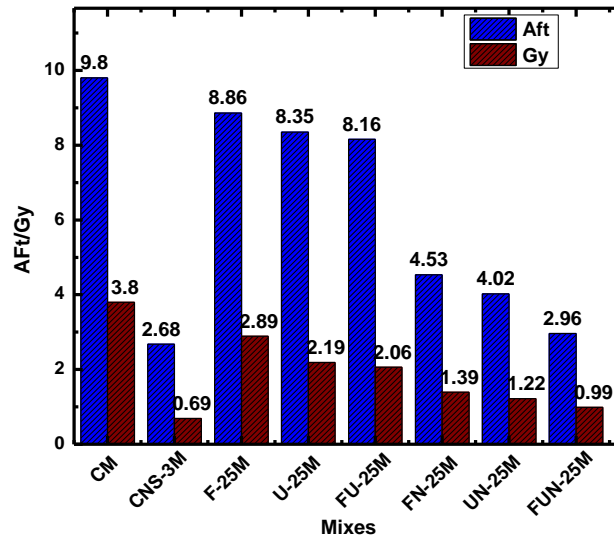
Figure 4.25: Quantified amounts of AFt and Gy for binary, ternary and quaternary mixes exposed to H₂SO₄ solution for 180 days

It can be observed from the figure that highest amount of AFt and Gy were formed for control mix, which is mainly allied to the greater concentration of CH due to the presence of high cement content. Hence, control mix is found to be more susceptible to deterioration by H_2SO_4. It can be observed from the figure that all the blended mixes shows lower amount of AFt and Gy as compared to that of control mix, which signifies the improved resistance to H_2SO_4. This was ascribed to the consumption of CH (foremost component targeted by sulfate ions) in blended cementitious composite mixes due to pozzolanic activity. Further, it was reported that less formation of AFt and Gy makes the cementitious system more stable and denser, thereby reduces the rate of compressive strength loss (Sahoo et al., 2017).

Among all the blended mixes, CNS-3M mix showed least formation of AFt and Gy compounds. This is mainly attributed to the fact that smaller particles of nano-silica accelerates the pozzolanic and hydraulic reactivity to greater extent than any other pozzolans and that aids in the formation of more stable C-S-H gel with improved microstructure (Kim et al., 2019). The optimistic resistance in formation of AFt and Gy was also found to be offered by other blended mixes, especially for ternary and quaternary

blended mixes consisting of nano-silica. The reasons associated to this could be as follows, a) improved particle packing density by the use of micro to nano sized finer particles, which minimizes permeable porosity and b) better-quality pozzolanic activity due to the presence of nano-silica, hence, improves the microstructure (Wang et al., 2016b)

It is important to point out that quaternary blended mix (FUN-25M) performed approximately similar to CNS-3M mix. Quaternary blended mix is found be more sustainable as the total replacement level of OPC here is 25%, whereas, CNS-3M mix could replace OPC only up to 3%.

4.3.5.3.1.2 Length change

Length change in terms of micro strain was measured for control and other multi-blended mixes exposed to H_2SO_4 solution at different exposure periods of 1, 3, 7, 14, 30, 60, 90, 120 and 180 days. The same are graphically represented in Figure 4.26.
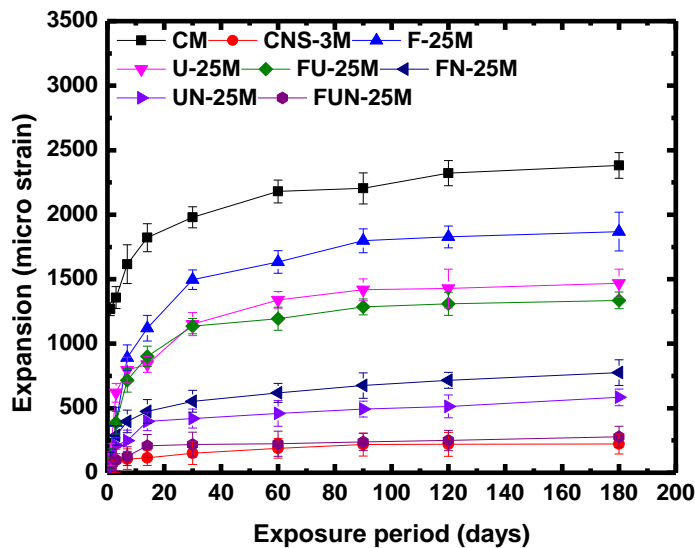
Figure 4.26: Length change for control and other multi-blended mixes exposed to H_2SO_4 solution at different exposure periods

It can be seen from Figure 4.26 that when specimens were exposed to H_2SO_4 solution, volume of all the samples found to increase due to the formation of expansive compounds such as gypsum (Gy) and etrringite (AFt). It is reported that the volume of ettringite is around seven times more than that of initial hydration compounds (Monteny et al., 2000).

Highest expansion was observed for control mix and the expansion strain was found to be around 2500 micro strain. This is attributed to the larger amount of Gy and AFt compounds (Figure 4.25) formed due to the reaction between sulfate ions from H_2SO_4 and CH.

Rate of expansion found to be reduced for all the blended mixes comprising of pozzolanic materials. CNS-3M was found to be the most resistant mix to expansion against H_2SO_4 exposure. Expansion value of CNS-3M mix for the exposure period of 180 days was found to be 130 micro strain, which is 95% lesser to that of control mix. The reason associated to this could be the development of densified microstructure in cementitious mortar due to the superior pozzolanic and nano-filler action of nano-silica. This mechanism restricts the easy diffusion of sulfate ions into the cementitious matrix, which significantly reduces the formation of Gy and AFt products (Figure 4.25).

In case of ternary (FN and UN mixes) and quaternary (FUN mixes) blended cementitious mixes comprising of superiorly performed nano-silica showed significant improvement in resistance to volumetric changes. Expansion rate for FN-25M, UN-25M and FUN-25M mixes at the exposure period of 180 days was found to be reduced by 79%, 88% and 94%, respectively in correspondent to that of control mix. Presence of small percentage of nano-silica in blended cementitious mixes tremendously reduces the formation of Gy and AFt (Figure 4.25), which results in significant drop in expansion strains.

4.3.5.3.2 Exposure to alkali (Na_2SO_4) solution

4.3.5.3.2.1 Density loss and strength loss

Density and strength losses underwent by control and blended mortar specimens exposed to 5% sodium sulfate (Na_2SO_4) solution for 30, 60, 90, 120 and 180 days are presented in Figure 4.27.
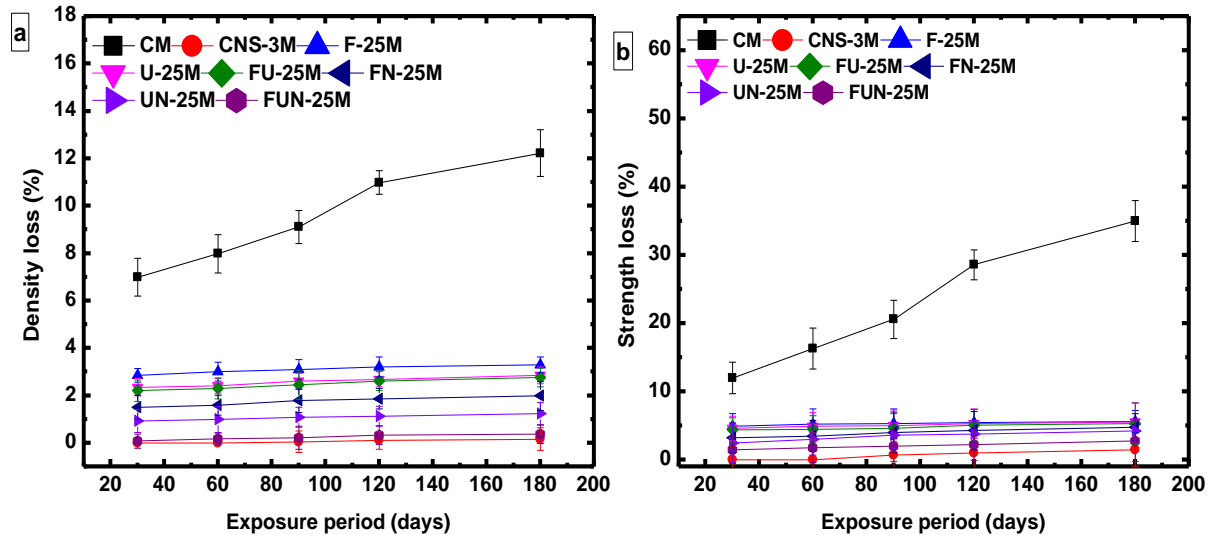
Figure 4.27: **Variation in a) density loss and b) strength loss percentage of blended cementitious mortar exposed to sodium sulfate (Na$_2$SO$_4$) for the period of 30, 60, 90, 120 and 180 days**

Similar trend of density and strength losses as like acid (H$_2$SO$_4$) exposure was observed for alkali (Na$_2$SO$_4$) exposure condition. But, intensity of losses were found to lesser to that of acid exposure. Control mortar showed highest value of density loss (12.5% at 180 days) and strength loss (35% at 180 days) among all the mixes. Density loss and strength loss for blended mortar mixes were found to be minimal as compared to that of control mix due to the presence of Pozzolans.

Among all the blended mixes CNS-3M mix showed lowest deterioration to Na$_2$SO$_4$ exposure. Density loss and strength loss experienced by CNS-3 mix was found be reduced by 99% and 94%, respectively with respect to control mix at the exposure period of 180 days. It can be understood from the results that use of SCMs in combination with nano-silica in the form of ternary and quaternary blends showed significant improvement in resistance to Na$_2$SO$_4$ exposure. Density loss and strength loss for quaternary blended mortar mix (FUN-25M) was seen to be lowered by 98% and 92%, respectively with respect to control mix at the exposure period of 180 days.

Ingression of sodium sulfate (Na_2SO_4) into cementitious medium undergoes sulfate attack in alkaline media. Distress caused by Na_2SO_4 exposure in cementitious composites is due to the development of expansive pressure due to formation of reaction products with relatively greater molar volume (Monteny et al., 2000). Diffusion of Na_2SO_4 into cementitious system undergoes sequence of chemical reactions as follows (Neville, 2008).

$2(3CaO.Al_2O_3.12\,H_2O) + 3(Na_2SO_4.2H_2O) \rightarrow 3CaO.Al_2O_3.3CaSO_4.31H_2O$ (ettringite)

$$+ 2Al(OH)_3 + 6NaOH + 17H_2O$$

$$(4.4)$$

$Ca(OH)_2 + Na_2SO_4.10\,H_2O \rightarrow CaSO_4.2H_2O$ (gypsum) $+2NaOH + 8\,H_2O$ \hfill (4.5)
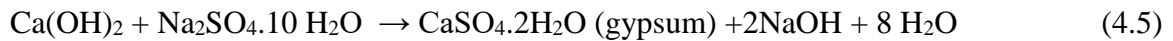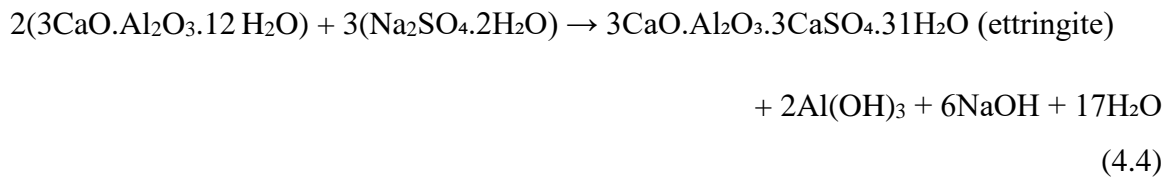
To identify the formation of Gy and AFt, TG-DTG analysis was carried out for Na_2SO_4 exposed cementitious samples. Figure 4.28 shows the TG-DTG plots for all the blended mixes exposed to Na_2SO_4 for the period of 180 days. For blended mixes exposed to Na_2SO_4 solution variation in TG-DTG curves were seen to be similar to H_2SO_4 exposure.
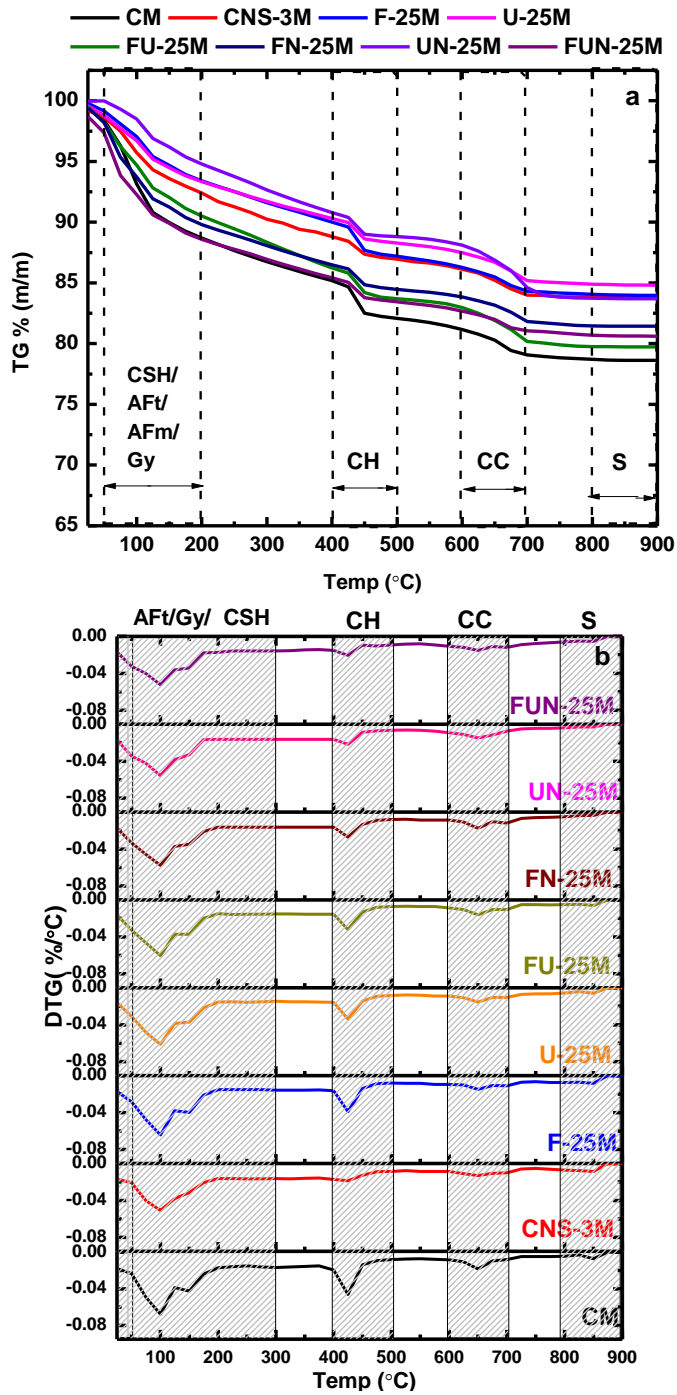
Figure 4.28: a) TG and b) DTG plots for control, binary, ternary and quaternary blended cementitious mixes exposed to Na₂SO₄ solution for the duration of 180 days

132

It can be observed from the Figure 4.28 that Na_2SO_4 attacked cementitious composites shows mass loss at various temperature boundaries of 25-50 °C, 50-300 °C, 50-120 °C, 120-150 °C, 150-300 °C, 400-500 °C, 600-700 °C and above 800°C, indicating the existence of free water molecules, ettringite (AFt), gypsum (Gy), portlandite (CH), calcium carbonate (CC), and sulfates (S), respectively similar to that of samples attacked by H_2SO_4.

Amount of AFt and Gy formed due to the action of Na_2SO_4 attack at the exposure period of 180 days were quantified using the Equations 3.10 and 3.11, respectively and the same are graphically presented in Figure 4.29.
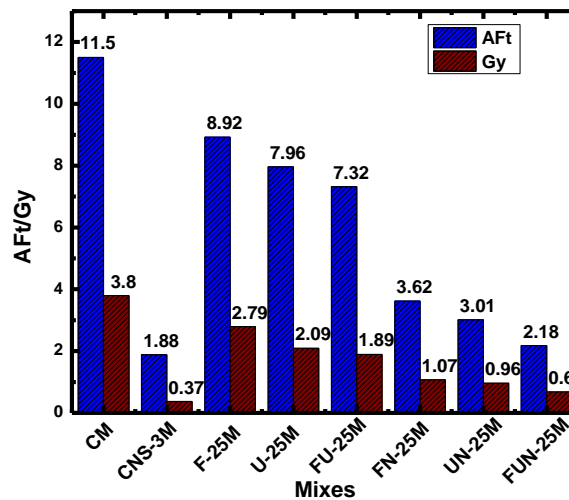
Figure 4.29: Quantified amounts of AFt and Gy for binary, ternary and quaternary mixes exposed to Na₂SO₄ solution for 180 days

It can be noticed from the figure that amount of Gy formed is much lesser as compared to the amount of AFt. Reason associated to this is that sulfate ions present in Na_2SO_4 solution starts reacting immediately with aluminate phases of cementitious system and possibly leads in the formation of AFt. Na_2SO_4 also undergoes similar chemical reactivity as like H_2SO_4 in cement system but are less hostile as it occurs in alkaline environment (pH>12.5). Control mix showed greater amount of AFt and Gy content. This is mainly due to the presence of high cement content possessing larger percentage of C_3A and CH component, which thereby makes the cementitious mortar more vulnerable to sulphate ions. Dissolution and decalcification of aluminate phases and CH leads to the development of reaction

products such as AFt and Gy, respectively owing to its chemical reaction with sulfate ions as shown in Equations 4.4 and 4.5 (Neville, 2008).

Use of Pozzolans in cementitious mortar in the form of binary, ternary and quaternary blends showed reduced formation of AFt and Gy that designates the improved resistance to sulfate ions. CNS-3M mix offers excellent resistance to sulfate attack showing significant drop in AFt and Gy values i.e. 83% and 90%, respectively with respect to control mix at 180 days of exposure. This was attributed to the densified microstructure instigated through the dual performance of nano-silica in cementitious system i.e. hasty reactivity with nucleation effect and nano-filler effect. Other multi-blended cementitious composites also showed resistance against sulfate attack. However, blended cementitious mixes comprising of nano-silica tremendously reduced the production of AFt and Gy i.e at the rate of 69%-81% and 71%-82%, respectively in correspondence to control mix at the exposure period of 180 days. This could be attributed to the facts that a) advanced pozzolanic activity in different scale (micro to nano), b) dense particle packing by filling up the nano sized pores and c) densified microstructure at the crucial points of interfacial transition zone (ITZ) owing to the improved binding ability (Sabry, 2013).

4.3.5.3.2.2 Length change
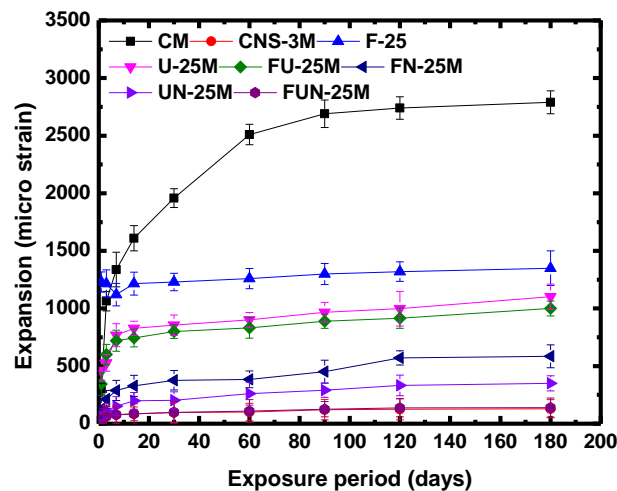
Figure 4.30: Length change associated to Na$_2$SO$_4$ solution at various exposure periods

Rate of length change for control and multi-blended mortar mixes exposed to 5% Na_2SO_4 solution are graphically represented in Figure 4.30. It can be seen from the figure that all the mixes, with and without Pozzolans were prone to expansion due to Na_2SO_4 exposure. It can be observed from the figure that pattern of length change curve for specimens exposed to Na_2SO_4 solution were seen to be similar to sulfuric acid effect. However, extent of expansion is quite high in Na_2SO_4 solution, since at the first introduction of sulfate ions into cementitious system it reacts with aluminates to form expansive solid phase i.e ettringite (AFt). Maximum expansion was seen for control mix i.e. about 2800 micro strain at 180 days of exposure period. The reason linking to this fact is the excessive formation of voluminous AFt and Gy, which is being promoted due to dissolution and decalcification of aluminates and portlandite (CH) (Chaudhary and Sinha, 2018).

Expansion rate found to reduce drastically for all blended mixes. It is well known fact that addition of Pozzolans could reduce proneness to Na_2SO_4 significantly. It could be attributed to following reasons (Al-Amoudi, 1999), i) amount of tri-calcium aluminate, gets reduced considerably; ii) CH get converted into stable CSH through pozzolanic reaction and thereby improves matrix characteristics; iii) ettringite turns into less expansive product owing to the reduction in pH value; and iv) formation of supplementary CSH compounds gets adsorbed on the surfaces of aluminates and other reactive phases, thus obstructing the development of secondary and final ettringite. For 180 days of exposure period, rate of expansion values for CNS-3M, F-25M, U-25M, FU-25M, FN-25M, UN-25M and FUN-25M were found to be 110 micro strain, 1468 micro strains, 1300 micro strains, 1280 micro strain, 476 micro strain, 254 micro strain and 115 micro strain, respectively. It can be noted that amongst all the blended mixes, binary blended CNS-3M mix showed superior resistance to expansion caused due to Na_2SO_4 exposure. It can also be seen from the figure that ternary (FN-25M and UN-25M) and quaternary blended (FUN-25M) mixes composed of nano-silica enhanced the resistance to expansion caused by sulfate attack than blended mixes without nano-silica.

4.3.5.3.3 Exposure to chloride (NaCl) solution

4.3.5.3.3.1 Density loss and strength loss

Figure 4.31 presents the variation in density loss and strength loss of cementitious mortar mixes exposed to 5% sodium chloride (NaCl) solution for the period of 30, 60, 90, 120 and 180 days.
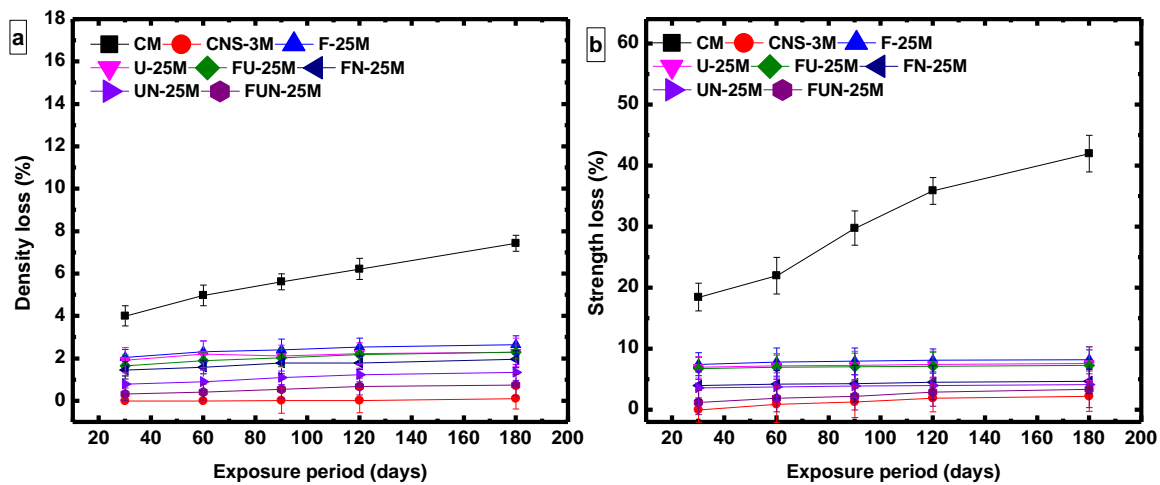
Figure 4.31: Variation in a) density loss and b) strength loss percentage of blended cementitious mortar exposed to sodium chloride (NaCl) for the period of 30, 60, 90, 120 and 180 days

It can be seen from Figure 4.31 that the trend in variation of density loss and strength loss for specimens exposed to 5% NaCl solution found to be similar to acidic and alkaline exposure. Control mix showed consistent rise in density and strength losses with respect to exposure period. Amid all the mixtures and highest percentage of density loss (7.5% at 180 days) and strength loss (42% at 180 days) amid all the mixtures. The effect of chloride on all blended mortar found to be very low as compared to that of control mix. Binary blended CNS-3 mix showed least percentage of density loss and strength loss compared to that of all other blended mixes i.e. 0.1% and 2.2% at 180 days of exposure period. It must be noted that FA and UFFA based ternary (FN-25M and UN-25M) and quaternary (FUN-25M)

136

blended mixes incorporated with nano-silica showed significant drop in deterioration compared to that of other blended mixes without nano-silica.

It is to be noted that the moment when NaCl solution permeates into the cementitious mixes, chloride ions reacts with unhydrated (C_3A or C_4AF) and hydrated (AFm) forms of aluminate phases to form Friedel's salt (Fs) and its analogues, this formation of Fs due to chloride binding in cementitious mixes is mainly depends on C_3A and C_4AF components in cement (Suryavanshi et al., 1996; Glass and Buenfeld, 2000; Kim et al., 2016). Chemical reaction involved between NaCl and component of C_3A is as follows (Suryavanshi et al., 1996).

$$Ca(OH)_2 + 2NaCl \rightarrow CaCl_2 + 2Na^+ + 2OH^- \qquad\qquad (4.6)$$

$$C_3A + CaCl_2 + 10H_2O \rightarrow C_3A.\ CaCl_2.\ 10H_2O \text{ (Friedel's salt)} \qquad (4.7)$$

$$C_3AF + CaCl_2 + 10H_2O \rightarrow C_3F.\ CaCl_2.\ 10H_2O \text{ (Friedel's salt iron analogue)} \qquad (4.8)$$
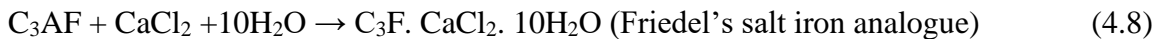
Reaction also takes place when chloride ion comes in contact with hydrated phase of aluminate i.e. AFm, where, sulfate ions gets replaced by chloride ions to form Friedel's salt (Suryavanshi et al., 1996).

$$2Cl^- + 3CaO.\ Al_2O_3.\ CaSO_4.\ 10\ H_2O \rightarrow 3CaO.\ Al_2O_3.\ CaCl_2.\ 10\ H_2O + SO_4^- \qquad (4.9)$$
$$\text{(Friedels salt)}$$
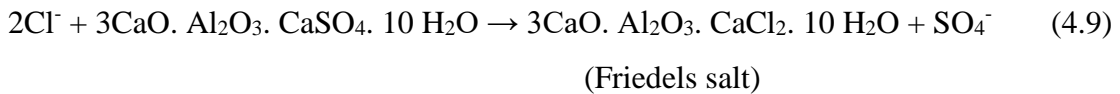
To characterize the influence of NaCl on blended cementitious samples thermogravimetric analysis (TG-DTG) was carried out for the samples exposed to the duration of 180 days and the same are presented in Figure 4.32.
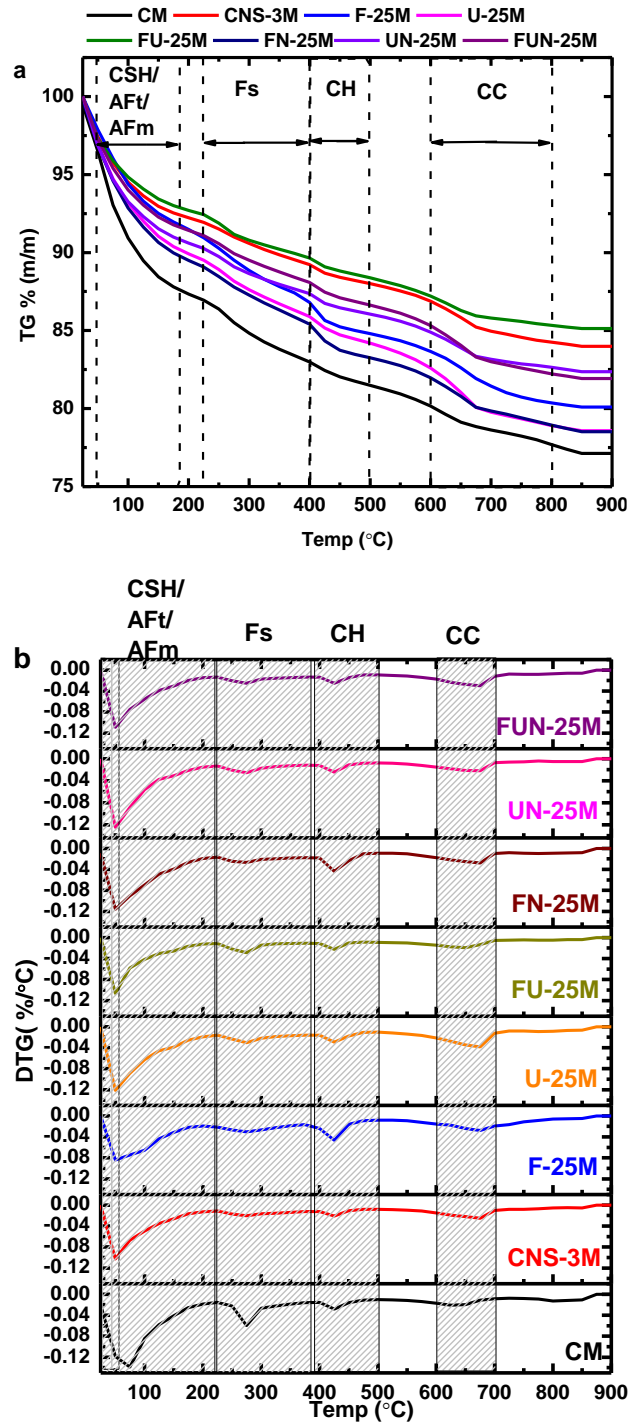
Figure 4.32: a) TG and b) DTG plots for control, binary, ternary and quaternary blended cementitious mixes exposed to NaCl solution for the duration of 180 days

It can be observed from the Figure 4.32 that thermogravimetric changes takes place at various ranges of temperature. Figure 4.32b shows the endothermic peaks at the temperature ranges of 25-50 °C, 50-300 °C, 230-380 °C, 400-500 °C and 600- 700 °C, which signifies the loss of free water molecules, dehydration of CSH/AFt/Fs, dehydration of Friedel's salt (Fs), dehydration of portlandite (CH) and decomposition of calcium carbonates, respectively. Endothermic peak observed at the temperature boundary of 230-380 °C, which indicates the formation of Friedel's salt is attributed to the loss of 6 moles of water (main layer water) from total 10 moles of water. While, rest 4 moles of water (interlayer water) loss from Friedel's salt is lost below 200 °C. However, amount of Fs formed can be quantified by determining the mass loss of 6 molecular main layer water from Fs at 230-380 °C (Glass and Buenfeld, 2000). Friedel's salt content (Fs, %) in cementitious mixes exposed to chloride ions was calculated using the Equation 3.12.

The amount of chemically bound Fs content in cementitious mixes exposed to 5% NaCl solution for 180 days is shown in Figure 4.33.
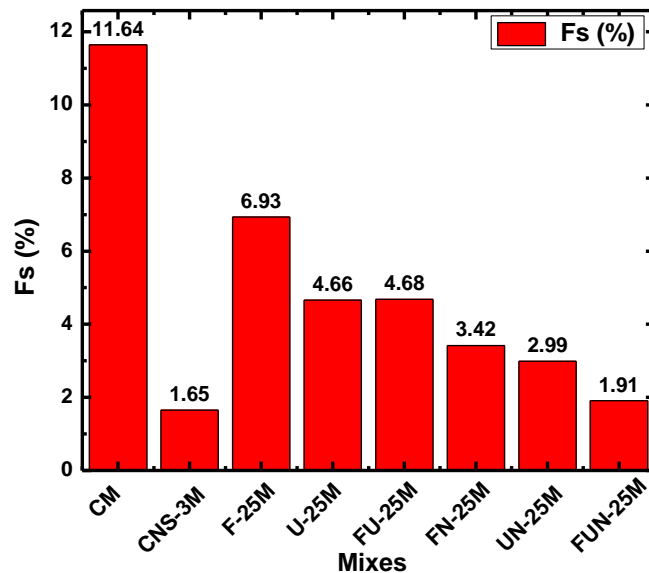
Figure 4.33: Quantified amount of Fs for binary, ternary and quaternary mixes exposed to NaCl solution for 180 days

Results shows that amount of Fs formation for control mix is higher than that of other blended cementitious mixes. This is due to the presence of maximum OPC fraction in

cementitious mix that contains larger proportion of aluminate phases (C_3A, C_4AF and AFm), which results in higher rate of chloride binding (i.e. > Fs formation). Further, higher concentration of portlandite (CH) in control mix leaches out with the ingress of NaCl solution, thereby adds in the increment of Fs content (Suryavanshi et al., 1996). Chloride ions are also known to interact with C-S-H at three stages i.e. as chemisorbed layer on surface of C-S-H, occupy the interlayer spaces in C-S-H and intimate bounding with lattice of C-S-H (Bosque et al., 2014). Even though, formation of Fs (chloride binding) reduced the migration force of chloride ion towards the embedded steel causing corrosion, decalcification and physical adsorption effect of chloride ions on hydration products weakens the microstructure of cementitious mixes by making the system more porous (Qiao and Suraneni, 2018). Further, it is to be noted that in laboratory high concentrated (5%) salt solutions is attacking the cementitious mortar continuously for the long period of 180 days, which is harsh and that is the reason for the formation of larger percentage of Fs (Sahoo et al., 2019).

Inclusion of pozzolanic materials as a partial replacement to cement showed significant reduction in the formation of Fs. Substantial drip in Fs content among all the mixes was observed for CNS-3M mix composed of 3% of nano-silica. This can be attributed to following factors: a) high rate of reactivity (hydraulic and pozzolanic) rate of nano-silica supported the formation of additional dense CSH, in addition to that nano-filler effect also supplemented in tailoring the microstructure of cementitious mixes by making the system least permeable, b) declination in pH value of pore solution (CH↓), and c) attenuation of C_3A content [21]. Utilization of Pozzolans such as FA and UFFA in the form of binary (F-25M and U-25M) and ternary (FU-25M) blended cementitious mixes also showed reduction in the formation of Fs. It is due to the fact that addition of SCMs has a promising role in enhancing the chemical stability and helps in reducing the detrimental changes in chemical phases of cementitious system.

It can be noted from the figure that small percentage of nano-silica in combination with FA or/and UFFA in the form of ternary (FN-25M and UN-25M) and quaternary (FUN-25M) blends showed improved reduction in Fs content than that of mixes without nano-silica.

140

This ascribed to the optimistic modification by nano-silica in cement hydration process by means of seeding effect, superior pozzolanic activity and accelerated hydration of C_3A at the early stage of hydration (Bosque et al., 2014). This could minimize the unreacted C_3A and CH availability at later age making the system less prone to chloride salt attack. Further, nano-scale impact due to the presence of nano-silica particles greatly modifies the micro-meso-macroscale behaviors of cementitious composites and makes the material more durable, strong and smart.

4.3.5.3.3.2 Length change

Variation in length change of control and blended cementitious mortar mixes exposed to 5% NaCl solution for the duration of 1, 3, 7, 14, 30, 60, 90, 120 and 180 days are presented in Figure 4.34.
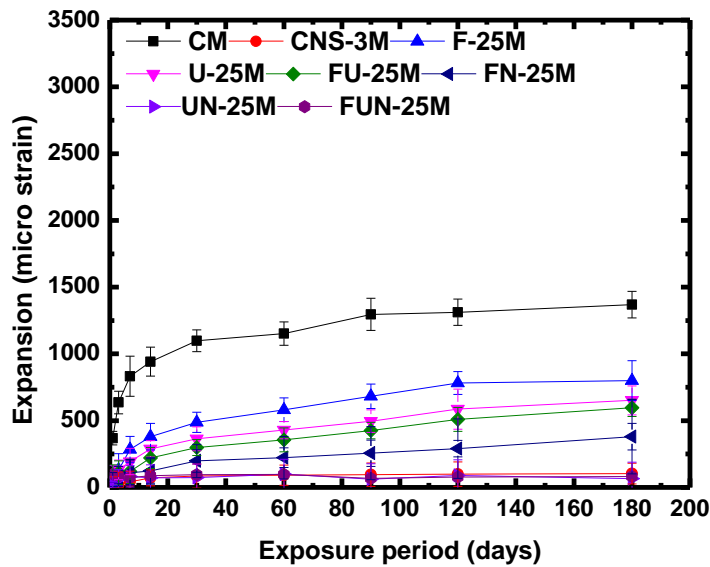
Figure 4.34: Length change associated to NaCl solution at various exposure periods

It can be seen from Figure 4.34 that when cementitious mixes exposed to 5% NaCl solution, all the mixes showed expansion over the period of exposure. The highest expansion (1300 micro strain at 180 days) was observed for control mix as chloride diffusivity is very high for 100% OPC mix. Major reason for the increased expansion could be due to binding of chloride ions with hydrated and unhydrated phases of C_3A and C_4AF to form voluminous

Fs (Figure 4.33). Even though, this is a beneficial reaction to avoid the deleterious effects of reinforcement corrosion caused by free chloride ions in pore solution, crystallization of Fs through chloride binding lead to expansive stresses. It is to be noted that hydration of unhydrated phases in cementitious mixes and the formation of Fs might be the two major possibilities that causes expansion in cementitious mixes when it gets interacted with NaCl solutions. Continuous exposure to chlorides media would contribute to cracking and ultimately deterioration of the reinforcement in structures.

Similar to other chemical exposure conditions, blended cementitious mortar exposed to NaCl solution also showed better resistance to volume change than that of control mix. CNS-3M mix showed least expansion of around 100 micro strain at 180 days of exposure. High pozzolanic activity, better-quality conversion rate of CH into stable CSH gel, seeding effect and nano-filler effect of nano-silica in cementitious mixes minimized the penetration rate of chloride ions. For binary blended F-25M and U-25M mixes expansion rate was seen to be 806 micro strain and 652 micro strain, respectively which found to be lower to control mix. The reduced expansion in these mixes is mainly attributed to the dilution effect caused by FA or UFFA replacement to cement, more than its pozzolanic effect.

It is important to note that incorporation of nano-silica in FA and/or UFFA blended mixes boosted the resistivity against expansion caused due to NaCl solution. This can be attributed to the presence of superior pozzolanic material i.e. nano-silica, which tailored the microstructure of cementitious mix along with the packing effect.

4.4 BLENDED CEMENTITIOUS PASTE

4.4.1   Setting time and surface temperature

The setting time of binary, ternary and quaternary blended cement pastes integrated with colloidal nano-silica are presented in Figure 4.35 to Figure 4.36.
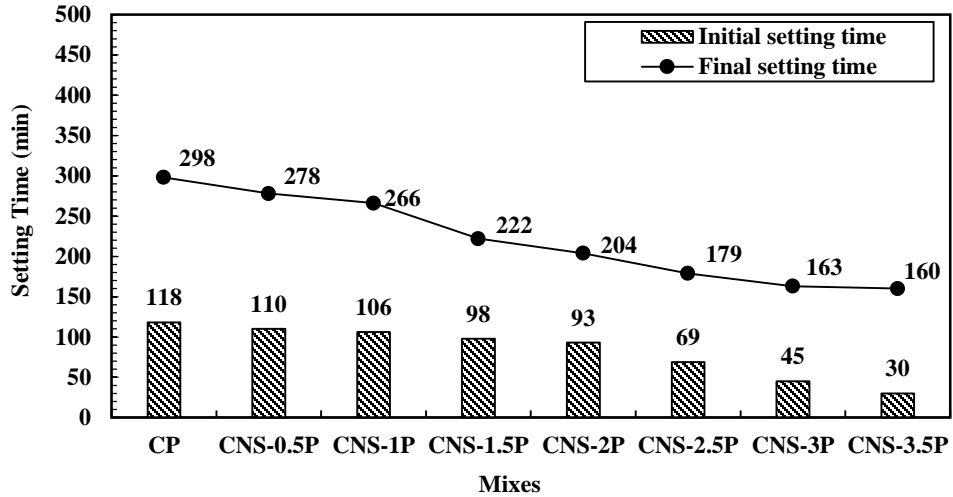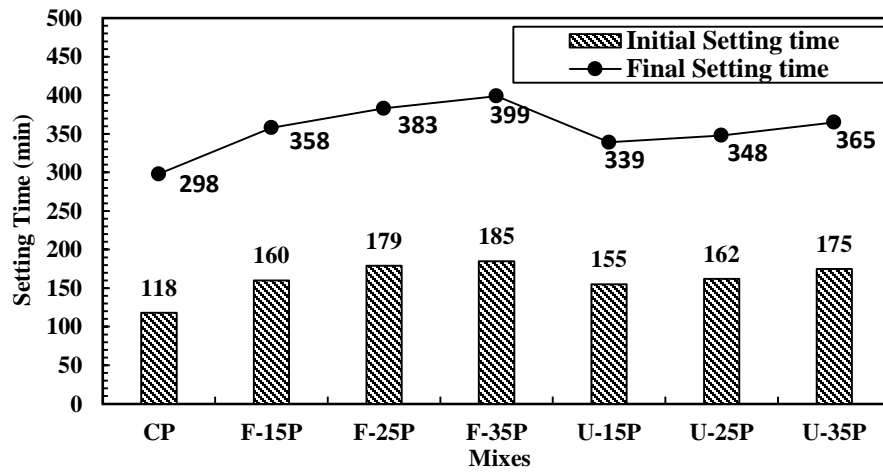
Figure 4.35: Setting time of binary blended a) CNS b) F and U cement paste mixes

It can be observed from the Figure 4.35a that there is a significant decline in initial and final setting time with increase in the content of nano-silica. Flash setting was observed after the replacement level of 3.5% nano-silica and hence not reported here. This accelerating effect in setting time of cement paste incorporated with nano sized silica particles can be attributed to the reduction in dormant period, faster rate of pozzolanic reactivity and hydration (Chithra et al., 2016).

Results indicated the increased initial and final setting time for binary blended F mixes i.e. at the rate of 36%-57% and 21%-34%, respectively with respect to that of control. This

may be attributed to slower initial pozzolanic reaction of fly ash particles. Whereas, in case of binary blended mixes consisting of ultra-fine fly ash particles, setting time was observed to be reduced with respect to F mixes, however, found to be greater than that of control. The percentage of delay in setting time for U mixes ranged between 30%-48% (initial setting time) and 14%-22% (final setting time). This reduced setting time of U mixes with respect to F mixes may be ascribed to the proliferated reactivity of ultra-fine fly ash particle as compared to that of fly ash particles (Obla et al., 2003)
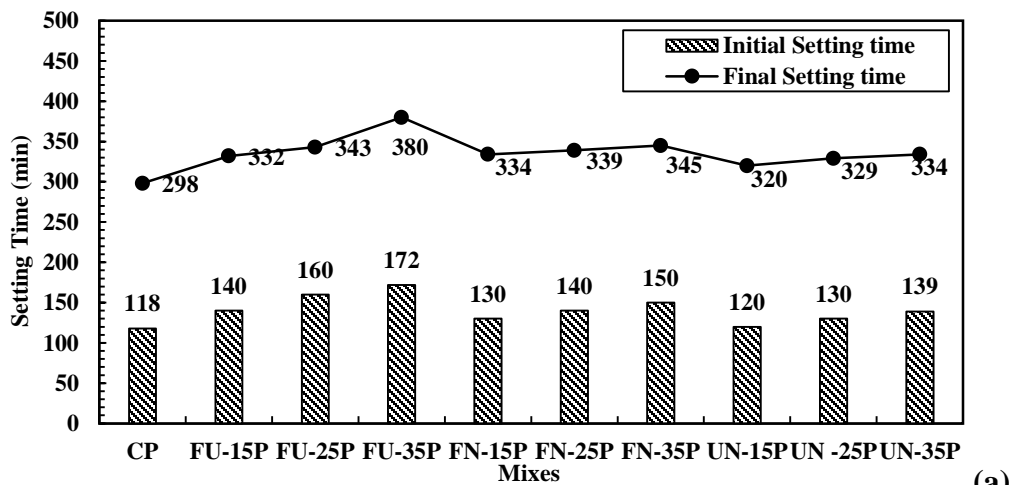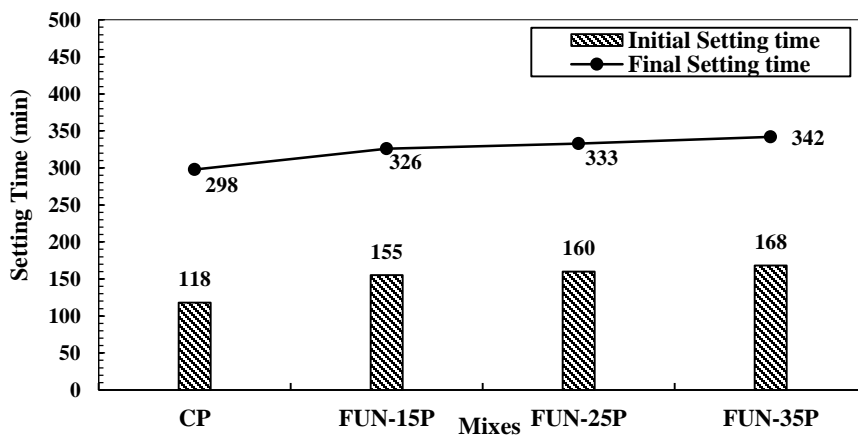
Figure 4.36: Setting time of a) ternary (FU, FN and UN) and b) quaternary blended (FUN) cement paste mixes

Figure 4.36a shows that compared to the control paste, ternary blended FU cement paste mixes proliferated the setting time by 18-40% in proportional to the percentage of

144

replacement. This retarding effect in setting time particularly with enhanced percentage of replacement can be ascribed to the dilution effect and slow rate of hydration (Hannesson et al., 2012). Whereas, nano-silica admixed FA and UFFA based ternary blended paste (i.e., FN and UN) exhibited the tailoring effect in setting time by balancing the retardation effect of FA and UFFA. The delay in initial setting time of FN and UN cement blends compared to control paste were seen to be between 8.5%-22% and 2.5%-22.8%, respectively. However, quaternary blended paste also showed similar trend of setting time as CNS admixed ternary blends i.e. percentage of delay in initial setting time ranged between 5.9% -23.7% (Figure 4.36b).

The results of surface temperature variation during setting time of binary blended cement pastes integrated with CNS is represented in the Figure 4.37.
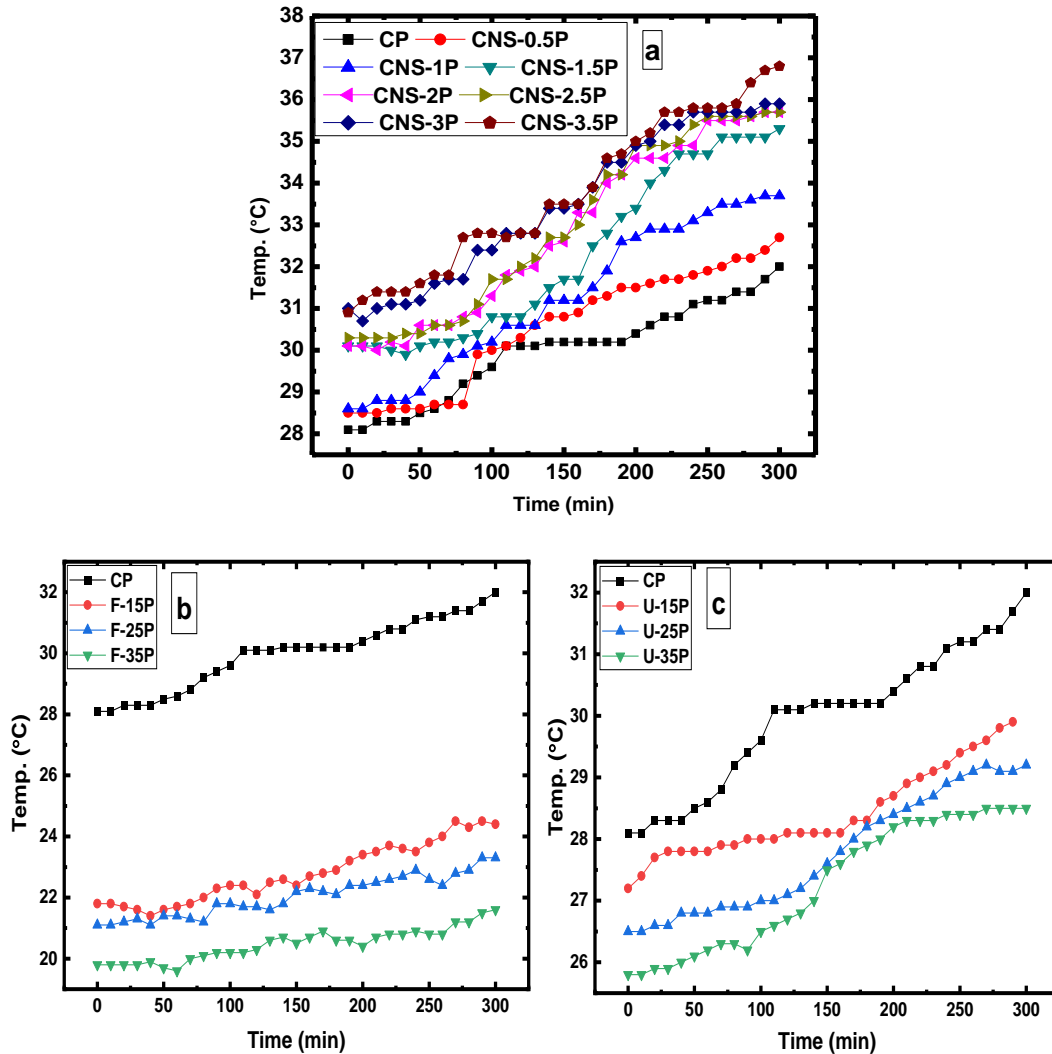
Figure 4.37: Surface temperature variations of binary blended cement a) CNS b) F and c) U paste mixes during the period of setting time

It can be noted from the Figure 4.37a that with increase in nano-silica content, surface temperature of cement paste increased substantially from the initial stage itself. For instance, initial rise in temperature of control paste is about 28 ℃ while, for CNS-3P mix, rise in temperature was found to be 31 ℃. It can be observed from the figure that pattern of rise in surface temperature is similar in correspondence to all binary CNS mixes. The reason behind this may be due to superior pozzolanic reactivity of nano-silica promoting

to faster hydration reaction, which may lead to higher heat liberation (Yu et al., 2014; Chithra et al., 2016). While, for all binary blended F mixes (Figure 4.37b) initial and peak surface temperature found to be much lower as compared to that of control that is in the range of 19 ℃-21.6 ℃ and 21 ℃- 24℃, respectively. This can be attributed to the delayed reactivity and dilution effect of FA blended cement paste. Further, UFFA admixed binary blended cement paste also showed reduced surface temperature as compared to that of control mix but found to be higher to that of binary blended FA mixes. Initial and peak surface temperature of binary blended U mixes increased approximately by 5 ℃ to 6 ℃ with respect to FA mixes. The reason associated to this would be the reduced particle size of UFFA initiated the chemical reactivity early as compared to that FA particles.

The variation in surface temperature for ternary blended and quaternary blended cement paste during the period of setting time is depicted in Figure 4.38 (b-c) and Figure 4.39, respectively.
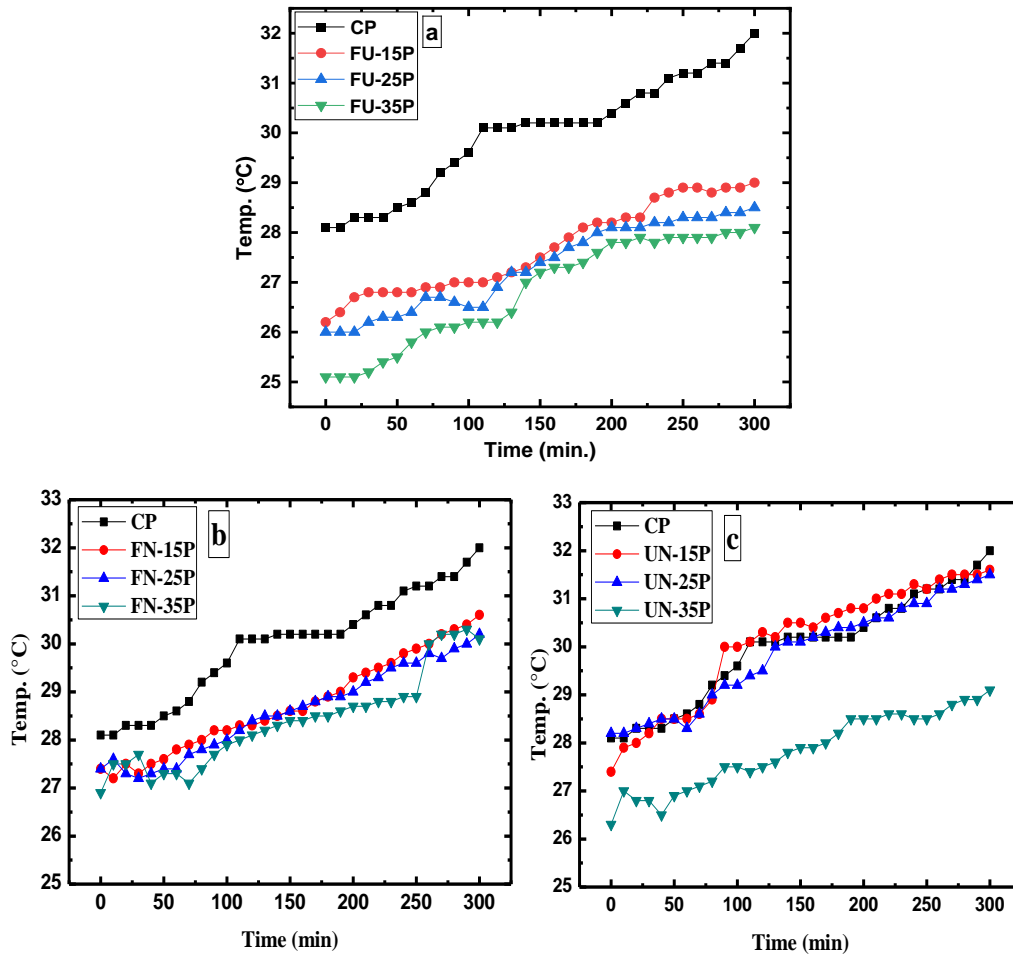
Figure 4.38: Surface temperature variations of ternary blended cement pastes during the period of setting time a) FU b) FN and (b) UN
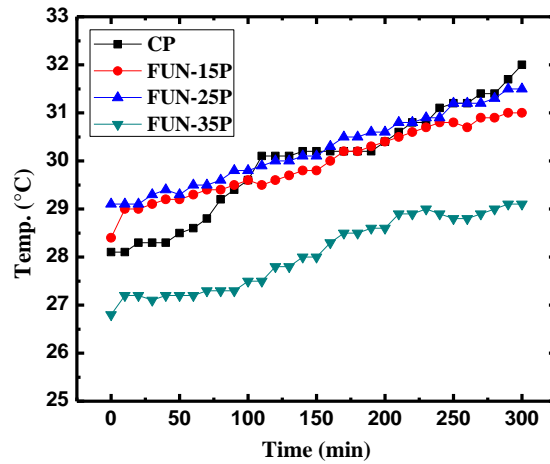
Figure 4.39: Surface temperature variations of quaternary blended FUN cement pastes during the period of setting time

It can be observed from the Figure 4.38a that for FU ternary blended paste mixes initial and peak surface temperature were also seen to be lower to that of control as like binary blended F and U mixes. It can be observed from the Figure 4.38 and 4.39 that nano-silica incorporated ternary and quaternary blends showed rise in surface temperature. Amongst all the nano-silica integrated blended paste, FN mixes showed lower peak temperature. This could be due to slow reactivity of FA particles, nevertheless presence of nano-silica played a role in slight increment in temperature. However, in case of nano-silica integrated ternary blended UN and quaternary blended FUN mixes (Figure 4.39b) the increase in surface temperature was noticeable compared to the ternary blended FN mixes. The peak temperature for ternary blended UN and quaternary blended FUN paste was found to be approximately similar to control paste. However, it is important to note that at replacement level of 35% for both UN and FUN mixes surface temperature was found to be lesser than that of control paste and the same could be attributed to the dilution effect and slow rate of hydration.

4.4.2 Workability

Influence of nano-silica on flow ability of binary blended cement paste is depicted in Figure 4.40a. It can be noticed from figure that increase in content of nano-silica in binary blended cement paste significantly reduced the flow diameter / flow value. The reason could be attributed to filling of voids by finer nano-silica particles, which lead to increased water demand as well as cohesion between the particles (Sneff et al., 2009; Yu et al., 2014).

Further, a subsequent drop in slump flow especially after nano-silica replacement level of 0.5% was modified by appropriate addition of superplasticizer to maintain stability of flow value with respect to control paste. The modified flow diameter and flow value of binary blended CNS cement paste with the aid of superplasticizer are represented in Figure 4.40b. It can be seen from the graphical representation that flow diameter of binary blend CNS cement paste modified with superplasticizer was maintained between 156 mm-157 mm.

The flow performance was observed to be increased for binary blended mixes containing FA and UFFA compared to that of control paste (Figure 4.41). This is attributed to the ball

bearing action of spherical shaped fly ash particles enhanced the flow ability (Copeland et al., 2001) However, UFFA showed an impact on flow properties and are noticed to be less workable compared to F mix owing to reduced particle size and increased specific surface area compared to that of FA particles.

(a)

(b)
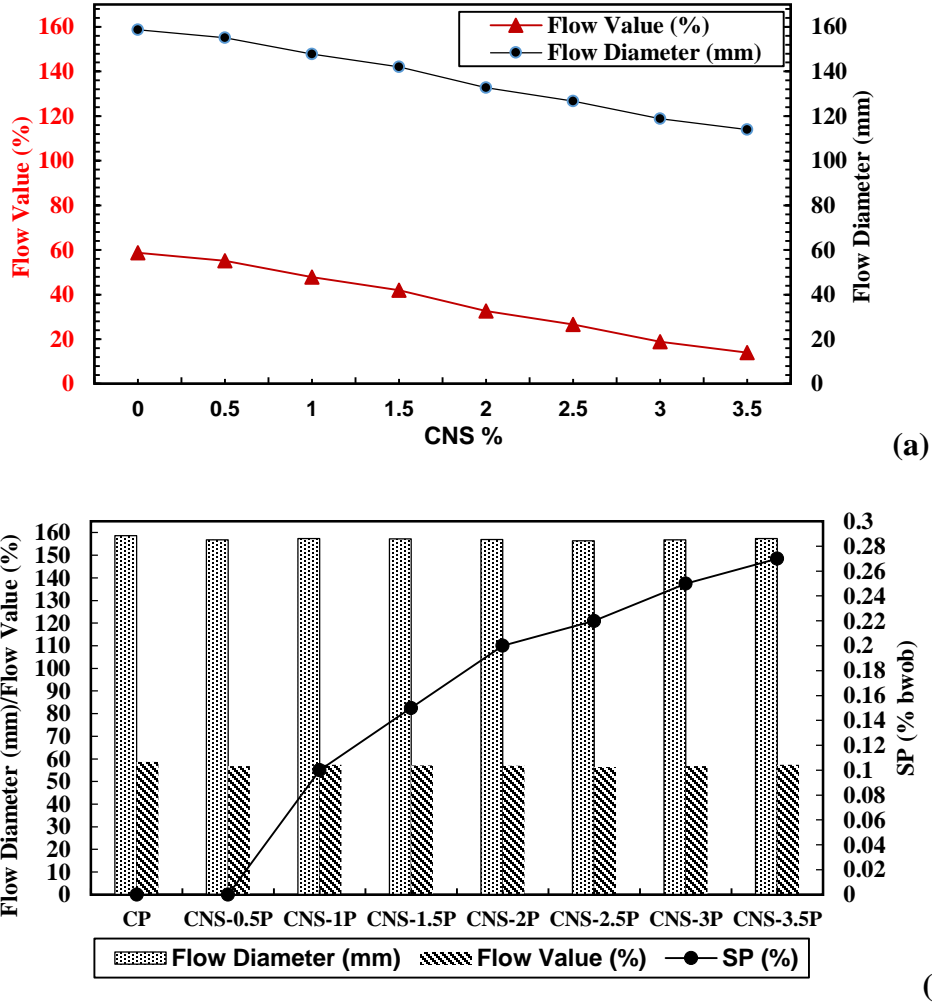
Figure 4.40: a) Influence of binary blend CNS cement paste on flow diameter and flow value b) Modified flow diameter and flow value of binary blend CNS cement paste
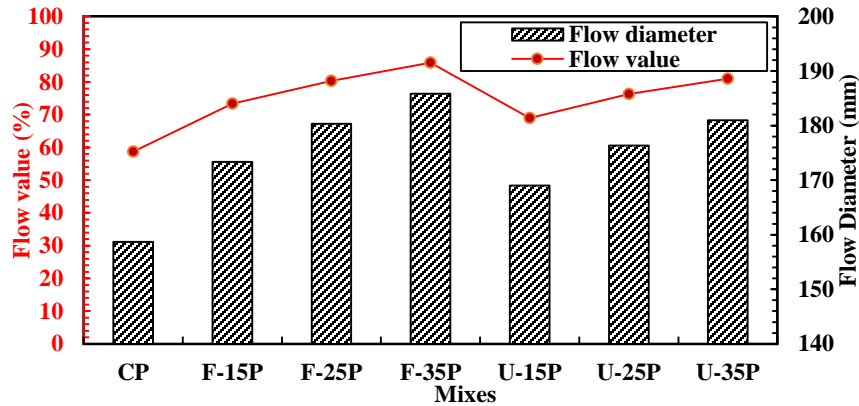
Figure 4.41: Influence of binary blended FA and UFFA cement paste mixes on flow diameter and flow value

The flow performance of ternary and quaternary blended cement paste is displayed in the Figure 4.42 (a-b).
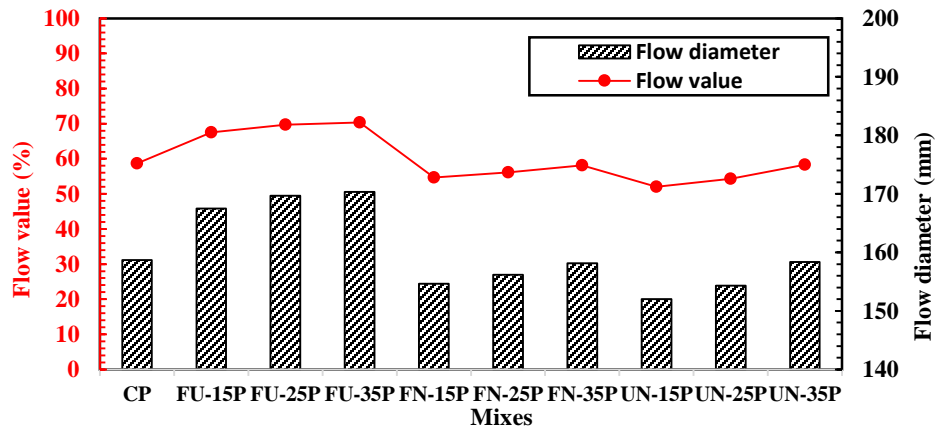
(a)
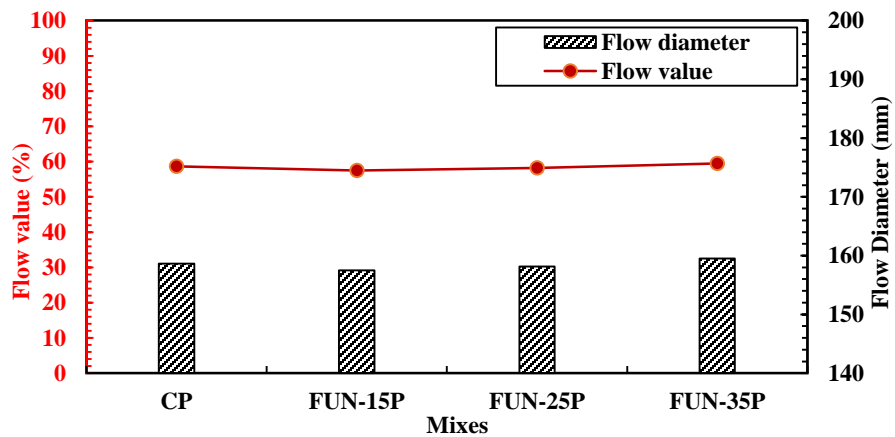
(b)

Figure 4.42: Influence of a) ternary (FU, FN and UN) and b) quaternary blended (FUN) cement paste on flow diameter and flow value

It can be noticed from the Figure 4.42a that the flow diameter/flow value improved in case of FU ternary blended paste than control mix. This may be attributed to the presence of spherical shaped FA and UFFA particles, which favoured the better workability performance (Copeland et al 2001). Whereas, the flow diameter/flow value for ternary blended pastes intermixed with nano-silica (i.e. FN and UN mixes) reduced marginally compared to that of control paste. This could be attributed to the larger surface area of nano-silica, which imbibes the water used for mixing thereby lowering the workability of cement paste (Hou et al., 2013, Chithra et al., 2016). However, it is noted that flow diameter of these mixes rests beyond 150 mm, which is closer to control paste without any addition of superplasticizer.

Furthermore, quaternary blended FUN mixes also showed the flow value nearby to the control paste in the range of 158 mm-160 mm (Figure 4.23b). Comparing Figure 4.40a and Figure 4.42 it can be understood that when the binary blend of CNS mixes are combined with FA/UFFA to form ternary and quaternary blends, the hindrance in workability of binary blends are stabilized. This can be attributed to ball bearing action of FA and UFFA particles (Obla et al., 2003; Yijin et al., 2004).

4.4.3 Chemical shrinkage

The chemical shrinkage results of binary blended cement paste admixed with different dosage of nano-silica at the ages of 1, 3, 7, 14, 28 and 56 days is presented in Figure 4.43a. Increased level of chemical shrinkage values was found for all binary mixtures of cement paste comprising of nano-silica. For instance, chemical shrinkage for CNS-3P was measured as 1.9, 2.8, 3.6 and 3.9 ml/100 gm at the age of 1, 3, 7 and 14 days, respectively and for control paste it is measured as 0.2, 0.7, 1.5, 2.1, 3.5 and 3.6 ml/100 gm at the age of 1, 3, 7, 14, 28 and 56 days, respectively. It is noticeable from this figure that after 28 days of curing age, the chemical shrinkage value for CNS-3P and CNS-3.5P is not reported. This is due to self-desiccation, which led to cracking and failure of flask (Figure 4.44). This may be attributed to presence of nano-sized silica particles having higher surface to volume ratio, where larger number of atoms are available at surface level, which makes the

152

cementitious system hyper-reactive in terms of hydration leading to increase in the value of chemical shrinkage (Chen and Lin, 2009).

It can be seen from the Figure 4.43b that binary blended F mixes showed lesser change in volume compared to all other binary blended mixes this is due to insignificant hydration activity during first few days and the increase in chemical shrinkage at early age is could be due to its chemical and filler effect (Givi et al., 2010; Saha, 2018) Whereas, in case of binary blended U mixes presence of ultra-finer particles of FA induced the volume change, which could be due to fine filler and faster reactivity owing to its size effect.
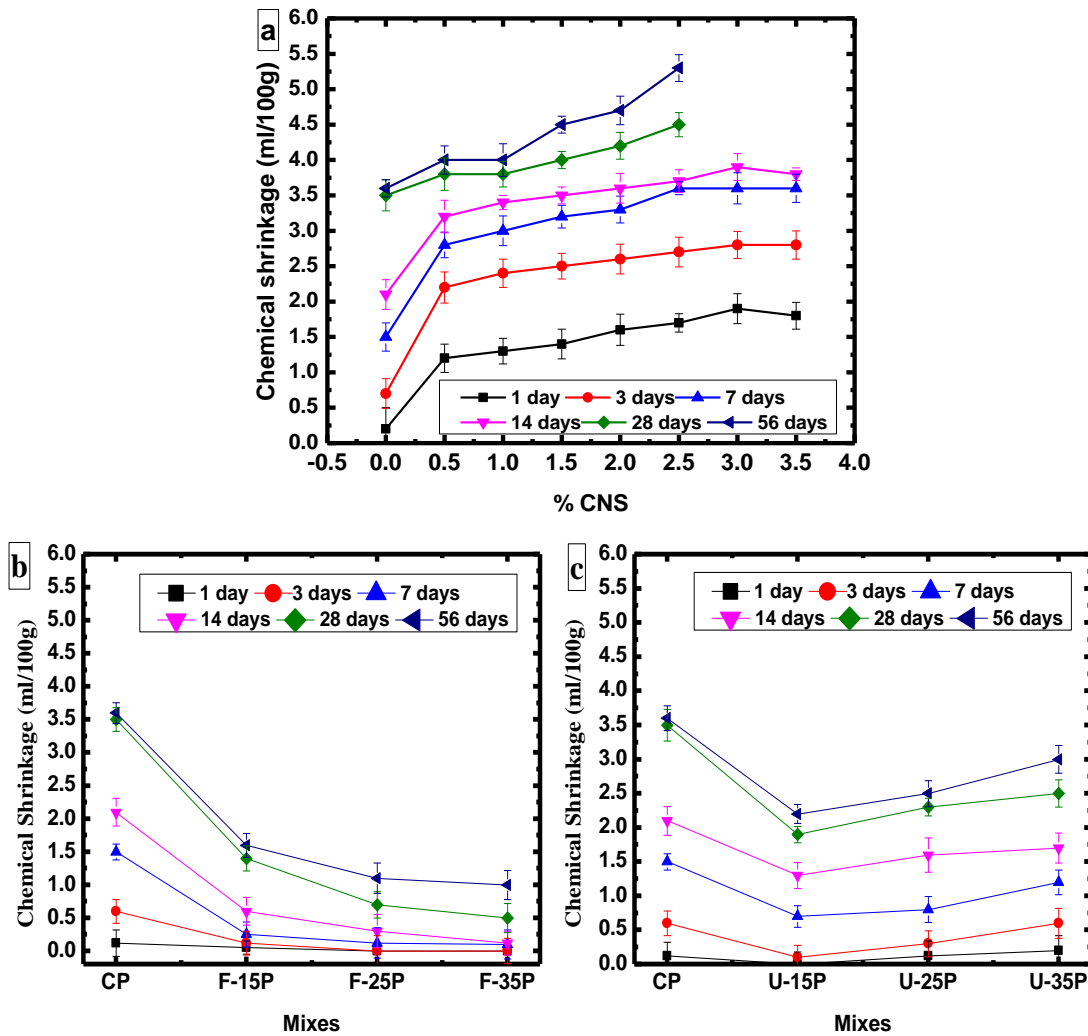
Figure 4.43: Chemical shrinkage for binary blended cement paste a) CNS mixes b) F mixes and c) U mixes
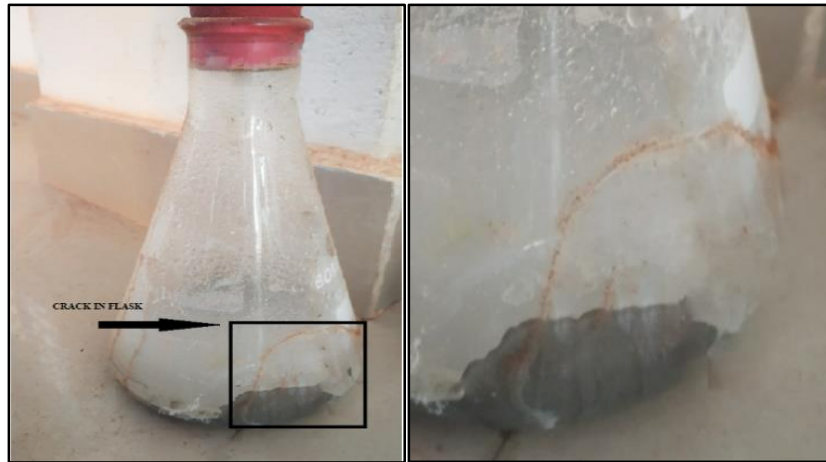
Figure 4.44: Test Specimen of chemical shrinkage resulted in failure of flask

Figure 4.45 (a-c) illustrates the response on chemical shrinkage of ternary blended paste at the ages of 1, 3, 7, 28 and 56 days.
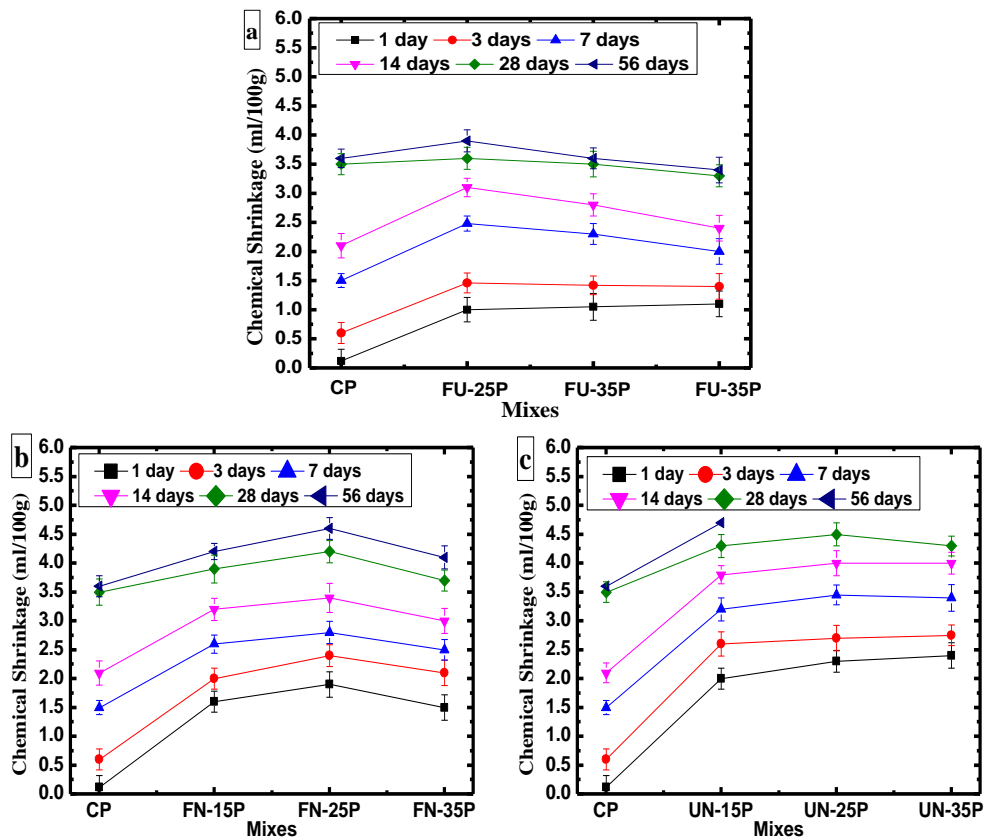
Figure 4.45: Chemical shrinkage for ternary blended cement paste integrated with CNS a) FU mixes b) FN mixes c) UN paste mixes

Figure 4.45a shows that for ternary blended FU paste development in chemical shrinkage was observed to be higher for FU-15P mix as compared to control paste. While, chemical shrinkage was seen to be reduced for FU-25P and FU-35P mixes. The reduction in chemical shrinkage at early age may be due to decelerated rate of pozzolanic activity in the presence of higher dosage of FA for FU-25P and FU-35P mixes that (Gaitero et al., 2008). It can be observed from the Figure 4.45 (b-c) that ternary blended pastes containing nano-silica (i.e. FN and UN mixes) shows higher rate of chemical shrinkage as compared to control paste. Maximum level of shrinkage was noted for FN-25P among FN mixes, volume change was measured to be between 2.5 to 4.5 ml/100 gm at the age of 1-56 days. Whereas, similar trend of increase in chemical shrinkage was observed for UN mixes, but after 56 days crack, in flask was noticed for both UN-25P and UN-35P mixes (Figure 4.44).

The chemical shrinkage values measured for all replacement levels of quaternary blended cement paste with FA, UFFA and CNS is potted in Figure 4.46.
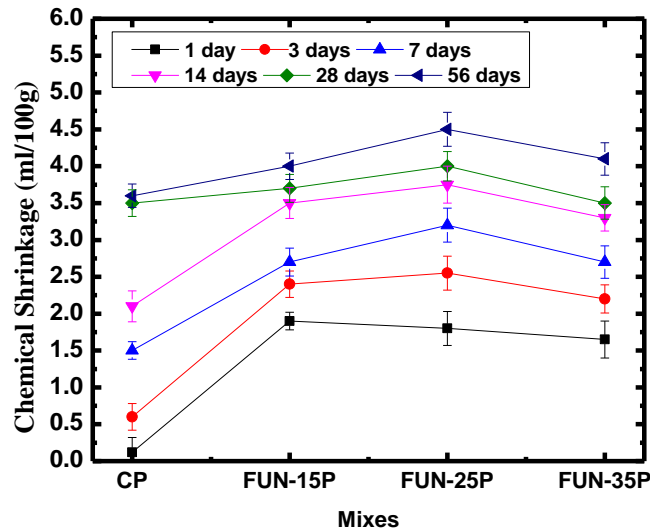
Figure 4.46: Chemical shrinkage for quaternary blended cement paste integrated with FA, UFFA and CNS paste mixes

Increased level of chemical shrinkage with time was observed up to the total replacement percentage of 25% (i.e. FUN-15P and FUN-25P) and then reduced for FUN-35P mix. The

chemical shrinkage value measured for quaternary blended composite cement paste found to be similar to FN mixes, however, lesser compared to the UN ternary blended mix.

4.4.4   Pozzolanic reactivity test: selective dissolution method (SDM)

Pozzolanic reaction degree (PRD) for binary, ternary and quaternary blended cementitious system determined by means of SDM are presented in Figure 4.47 to Figure 4.49.
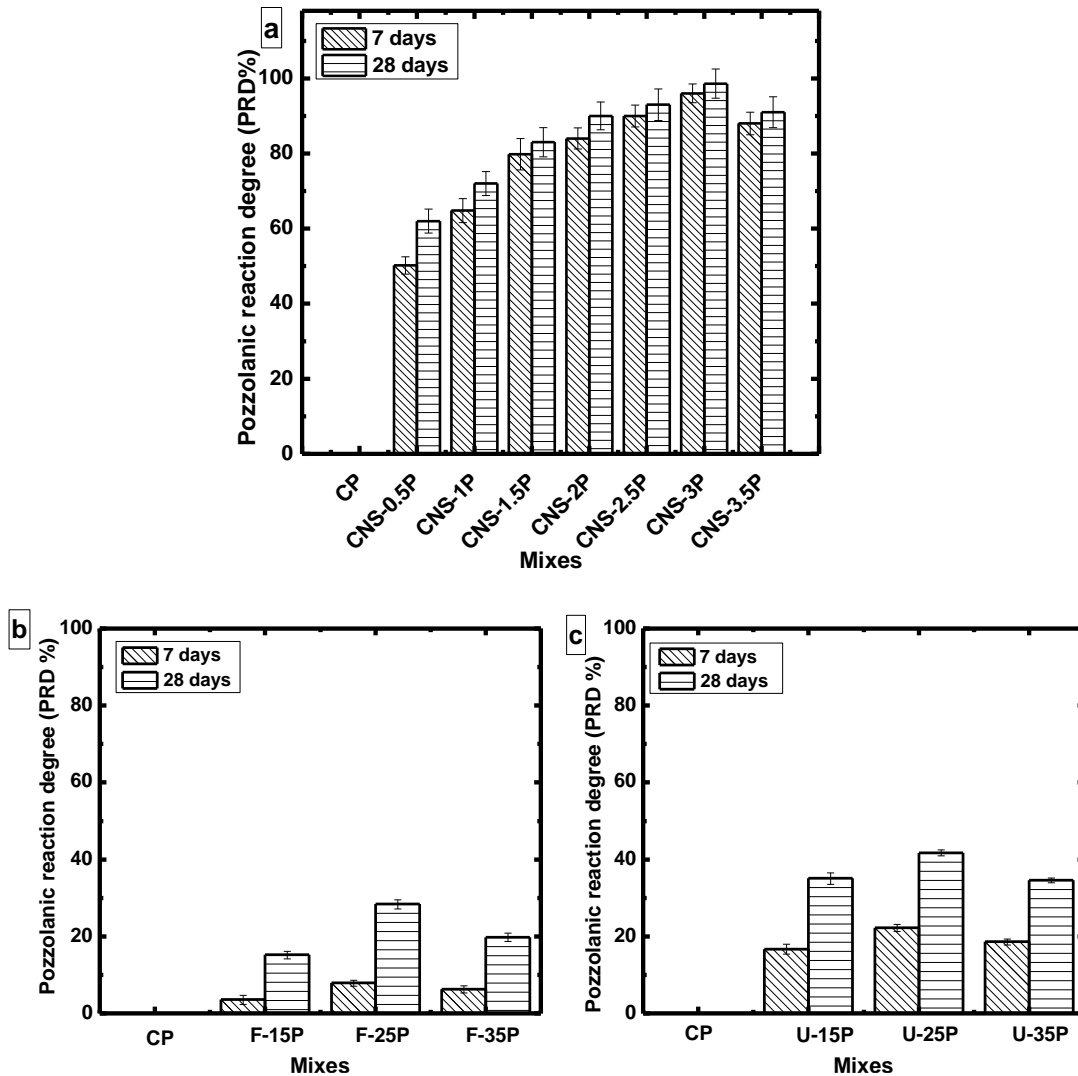
Figure 4.47: Pozzolanic reaction degree for binary blended cementitious paste a) CNS mixes b) F mixes c) U mixes

It can be seen from the Figure 4.47a that pozzolanic reaction degree (PRD) of binary blended CNS mixes were tends to increase with the percentage of nano-silica. Among all

the mixes CNS-3P mix showed maximum degree of pozzolanic reaction at both the ages of 7 (96%) and 28 days (98.6%). This may be attributed to the more rapid reactivity of nano-silica particles in cementitious system. Nano-silica possess superior specific surface area, which contributes in topo-chemical reaction of cement particles on account of its CSH seeding effect and there by aids in promoting hydration (Kim et al., 2019).

Other binary blended F and U mixes showed slower rate of pozzolanic reactivity especially at early age of 7 days (less than 25%) and found to be increased at later age of 28 days. Highest PRD% for F and U mixes were seen at the percentage replacement of 25% and PRD value F-25P and U-25P were found to be 28.4% and 41.8%, respectively at the age of 28 days. This was ascribed to the initial filler behavior of fly ash and ultra-fine fly ash particles that remained inert in terms of pozzolanic/ hydraulic reactivity (Sahoo et al., 2017).
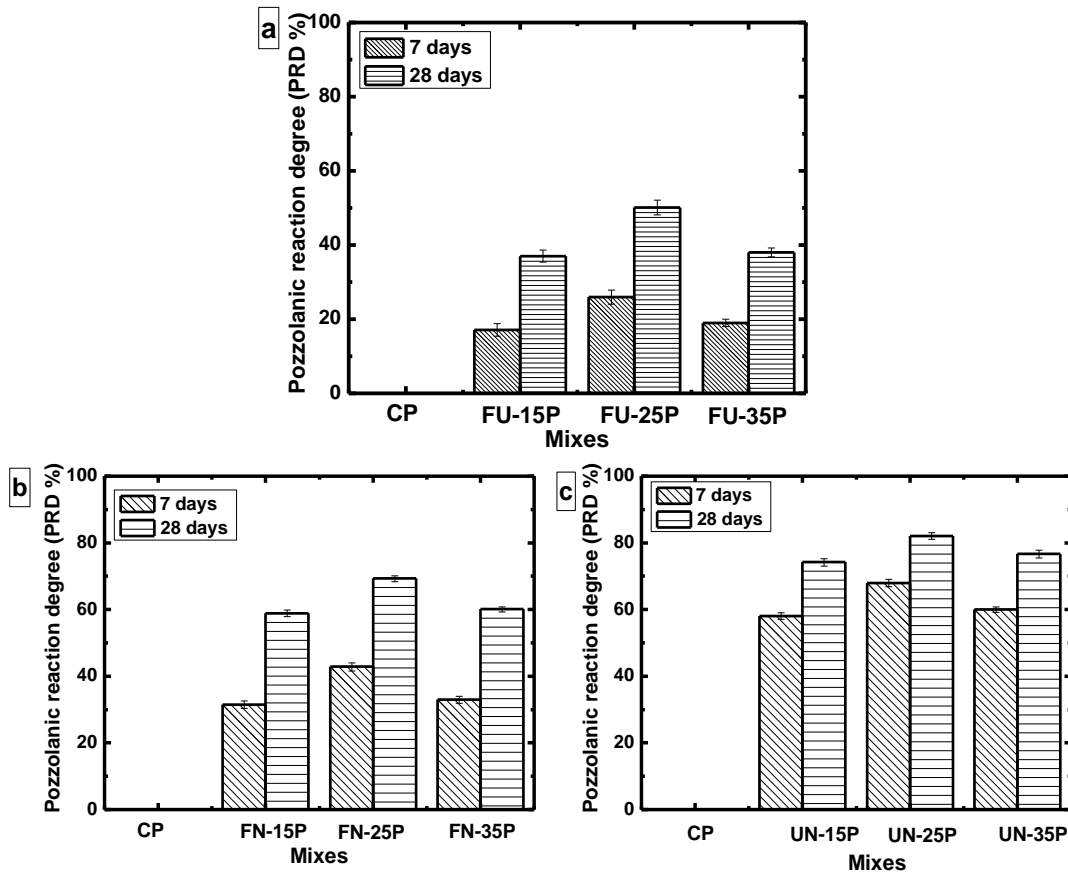
Figure 4.48: Pozzolanic reaction degree for ternary blended cementitious paste a) FU mixes b) FN mixes c) UN mixes
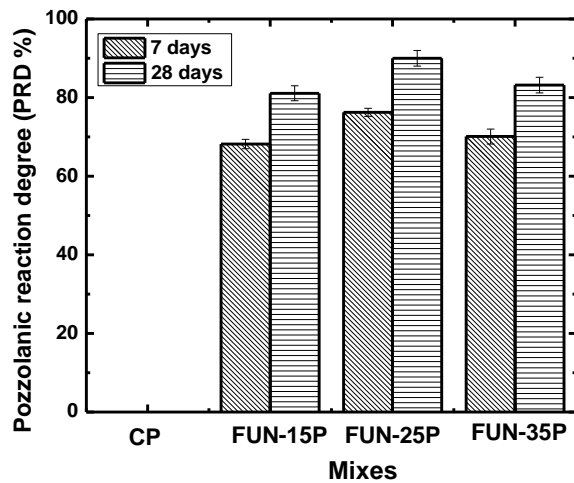
Figure 4.49: Pozzolanic reaction degree for quaternary blended cementitious paste

It can be observed from the Figure 4.48a that in case of FU mixes PRD was found to be similar to that of binary blended U mixes and FU-25P mix showed highest rate of pozzolanic reactivity among other FU mixes with a value 24.8% and 50%, respectively at the age of 7 and 28 days. On the other hand, it is important to note that ternary (FN and UN) and quaternary blended (FUN) cementitious system comprised of nano-silica showed superior pozzolanic reactivity even at the early age of 7 days compared to that of blended mixes without nano-silica. This may be attributed to the presence of highly pozzolanic nano-silica particles possessing high surface to volume ratio, which tailored the pozzolanic reactivity in conjunction with FA or/and UFFA particles owing to its greater ability to consume lime. Pozzolanic reaction degree of FN-25P, UN-25P and FUN-25P at the age of 28 days was 72%, 86% and 92% respectively. It can be noticed that optimized quaternary blended FUN-25P mix resulted in approximately 93% reactivity with respect to CNS-3P mix at the age of 28 days. Even though, binary blended CNS-3P mix performed better in terms of reactivity it was capable of replacing lower percentage of cement i.e. 3% (beyond 3% may affect negatively, which will not effectually contribute in environmental sustainability, in this view point quaternary blended FUN-25P mix with optimized particle packing, which can replace OPC by 25% can be a sustainable solution.

4.4.5 Thermo gravimetric analysis (TGA)

The TG-DTG curve for binary, ternary and quaternary blended cement paste specimens at the age of 7 and 28days are presented in Figure 4.50 to Figure 4.51. Thermogravimetric mass loss takes place at specific temperature boundaries when hydrated cement paste samples are exposed to an elevated temperature, owing to loss of free water, dehydration, de-hydroxylation and de-carbonation of hydration products (Yu et al 2014). From TGA results, it can be observed that significant weight losses took place between temperature ranges of 110 ˚C-300 ˚C, 400 ˚C-500 ˚C and 600 ˚C-800 ˚C. Temperature boundaries of various decomposition phenomenon of hydration products were identified by means of differential thermogravimetry curve (DTG). Weight loss seen in the range of 110 ˚C-300 ˚C signifies the dehydration of water molecules associated to calcium silicate hydrate gel (C-S-H) (Soriano et al., 2014; Singh et al., 2015). Further, the weight loss observed

between the ranges of 400 ˚C-500 ˚C represents the de-hydroxylation of calcium hydroxide (CH, Singh et al 2015) and thermal degradation happens between the temperature ranges of 600 ˚C-800 ˚C relating to de-carbonation of calcium carbonate (CC).

(a)

(b)

(c)

(d)

(e)
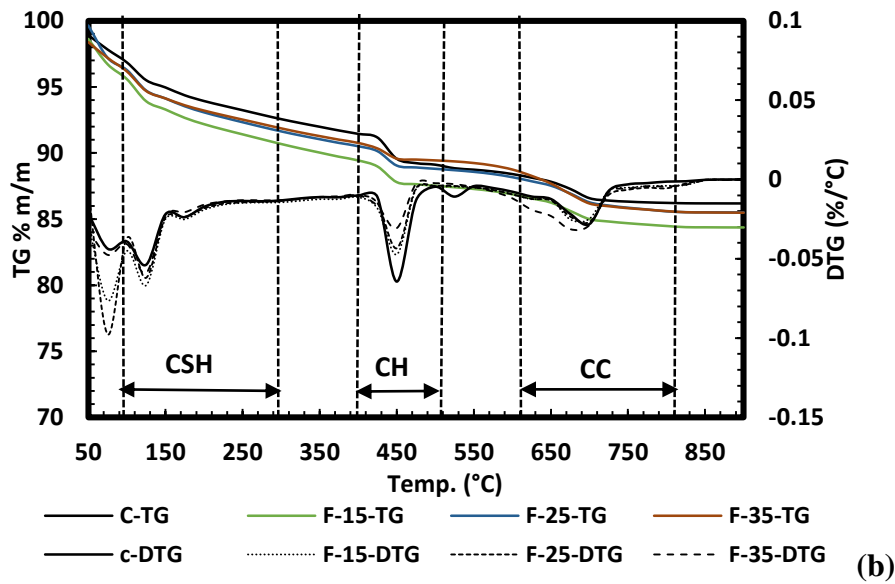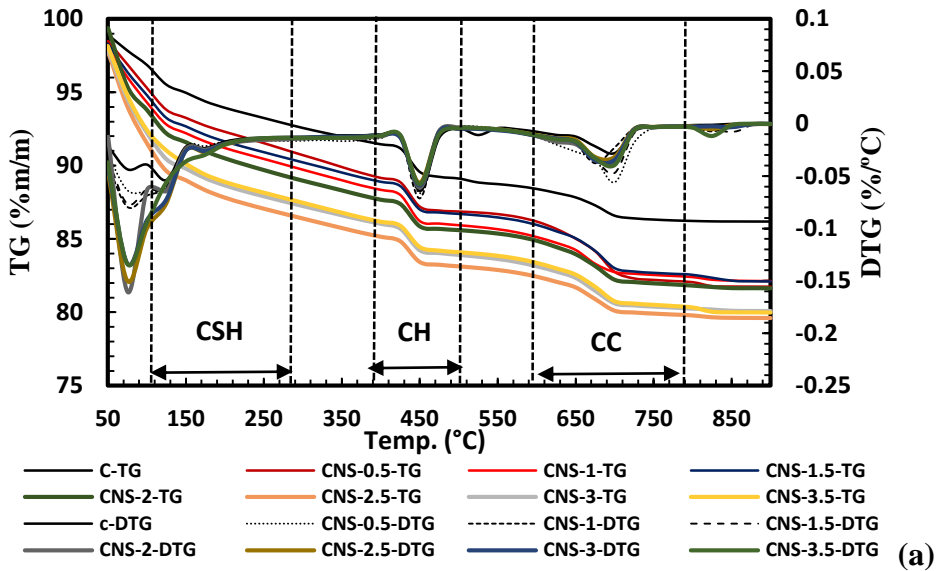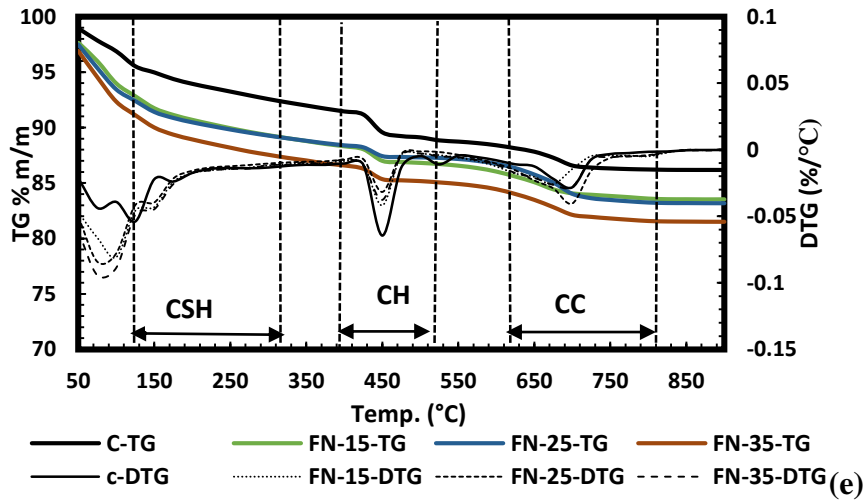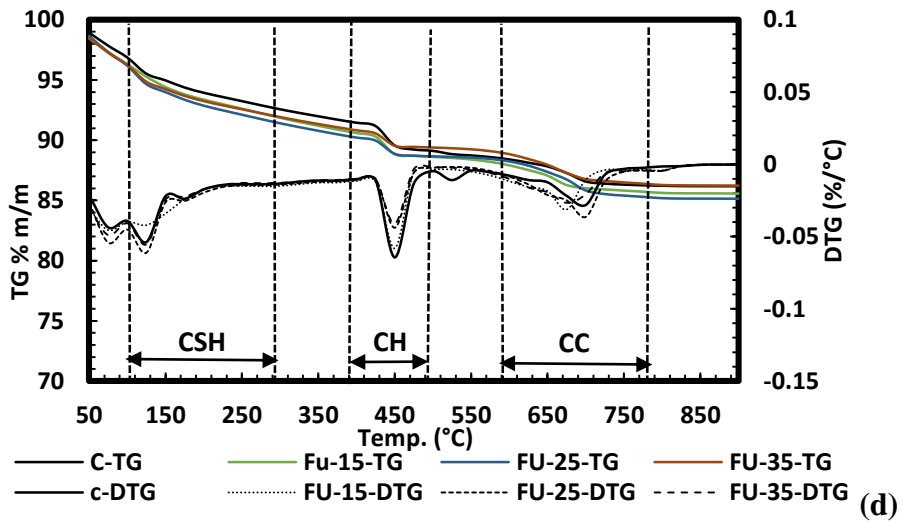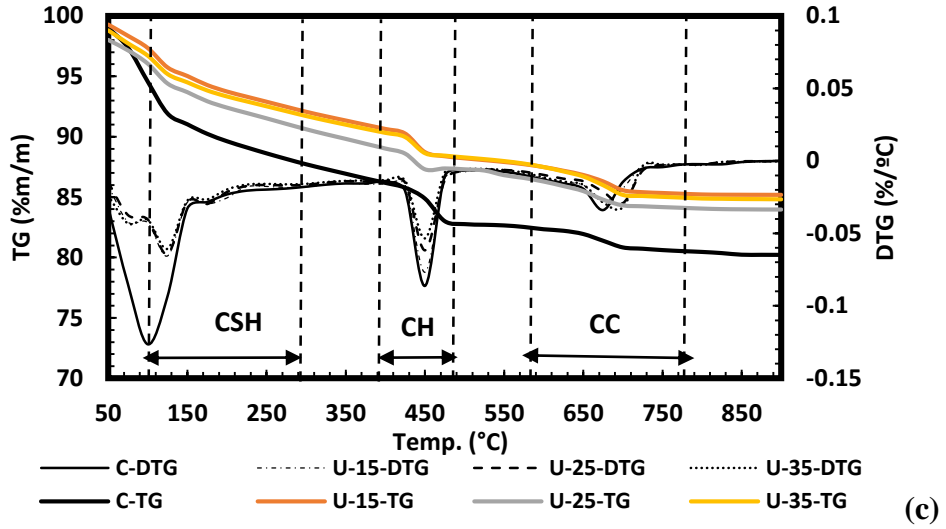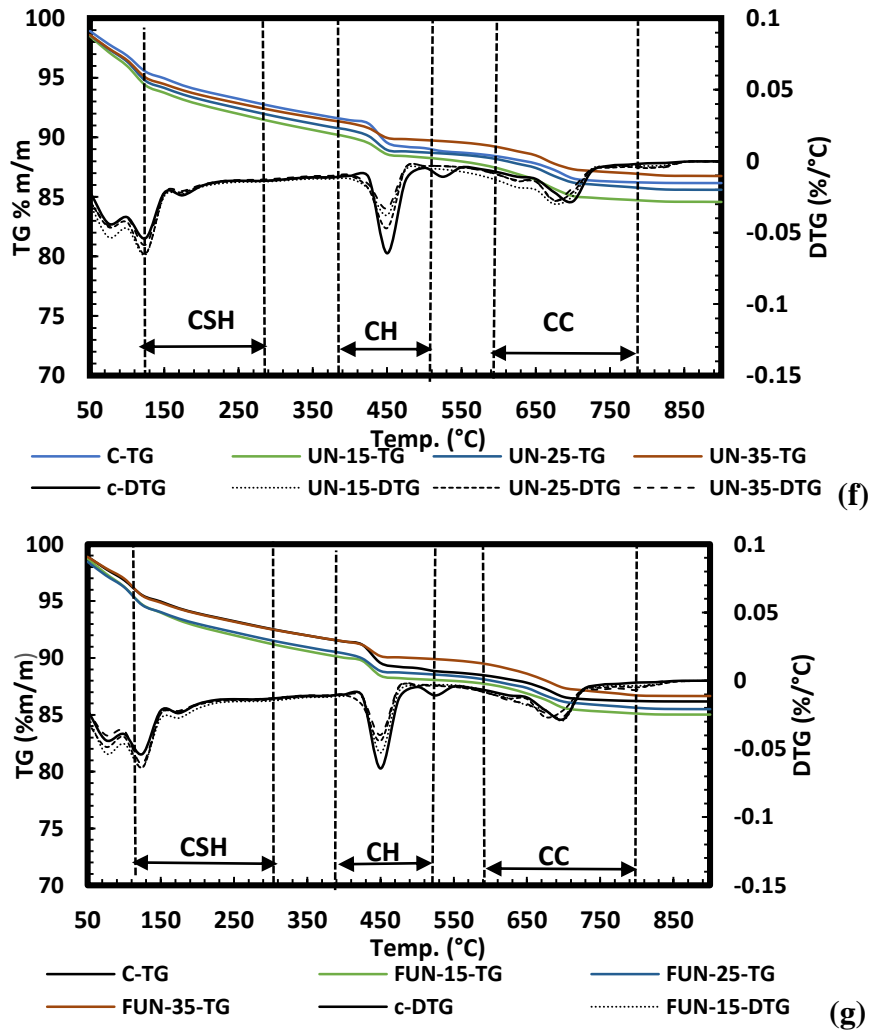
Figure 4.50: TG-DTG curves of binary, ternary and quaternary blended paste specimens at the age of 7 days a) CNS, b) F, c) U, d) FU, e) FN, f) UN and g) FUN mixes

(d)

(e)

(f)

164
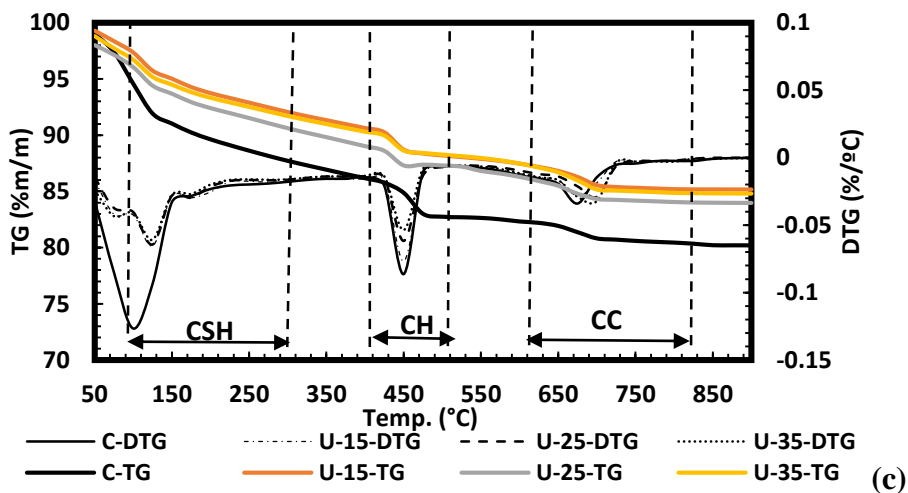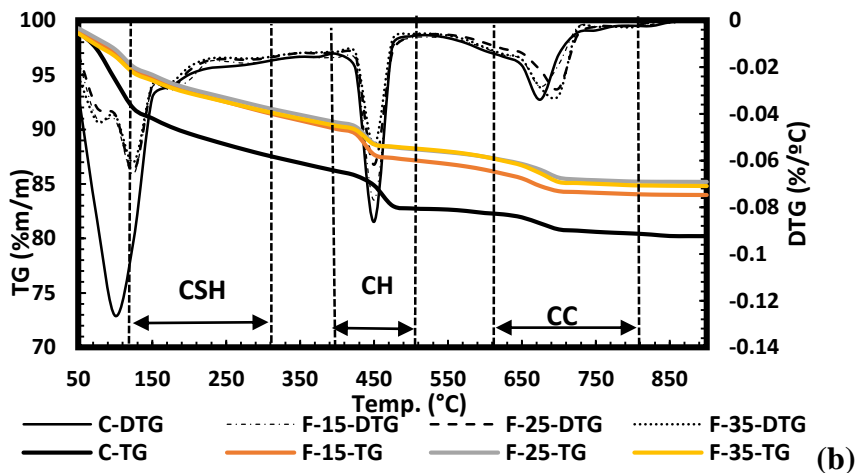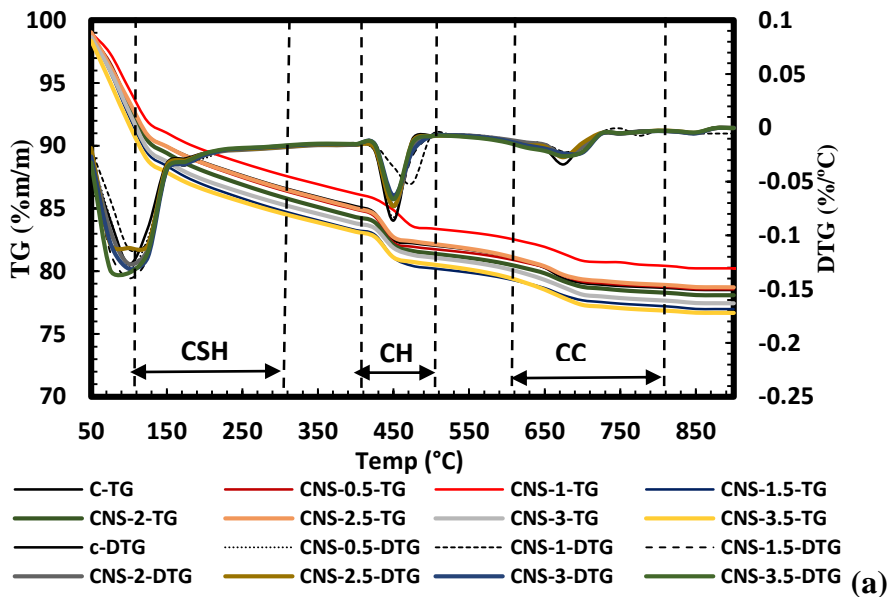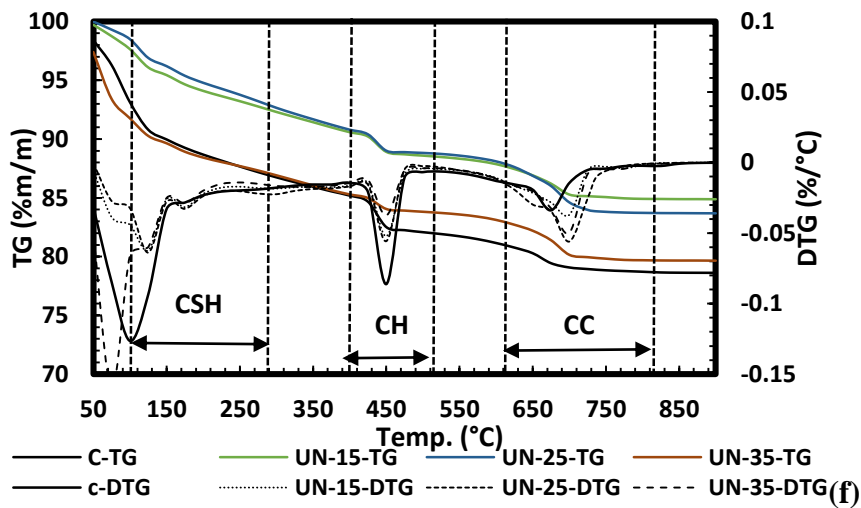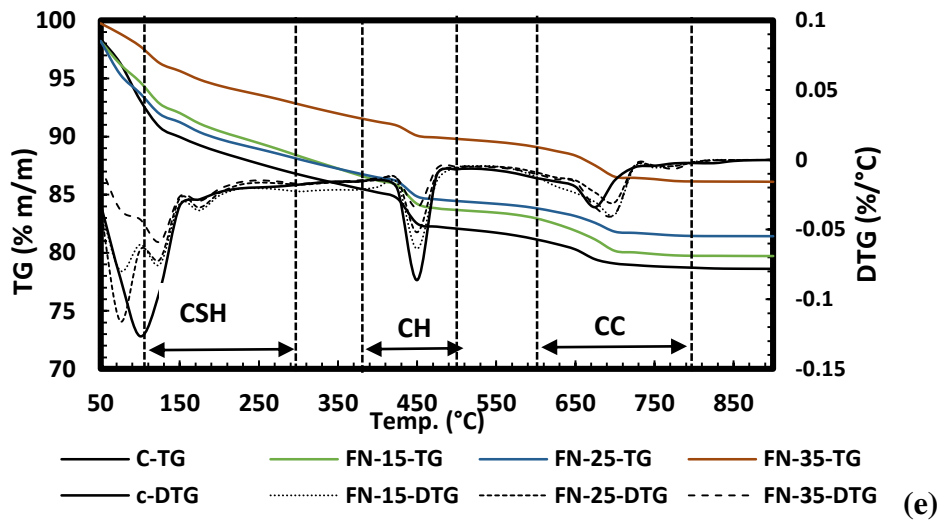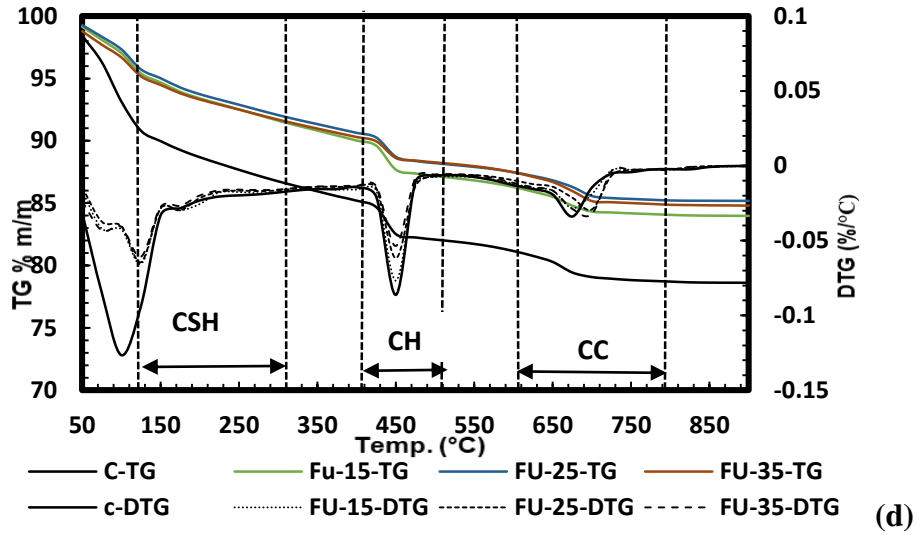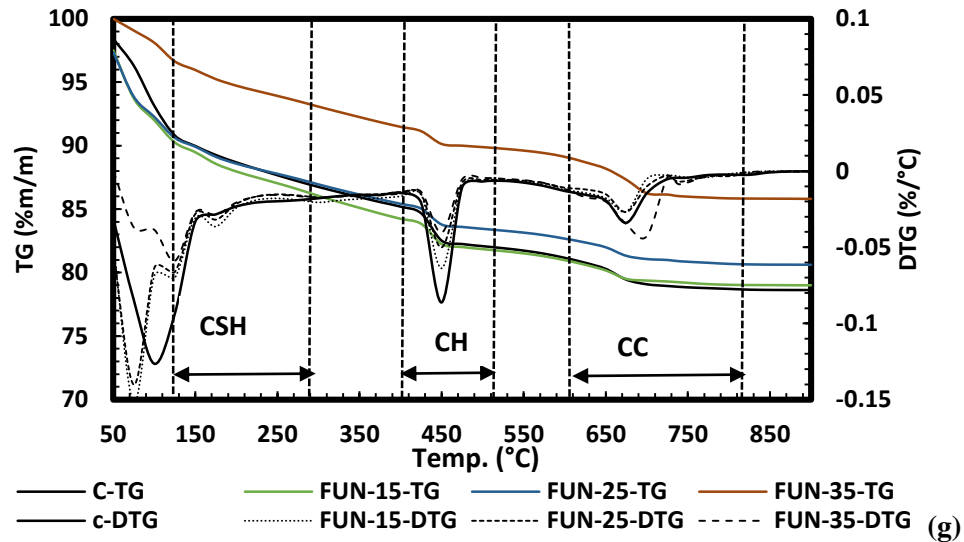
Figure 4.51: TG-DTG curves of binary, ternary and quaternary blended paste specimens at the age of 28 days a) CNS, b) F, c) U, d) FU, e) FN, f) UN and g) FUN mixes

The quantification of hydration products was done on the basis of the observed mass loss at particular temperature ranges. The amount of calcium hydroxide (CH) and water associated to hydration product (WH) excluding CH content for all the samples were calculated according to the Equation 3.8 and Equation 3.9, respectively. The calculated values of CH and WH for all blended paste samples are presented in Table 4.2.

Table 4.2: **CH and WH content of blended mixes at 7 and 28 days of curing age**

Blends	Specimen	CH (%)		WH (%)	
		7 days	28 days	7 days	28 days
Control	CP	11.90	19.98	13.98	16.92
Binary blends	CNS 0.5P	9.01	14.06	14.82	17.73
	CNS 1.0P	7.99	12.89	14.95	18.14
	CNS 1.5P	7.02	10.54	16.38	19.27
	CNS 2.0P	6.00	9.56	16.99	20.135
	CNS 2.5P	5.68	9.13	17.10	21.85
	CNS 3.0P	5.21	7.69	19.99	23.835
	CNS 3.5P	5.23	8.00	18.88	22.70
	F-15P	10.30	17.00	11.20	15.50
	F-25P	9.90	16.20	12.50	16.00
	F-35P	9.10	14.10	13.00	16.20
	U-15P	9.90	16.50	12.60	16.80
	U-25P	9.20	15.50	13.90	17.30
	U-35P	8.10	13.10	14.10	17.80
Ternary blends	FU-15P	9.80	16.30	12.80	17.00
	FU-25P	9.00	15.41	13.99	17.50
	FU-35P	8.00	13.00	14.30	17.90
	FN-15P	9.32	15.88	14.98	18.03
	FN-25P	8.52	14.32	15.32	18.69
	FN-35P	7.00	12.02	15.99	19.12
	UN-15P	8.06	14.12	15.06	18.78
	UN-25 P	7.42	13.33	15.79	19.072
	UN-35P	6.98	11.96	16.39	19.32
Quaternary blends	FUN-15P	8.02	14.001	15.12	18.85
	FUN-25P	6.92	11.99	16.859	20.15
	FUN-35P	6.87	11.96	16.92	20.49

For binary blended CNS mixes, with the increase in dosage of nano-silica significant reduction in CH percent and increase in WH percent was observed as compared to control mix. It is important to note that, after 3% dosage of nano-silica there was no further deviation in CH and WH quantity, which means that incorporation of nano-silica content exceeding 3% may not be effective in hydration activity. The reduction in CH% and increase in WH% with the integration of nano-silica might be due to its rapid pozzolanic

reaction that significantly consumed the CH content produced during the process of cement hydration especially at the age of 7 days (Hou et al., 2013; Yu et al., 2014). In addition, nano-silica particles acts as nucleation site for the production of C-S-H and thereby stimulates the hydration reaction of cement (Yu et al., 2014, Singh et al., 2015). It is reported that introduction of nano-silica in cementitious system enhances the pozzolanic activity producing greater C-S-H formation, which eventually modifies the cement paste in nano-scale resulting in higher compressive strength (Qing et al., 2007; Sobolev et al., 2009).

Binary blended F and U mixes showed slower rate of reduction in CH % and increase in WH%. However, U mixes showed better result compared to that of F mixes. This is attributed to the slower rate of reactivity of FA particles especially at early ages.

It can be observed from the table that ternary blended FU mixes performed similar to binary blended F and U mixes in terms of CH and WH content. However, slight improvement was seen compared to F and U mixes, this may be linking to the particle packing and synergic effect of micron/submicron level particles in reactivity. It is important to note that with intrusion of CNS in ternary blended FN and UN mixes, there found to be an intensified reduction in CH% and pronounced increase in WH% compared to that of control mix. This could be attributed to the more active pozzolanic reactivity of FA and UFFA in presence of highly reactive nano-silica particles.

Quaternary blended paste samples also showed reduction in CH content and increase in WH content as like CNS incorporated ternary blended samples, but in a higher rate. The CH and WH values obtained are observed to be closer to that of binary blended CNS samples.

4.4.6 Mineralogical characterization (XRD)

Mineralogical characteristics of hydrated binary blended cement paste incorporated with different proportions of CNS, FA and UFFA were studied by means XRD analysis at the age of 7 and 28 days and the XRD pattern are shown in Figure 4.52- Figure 4.54.
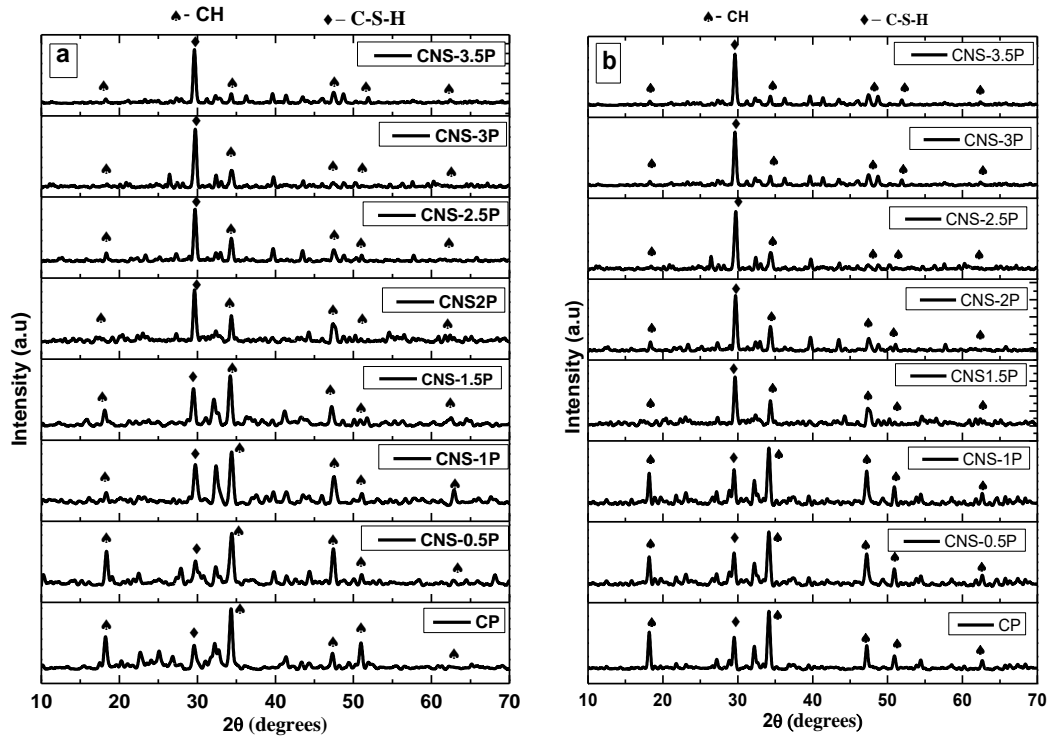
Figure 4.52: XRD pattern of binary blended and CNS admixed paste samples at the age of a) 7 and b) 28 days
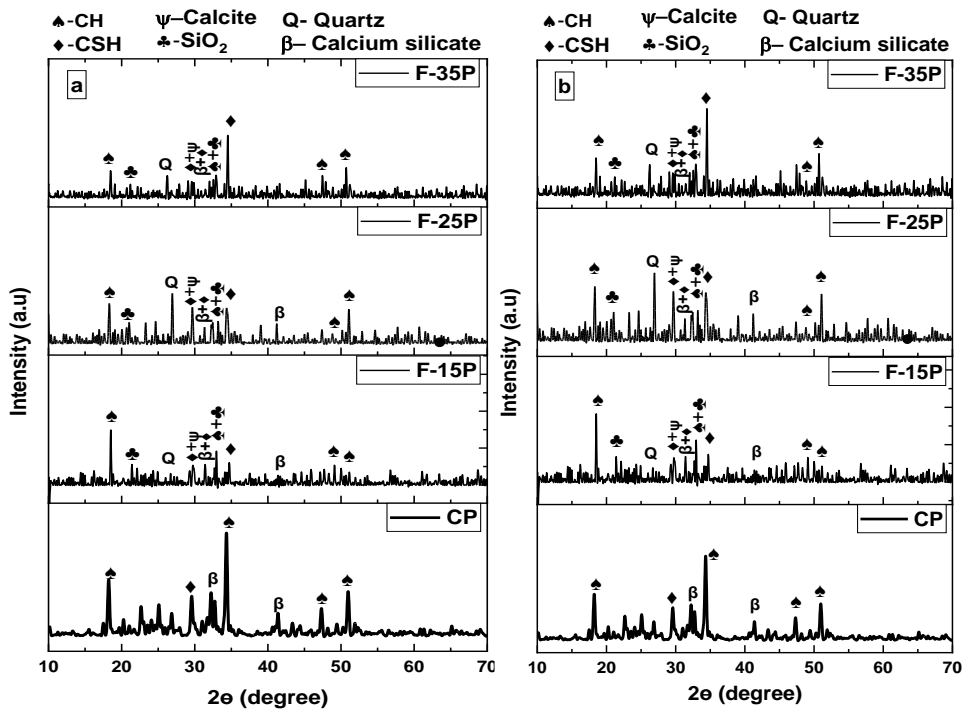
Figure 4.53: XRD pattern of binary blended FA admixed paste samples at the age of a) 7 and b) 28 days
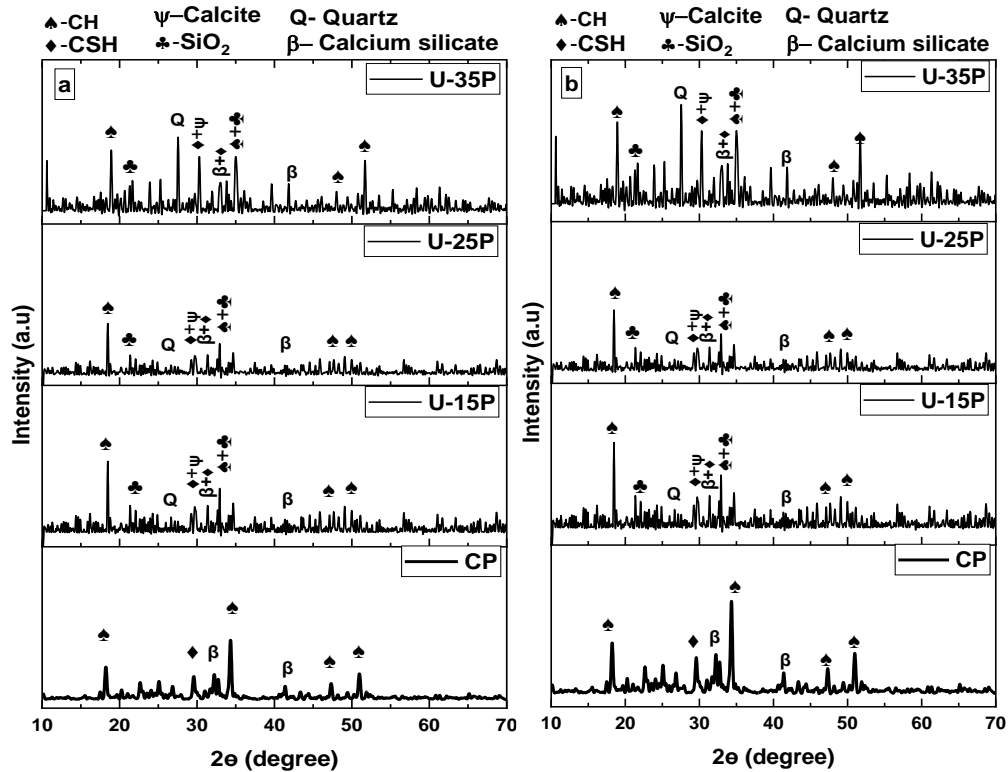
Figure 4.54: XRD pattern of binary blended UFFA admixed paste samples at the age of a) 7 and b) 28 days

It can be seen from the figure 4.52 that most prominent peaks obtained from the analysis are calcium silicate hydrate (C-S-H) and calcium hydroxide (CH). The intensity of peak for CH was found to decrease with increase in amount of CNS content compared to that of control paste at 7 and 28 days. Whereas, the intensity of C-S-H peak increased with increase in CNS content. The intense peak of CH was positioned at 2θ angle of 18.2° and 34.171°, whereas C-S-H was at 29.47°.

It can be observed from the Figure 4.53 and Figure 4.54 that intensity of decrease in CH peak (2θ angle: 18.2° and 34.216°) and increase in CSH peak (2θ angle: 29.766° and 32.282°) found to be less compared to that of CNS mixes. Further, additional peaks such as quartz, SiO$_2$, calcite and calcium silicate were seen in FA and UFFA admixed binary mixes. It is important to note that CH peak found to increase at the age of 28 days as compared to 7 days. This could be attributed to the slow rate of initial hydration and slow

pozzolanic activity of FA particles and this can be associated with CH% calculated from TG analysis (Table 4.2). However, U mixes designated better hydration activity compared to F mixes

Figures 4.55 - 4.58 XRD pattern for ternary and quaternary blended mixes, which shows the peaks of calcium hydroxide (CH) in the form of portlandite, calcium silicate hydrate (C-S-H) in the form of tobermorite, pure silicon dioxide (SiO_2) in the form of quartz low syn, calcium silicates (unhydrated cement particles) and calcite. Strong peaks were observed for all the blended paste samples are CH (2θ angle: 18.2° and 34.216°) and C-S-H (2θ angle: 29.766° and 32.282°). In addition, quartz peaks were also noticed for samples containing FA and UFFA.
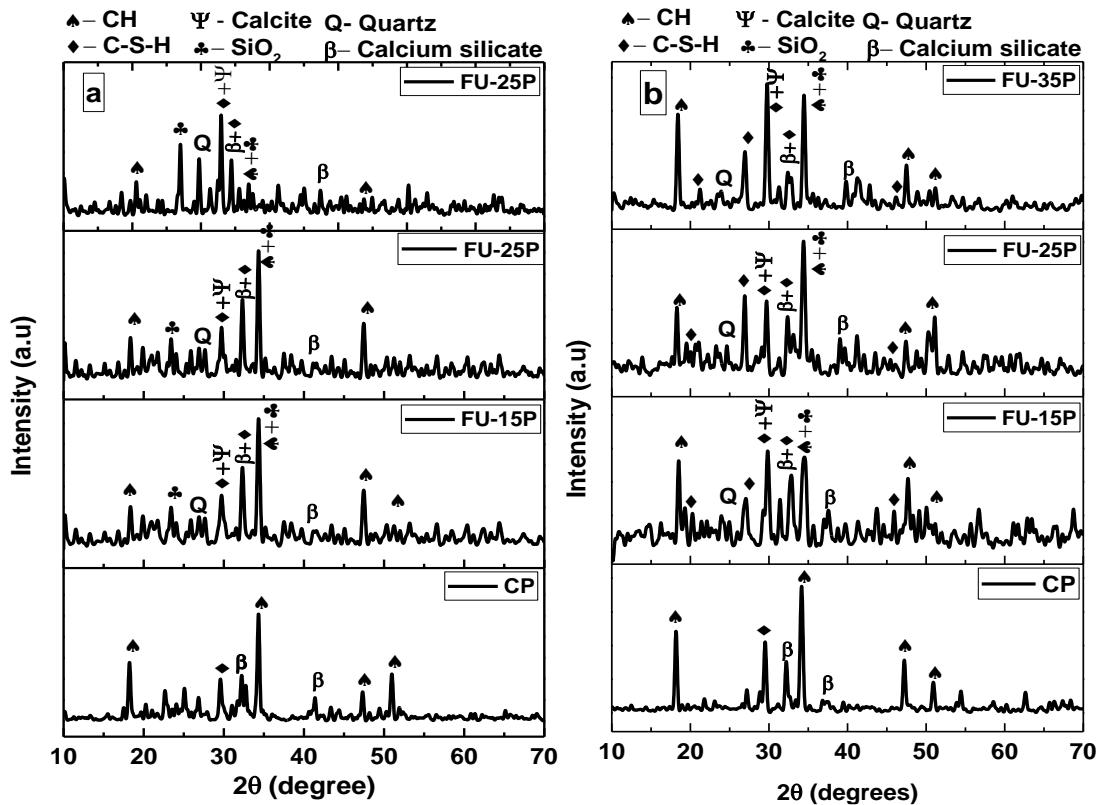
Figure 4.55: XRD patterns of FU ternary blended hydrated cement paste samples at (a) 7days (b) 28 days

170
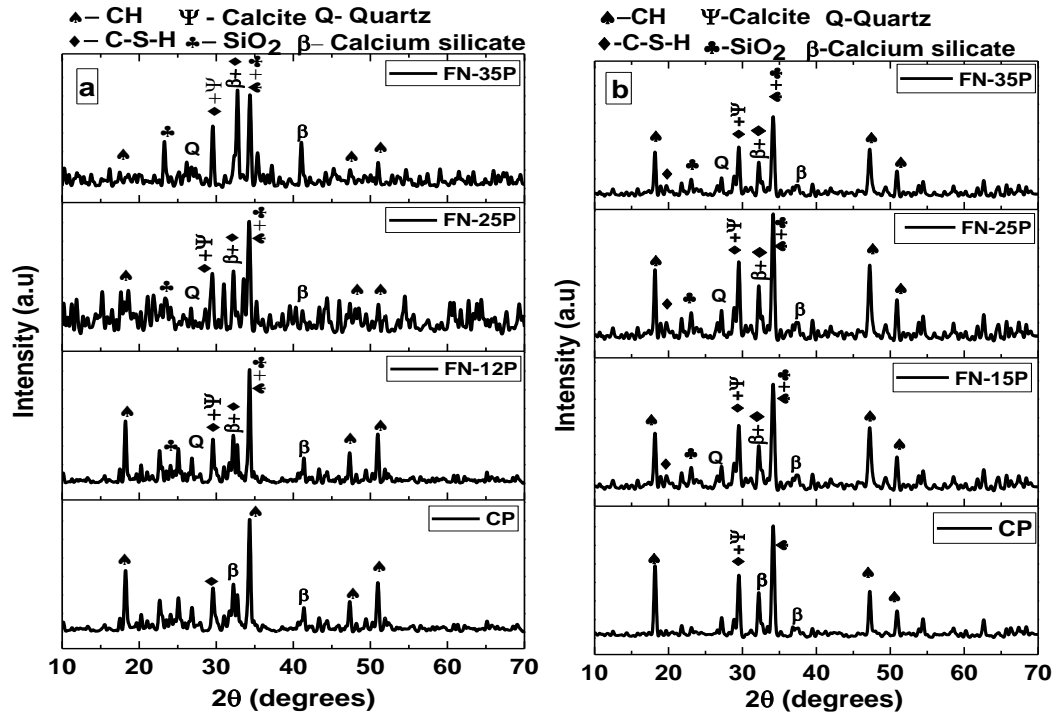
Figure 4.56: XRD patterns of FN ternary blended hydrated cement paste samples at (a) 7days (b) 28 days
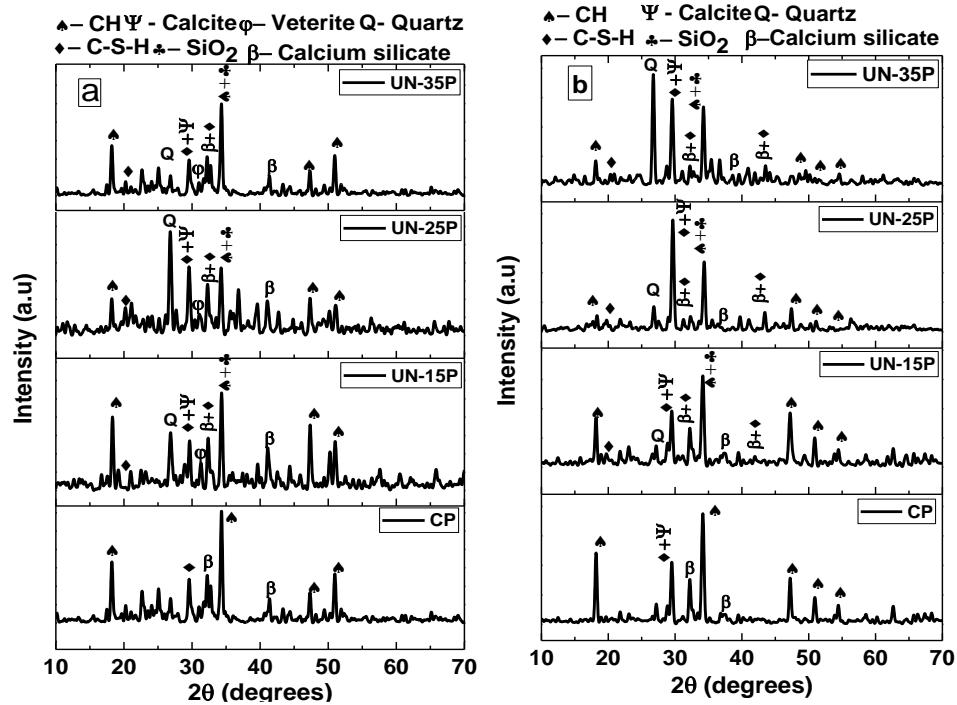
Figure 4.57: XRD patterns of UN ternary blended hydrated cement paste samples at (a) 7days (b) 28 days

It can be observed from the XRD pattern (Figure 4.55) of FU ternary blended paste samples that compared to the control paste CH peak reduces with the increase in dosage of supplementary cementitious materials. But it is important to note that after 25% of replacement level CH peak was observed to be increased especially at 28 days. The pattern indicates that compared to the early age of 7 days the CH peak was seen to be higher at the age of 28 days and CSH peak also found to be increased similar to that of binary blended F and U mixes. Further, the peaks of unhydrated cement particle i.e. calcium silicate was detected and noticeable increase in qutartz/SiO_2 peaks was also seen with increase in replacement level.

It can be observed from Figure 4.56 and Figure 4.57 that compared to control samples, presence of nano-silica in both FN and UN samples amplified the peak of C-S-H and dramatically reduced the peak of CH. However, among FN and UN ternary blended samples, UN showed higher intensity of C-S-H and lower CH peak. It is important to note that suppressed peak of CH and extra peak of C-S-H was seen at the age of 28 days. Quartz peak was also observed and found to be intensified with the enhancement in replacement level in both FN and UN mixes.
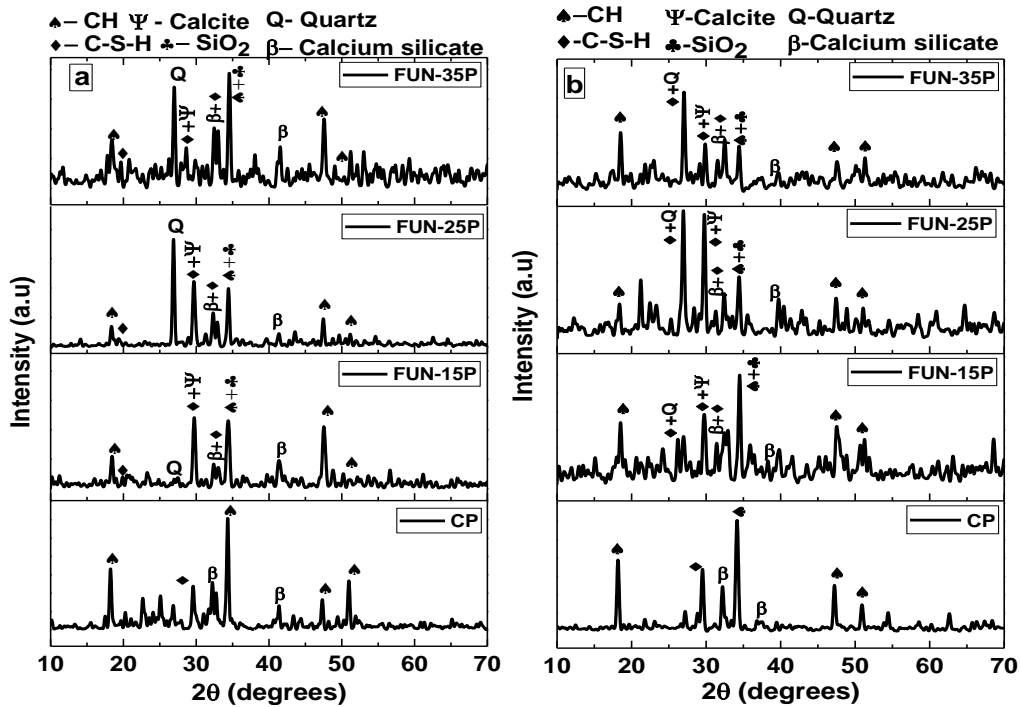
Figure 4.58: XRD patterns of FUN quaternary blended hydrated cement paste samples at (a) 7days (b) 28 days

Similar trend of peaks like other CNS integrated ternary blended samples were also noticed in quaternary blended paste samples (Figure 4.58). Extra peak of C-S-H at the age of 7 days itself was detected, however greater number of C-S-H peaks are found at 28 days. Reduced peak of CH was also noticed in both the ages. Among ternary and quaternary blended paste samples, quaternary blended paste samples indicated larger formation of C-S-H and were seen to be more noticeable at the age of 28 days.

4.4.7 Microstructural analysis (SEM-EDS)

The SEM-EDS analysis was carried out for all the hydrated paste samples at curing age of 7 and 28 days. The Ca/Si atomic ratio was determined for all samples on the basis of elemental compositions obtained from EDS analysis (carried out as area analysis). In view of conciseness, SEM-EDS image of control and CNS-3P samples at the age of 28 days is presented in Figure 4.59. It can be noticed from SEM images that compared to control sample, CNS-3P showed a denser matrix.
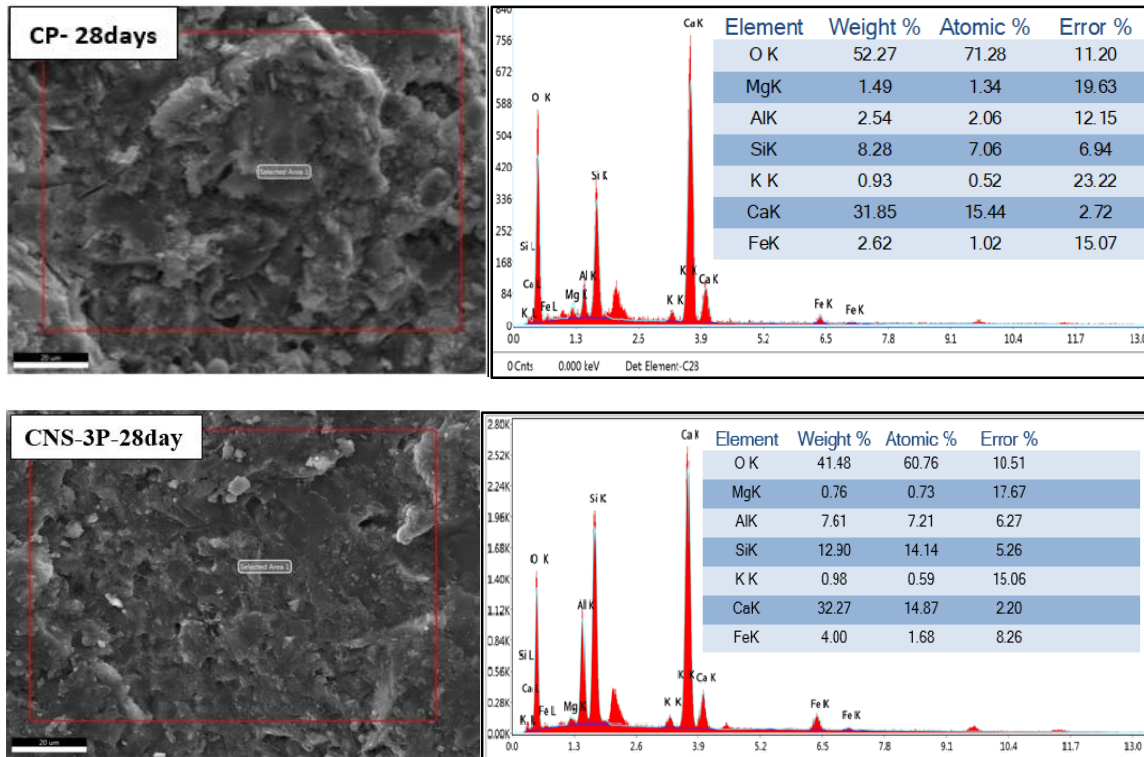
Figure 4.59: Illustration of SEM-EDS analysis for control paste and CNS-3P sample at the curing age of 28days

The atomic ratio of Ca/Si, calculated from EDS study was used to analyse the chemistry of C-S-H formation in the matrix of hydrated cement paste. It is reported that chemistry of C-S-H formation greatly relies on the chemical activity of existing calcium (Ca) and silicate (Si) ions in pore solution, which are produced during the process of hydration (Hu et al., 2016)

Literature states that lower value of Ca/Si ratio characterizes the compact and densified microstructure of cement matrix due to the development of stronger network of C-S-H (Goudar et al., 2019).

The resulted Ca/Si values for all samples at the curing age of 28 days arrived from the EDS analysis are summarized and are presented in Table 4.3.

Table 4.3: Ca/Si atomic ratio for control binary, ternary and quaternary blended cement paste at the age of 28 days

Blends	Specimen	Ca/Si Atomic ratio (%)
		28 days
Control	CP	2.186
Binary blends	CNS 0.5P	1.903
	CNS 1.0P	1.694
	CNS 1.5P	1.593
	CNS 2.0P	1.382
	CNS 2.5P	1.276
	CNS 3.0P	1.051
	CNS 3.5P	1.185
	F-15P	1.951
	F-25P	1.903
	F-35P	1983
	U-15P	1.878
	U-25P	1.805
	U-35P	1.891
Ternary blend	FU-15P	1.823
	FU-25P	1.790
	FU-35P	1.830
	FN-15P	1.768
	FN-25P	1.628
	FN-35P	1.815
	UN-15P	1.656
	UN-25 P	1.446
	UN-35P	1.761
Quaternary blends	FUN-15P	1.554
	FUN-25P	1.147
	FUN-35P	1.697

The EDS analysis demonstrates the reduced value of Ca/Si ratio for all the blended cement paste samples incorporated with various combinations of FA, UFFA and CNS compared to that of control paste. The reduction of Ca/Si ratio is intense in CNS incorporated blended mixes and this could be due to accelerated reactivity of nano-silica and the additional formation of C-S-H (Singh et al., 2015). The lowest value of Ca/Si ratio, in binary blended F and U mixes were seen for F-25P and U-25P mixes and in case of ternary blended FU,

FN and UN mixes FU-25P, FN-25P and UN-25P mixes showed lower Ca/Si ratio. The quaternary blended cement paste showed comparatively lower Ca/Si ratio than control as well as ternary blends. However, it is noticed that there is an increase in Ca/Si ratio for all binary, ternary and quaternary blended samples having higher percentage of cement replacement i.e. 35%.

4.4.8 Relationship between Ca/Si ratio and water related to hydration products (WH)

Quantified C-S-H from TG analysis in the form of water related to hydration products (WH) was correlated with Ca/Si ratio and the same is presented in Figure 4.60. It can be seen from figure that Ca/Si ratio found to be inversely proportional and is fitting linearly with WH% with a precision value of "$R^2 = 0.9385$". It is to be noted that higher WH% relates to lower Ca/Si atomic ratio, which signifies solid microstructure of cementitious system on account of larger formation of C-S-H.
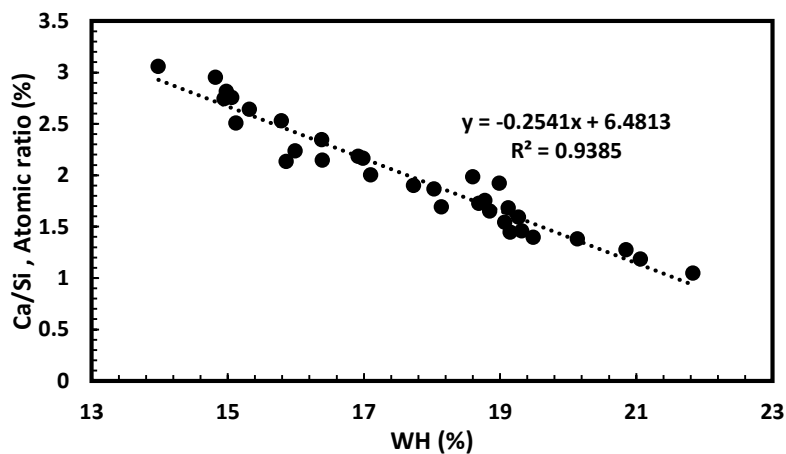
Figure 4.60: Variation of Ca/Si ratio versus water related to hydration products (WH) excluding CH content

4.4.9 Comparison of pozzolanic activity tests: strength activity index (SAI) test, selective dissolution method (SDM)-pozzolanic reaction degree (PRD) and thermogravimetric analysis-CH content

Reactivity of lime fraction with different Pozzolans and their combination differs greatly depending on its physico-chemical and mineralogical properties (Das and Pandey, 2011).

Further, temperature and humidity also play a significant role in pozzolanic reactivity of the materials (Dalinaidu et al., 2007). This signifies that it is difficult to interpret the reactivity of Pozzolans specifically. In this perspective, three different methods (SAI, SDM and TGA) was adopted to estimate the reactivity of Pozzolans in terms of compressive strength, reaction degree and amount of CH. It is a well-known fact that increase in strength of blended cementitious composites relates to the degree of SCM (individual/combined form) reactions and depletion of CH content. Further, pozzolanic reaction degree of SCMs is directly linked to the rate of CH consumption. Correlation between a) strength activity index (SAI) and pozzolanic reaction degree (PRD) and b) strength activity index (SAI) and CH content and are presented in Figure 4.61.
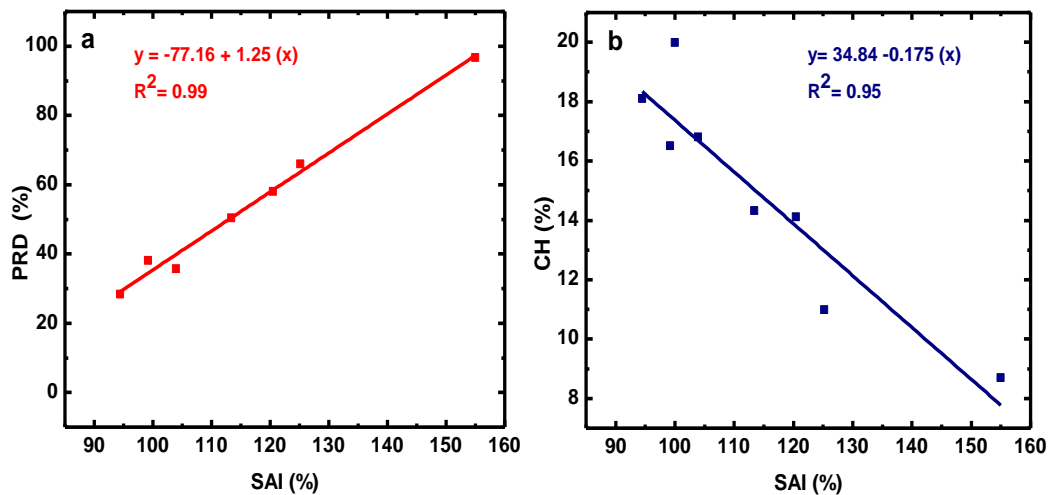
Figure 4.61: Correlation plot between a) SAI and PRD and b) SAI and CH

It can be noticed from the Figure 4.61a that SAI and PRD are directly proportional to one another. While, SAI is found to be inversely related to CH content (Figure 4.61b). All the three techniques adopted are found to be inter connected and are well related to one another. Hence, it is possible to predict the reaction degree and CH content using the following derived equations for the multi-blended mixes.

$$y = -77.16 + 1.25 \ (x) \tag{4.10}$$

$$z = 34.84 - 0.175 \ (x) \tag{4.11}$$

where, x, y and z represent SAI, PRD and CH percentage values, respectively.

4.4.10 Relationship between pozzolanic reactivity indices (PRD and SAI) and drying shrinkage

In order to understand the influence of pozzolanic reactivity and shrinkage associated to ambient drying, drying shrinkage values of all the blended cementitious composites were made to correlate with pozzolanic reactivity indices i.e., pozzolanic reaction degree (PRD%) and strength activity index (SAI %). The same is presented in the Figure 4.62. It can be noticed from the figure that, when drying shrinkage values of all multi-blended mixes were made to correlate with pozzolanic reactivity indices i.e., SAI, PRD and CH, there found to be a linear correlation (with $R^2 \approx 0.9$). The relationship between drying shrinkage and the pozzolanic reactivity indices are presented in the following equations.

$$D = 2813.73 - 37.04\,(x) \tag{4.12}$$

$$D = 260.09 - 32.55\,(y) \tag{4.13}$$

$$D = -4167.72 + 198.21\,(z) \tag{4.14}$$

Where, D denotes drying shrinkage (micro strain) and x, y and z signify SAI, PRD and CH percentage values, respectively.
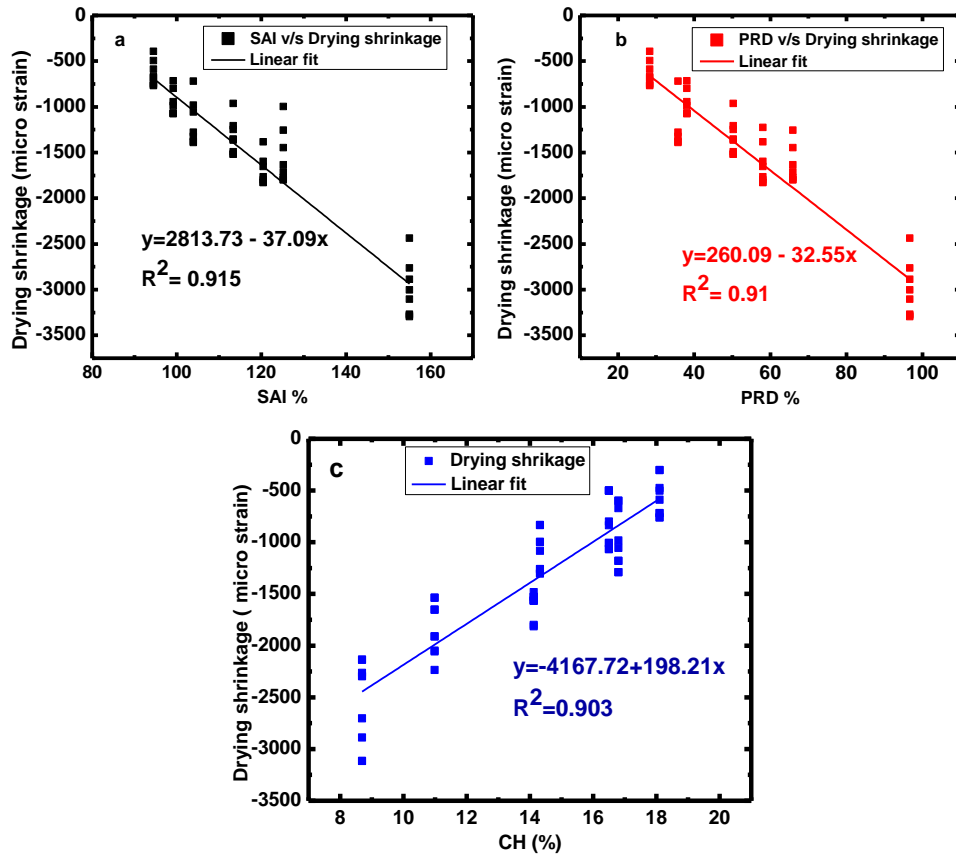
Figure 4.62: Relationship plot between a) SAI v/s drying shrinkage b) PRD v/s drying shrinkage c) CH content v/s drying shrinkage

Measurement of drying shrinkage for cementitious composites enables the estimation of possible volumetric changes caused due to internal and external environment. Estimation of volumetric strain is one of the significant parameters that influences the durability of the structure particularly in fluctuating climatic condition. Use of blended mixes influences optimistically on volumetric changes owing to its additional physical and chemical action i.e., filler and pozzolanic effect. However, assessment of drying shrinkage of cementitious composites is a tedious and time-consuming process. But it is to be noted that measurement of pozzolanic reactivity of blended cementitious composites in terms of SAI (using the values of compressive strength), PRD (using selective dissolution method) and CH content (using TGA) is the fast measuring procedure compared to that of long-term drying shrinkage measurement. Hence, determination of drying shrinkage using pozzolanic reactivity indices such as SAI, PRD and CH would make things much quicker.

4.5 SUMMARY

- Implementing the theory of particle packing i.e. modified Andreasen and Andersen model, the right proportions of mineral admixtures could be proportioned for the production of multi blended cement paste and mortar.

- In binary blended cement mortar the highest compressive strength and lowest chloride ion permeability was corresponded to the optimum nano-silica dosage i.e. at 3%. While, compared to control and ternary blended samples, quaternary blended samples performed the best at all the curing ages owing to its better particle packing and pozzolanic effect.

- With respect to the linear expansion, quaternary blended mix and 3% nano-silica mix were having the least micro strain measurement.

- Under acid and alkali attack, interaction of aggressive ions (SO_4^{2-}) with in cementitious system directed to CH disbanding and formation of aggressive products (AFt and Gy) causing deterioration in cementitious mixes through expansion, strength and density loss.

- It can be concluded from TGA results of blended paste samples that the presence of SCMs with nano-silica combination showed the potential reduction in CH amount and improvement in WH quantity.

- XRD analysis of binary blended paste samples revealed the significant increase in C-S-H peak and drastic reduction in CH peak with the increase in nano-silica content even at the early age of 7days. In ternary and quaternary blended samples presence of nano-silica had an immense effect in C-S-H and CH peak, but the additional C-S-H peaks are much stronger after 28days.

- Ca/Si atomic ratio attained from the results of SEM-EDX analysis was found to be lower for binary blended samples at all the ages indicating denser formation of C-S-H. However, all the composite samples showed the lower value of Ca/Si ratio compared to control sample. Quaternary blended samples executed the lowest Ca/Si ratio compared to control and other ternary blended samples.

CHAPTER – 5

INFLUENCE OF PHASE CHANGE MATERIALS ON THERMO-MECHANICAL AND DURABILITY PROPERTIES OF CEMENTITIOUS MORTAR INTEGRATED WITH NANO-SILICA

5.1 GENERAL

This Chapter deals with the results of the experimental investigation carried out to study the influence of bulk phase change materials (PCMs) on early age, hydration, thermal, mechanical, microstructure and durability properties of nano silica admixed cementitious composites. First, desired proportion of PCMs were identified pertaining to a designated compressive strength of 35 MPa at the curing age of 28 days. Next, best performing PCM admixed cementitious mortar with respect to desired compressive strength was integrated with optimized dosage of nano-silica. Advanced characterization such as thermo gravimetric analysis (TGA), x-ray diffraction (XRD) and scanning electron microscopy (SEM) were carried out to study hydration and microstructure properties of cementitious composites, respectively. Further, thermal properties were determined by means of differential scanning calorimeter (DSC).

5.2 PCM ADDED CEMENTITIOUS MORTAR

5.2.1 Compressive strength

Figure 5.1 shows the compressive strength of cement mortar integrated with different type and proportion of PCMs for the curing ages of 3, 7 and 28 days. Apt PCM on the basis of the attainment of designated compressive strength of 35 MPa at the age of 28days was identified.
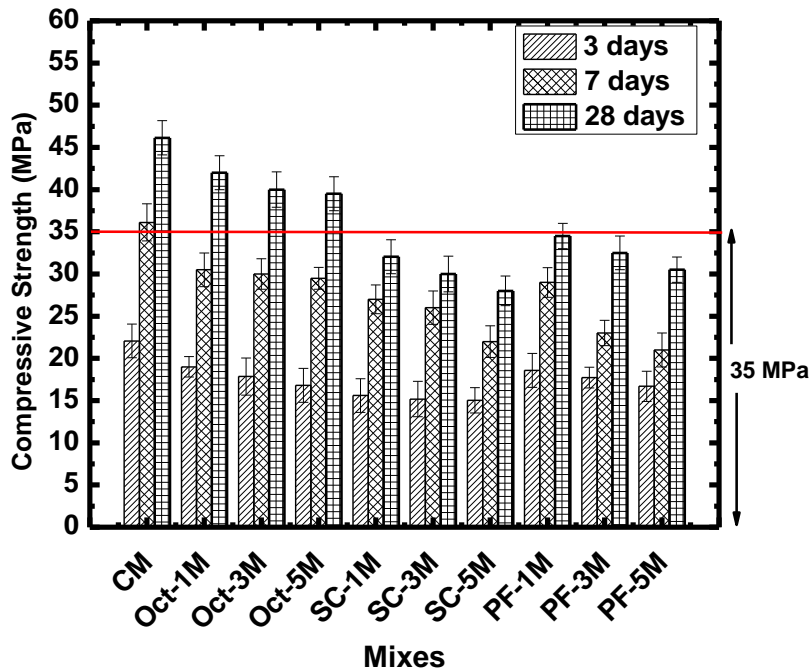
Figure 5.1: Compressive strength results of PCM admixed mortar

However, substantial reduction in compressive strength was noticed in PCM admixed mortar irrespective of curing ages as compared to that of control mortar. This reduction in compressive strength in PCM modified mortar is found to be directly proportional to the dosage of PCM. The percentile reduction in compressive strength of PCM modified cement mortar at the curing age of 28 days ranges from 15% - 30% for n-octadecane based mortar (oct-mixes), 31% - 46% for sodium carbonate hydrate-based mortar (SC-mixes) and 27% - 38% for paraffin wax-based mortar (PF-mixes). However, experimental results showed that in the midst of various PCMs admixed cement mortar, oct-1M, oct-3M and oct-5M cement mortar mixes achieved the desired 28 days compressive strength (35MPa), i.e. 42 MPa, 40 MPa and 38 MPa, respectively. Presence of PCMs of any form in cementitious composites indicated the lowered strength (Ling and Poon, 2013; Sahu et al., 2017; Cellat et al., 2017). It was reported that presence of PCM in cementitious system may possibly coat on the surface of unhydrated cement particles obstructing the hydration reaction (Sakulich and Bentz., 2012).

In the next stage, optimized dosage of nano-silica mix (CNS-3M) were admixed with the identified PCM proportions (i.e. oct-1M, oct-3M and oct-5M) and were designated as CNS/oct-

1M, CNS/oct-3M and CNS/oct-5M, respectively. Figure 5.2 demonstrates the compressive strength plot for nano-silica modified PCM mixes (CNS/oct-1M, CNS/oct-3M and CNS/oct-5M).

It can be perceived from the Figure 5.2 that with the integration of 3% nano-silica to the varied proportions of n-octadecane added mortar, compressive strength found to be improved by 15%, 13 % and 10% at the age of 28 days with respect to oct-1%, oct-3% and oct-5% mixes. This improvement in strength of CNS/oct mortar mixes may be ascribed to the compensation of disturbance in hydration product due to the interference of PCMs by the addition of highly reactive nano sized silica particles (Qing et al., 2007; Land et al., 2012; Singh et al., 2015).
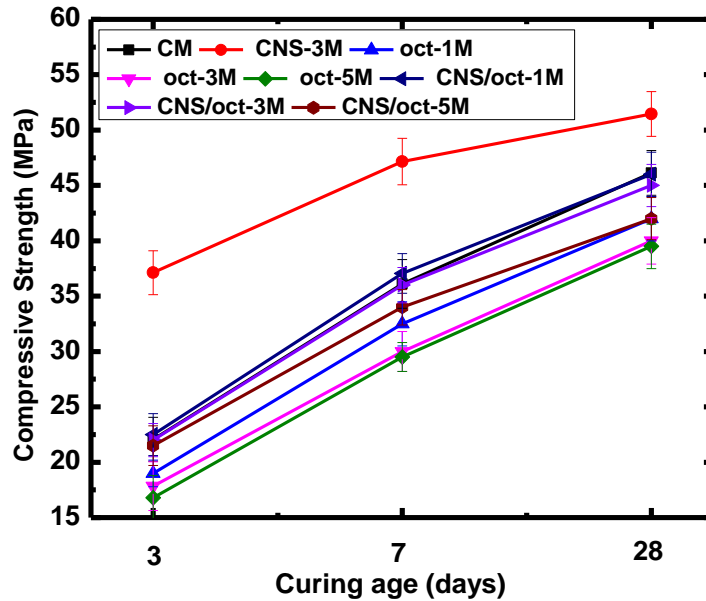
Figure 5.2: Compressive strength plot for nano-silica modified n-octadecane PCM mixes

5.2.2 Density

The results of density for selected cementitious mortar with the incorporation of nano-silica and PCMs at the age of 3, 7 and 28 days is demonstrated in Table 5.1.

Table 5.1: Density values of control, optimized nano-silica, PCM (n-octadecane) and nano-silica modified PCM admixed cementitious mortar

Mix	Density (g/cc)		
	3 days	**7 days**	**28 days**
CM	2.16	2.24	2.32
CNS-3M	2.36	2.40	2.46
oct-1M	2.15	2.18	2.20
oct-3M	2.14	2.20	2.25
oct-5M	2.10	2.12	2.16
CNS/oct-1M	2.17	2.24	2.35
CNS /oct-3M	2.16	2.23	2.33
CNS /oct-5M	2.15	2.23	2.30

It can be perceived from the Table 5.1 that CNS-3M mix has greater potential to increase the density as compared to that of control mortar. CNS-3M mortar sample increased the density by 6% with respect to control mortar at the age of 28 days. This may be due to the dual performance of nano-silica particle acting both as a nano-filler and pozzolanic activator (Du et al., 2014). Further, it can be understood that for PCM (n-octadecane) based cement mortar density was found to be decreased, this could be due to the incompatibility of PCMs within the cementitious system. Whereas, for CNS/oct mortar mixes, density values were found to be tailored due to the presence of nano-silica content. The density value for CNS/oct mixes were found to be increased by 6% - 7% in correspondence to PCM based mortar mixes (oct- mortar mixes) at the age of 28 days.

5.2.3 Drying shrinkage

Drying shrinkage values (micro strain) of control, CNS-3M, PCM (n-octadecane) admixed cementitious mortar mixes as well as PCM mixes modified with 3% nano-silica were plotted as a function of exposure period (i.e. 1, 3, 7, 14, 30, 60, 90, 120 and 180 days) and the same is presented in Figure 5.3.
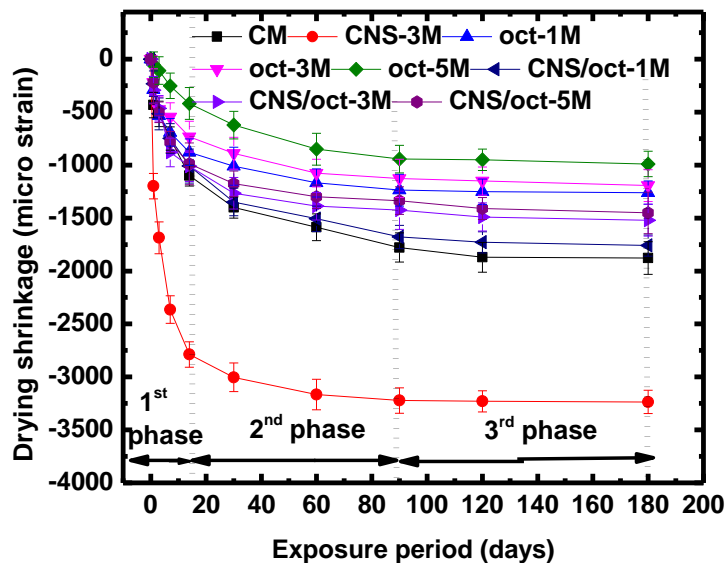
Figure 5.3: Drying shrinkage values of control, CNS-3M and all PCM based cementitious mortar

Figure 5.3 indicates that CNS-3M mix, which comprises of 3% nano-silica as a replacement to cement shows greater shrinkage value. Shrinkage value for CNS-3M mix at the maximum exposure period of 180 days was 3236 micro strain and that is found to be 80 times higher to that of control mortar. The probable reason attributed to the increased shrinkage characteristics for nano-silica mix is that it acts as an activator to accelerate the cement hydration owing to its higher surface area and that greatly results in higher consumption of water. Further, due to high heat of hydration initial age (1 to 14 days) shrinkage caused due to chemical reactivity is found to be higher.

On the other hand, substantial reduction in drying shrinkage was noticed for PCM admixed mortar as compared to that of control mortar. It can also be seen from the figure that rate of drying shrinkage for PCM admixed cementitious mortar is inversely proportional to PCM dosage. Drying shrinkage values for oct-1M, oct-3M and oct-5M at the exposure period 180 days were found to be 1260, 1193 and 990 micro strain, respectively. PCM being a latent heat storage material has an ability to absorb the heat generated during the period of hydration and this would control the initial shrinkage rate caused due to heat of hydration (Fernandes et al.,

2014), hence, initial shrinkage found to be lower. However, it can be inferred from the figure that for nano-silica admixed PCM based cementitious mortar mixes (CNS/oct) drying shrinkage values were seen to be modified due to the dual action of nano-silica (high reactivity) and PCM. Rate of drying shrinkage for CNS/oct-mixes falls between PCM mixes and control mix. Drying shrinkage value of CNS/oct-mixes were seen to be in the range of 1500 to 1451 micro strains and are much lower to that of CNS-3M mix.

Similar trend of drying shrinkage curve expressing a three phase drying system was observed for all the PCM admixed cementitious mortar mixes. Section 4.3.3 clearly demonstrates the three phase system of drying shrinkage curve.

5.2.4 Durability properties

5.2.4.1 Permeable porosity

The percentage of permeable porosity for control, optimized nano-silica, identified PCM and nano-silica admixed PCM based cementitious mortar at the age of 3, 7 and 28 days are presented in Table 5.2.

Table 5.2: Permeable porosity of control, optimized nano-silica, PCM (n-octadecane) and nano-silica modified PCM admixed cementitious mortar

Mix	Permeable porosity (%)		
	3 days	7 days	28 days
CM	18.19	15.91	13.64
CNS-3M	11.63	9.23	8.7
oct-1M	19.61	19.04	16.48
oct-3M	20.74	19.89	16.77
oct-5M	21.03	20.18	17.05
CNS/oct-1M	18.76	15.91	13.92
CNS /oct-3M	19.04	16.20	14.21
CNS /oct-5M	20.74	17.05	15.06

It can be observed from the table that significant reduction in permeable porosity percentage was seen for CNS-3M mix. Permeable porosity of CNS-3M mix was found to be reduced by

36% with respect to control mix at the age of 28 days. The reason associated to this is that smaller particle of nano-silica has an advantage to act as a fine filler along with superior reactivity. In case of PCM (n-octadecane) based cement mortar permeable porosity was found to be increased with the increase in PCM dosage, this could be due to the development of air gaps within the cementitious system causing disruption in binding ability. When identified PCM (n-octadecane) based cement mortar were integrated with nano-silica i.e. CNS/oct mortar mixes, percentage of permeable porosity were seen to modified due to the action of nano-silica as reported in section 5.2.2. The permeable porosity value for CNS/oct mixes were found to be reduced at the rate of 13% - 17% in correspondence to octadecane based PCM mixes.

5.2.4.2 Rapid chloride-ion penetration test (RCPT)

The results of total charge passed through the various mixes at the age of 7 and 28 days are plotted in the Figure 5.4.
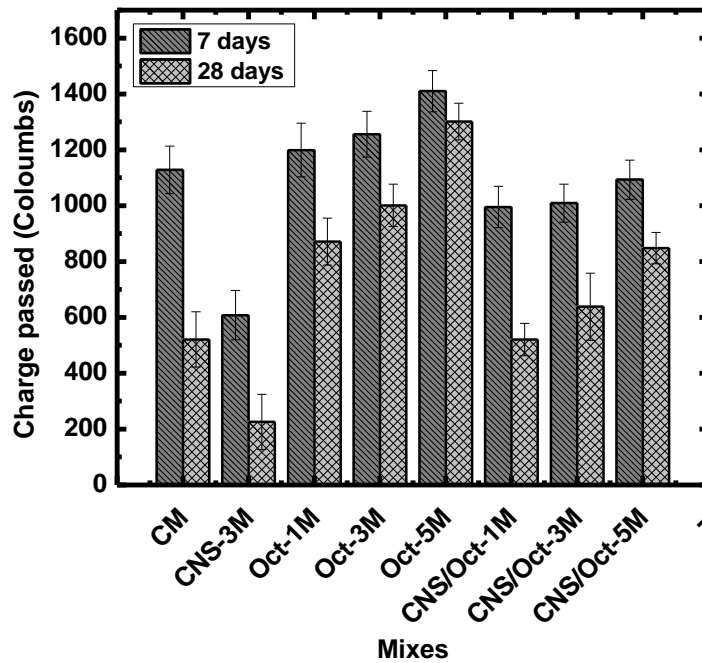
Figure 5.4: Variation of charge passed for nano-silica, PCM (n-octadecane) and nano-silica/PCM admixed mortar mixes at curing ages of 7 and 28 days

From the plotted results, it can be observed that, as the curing period increases the chloride ion permeability decreases for all the cement mortar samples. The graphical representation clearly depicts the dramatic reduction in charge passing for CNS-3M mix. The charge passed for CNS-3M mix at the curing age of 28 days is 226 coulombs, which is well within the limit of 100 to1000 coulombs that can be designated to very low chloride ion penetrability as per ASTM C 1202. But, for the identified PCM (n-octadecane) added mortar mixes, it was observed from the results that as the dosage of PCM increased the charge passed found to be increased. This may be owing to the increase in porosity and alteration in cementitious matrix in the occurrence of PCMs (Ling and Poon, 2014). However, the charge passed through n-octadecane based PCM mortar was observed to be reduced when 3% nano-silica was introduced into the mix.

5.2.4.3 Acid, alkali and chloride resistance

5.2.4.3.1 Exposure to acid (H$_2$SO$_4$) solution

5.2.4.3.1.1 Density loss and strength loss

Results of density loss and strength loss for control, optimized nano-silica, identified PCM and nano-silica admixed PCM based cementitious mortar exposed to 1% sulfuric acid (H$_2$SO$_4$) solution for the exposure periods of 30, 60, 90, 120 and 180 days are presented in Figure 5.5.
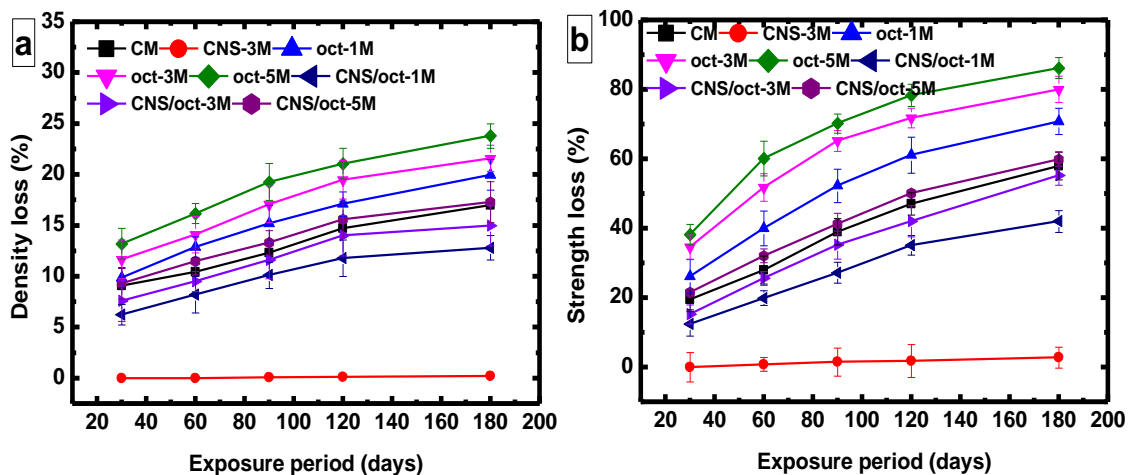
Figure 5.5: a) Density loss and b) strength loss percentage for PCM admixed cementitious mortar exposed to sulfuric acid (H$_2$SO$_4$)

It can be observed from the figure that CNS-3M mortar mix experiences least deterioration with density and strength loss percentage of 0.23% and 2.4%, respectively at the exposure

period of 180 days. This could be attributed to the reduction in initial calcium hydroxide content due to the high pozzolanic activity of nano-silica, thereby makes the cementitious matrix dense and hence controls the further diffusion of aggressive ions. While, PCM admixed cementitious mortar (oct-mixes) encounters greater deterioration as compared to that of control mortar with the increase in PCM dosage when exposed to H_2SO_4. Cementitious mortar comprising of 5% octadecane (oct-5M mix) experienced a density and strength loss of 24% and 80%, respectively at the exposure period of 180 days. This was mainly attributed to the deleterious act of sulphuric acid (H_2SO_4) on the cementitious matrix due to the combined effect of acid and sulphate attack (Barbhuiya and Kumala, 2017). Further, exposure to H_2SO_4 would cause dissolution and leaching of acid-susceptible constituents such as calcium hydroxide (Chemical reaction involved are described in Section 4.3.5.3.1.1). It was reported that this action results in an increase in capillary porosity, loss of cohesiveness and eventually losses the strength (Barbhuiya and Kumala, 2017).

It can be understood from the obtained results that by incorporating 3% nano-silica to PCM based cementitious mortar (CNS/oct), which are vulnerable to H_2SO_4, the rate of deterioration can be minimized. Figure also depicts that CNS/oct-1M and CNS/oct-3M exhibits lower percentage of density and strength losses compared to that of control mortar irrespective of exposure period. While, density and strength losses suffered by CNS/oct-5M found to be 2% and 3%, higher to control mortar, respectively. Hence, it can be inferred that to reduce the deterioration of the PCM based cementitious matrix by acid intrusion it is desirable to incorporate highly active pozzolanic ingredient that aids in improving the density and uniformity of the cementitious matrix.

In order to understand the influence of H_2SO_4 on PCM added cementitious composites thermogravimetric analysis (TG-DTG) was carried out. Figure 5.6 demonstrates TG-DTG plots for control, optimized nano-silica, identified PCM and nano-silica admixed PCM based cementitious mortar exposed to 1% H_2SO_4 solution for the period of 180 days.
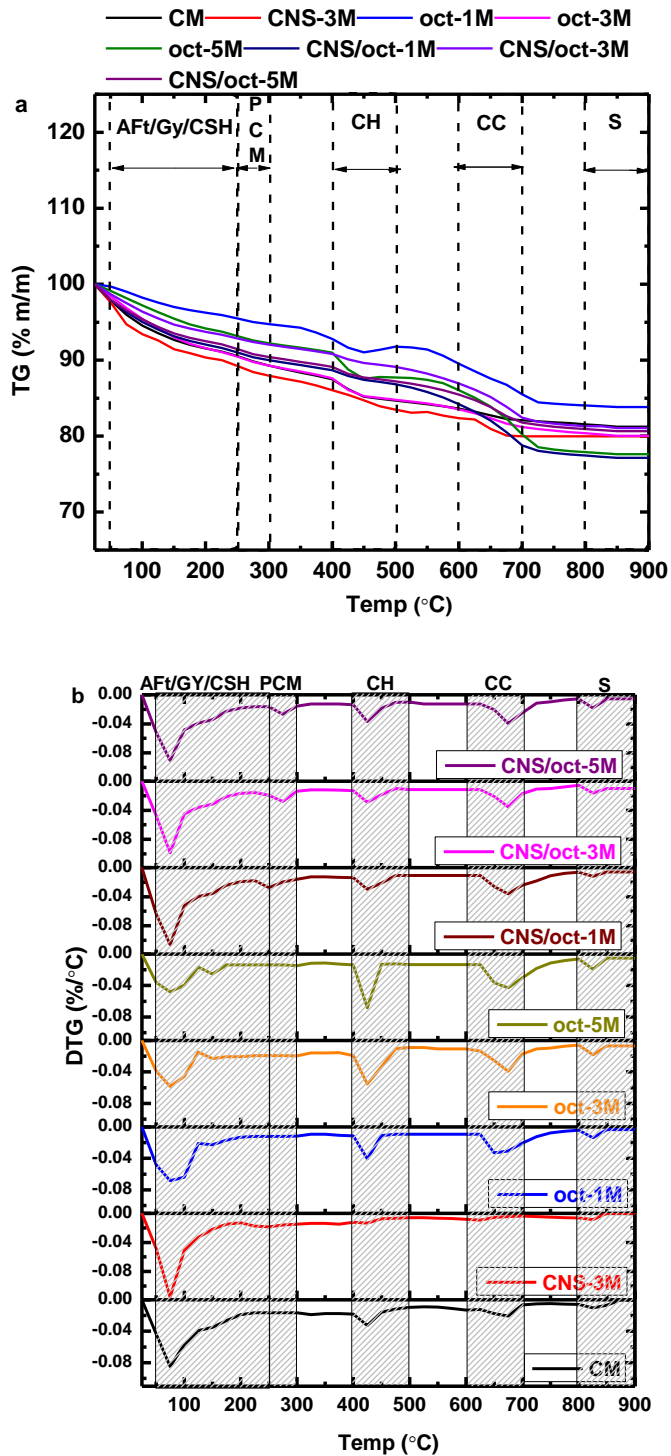
Figure 5.6: a) TG and b) DTG plots of control, nano-silica, PCM (n-octadecane) and nano-silica/PCM admixed mortar mixes exposed to H$_2$SO$_4$ solution for the duration of 180 days

It can be seen from the Figure 5.6 that thermogravimetric mass losses for control, CNS-3M and all PCM based cementitious mixes occurred at the different ranges of temperature i.e. a) 25-50 °C indicating the loss of free water molecules present in the system b) 50-300 °C signifies the three key decomposition events, relating to the dehydration of ettringites (AFt, 50-120 °C), gypsum (Gy, 120-150 °C) and chemically bound water from calcium silicate hydrates (CSH, 150-300 °C), c) 400-500 °C indicates the dehydroxylation of calcium hydroxide (CH) and d) 600-700 °C symbolizes the and decarbonation of calcium carbonate (CC). Further, DTG peak noticed beyond 800 °C designates the decomposition of sulfates (S) (Chen et al., 2000). It was important to note from the DTG curves (Figure 5.6b) that for CNS/PCM mixes additional endothermic peak was observed at the temperature boundaries of 250-300 °C that indicates the decomposition of PCM (octadecane). However, endothermic peak referring to PCM was found to be absent in PCM based cementitious mixes without nano-silica (oct-mixes). This could be attributed to extermination of PCM in cementitious mixes exposed to H_2SO_4. Whereas, presence of nano-silica in PCM admixed cementitious mixes controlled the deterioration of PCM caused due to H_2SO_4 exposure owing to the refinement of microstructure of cementitious matrix through the action of nano-silica. This demonstrates that in CNS/oct- mixes PCMs are still active as a thermal storage material after the 180 days of exposure to H_2SO_4.

Section 4.3.5.3.1.1 clearly depicts that ettringite (AFt) and gypsum (Gy) are the two major compounds that are responsible to the deterioration of cementitious composites. On the basis of TG-DTG results amount of AFt and Gy formed for control, 3% nano-silica and all PCM based cementitious (with and without nano-silica) mixes during 180 days of H_2SO_4 exposure were quantified (using Equation 3.10 and Equation 3.11) and the same are graphically presented in Figure 5.7.
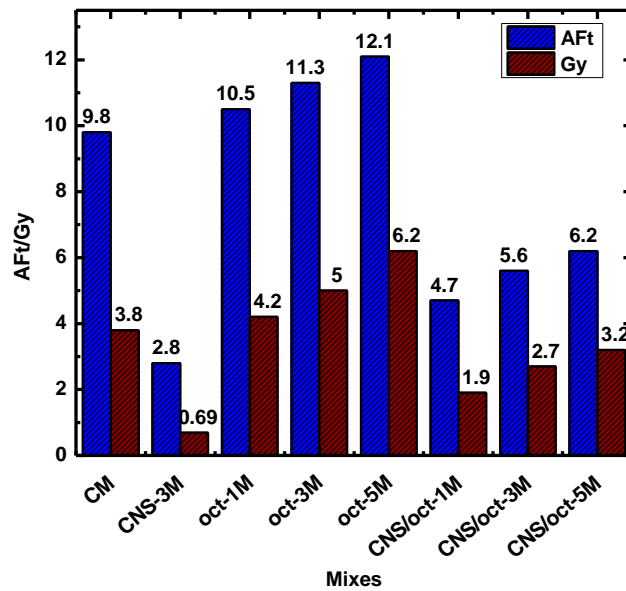
Figure 5.7: Quantified amounts of AFt and Gy for control, nano-silica, PCM (n-octadecane) and nano-silica/PCM admixed mortar mixes exposed to H_2SO_4 solution for 180 days

It can be observed from the figure that least formation of AFt and Gy was obtained for CNS-3M mix. This is attributed the greater consumption of CH by means of high reactivity rate of nano-silica and formation of densified cementitious matrix owing to its physico-chemical activity (Black et al., 2006). Further, it is evident from the figure that AFt and Gy content for PCM added cementitious mixes (oct-mixes) found to be higher to that of control mix. It can also be inferred from the figure that AFt and Gy content for oct-mixes increases with the increase in PCM dosage. This was ascribed to the increase in CH content with the increased dosage of PCM in cementitious mixes and this can be substantiated through the increase in endothermic peak height associated to dehydroxylation of CH (at 400-500 °C) with the increase in PCM content. It is to be noted from the figure that amount of formation of AFt and Gy for PCM based cementitious mixes were found to be modified by the integration of 3% highly reactive nano-silica i.e CNS/oct mixes. Formation rate of AFt and Gy content for CNS/oct mixes were found to be reduced by ≈50% with respect to PCM based cementitious mixes without nano-silica (oct-mixes). This is mainly attributed to the tailoring action of nano-silica on PCM added cementitious mixes by minimizing the pores

192

generated through the incorporation of PCMs, instigating the pozzolanic reactivity and reducing the concentration of CH with in PCM based cementitious system.

5.2.4.3.1.2 Length change
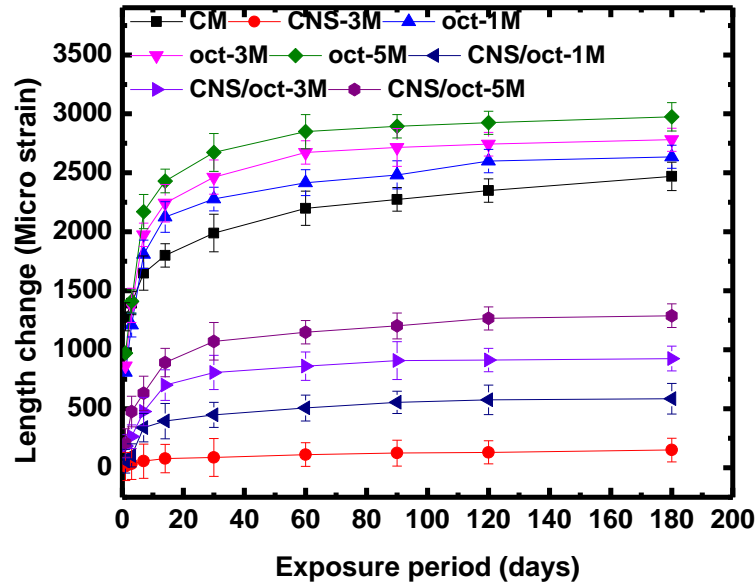
Figure 5.8: **Length change values of PCM admixed cementitious mortar mixes exposed to H₂SO₄ solution at different exposure periods**

Length change experienced by control, optimized nano-silica mix (CNS-3P), identified PCM mixes (oct-1P, oct-3P and oct-5P) and nano-silica modified PCM mixes (CNS/oct-1P, CNS/oct-3P and CNS/oct-5P) exposed to 1% H_2SO_4 expressed in terms of micro strain submerged is presented in Figure 5.8. All mortar specimens with and without PCMs exposed to H_2SO_4 undergoes expansion over the period of exposure. It has been described in Section 4.3.5.3.1.2 is that this expansion is caused due to the development of expansive products such as Aft and Gy owing to the reactivity of sulphate ions with hydrated calcium hydroxide (CH) and calcium aluminates (C_3A). It can be perceived from the figure that control mortar experiences a length change of approximately 2500 micro strains at the exposure period of 180 days. From the figure it can be observed that CNS-3M mortar mix comprising of 3% nano-silica experiences lowest length change days as compared to that of control mortar and other PCM based mortar mixes with a maximum value of 130 micro strain at the age of 180. This

could be ascribed to the reduction in CH content and development of more uniform/dense microstructure of cementitious mortar owing to the high pozzolanic and nano filling action of nano-silica.

Figure also demonstrates that rate of expansion increases with the increase in PCM dosage for all the n-octadecane PCM based cementitious mixes (oct-mixes) and found to be higher than that of control mix. Length change values for oct-1M, oct-3M and oct-5M at the maximum exposure age of 180 days were seen to be 2636 micro strain, 2781 micro strain and 2975 micro strain, respectively. This could be attributed higher percentage of calcium hydroxide with the addition of PCMs and cross linking of PCM with hydration products that weakens the microstructure thereby making the system susceptible to deleterious ions (Sharma, 2013). Increase level of CH in PCM admixed cementitious system increased the amount of Gy and AFt formation, which are highly expansive compounds. It can be noticed from the Figure 5.7 that Gy and AFt amount were found to be 7-24% and 11-60% higher to that of control mortar at the age of 180 days, respectively. It was reported that these compounds are responsible for increase in volume to about 1.2 and 2.5 times, respectively (lrassar et al., 1995). It can be observed from the figure that PCM admixed cementitious mortar integrated with 3% nano-silica (i.e. CNS/oct) experiences a length change in the range of 586 to 1289 micro strain that falls lower to that of control mortar. It is evident from the results that rate of expansion corresponding to H_2SO_4 exposure can be controlled by the intrusion of optimized dosage of highly reactive nano-silica to PCM based cementitious mortar. Further, formation of AFt and Gy were found to be significantly reduced for CNS/oct-mixes compared to that of PCM based cementitious mixes without nano-silica that would be the probable reason for the reduction in expansion rate. The reason associated to this is the increased consumption rate of lime due to the presence of highly pozzolanic nano-silica and improved microstructure.

5.2.4.3.2 Exposure to alkali (Na_2SO_4) solution

5.2.4.3.2.1 Density loss and strength loss

Figure 5.9 shows the density and strength losses endured by control, optimized nano-silica mix (CNS-3P), identified PCM mixes (oct-1P, oct-3P and oct-5P) and nano-silica modified PCM

mixes (CNS/oct-1P, CNS/oct-3P and CNS/oct-5P) exposed to 5% sodium sulfate (Na$_2$SO$_4$) solution for the exposure periods of 30, 60, 90, 120 and 180.
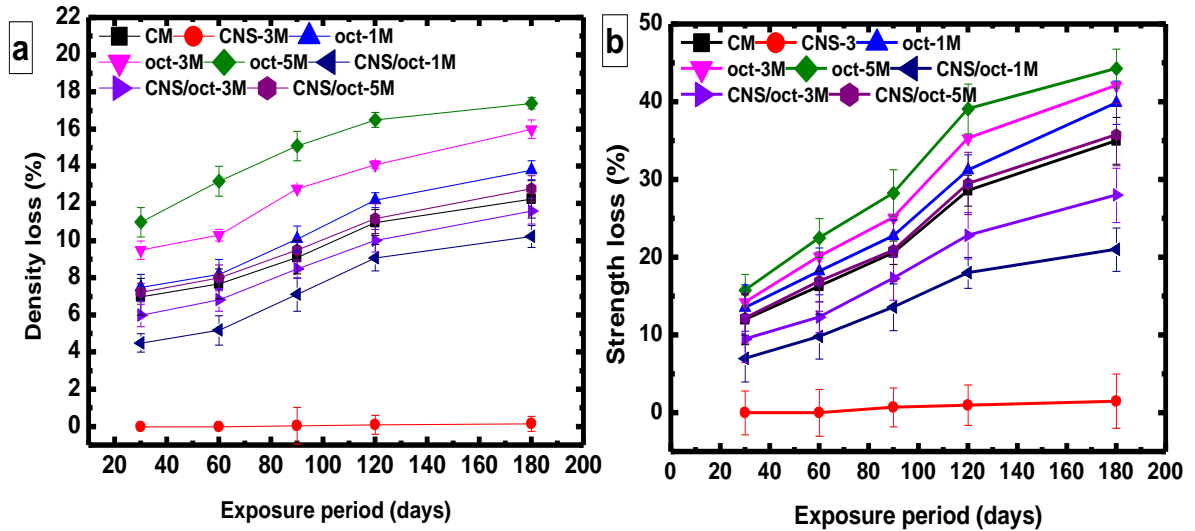
Figure 5.9: a) Density loss and b) strength loss percentage for PCM admixed cementitious mortar exposed to sodium sulfate (Na$_2$SO$_4$) solution

It can be observed from the figure that as like H$_2$SO$_4$ exposure, CNS-3M mix showed least deterioration in correspondence alkali (Na$_2$SO$_4$) exposure. Density loss and strength loss values for CNS-3M mix at the exposure period of 180 days was found to be 0.16% and 1.5%, respectively. While, PCM admixed cementitious mortar mixes (oct-mixes) experienced greater deterioration as compared to that of control mortar. However, alkaline based Na$_2$SO$_4$ solution found to be less aggressive compared to that of H$_2$SO$_4$ solution owing to its acidic nature. Among PCM based cementitious mortar mixes, mix comprising of 5% PCM (oct-5M) suffers the highest deterioration with maximum value of density and strength losses of 17% and 44%, respectively at the exposure period of 180 days. Further, it can be understood from the figure that PCM admixed cementitious mortar when integrated with 3% nano-silica (CNS/oct- mixes) deteriorated caused due to Na$_2$SO$_4$ exposure found to be reduced. It can be seen from the figure that density and strength losses for CNS/oct-1M and CNS/oct-3M were found to be lower to that of control mortar. Density loss and strength loss experienced by CNS/oct- mixes mix was found be reduced by around 27% and 35%, respectively with respect to oct-mixes at the exposure period of 180 days. This controlled level of deterioration was due to the presence of

nano-silica, which compensated the negative impact of PCMs on the performance of cementitious composites.

Diffusion of Na_2SO_4 into cementitious matrix also leads in the formation of voluminous compounds such as AFt and Gy. Chemical reactions involved during Na_2SO_4 exposure are presented in Section 4.3.5.3.2.1.

TG-DTG results of control mix, optimized nano-silica mix, identified n-octadecane based PCM mixes and nano-silica modified PCM mixes exposed to 5% Na_2SO_4 solution for the period of 180 days are presented in Figure 5.10.

It can be observed from the figure that the trend of TG-DTG curves (i.e. mass loss and endothermic peak) for Na_2SO_4 exposed PCM based cementitious mixes were found to be similar to H_2SO_4 exposure condition. It is important to note that in case of Na_2SO_4 exposure condition endothermic peak at the temperature range of 250-300 °C, which signifies the PCM decomposition was also seen to be in oct-3M and oct-5M mixes without nano-silica that indicates the existence of PCM in alkali exposed cementitious mixes at 3-5% PCM dosages. Further, AFt and Gy formed during Na_2SO_4 exposure of PCM based cementitious mixes are weak and voluminous compounds, which leads to the deterioration of cementitious system.
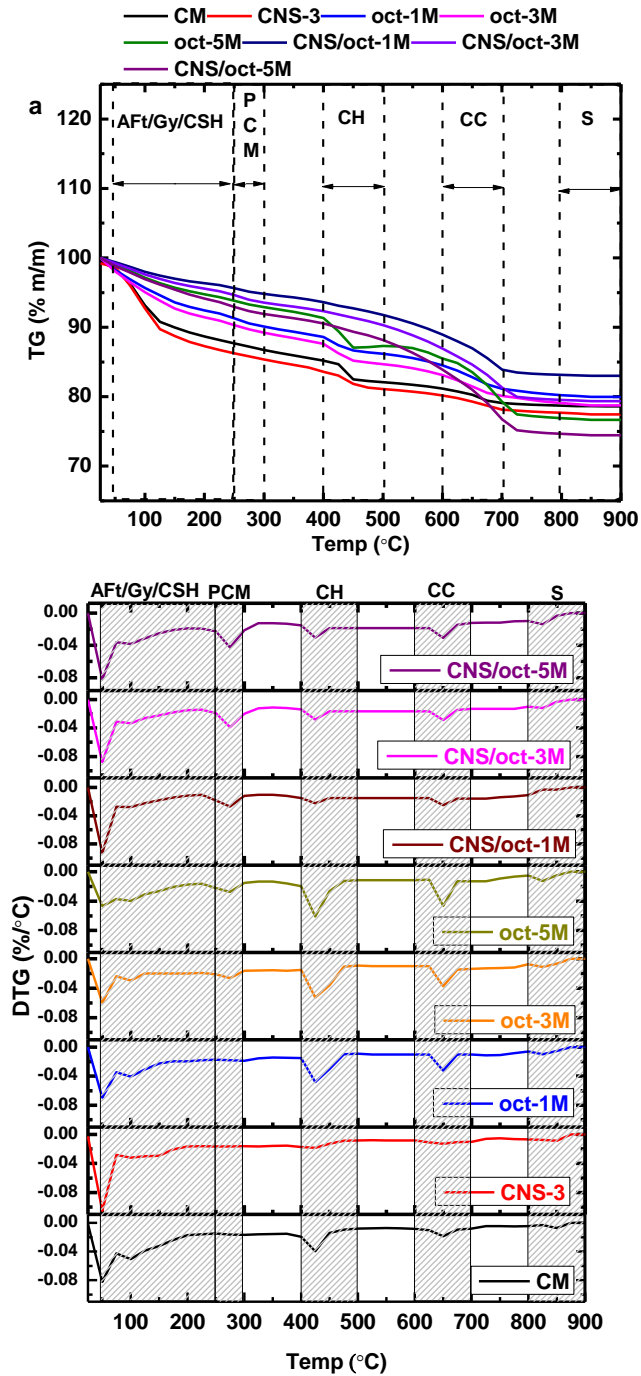
Figure 5.10: a) TG and b) DTG plots of control, nano-silica, PCM (n-octadecane) and nano-silica/PCM admixed mortar mixes exposed to Na$_2$SO$_4$ solution for the duration of 180 days

Quantified amount of AFt and Gy (using Equation 3.10 and Equation 3.11) for control, 3% nano-silica, PCM (n-octadecane) and nano-silica/PCM added mortar mixes exposed to Na_2SO_4 solution for 180 days are plotted in the form of histogram and presented in Figure 5.12.
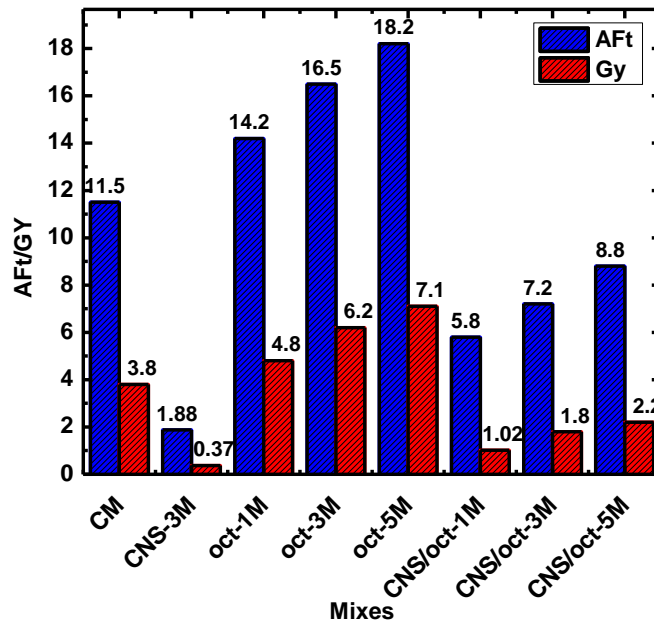
Figure 5.11: Quantified amounts of AFt and Gy for control, nano-silica, PCM (n-octadecane) and nano-silica/PCM admixed mortar mixes exposed to Na_2SO_4 solution for 180 days

It can be seen from the figure that CNS-3M mix with 3% nano-silica tremendously reduced the formation of voluminous compounds such as AFt and Gy. This minimized formation of AFt and Gy for CNS-3M mix could be attributed to the existence of negligible CH traces, this fact is evinced from the mass loss curve associated to dehydroxylation of CH (Figure 5.10). On the other end, the rate of formation of AFt and Gy for Na_2SO_4 exposure condition was higher for PCM based cementitious mixes and found to be increase with the increase in the percentage addition of PCM. AFt and Gy content for oct mixes were found to be increased by 23 -58% and 26 -87%, respectively with respect control mix at the exposure age of 180 days. This is attributed to the increase in free lime (CH) and larger availability of un-hydrated aluminate compounds such as C_3A and C_4AF in cementitious matrix owing to the presence of

PCM and 100% OPC. It is reported that PCMs are responsible for increase in capillary porosity in cementitious paste owing to its negative impact on binding. Further, it can be noticed from the figure that for CNS/oct- mixes formation of AFt and Gy were seen to be curtailed in correspondence to oct-mixes. Amount of AFt and Gy formed for CNS/oct- mixes were found to be reduced by 51 -60% and 69 -79%, respectively in correspondence to PCM admixed cementitious mixes without nano-silica (oct-mixes). This could be due to the occurrence of highly reactive nano-silica yields in the reduction of CH concentration and also complement in minimizing the capillary pores generated through PCM as well as by CH.

5.2.4.3.2.2 Length change

Resulted length change values for control mix, 3% nano-silica mix and PCM added cementitious mixes (with and without nano-silica) exposed to alkali solution (5% Na_2SO_4) at different exposure periods are shown in Figure 5.12.
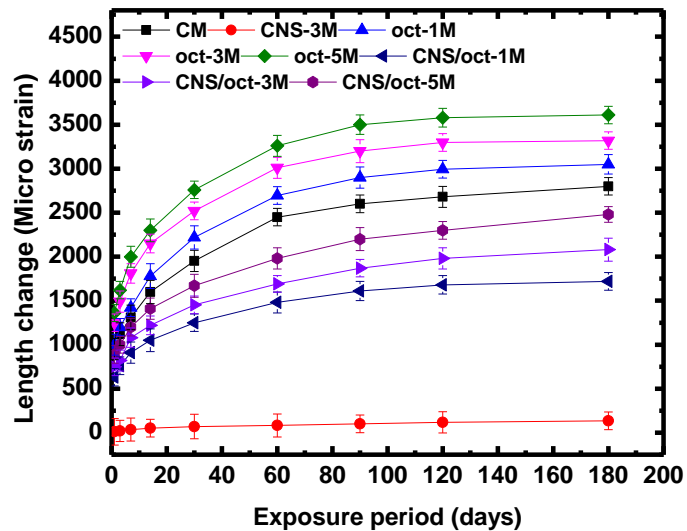
Figure 5.12: Length change values of PCM admixed cementitious mortar mixes exposed to Na_2SO_4 solution at different exposure periods

From the obtained results it is noticed that all the mixes exhibited an expansive behaviour when exposed to Na_2SO_4 solution and found to be higher to that of H_2SO_4 exposure. This could be attributed to the immediate formation of voluminous compounds such as AFt and Gy at the instant when sulphate ion contacts with cementitious system (Black et al., 2006).

199

It can be noticed from the figure that expansion rate for CNS-3M mix with 3% nano-silica (as partial replacement to cement) was found to be least i.e. 152 micro strain at 180 days of exposure. High pozzolanic nature of nano-silica significantly reduced the amount of CH and C_3A content, which are susceptible to the formation of voluminous AFt and Gy. It can also be seen from the Figure 5.11 that the CNS-3M mix resulted in very low amount of AFt and Gy i.e.1.88% and 0.37%, respectively at the exposure period of 180 days. Further, figure also illustrates that with the increase in addition of PCM content in cementitious mortar rate of expansion also found to be increased. PCM added cementitious mixes (oct-mixes) showed higher expansion than control i.e. in the range of 3050 to 3610 micro strain. This could be ascribed to the to the presence of PCMs that disturbed the hydration process by cross linking with the hydrated products to form large traces of calcium hydroxide (Figure 5.10b) and diminishing the formation CSH, hence leading to larger formation of AFt and Gy content (Figure 5.11). But, the rate of expansion of PCM admixed cementitious mixes can be reduced with the addition of 3% nano-silica. Rate of expansion for CNS/oct-mixes was found to be reduced by 31%-44%. This is could be due to the presence of nano-silica that accelerated the pozzolanic and hydration activity of CNS/oct- mixes thereby resulting in lesser formation of AFt and Gy (Figure 5.11).

5.2.4.3.3 Exposure to chloride (NaCl) solution

5.2.4.3.3.1 Density loss and strength loss

Figure 5.13 presents the density loss and strength loss for control, 3% nano-silica mix (CNS-3M), PCM added mixes (oct) and nano-silica modified PCM added mixes (CNS/oct) exposed to 5% sodium chloride (NaCl) solution for the duration of 30, 60, 90, 120 and 180 days.
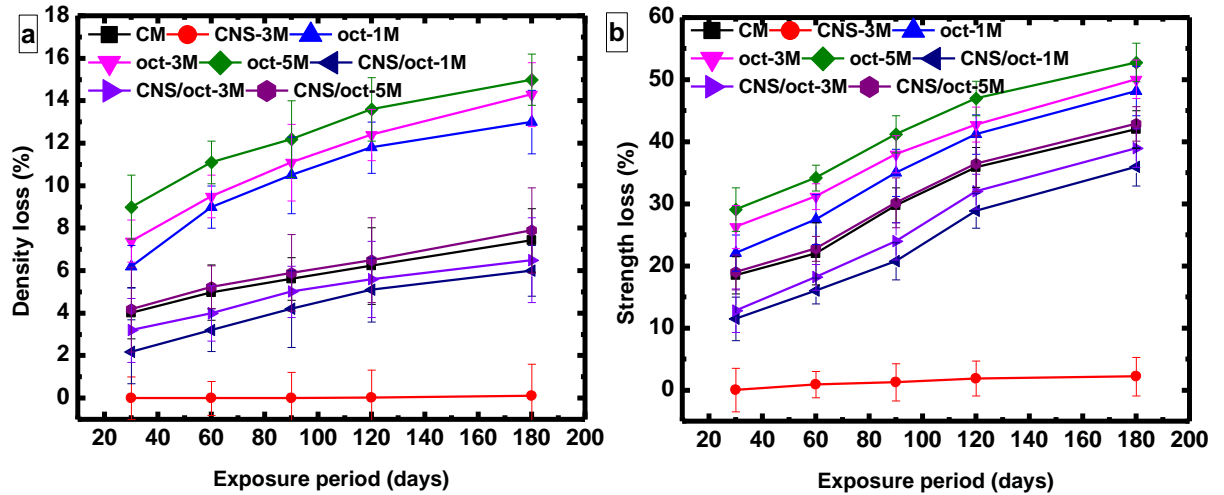
Figure 5.13: a) Density loss and b) strength loss percentage for PCM admixed cementitious mortar exposed to sodium chloride (NaCl) solution

It can be observed from the figure that as like acid and alkali exposure, CNS-3M mix showed least deterioration rate. It is understood that nano-silica has a greater role in resisting the action of chloride ions on cementitious system owing to its enhanced physical and chemical activity. In contrast, PCM added cementitious mortars (oct-mixes) showed highest rate of deterioration at 5% NaCl exposure. Density and strength losses suffered by oct-mixes were found to be increased by 75-90% and 20-30%, respectively with respect to control mix at 180 days of exposure. This could be ascribed to the deleterious facts such as decalcification, leaching of calcium chloride and formation of porous C-S-H (Chaudhary and Sinha, 2018). Further, integration of optimized nano-silica content (i.e. 3%) into the chloride susceptible PCM added cementitious mortar (CNS/oct- mixes) altered the rate of deterioration. Density and strength losses experienced by CNS/oct- mixes were found to be reduced by 47-55% and 26-30%, respectively in correspondence to oct-mixes without nano-silica. This could be attributed to the modified microstructure of PCM added cementitious mortar in the presence of highly reactive nano-silica reduced the diffusion capacity of chloride ions into the cementitious system.

Interaction of NaCl with un-hydrated and hydrated phases of aluminates of cementitious system leads to the formation of Friedel's salt (Fs) and its analogues and the endured reactions are presented in Section 4.3.5.3.3.1.

To analyse the action of NaCl on PCM added cementitious samples and the same in the presence of 3% nano-silica thermogravimetric analysis (TG-DTG) was carried out for the samples exposed to the duration of 180 days and the same are presented in Figure 4.32.

It can be observed from the Figure 5.14 that when 180 days NaCl exposed PCM admixed mortar mixes (with and without nano-silica) were subjected to thermogravimetric analysis series of thermogravimetric mass losses takes place at various ranges of temperature. It can be noticed from the Figure 5.14b that as like acid and alkali attack there exists endothermic peaks at 25-50 °C, 50-300 °C, 400-500 °C and 600- 700 °C, which indicates the dehydration of free water molecules, dehydration of CSH/AFt/Fs, dehydration of portlandite (CH) and decomposition of calcium carbonates, respectively. Further, it is to be noted that in case of NaCl exposure at the temperature range of 230-380 °C there exist a broadened endothermic peak. This was due to the overlapping of endothermic peaks developed through the decomposition of two compounds i.e. Friedel's salt (Fs, 230-380 °C) and PCM (250-300 °C).
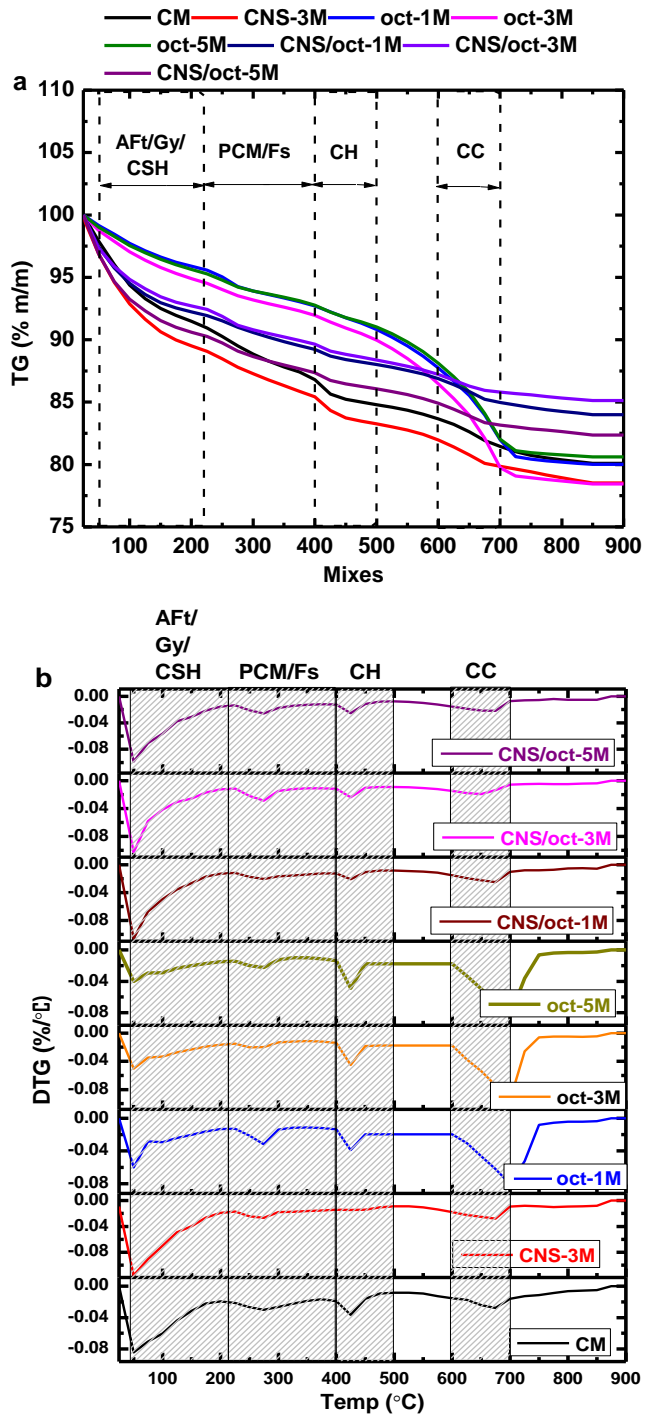
Figure 5.14: a) TG and b) DTG plots of control, nano-silica, PCM (n-octadecane) and nano-silica/PCM admixed mortar mixes exposed to NaCl solution for the duration of 180 days

Quantified amount of chemically bound Fs content (using Equation 3.12) for control, nano-silica, PCM (n-octadecane) and nano-silica/PCM admixed mortar mixes exposed to 5% NaCl solution is shown in Figure 5.15.
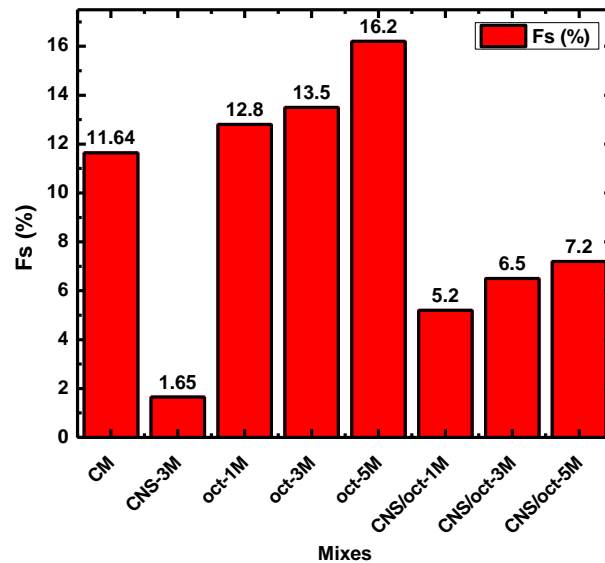
Figure 5.15: Quantified amounts of Fs for control, nano-silica, PCM (n-octadecane)
and nano-silica/PCM admixed mortar mixes exposed to NaCl solution for 180 days

Figure demonstrates the significant drop in Fs content for CNS-3M mix i.e. 86% lower to that of control mix. This could be attributed to the action of nano-silica in consuming the CH, supplementary formation of dense C-S-H, nano filler effect and reduced concentration of chloride vulnerable compounds such as C_3A and C_4AF. At the same time, amount of Fs formed for PCM added cementitious mixes (oct-mixes) were found to be increased by 10-40% with respect to that of control mix and are in directly proportional to the percentage of PCM added. This could be attributed to higher concentration of portlandite (CH) and aluminate phases (C_3A, C_4AF and AFm). Further, in case of nano-silica modified PCM added cementitious mixes (CNS/oct- mixes) despite of the disruption in hydration caused by PCM, presence of highly reactive nano-silica tailored the formation of Fs. Amount of Fs formed in CNS/oct mixes were found to be reduced by 52-55% in correspondence to oct-mixes without nano-silica. This indicates that resistance to chloride ion for PCM added cementitious mixes can be enhanced by integrating 3% of nano-silica.

5.2.4.3.3.2 Length change

Variation in length change for control mix, 3% nano-silica mix, n-octadecane PCM added mixes and 3% nano-silica modified PCM added mixes exposed to 5% NaCl solution for the duration of 1, 3, 7, 14, 30, 60, 90, 120 and 180 days are presented in Figure 5.16.
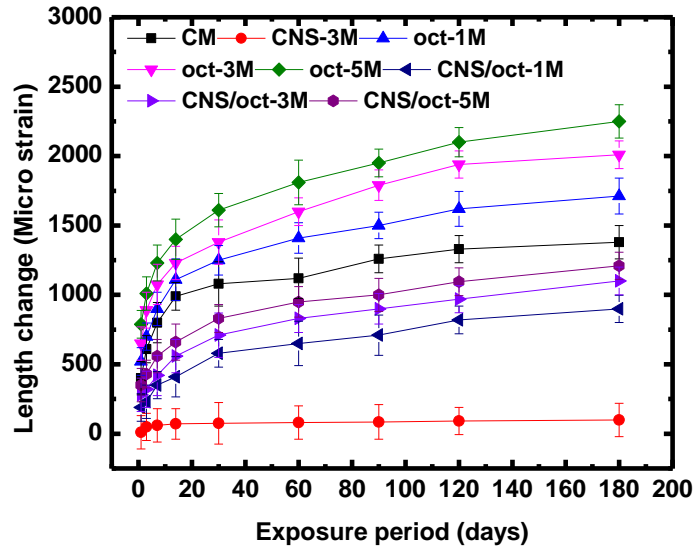
Figure 5.16: Length change values of PCM admixed cementitious mortar mixes (with and without nano-silica) exposed to NaCl solution at different exposure periods

It can be observed from the figure that the trend in variation of length change for control, CNS-3M and PCM added cementitious mortar (with and without nano-silica) specimens exposed to 5% NaCl solution was found to be similar to acidic and alkaline exposure. CNS-3M mix comprising of 3% nano-silica showed greater resistance to chloride exposure. Expansion value of CNS-3M mix at the exposure age of 180 days was seen to be <100 micro strain. This could be attributed to the least formation of Fs owing to its superior reactivity and filler property, which resists the diffusion of chloride ions and formation of Fs (Qiao et al., 2018). PCM added cementitious mortar mixes (oct-mixes), which encompasses larger Fs content (Figure 5.15) showed highest rate of expansion. Expansion value for oct-mixes at the exposure age of 180 days was found to be in the range of 1750-2250 micro strain, which is greater to that of control mix (1300 micro strain). This is mainly attributed to the voluminous nature of Fs, which

develops expansive stresses with the hardened cementitious system. It was important to note that incorporation of nano-silica in PCM added cementitious mixes controlled the rate of expansion caused due to NaCl solution. Expansion value for CNS/oct-mixes at the age of 180 days falls in the range of 750-1150 micro strain PCM based cementitious mortar in the presence of nano-silica exhibited better-quality microstructure by tailoring the interruption caused by PCM within the cementitious matrix.

5.3 PCM ADDED CEMENTITIOUS PASTE

5.3.1   Setting time

The results of setting time for control, optimized nano-silica mix (CNS-3P), identified PCM mixes (oct-1P, oct-3P and oct-5P) and nano-silica modified PCM mixes (CNS/oct-1P, CNS/oct-3P and CNS/oct-5P) were plotted and presented in Figure 5.17.
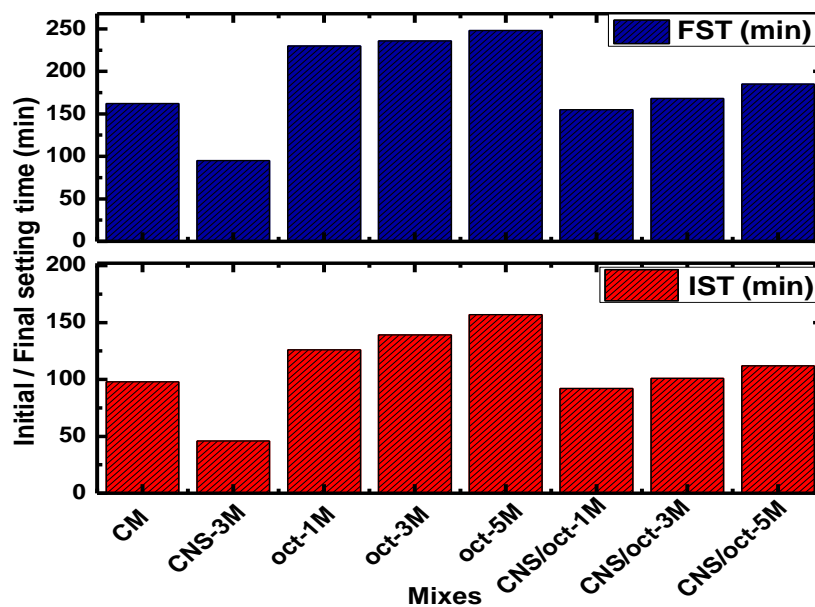
Figure 5.17: Variation in setting time of PCM admixed cement paste and nano-silica modified n-octadecane PCM admixed cement paste

It can be perceived from the Figure 5.17 that for CNS-3P mix initial and final setting time was lowered by 73 minutes and 66 minutes, respectively with respect to control mix. This can be attributed to the accelerated dissolution and precipitation process of cement particles and

hydrates at the initial stage reaction, and thus proliferating the hydration process (Gaitero et al., 2008). Further, for n-octadecane PCM mixes prolongation in setting time is found to be observed. Initial setting time of oct-1P, oct-3P and oct-5P samples were extended by 28 minutes, 41 minutes and 59 minutes, respectively with respect to control mix and final setting time was enhanced by 68 minutes, 74 minutes and 86 minutes, respectively.

On the other way, the prolonged setting time of n-octadecane PCM added cement paste was noticed to be altered with the integration of 3% nano-silica particles (Figure 4.42). The initial and final setting time of CNS/oct-1P was reduced by 6 minutes and 7 minutes, respectively in correspondence to control. However, for CNS/oct-3P and CNS/oct-5P initial setting time was prolonged by 3 minutes and 14 minutes and final setting time by 6 minutes and 16 minutes, respectively pertaining to control sample.

5.3.2   Surface temperature

The variation in surface temperature for control, optimized nano-silica mix (CNS-3P), identified PCM mixes (oct-1P, oct-3P and oct-5P) and nano-silica modified PCM mixes (CNS/oct-1P, CNS/oct-3P and CNS/oct-5P) were plotted and presented in Figure 5.18.
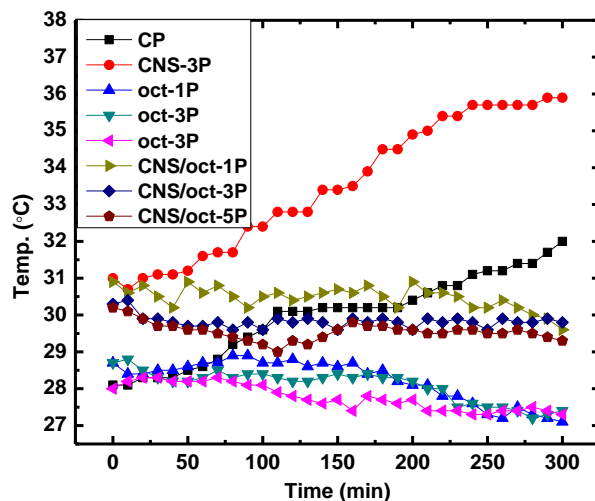
Figure 5.18: Surface temperature variation of PCM admixed cement paste and nano-silica modified n-octadecane PCM admixed cement paste

It can be inferred from the Figure 5.18 that initial and peak temperature of CNS-3P is observed to be high compared to that of control paste. This would be attributed to the instantaneous

increase in heat of hydration of cementitious system in the presence of highly reactive nano-silica and there by promotes the accelerated setting. Whereas, cement paste incorporated with n-octadecane PCM lowered the surface temperature over the time. This may be attributed to the absorption of heat produced during hydration of cement by PCMs owing to its phase changing functionality (Choi et al., 2014; Fernandes et al., 2014). On the other hand, intervention of nano-silica into PCM (n-octadecane) admixed samples i.e. CNS/oct-mixes, modified the variation in surface temperature. The peak surface temperature of CNS/oct-mixes were found to be in the range of control mix, rather a slight downward trend is observed at the end as compared to the control mix.

5.3.3   Chemical shrinkage

Chemical shrinkage values for selected cementitious mortar with the incorporation of nano-silica and PCMs at the age of 1, 3, 7, 14 and 28 days are plotted and presented in Figure 5.19.
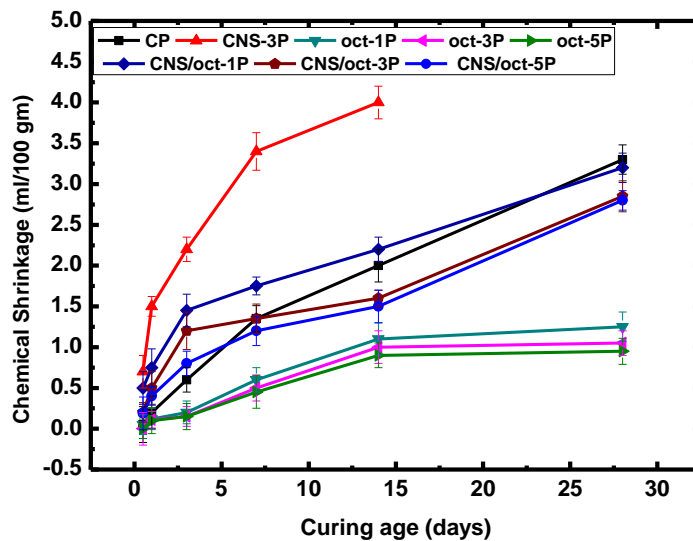
Figure 5.19: Chemical shrinkage values of nano-silica modified PCM (n-octadecane) added cementitious samples

The plot clearly infers the significant increase in chemical shrinkage for CNS-3P mix right from the beginning of 1 day to 14 days of hydration compared to that of control sample. It is important to note that for CNS-3P mix no values of chemical shrinkage were reported beyond 14 days because of development of cracks in the flask. This failure in flask may be attributed

to the accelerated heat of hydration in the presence of nano-silica leading to self-desiccation and thermal stresses in cementitious system (Roychand et al., 2016).

While, n-octadecane PCM added cementitious system (oct-mixes) showed much lower chemical shrinkage value compared to that of control paste. The chemical shrinkage value of control mix at the age of 1 day to 28 days laid in the boundaries of 0.5 ml/100 gm to 3.5 ml /100gm. However, for oct-1P, oct-3P and oct-5P samples it is observed to be in the range of 0.1-1.5 ml/100 gm, 0.1-1.3 ml/100 gm and 0.1-1.2 ml/100 gm, respectively. The low chemical shrinkage can be attributed to the existence of PCM, which has the ability to control the thermal variation by storing heat at the narrow range of temperature by changing the phase from solid to liquid and vice versa (Fernandes et al., 2014). However, on bringing PCM (n-octadecane) in conjunction with optimized nano-silica 3% into cementitious system i.e. CNS/oct-mixes, resulted in condensed volume change compared to that of control (CP) and CNS-3P cementitious mix, especially for CNS/oct- 3P and CNS/oct- 5P mixes. Chemical shrinkage values for CNS/oct-1P, CNS/oct- 3P and CNS/oct- 5P lies between 0.5-3.3 ml/gm, 0.3-3.1 ml/100 gm and 0.3-3 ml/100 gm from 1 day to 28 days, respectively. These results give the idea that there is an absolute possibility of controlling initial shrinkage of nano-silica admixed cement composites observed during early hydration with the optimal inclusion of PCMs.

5.3.4 Differential scanning calorimeter

DSC curve for n-octadecane PCM mixes (oct-mixes) and nano-silica modified n-octadecane mixes (CNS/oct-mixes) in comparison with control samples at the age of 28 days is represented in Figure 5.20 (a and b), respectively. Figure 5.21 demonstrates the comparison plot of DSC curve for CP, CNS-3P, oct-5P mix and CNS/oct-5P at the curing age of 28 days.
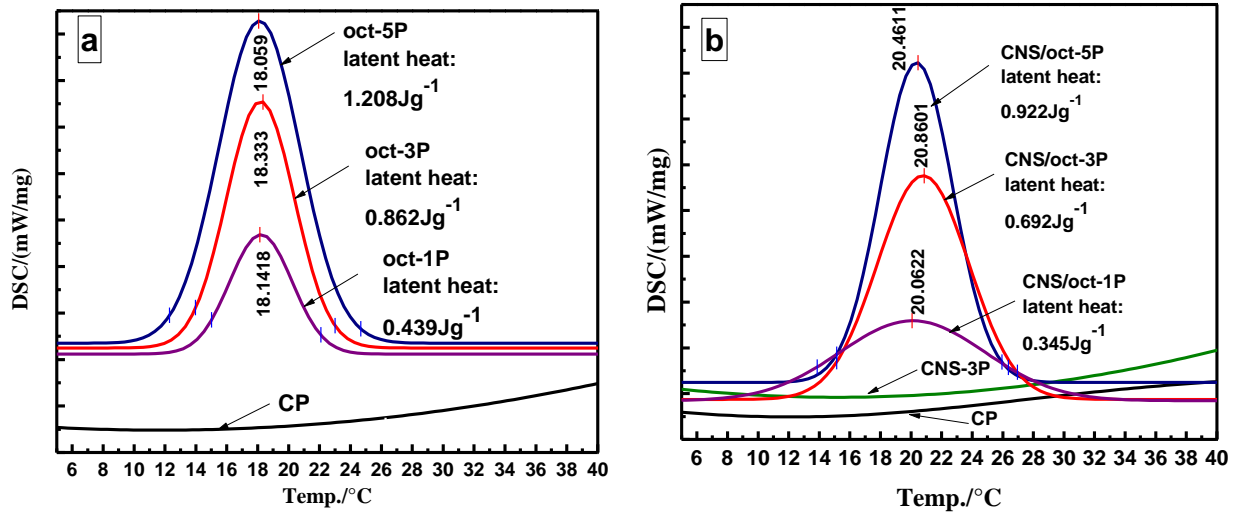
Figure 5.20: DSC curves (endothermic) for a) n-octadecane PCM based mortar samples b) 3% nanosilica modified PCM based mortar samples

It can be noticed from the Figure 5.20a and Figure 5.20b that heat capacity of n-octadecane PCM added cementitious samples increase with the increase in dosage of PCM. The onset and end temperature of DSC curve for n-octadecane PCM admixed cementitious samples ranges from 13±2 °C to 27± 2 °C and peak temperature is found to be 18.2± 0.2 °C (Figure 5.20a). Enthalpy (ΔH) of change in phase was measured as area under the DSC curve (Jayalath et al., 2016). The latent heat capacity of cement mortar for oct-1P was 0.439 Jg^{-1}. Further, for oct-3P and oct-5P mixes the latent heat capacity was noticed to be increased by two times and three times, respectively as compared to that of oct-1P mix.

Whereas, in case of CNS/oct mixes reduced heat capacity was observed (Figure 5.20b), in addition to the shift in peak temperature (from 18± 0.2 °C to 20.3± 0.2 °C). Further, temperature boundaries of DSC curve were observed to be slightly higher as compared to n-octadecane PCM mixes (oct-mixes). The latent heat capacity of CNS/oct-1P, CNS /oct-3P and CNS/oct-5P was 0.345 Jg^{-1}, 0.692 Jg^{-1} and 0.922 Jg^{-1}, respectively. Latent heat was observed to be reduced by 25%-50% compared to that of n-octadecane PCM based cement mixes (oct-1P, oct-3P and oct-5P). However, no peaks were noticed for control and CNS-3P samples, which do not possess PCM dosage. Figure 5.21 clearly designates the swing in peak temperature and drop in latent heat capacity for CNS /oct-5P mixes due to the inclusion of

210

3% nano-silica. Nevertheless, presence of PCM (n-octadecane) in nano-silica admixed cement composites was able to sustain an absolute amount of latent heat capacity.
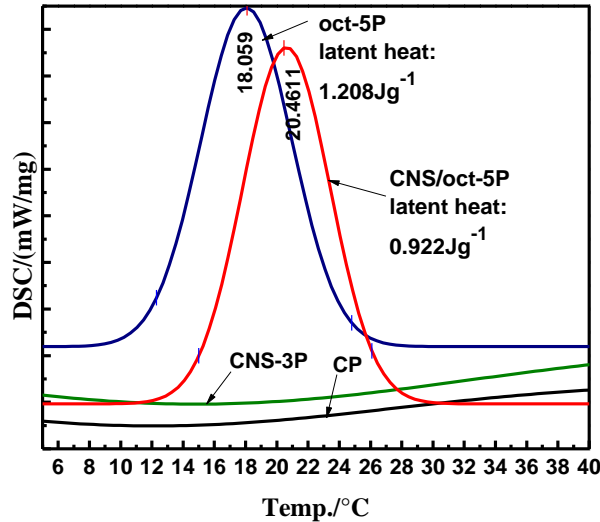
Figure 5.21: Comparison plot of DSC curves (endothermic) for oct-5% and Ns/oct-5% at the curing age of 28 days

5.3.5 Thermo gravimetric analysis (TGA)

Figure 5.22 demonstrates the results of TG/DTG analysis for control, optimized nano-silica mix (CNS-3P), identified PCM mixes (oct-1P, oct-3P and oct-5P) and nano-silica modified PCM mixes (CNS/oct-1P, CNS/oct-3P and CNS/oct-5P) at the age of 28 days.

It can be noticed from the figure that mass loss occurs at three stages. First, at temperature range of 50–230°C due to dehydration of ettringites and calcium silicate hydrates (CSH). Second, at temperature range of 400–500°C due to dehydroxylation of CH. Third, at temperature range of 600–800°C due to decarbonation of calcium carbonate (CC). For brevity, a comparison plot of DTG curves for control, CNS-3P, oct-5P and CNS/oct-5P are presented in Figure 5.23. It can be noted from the figure that for PCM admixed samples, additional thermal degradation curves at the temperature range of 230–300°C is found to be observed, that could be attributed to the thermal decomposition of PCMs.

It can be noticed from the plot (Figure 5.22) that CNS-3P mix showed immense effect in reducing the mass loss associated to CH content compared to that of control sample. Whereas,

for n-octadecane PCM based mixes (oct-1P, oct-3P and oct-5P), CH content is found to be increased. Nevertheless, presence of 3% nano-silica in PCM mixes (CNS/oct) tailored the mass loss effect relating to the decomposition of CH content. This reduced mass loss associated to CH content in the presence of nano-silica is ascribed to the profound pozzolanic reactivity of nano-silica, which made possible in consuming the CH content produced during hydration of cement (Singh et al., 2012a; Singh et al., 2015).
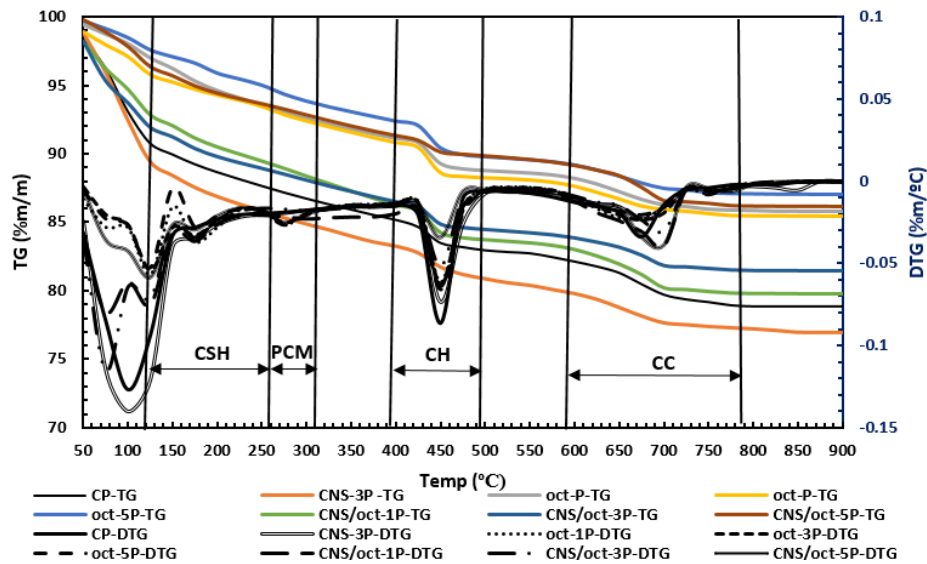
Figure 5.22: TG-DTG curve for control, optimized nano-silica mix, n-octadecane PCM mixes and nano-silica modified PCM mixes
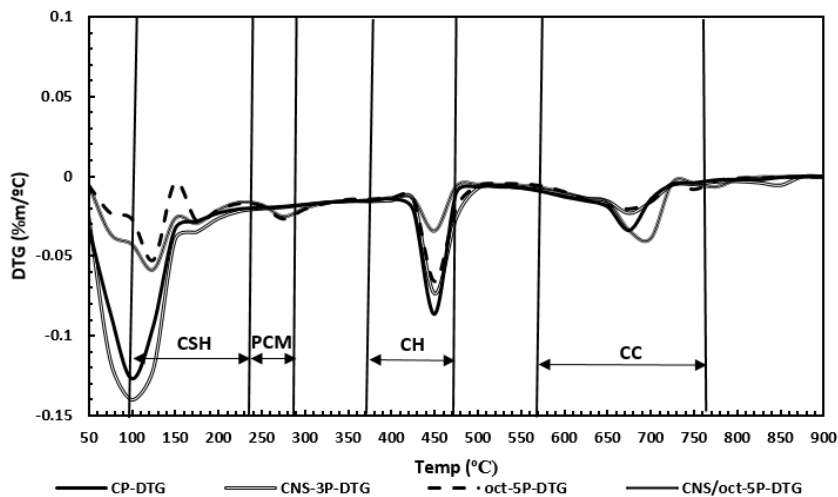
Figure 5.23: Comparison plot of DTG curves for CP, CNS-3P, oct-5%P and CNS/oct-5%P cementitious composite mixes

212

Quantified values of CH content and water content related to hydration product (WH) from the available TGA data for 3% nano-silica mix, n-octadecane PCM added cementitious mixes and nano-silica modified n-octadecane PCM admixed mixes at the curing age of 28 day is presented in Figure 5.24.
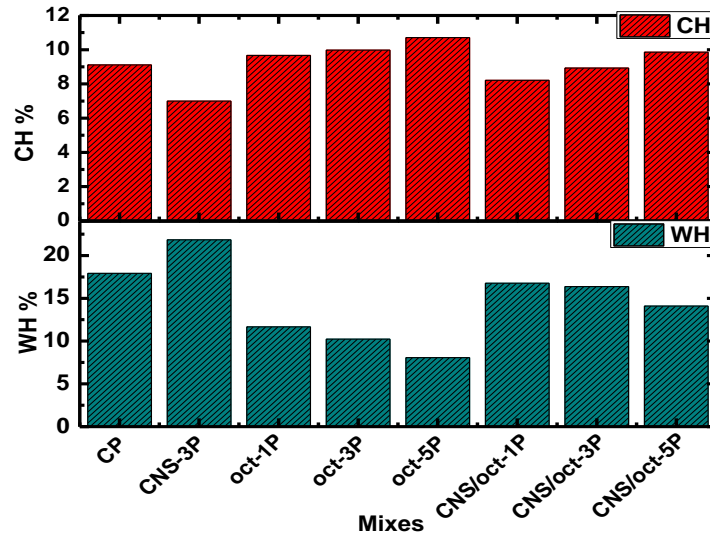
Figure 5.24: Values of CH % for control mix, 3% nano-silica mix, n-octadecane PCM admixed mixes and nano-silica modified n-octadecane PCM based mixes

It can be noticed from the plot (Figure 5.24) that for CNS-3P samples increased WH% and reduced CH% compared to the control samples was observed. CH% for CNS-3P mix was found to be reduced by 28% at the age of 28 days with respect to that of control sample, in addition to that WH% was seen to be increased by 30%. This indicated the amplified degree of hydration owing to the occurrence of additional CSH formation and absorption of CH by the nucleation and pozzolanic activity of nano-silica particles.

On other view, it can be observed from the Figure 5.24 that integration of n-octadecane PCM in cementitious system increased CH% with increase in PCM dosage. The calculated CH content for n-octadecane, based PCM cementitious sample was in the range of 9.67%-10.71% and for control sample it was seen to be 8.9%. Increased percentage of CH for PCM-based samples could be ascribed to the fact that the mass loss curve related to PCMs degradation spreads out into the curve linking to the dehydroxylation of CH (Sharma, 2013). Whereas,

WH% of hydrated cementitious system was seen to be reduced drastically in the presence of PCM. This may be attributed to the fact that direct incorporation of PCM could have disturbed the matrix of hydration product (Yu et al., 2014; Zapata et al., 2013). It was expected that PCMs intermix with CSH/cement hydrates and adsorbs on the surface of unhydrated cement particle blocking it from undergoing hydration reaction, which might be the prior reasons behind reduction of WH% in cementitious mix admixed with PCMs. WH% for n-octadecane, based PCM cementitious sample was in the range of 11.66%-8.06%, which is lower compared to the control sample (17.5%).

However, it can be noticed from the plot that CH% was reduced for n-octadecane PCM cementitious samples containing 3% nano-silica and correspondingly WH% was seen to be increased (Figure 5.24). The presence of nano-silica might have played a vital role in balancing the adverse effect of PCM on hydration products. This was made possible due to the nano-scale hydraulic and pozzolanic reactivity of nano-silica particles (Zapata et al., 2013; Yu et al., 2014). The CH% for CNS/oct- 1P, CNS /oct-3P and CNS /oct 5P samples was observed to be 8.2%, 9% and 9.9% respectively. While, WH% was found to be 16%, 15.6% and 14% respectively.

5.3.6 Mineralogical characterization (XRD)

Figure 5.25 illustrates the XRD pattern of 3% nano-silica, PCM (n-octadecane) and nano-silica modified n-octadecane PCM based mixes at the curing age of 28 day
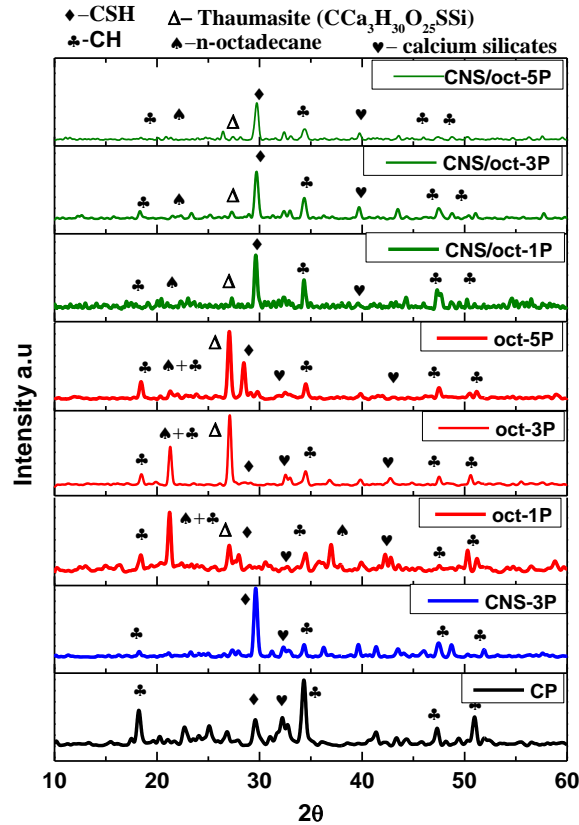
Figure 5.25: XRD patterns for of 3% nano-silica, PCM (n-octadecane) and nano-silica modified n-octadecane based PCM admixed cementitious samples at the age of 28 days

The pattern of XRD for CNS-3P showed the prominent peaks of calcium silicate hydrates in tobermorite form and portlandite (CH). Intense peak of CSH and suppressed peak of CH was noticed for CNS-3P samples as compared to that of control samples. The prominent peaks of control samples are observed at an angle of 18.12°, 34.8° (portlandite, CH), 29.36° (tobermorite, CSH) and 32.6° (unhydrated calcium silicates). XRD pattern of n-octadecane PCM based cementitious samples indicated the additional peaks of n-octadecane (22.1° and 26.8°) as compared to that of control sample and observed to be intensified with the increased dosage of PCM. In addition to that peak, thaumasite (calcium carbonate silicate sulphate hydroxide hydrate, $CCa_3H_{30}O_{35}SSi$) was observed at an angle of 27.2° that is giving an evidence of possible intervention of n-octadecane (C_8H_{38}) PCM with hydration products. It can also be noticed that intensity of CSH (in the form of tobermorite) peak tends to reduce in PCM

215

based cementitious mixes. However, it can be observed from the XRD pattern of CNS/oct-mixes that, presence of nano-silica strengthened the tobermorite (CSH) peak at 29.36° and reduced the peak of CH (18.2° and 34.8°) and thaumasite ($CCa_3H_{30}O_{35}SSi$, 27.2°) as compared to that of n-octadecane PCM based cementitious samples. It was also observed that with increase in the dosage of n-octadecane in CNS/oct- mixes, there found to be a gradual reduction in the intensity of CSH peak.

5.3.7 Microstructural analysis (SEM-EDS)

A detailed study was carried out in obtaining the micrographs and elements for all samples through SEM-EDS. However, for brevity, morphology and elemental composition of control, CNS-3P, oct-5P and CNS/oct-5P mortar samples at the age of 28 days were illustrated in Figure 5.26. It is to be noted that for hydrated cement mortar, capillary pores are the darkest, calcium hydroxide (CH) is light grey, calcium silicate hydrate (CSH) and other (aluminate) hydration products are dark grey (Bentz and Stutzman, 2006).
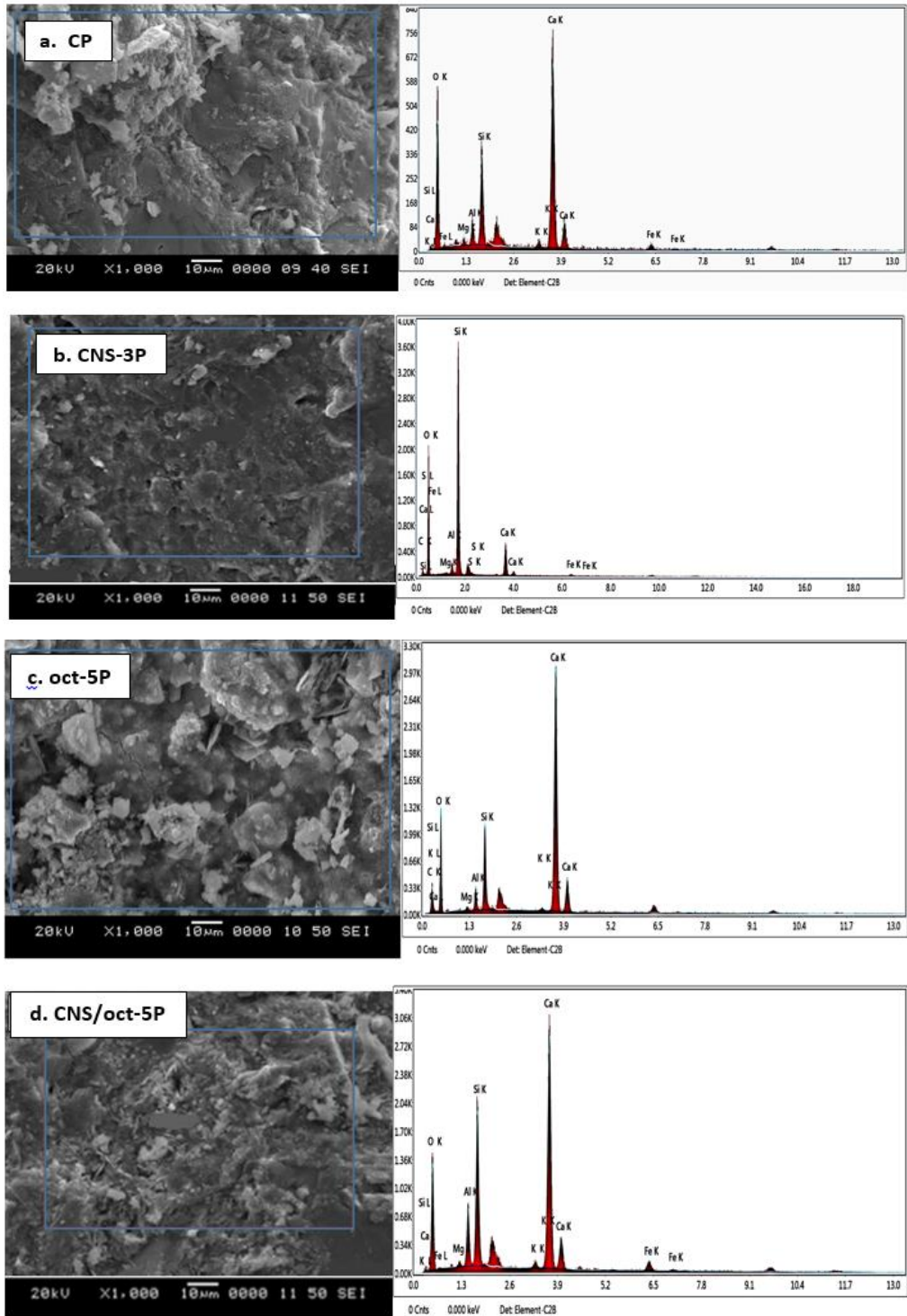
Figure 5.26: SEM-EDS images of a) CP b) CNS-3P c) oct-5P d) CNS/oct-5P at the age of 28 days

The morphology of nano-silica admixed mortar (CNS-3P) confirms the densified microstructure of cement mortar with solid mass of CSH formation and negligible CH concentration due to significant pozzolanic action of nano-silica. EDS image also indicated the intense peak of Silica (Si). Further, it can be observed from the Figure 5.26c that presence of PCM in mortar mix (oct-5P) developed more porous system with large traces of CH compared to that of control mortar. On the other hand, CNS/oct-5P shows the dense microstructure compared to that of oct-5P that specifies the inclusion of nano-silica in n-octadecane PCM mix modified the microstructure of PCM based mixes by lowering the porosity, concentration of CH and increasing the dark grey mass of CSH. The variability in Ca/Si atomic ratio of selected mixes like control, CNS-3P, PCM based samples (oct-1P, oct-3P,oct-5P) and nano-silica modified PCM added samples (CNS/oct-1P, CNS/oct-3P and CNS/oct-5P) at the age of 28days are presented in Table 5.3.

Table 5.3: Ca/Si ratio of PCM admixed cementitious composites at the curing age of 28 days

Mix	Ca	Si	Ca/Si
	Atomic %		
CP	15.01	8.8	1.71
CNS-3P	5.15	22.52	0.23
oct-1P	16.19	8.21	1.97
oct-3P	20.12	8.31	2.42
oct-5P	21.04	8.05	2.61
CNS/oct-1P	15.19	8.8	1.73
CNS /oct-3P	17.01	8.8	1.93
CNS /oct-5P	17.2	8.7	1.98

Ca/Si ratio is the indicator to portray the dense and solid microstructure of cementitious system, lesser value of Ca/Si ratio represents the larger C-S-H formation with the consumption of CH (Hu et al., 2016; Goudar et al., 2019). It can be noticed from the table that for nano-silica mortar samples (CNS-3P) the Ca/Si ratio is found to be 0.23 which is considerably lower compared to that of control samples. This would be made possible by the acceleration of C_3S dissolution and rapid formation of CSH owing to the influence of extremely smaller size of silica particles (Singh et al., 2015).

From the table it can also be understood that inclusion of PCM in cementitious matrix has increased the Ca/Si ratio (1.97-2.61), which was much higher compared to the control sample (1.71). This represents a disturbed hydration system in the presence of PCM. However, it was important to note that with the inclusion of 3% nano-silica to cementitious mixes comprising of n-octadecane PCMs (CNS/oct-mixes), Ca/Si ratio dramatically dropped to the range of 1.73 to1.98. Hence, it was evident that nano-silica compensated the damages induced by the PCM content on the microstructure.

5.4 SUMMARY

- Compressive strength was found to be enhanced by 15%, 13% and 10% for CNS/oct-1M, CNS/oct-3M and CNS/oct-5M compared to that of PCM based cementitious mortar.

- Nano-silica 3% mix has a greater potential to reduce porosity and charge passing compared to control and n-octadecane PCM admixed mortar.

- In acid, alkali and chloride exposure conditions incorporation of PCM in cementitious composites induced significant effect on density, strength as well as on length change owing to the amplified formation of voluminous compounds such as AFt, Gy and Fs.

- PCM added cementitious composites integrated with nano-silica showed improved résistance against aggressive ions and also was able retain the thermal effectiveness within the system.

- PCMs played a vital role in controlling the chemical and drying shrinkage. PCM added nano-silica cementitious samples showed much lower volume change compared to that of control and 3% nano-silica cementitious mix.

- DSC curve signified the increase in heat flow capacity for PCM (n-octadecane) added cementitious sample associated to the PCM dosage. Presence of nano-silica in PCM (n-octadecane) added cementitious composites reduced the heat storage capacity, nevertheless, it was able to sustain an absolute amount of latent heat capacity.

- Reduced value of CH was found for optimized nano-silica mix (CNS-3P). Whereas, for n-octadecane PCM mortar it was found to be in reverse manner. However, presence of nano-silica in PCM (n-octadecane) admixed cementitious mixes was able to balance the adverse effect of PCM on hydration products.

- The mineralogical and SEM-EDS study portrayed the interruption of hydration products for PCM admixed cementitious mix and it also confirmed the modification of the same with the intrusion of highly pozzolanic nano-silica particles.

- Hence, it is understood that direct incorporation of bulk PCMs without highly active pozzolanic ingredient may not be feasible for structural utility.

CHAPTER – 6

CONCLUSIONS AND SCOPE FOR FUTURE RESEARCH

6.1 CONCLUSIONS

Implementing the theory of particle packing i.e. modified Andreasen and Andersen model, the right proportions of mineral admixtures could be proportioned for the production of multi blended cement paste and mortar. The multi-blended composite could achieve the best possible particle packing in improving the mechanical, durability and microstructural properties. In binary blended cement mortar the highest compressive strength and lowest chloride ion permeability was corresponded to the optimum nano-silica dosage i.e. at 3%. As compared to control and ternary blended samples, quaternary blended samples performed the best at all the curing ages owing to its better particle packing and pozzolanic effect.

Under concentrated acid and alkali exposure condition, interaction of aggressive ions (SO_4^{2-}) with in cementitious system directed to CH disbanding and formation of voluminous aggressive products (AFt and Gy) causing deterioration in cementitious mixes through expansion, strength and density loss. Further, ingression of chloride ion (Cl^-) resulted in the crystallization of Fs which weakens the microstructure of cementitious mixes leading to its deterioration. Implementing the concept of particle packing theory (modified Andreasen and Andersen model) in optimizing the proportion of micro-nano scale ingredients of mortar mixture would support in enhancing the resistance of blended mortar mixes to aggressive ions. At this point of time, it can be understood from the experimental investigation that it is possible to attain sustainable cementitious mortar by blending fly ash or/and ultrafine fly ash along with highly reactive nano-silica particles. Performance of 3% nano-silica admixed binary blended mix was found to be the best with respect to acid, alkali and chloride exposure. But, nano-sized silica particles has certain limitation in regard to high heat of hydration, workability, cost and percentage of replacement to OPC. Therefore, quaternary blended cementitious mix admixed with small percentage of nano-silica, if designed and blended appropriately with other SCMs, could

potentially absorb the aggressivity. Further, design and development of blended mixes are found to be highly performing, sustainable and also durable.

This experimental study also gives an understanding that PCMs and nano-silica can be combined in cementitious composites to a suitable proportion that would give the best performance with respect to the compressive strength development, hydration, microstructure development and minimization of shrinkage. In addition, a PCM admixed cementitious composite can be proportioned to store suitable amount of heat energy. Blended mortar (having both nano-silica and PCMs) showed superior strength gain at early age, better durability resistance, low chemical shrinkage and superior thermal performance.

6.2 RESEARCH CONTRIBUTIONS

- This investigation gives information to concrete producers, practitioners and researchers about the adoption of particle packing concept in the design of high performance and sustainable cementitious mixes.
- This work demonstrates the possible way of overcoming defies in identifying, characterizing and implementing the right type and suitable proportion of secondary cementitious materials (SCMs) in cementitious composite mixes.
- This study also proves the efficiency of a small percentage of nano sized silica particles when designed and blended appropriately with other SCMs has a capacity to substantiate in eliminating the permeable pores, responsible for durability of concrete structures.
- The deleterious compounds such as ettringite ($Ca_6Al_2(SO_4)_3(OH)_{12}.26H_2O$, AFt), gypsum ($CaSO_4.2H_2O$, Gy) and Friedel's salt ($Ca_4Al_2(OH)_{12}Cl_2.4H_2O$, Fs) formed due to the chemical exposure were quantified, which can be a basis in understanding the deterioration of concrete structures exposed to aggressive conditions.
- This experimental investigation proposes that there exists a "three-phase drying system" for all kind of cementitious mixes. In addition there found to be a linear relationship between drying shrinkage and pozzolanic reactivity indices, which would help the research fraternity significantly.

- This study also defines a methodology of admixing PCMs with suitable amount of nano-silica for the development of high performing thermal storage material.

6.3 SCOPE FOR FUTURE RESEARCH

- From the present research work it was found that using micron and submicron level fly ash in combination with nano-silica it was able to attain high performance sustainable cementitious mix. However, there is a scope to study the performance of multi-blended cementitious mixes with other SCMs in combination with nano-silica.
- Studies can be focused on using alternative for sand with different gradation to achieve at optimized particle packing by filling up the gaps in the micron to millimetre scale.
- There is a scope to study the performance of encapsulated PCMs in conjunction with highly reactive nano-silica particles.
- Suitability of the nano-silica admixed multi-blends mixes at cold and high temperatures is to be studied for its better application.
- There is a scope available to go for extensive statistical analysis such as ANOVA for the results obtained within this experimental investigation.

6.4 LIMITATIONS

- Cost of nano-silica is found to be very high.
- Nano-silica was sourced from a supplier and it was difficult to receive the material in time.
- Since, particle size of nano-silica is very small, mixing or proportioning was found to be difficult. Hence, it was required to obtain the nano-silica in colloidal form that led to additional increase in the cost of the material.

REFERENCES

Aitcin, P.C. (2000). "Cements of yesterday and today: concrete of tomorrow." *Cement and Concrete Research*, 30 (9), 1349–1359.

Al-Amoudi, O. S. B. (1999). "Mechanisms of sulfate attack in plain and blended cements: a review." R. K. Dhir, P.C. Hewlett (Eds.), Proceedings of the international congress creating with concrete, ASCE, Thomas Telford Ltd., Dundee, 247-260.

Andersen, P. J. and Johansen, V. (1991). "Particle packing and concrete properties". *Material Science of Concrete: II, Skalny J and Mindess S* (Edited), The American Ceramic Society, Inc., Westerville, Ohio, 111-147.

ASTM (2007) C 311, (2007). "Standard Test Methods for Sampling and Testing Fly Ash or Natural Pozzolans for Use in Portland-Cement Concrete." *American Society for Testing and Materials, United States*.ASTM C 989-93, (1993). "Specification for ground granulated blast-furnace slag for use in concrete and mortars." *American Society for Testing and Materials, United States*.

ASTM C 1202, (2005). "Standard test method for electrical indication of concrete's ability to resist chloride ion penetration." *American Society for Testing and Materials, United States*.

ASTM C 157/ C 157M, (2017). "Standard Test Method for Length Change of Hardened Hydraulic-Cement Mortar and Concrete." *American Society for Testing and Materials, United States*.

ASTM C 1608, (2017). "Standard Test Method for Chemical Shrinkage of Hydraulic Cement Paste." *American Society for Testing and Materials, United States*.

ASTM C 596-18, (2018). "Standard Test Method for Drying Shrinkage of Mortar Containing Hydraulic Cement." *American Society for Testing and Materials, United States.*

ASTM C 618-15, (2015). "Standard Specification for Coal Fly Ash and Raw or Calcined Natural Pozzolan for Use in Concrete." *American Society for Testing and Materials, United States*.

ASTM C490 / C490M, (2017). "Standard Practice for Use of Apparatus for the Determination of Length Change of Hardened Cement Paste, Mortar, and Concrete." *American Society for Testing and Materials, United States*.

Augustine, C., Byrne, A., Gimon, E., Goerner, T., Hoffman, I., Kammen, D. M., Kantner, J., J. Levin, T. Lipman, A. Mileva, R. Muren, S. Paul, S. Sapatari, Thorsteinsson, H and Tominks, C. (2009). "Gigaton throwdown: Redefining what's possible for clean energy until 2020." *Renewable and Appropriate Energy Laboratory report*.

AZoNano. (2013). "Silicon dioxide, silica (SiO_2) nanoparticles – properties, applications." Article ID-3398.

Bagheri, A. R., Zanganeh, H., Moalemi, M. M. (2012). "Mechanical and durability properties of ternary concretes containing silica fume and low reactivity blast furnace slag." *Cement and Concrete Composites*, 34(5), 663-670.

Balaguru, P. and Chong, K. (2008). "Nanotechnology and concrete: research opportunities." *Proceedings of ACI sessions on: Nanotechnology of concrete: Recent developments and future perspectives*, National Science Foundation, Denver, USA, pp.15-28.

Ballim, Y. and Graham, P. (2009). "The effects of supplementary cementing materials in modifying the heat of hydration of concrete." *Material Structures,* 42, 803–811.

Barbhuiya, S. and Kumala, D. (2017). "Behaviour of a Sustainable Concrete in Acidic Environment." Sustainability, 9 (9), 1556.

Bartos, P. J. M., Sonebi, M. and Tamimi, A. K. (2002). "Workability and rheology of fresh concrete: compendium of tests." Report of RILEM TC 145-WSM, RILEM, Bagneux, France.

Bentz, D. P and Turpin, R. (2007). "Potential applications of phase change materials in concrete technology." *Cement and Concrete Composites,* 29, 527–532.

Bentz, D.P., and Stutzman, P. (2006). "Curing, hydration and microstructure of cement paste." *ACI materials Journal,* 103 (5), 348-356.

Berra, M, Carassiti, F., Mangialardi, T., Paolini, A.E. and Sebastiani, M. (2012). "Effects of nanosilica addition on workability and compressive strength of Portland cement pastes." *Construction and Building Materials, 35,* 666–675.

Birgisson, B., Taylor, P., Armaghani, J. and Shah, S. P. (2010). "American road map for research for nanotechnology-based concrete materials." *Transportation Research Record*, No. 2142, 130-137.

Biricik, H. and Sarier, N. (2014)." Comparative study of the characteristics of nano-silica–, silica fume– and fly ash–incorporated cement mortars." *Materials Research, 17(3),* 570-582.

Bjornström, J., Martinelli, A., Matic, A., Borjesson, L. and Panas, I. (2004). "Accelerating effects of colloidal nano-silica for beneficial calcium-silicate-hydrate formation in cement." *Chemical Physics Letters, 392*, 242-248.

Black, L., Breen, C., Yarwood, J., Deng, C. S., Phipps, J. and Maitland, G. (2006). "Hydration of tricalcium aluminate (C3A) in the presence and absence of gypsum—studied by Raman spectroscopy and X-ray diffraction." *Journal of Materials Chemistry*, 16, 1263-1272

Bleeck, T. H. (2011). "Particle packing; an effective approach to optimized design of ultra-high strength and self-compacting concretes." *ADFA Journal of Undergraduate Engineering Research*, 4(1).

Borges. P. H. R., Fonseca, L. F., Nunes, V. A., Panzera, T. H and Martuscelli, C. C. (2016). "Andreasen Particle Packing Method on the Development of Geopolymer Concrete for Civil Engineering." *Journal of Materials in Civil Engineering*, 26, 692-697.

Bosque, I. F. S. D., Ramírez, S. M., Pastor, M. M. and Varela, M. T. B. (2014). "Effect of the addition of nanosilica on white cement hydration at 25°C." *MATEC Web Conference.* 11, 01006.

Brouwers H. J. H. and Radix H. J. (2005). "Self-compacting concrete: the role of the particle size." *First International Symposium on Design, Performance and Use of Self-Consolidating Concrete SCC*.

BS EN 1015-3. "Methods of test for mortar for masonry. Determination of consistence of fresh mortar (by flow table)", *British Standards Institution-BSI and CEN European Committee for Standardization*, 1999.

BS EN 196-3: 2016. "Methods of testing cement – Part 3: Determination of setting times and soundness". *British Standards Institution-BSI and CEN European Committee for Standardization*, 2016.

BS-EN-196-1. "Methods of testing cement – Part 1: determination of strength". *British Standards Institution-BSI and CEN European Committee for Standardization*, 2016.

Cai, W. (2017). "Effect of particle packing on flow property and strength of concrete mortar." *Graduate Theses and Dissertations*, 15271.

Cao, V. D., Pilehvar, S., Bringas, C.S., Szczotok A M., Rodriguez, J.F., Carmona, M., Al-Manasir, N. and Kjoniksen, A. L. (2017). "Microencapsulated phase change materials for

enhancing the thermal performance of Portland cement concrete and geopolymer concrete for passive building applications." *Energy Conversion and Management*, 133, 56–66.

Cellat, K., Beyhan, B., Kazanci, B., Konuklu, Y. and Paksoy, H. (2017). "Direct Incorporation of Butyl Stearate as Phase Change Material into Concrete for Energy Saving in Buildings." *Journal of Clean Energy Technologies*, 5 (1), 64-68.

Chaudhary, S. K. and Sinha, A. K. (2018). "Effect of Nano Silica on Acid, Alkali and Chloride Resistance of Concrete." *International Journal of Civil Engineering and Technology*, 9(8), 853-861.

Chen, L. and Lin, D. (2009). "Application of sewage sludge ash and nano-SiO_2 to manufacture tile as construction material." *Construction Building Materials*, 23, 3312-3320.

Chen, W., Huang, B., Yuan, V. and Deng, M. (2000). "Deterioration process of concrete exposed to internal sulfate attack." *Materials*, 13, 1336.

Chithra, S., Senthil Kumar, S. R. R. and Chinnaraju, K. (2016). "The effect of colloidal nano- silica on workability, mechanical and durability properties of high performance concrete with copper slag as partial fine aggregate." *Construction and Building Material*, 113, 794–804.

Choi, W. C., Khil, B. S., Chae, Y. S., Liang, Q. B. and Yun, H. D. 2014. "Feasibility of Using Phase Change Materials to Control the Heat of Hydration in Massive Concrete Structures." *Hindawi Publishing Corporation the Scientific World Journal,* Article ID 781393, 1-6.

Copeland, K. D., Obla, K., Hill, R. L and Thomas, M. D. A. (2001). "Ultrafine fly ash for high performance concrete." *Conference: Construction Institute Sessions at ASCE Civil Engineering Conference*, Houston, Texas, United States.

Dai, J., Wang, Q., Xie, C., Xue, Y., Duan, Y. and Cui, X. (2019). "The effect of fineness on the hydration activity index on ground granulated blast furnace slag." *Materials*, 12(18), 2984.

Dalinaidu, A., Das, B. B., Singh, D. N. and Pandey, S. P. (2007). "Methodology for rapid determination of pozzolanic activity of materials." *Journal of ASTM international (JAI)*, 4(6).

Das, B. B and Pandey, S. P. (2011). "Influence of fineness of fly ash on the carbonation and electrical conductivity of concrete." *Journal of Materials in Civil Eng*ineering, 23(9), 1365-1368.

Das, B. B, Singh, D. N. and Pandey, S. P. (2014). "Influence of initial curing humidity on compressive strength and ultrasonic properties of concrete." *Indian Concrete Journal* 88(2), 48-55.

Das, B. B., Singh, D. N. and Pandey, S. (2012). "Rapid Chloride Ion Permeability of OPC and PPC Based Carbonated Concrete." *Journals of materials in Civil Engineering, ASCE,* 24, 606-611.

Das, B. B., Singh, D. N. and Pandey, S. P. (2010). "A comparative study for determining pore volume of concrete." *Indian Concrete Journal,* 84 (12), 7-12.

De Larrad. "Concrete Mixture Proportioning - A Scientific Approach." E & FN Spon, London, 1998

Demirbas M. F. (2006). "Thermal energy storage and phase change materials: an overview." *Energy Sources Part B*, 1, 85–95.

Dewar, J. D. "Computer Modeling of Concrete Mixtures." E and FN Spon, London, 1999

Diab, A. M., Awad, A. E. M., Elyamany, H. E. and Elmoaty, M. A. (2012). "Guidelines in compressive strength assessment of concrete modified with silica fume due to magnesium sulfate attack." Construction Building Materials, 36, 311–318.

Dinger, D. R. and Funk, J. E. (1997). "Particle-packing phenomenon and their application in materials processing." *MRS Bulletin*, 19-23.

Du, H., Du, S. and Liu, X. (2014). "Durability performances of concrete with nano-silica." *Construction and Building Materials,* 73, 705-712.

Duan, S., Liao, H., Ma, Z., Cheng, F., Fang, L., Gao, H. and Yan, H. (2018). "The relevance of ultrafine fly ash properties and mechanical properties in its fly ash-cement gelation blocks via static pressure forming." *Construction and Building Mater*ials, 186, 1064-1071.

Dunster, A. (2009). "Silica fume in concrete." *Information paper Nº IP5/09*, IHS BRE press, Garston UK.

Eddhahak-Ouni, A., Drissi, S., Colin, J., Neji, J. and Care, S. (2014). "Experimental and multi-scale analysis of the thermal properties of Portland cement concretes embedded with microencapsulated phase change materials (PCMs)." *Applied Thermal Engineering*, 64 (1), 32–39.

Ehsani, A., Nili, M. And Shaabani, K. (2017)." Effect of nanosilica on compressive strength development and water absorption properties of cement paste and concrete containing fly ash." *KSCE Journal of Civil Engineering,* 21(5), 1854–1865.

Falzone, G., Falla, G. P., Wei. Z., Zhao, M., Kumar, A., Bauchy, M., Neithalath, N., Pilon, L. and Sant, G. (2016). "The influences of soft and stiff inclusions on the mechanical properties of cementitious composites." *Cement and Concrete Composites,* 71, 153-165.

Farnam Y., Krafcik M., Liston L., Washington T., Erk K., Tao B. and Weiss W. J. (2015). "Evaluating the use of phase change materials in concrete pavement to melt ice and snow." Journal of Materials of Civil Engineering, 28.

Felske, J. D. (2004). "Effective thermal conductivity of composite spheres in a continuous medium with contact resistance." *International Journal of Heat Mass Transfer*, 47(14), 3453–3461.

Feng, J., Liu, S. and Wang, Z. (2015). "Effect of ultrafine fly ash on the properties of high strength concretes." *Journal of Thermal Analysis and Calorimetry*. 121 (3), 1213–1223.

Fennis, S. A. A. M. and Walgreen, J. C. (2012). "Using particle packing technology for sustainable concrete mixture design." *Heron*.

Fenollera, M., Míguez, J. L., Goicoechea, I., Lorenzo, J. and Ángel Álvarez, A. (2013). "The Influence of Phase Change Materials on the Properties of Self-Compacting Concrete." *Materials*, 6, 3530-3546.

Fernandes, F., Manari, S., Aguayo, M., Santos, K., Oey, T., Wei, Z., Falzone, G., Neithalath, N. and Sant, G. (2014). "On the feasibility of using phase change materials (PCMs) to mitigate thermal cracking in cementitious materials." *Cement and concrete composites,* 51, 14-26.

Fuller, W. B. and Thompson, S. E. (1907). "The laws of proportioning concrete." *Transactions of American Society of Civil Engineers*, 33 (2), 223-298.

Furnas, C.C. "Grading Agrregates I-Mathematical Reltions for Beds of Broken Solids of Maximum Density." U. S. Bureau of Mines. 23(9), 1052-1058, 1931.

Gaitero, J. J., Campillo, I. and Guerrero, A. (2008). "Reduction of the calcium leaching rate of cement paste by addition of silica nanoparticles." *Cement and Concrete Research*, 38, 1112–1118.

Ge, Z., Ye, F., Cao, H., Leng, G., Qin, Y. and Ding, Y. (2014). "Carbonate-salt-based composite materials for medium- and high-temperature thermal energy storage." *Particuology*, 15, 77–81.

Giner, T., Ivorra, S., Baeza, F. J., Zornoza, E., Ferrer, B. (2011). "Silica fume admixture effect on the dynamic properties of concrete." *Construction Building Materials*, 25 (8), 3272-3277.

Givi, A. N., Rashid S A., Aziz, F. N. A. and Salleh, M. A. M. (2010). "Experimental investigation of the size effects of silica nano-particles on the mechanical properties of binary blended concrete." *Cement and Concrete Composites, 41*, 673–677.

Glass, G. K. and Buenfeld, N. R. (2000). "The influence of chloride binding on the chloride induced corrosion risk in reinforced concrete." *Corrosion Science*, 42(2), 329-344.

Goodarzi, F. (2006). "Characteristics and compositions of fly ash from canadial coal fired power plant." *Fuel,* 85, 1418-1428.

Gopalakrishnan, K. (2011). "Nanotechnology in civil infrastructure: a paradigm shift." *Springer*, USA.

Gopinath, S., Murthy, R. A., Ramya, D. and Iyer, N. R. (2011). "Optimised mix design for normal strength and high performance concrete using particle packing method." *Archives of Civil Engineering*, LVII, 4.

Goudar S. K., Das, B. B. and Arya, S. B. (2019). "Microstructural study of steel-concrete interference and its influence on bond strength of reinforcement concrete." *Advanced Civil Engineering Materials*, 8 (1), 171-189.

Hannesson, G., Kuder, K. G., Shogren, R and Lehman, D. (2012). "The influence of high volume of fly ash and slag on the compressive strength of self-consolidating concrete." *Construction and Building Materials*, 30, 161–168.

Haruehansapong, S., Pulngern, T and Chucheepsakul, S. (2017). "Effect of nanosilica particle size on the water permeability, abrasion resistance, drying shrinkage, and repair work properties of cement mortar containing nano-SiO_2." *Advances in Materials Science and Engineering,* Article ID 4213690.

Hawes, D. W., Feldman, D. and Banu, D. (1993). "Latent heat storage in building materials". *Energy and buildings*, 20(1), 77-86.

Hewlett, P. C. (1998). "Lea's Chemistry of Cement and Concrete." 4th Edition, edited by Hewlett P.C Arnold, Great Britain, 11053.

Hou, P. K., Kawashima, S., Wang, K. J., Corr, D. J., Qian, J. S. and Shah, S. P. (2013). "Effects of colloidal nanosilica on rheological and mechanical properties of fly ash-cement mortar." *Cement and Concrete Composites*, 35, 12-22.

Hou, P., Kawashima, S., Kong, D., Corr, D. J., Qian, J. and Shah, S. P. (2014). "Modification effects of colloidal nanoSiO$_2$ on cement hydration and its gel property." *Composites Part B: Engineering*, 45(1), 440-448.

Hu, Q., Aboustait, M., Kim, T., Ley, M. T., Hanan, J. C. J, Bullard, J., Winarski, R. and Rosed, V. (2016). "Direct three-dimensional observation of the microstructure and chemistry of C3S hydration." *Cement Concrete Research,* 88, 157–169.

Hummel, A. (1959). "Das beton-ABC- Ein Lehrbuch der technology des schwerbetons and des leichtbeton." *11th edn, Wilhelm Ernst and Sohn, Berlin*.

Hunger M. and Brouwers H. J. H. (2009). "Flow analysis of water powder mixtures: Application to specific surface area and shape factor." *Cement and concrete composites,* 31, 39-59.

Hunger, M., Entrop, A. G., Mandilaras, I., Brouwers, H. J. H. and Founti, M. (2009). "The behavior of self-compacting concrete containing micro-encapsulated Phase Change Materials." *Cement and Concrete Composites,* 31, 731–743.

Huntzinger, D. N. and Eatmon, T. D. (2009). "A life-cycle assessment of cement manufacturing: comparing traditional process with alternative technologies." *Journal of Cleaner Production,* 17(7), 668-675.

Irassar, E. F., Di Maio, A. and Batic. O. R. (1995). "Sulfate attack on concrete with mineral admixtures." *Cement and Concrete Research*, 26 (1), 113-123.

IS 12269: 2013 "Ordinary Portland cement, 53 grade – Specification". *Bureau of Indian Standards*, New Delhi, India.

IS 2386:1963 "Methods of Test for Aggregates for Concrete". *Bureau of Indian Standards*, New Delhi, India

IS 3812: 2003 "Specification for pulvarized fly ash". Bureau of Indian Standards, New Delhi, India

IS 383:2016 "Coarse and Fine Aggregate for Concrete – Specification", *Bureau of Indian Standards*, New Delhi, India

IS 4031 (Part 5) -1988 "Methods of physical tests for hydraulic cement part 5 determination of initial and final setting times", *Bureau of Indian Standards*, New Delhi, India.

IS 4031 (Part 6) -1988 "Determination of compressive strength of hydraulic cement other than masonry cement". *Bureau of Indian Standards*, New Delhi, India.

IS 9103: 1999 "Concrete admixtures –Specifications". *Bureau of Indian Standards*, New Delhi, India.

IS: 10500: 2012 "Drinking Water — Specification". *Bureau of Indian Standards*, New Delhi, India.

Isfahani, F. T., Redaelli, E and Sun, Y. (2017). "Effects of Nanosilica on early age stages of cement hydration." Journal Nanomaterials, Article ID 4687484.

Izzat, A. M., Al Bakri, A. M. M., Kamarudin, H., Sandu, A. V., Ruzaidi, G. C. M. Faheem, M. T. M. and Moga, L. M. (2013). "Sulfuric acid attack on ordinary Portland cement and geopolymer material." Revista De Chimie (Bucharest), 64(9), 1011-1014.

Jayalath, A., Nicolas, R. S., Sofi, M., Shanks, R., Ngo, T., Ayea, L. and Mendis, P. (2016). "Properties of cementitious mortar and concrete containing micro-encapsulated phase change materials." *Construction and Building Materials,* 120, 408–417.

Jittabut, P., Pinitsoontorn, S., Thongbai, P., Amornkitbamrung, V. and Chindaprasirt, P., 2016. "Effect of nano-silica addition on the mechanical properties and thermal conductivity of cement composites." *Chiang Mai Journal Science,* 43(5), 1160-1170.

Jo, B. W., Kim C. H., Tae, G. H. and Park J. B. (2007). "Characteristics of cement mortar with nano-SiO$_2$ particles." *Construction and Building Materials*, 21, 1351–1355.

Kanimozhi, B., Harish, K., Tarun, B. S., Reddy, P. S. S. and Sujeeth, P. S. (2007). "Charging and Discharging Processes of Thermal Energy Storage System Using Phase change materials." *IOP Conference Series Material Science Engineering*, 197, 012040.

Kennedy, T., Huber, G., Harrigan, E., Cominsky, R., Hughes, C., Quintus, H. and Moulthrop, J. (1994). "Superior performing ashphalt pavements (superpave): the product of SHRP asphalt research program.".*National research council, SI-IRP-A-410*.

Khitab, A. and Arshad, M. T. (2014). "Nano construction materials: review." *Revised Advanced Materials Science*, 38, 181-189.

Kim, H. S., Lee, S. H. and Moon, H. Y. (2007). "Strength properties and durability aspects of high strength concrete using Korean metakaolin." *Construction and Building Material,* 21, 1229-1237.

Kim, M. J., Kim, K. B. and Ann, K. Y. (2016). "The Influence of C3A Content in Cement on the Chloride Transport." *Advances in Material Science Engineering*, Article ID 5962821.

Kim, T., Hong, S., Seo, K. Y. and Kang, C. (2019). "Characteristics of ordinary portland cement using the new colloidal nano-silica mixing method." Applied Sciences, 9(20), 4358.

Kiviste, M. and Lindberg, R. (2014). "The feasibility of phase change materials in building structures for saving heating energy in the Nordic climate." *Agronomy Research*, 12(3), 989-998.

Kong, D., Du, X., Wei, S., Zhang, H., Yang, Y. and Shah, S. P. (2012). "Influence of nano-silica agglomeration on microstructure and properties of the hardened cement-based materials." *Construction and Building Materials,* 37, 707–715.

Kosmatka, S. H., Kerkhoff, B. and William, C. (2003). "Design and control of concrete mixtures." 14th Edn, *Portland Cement Association*, USA.

Kulakarni, S. B. (2011). "Significance of Curing of Concrete for Durability of Structures." *NBM and CW Infra Construction and Equipment Magazine*.

Kumar, S.V. and Santhanam, M., 2003. "Particle packing theories and their application in concrete mixture proportioning: A review". *Indian Concrete Journal*, 77(9), pp. 1324-1331.

Land, G. and Stephan, D. (2012). "The influence of nano-silica on the hydration of ordinary Portland cement." *Journal of Materials Science,* 47(2), 1011-1017.

Land, G. and Stephan, D. (2015). "Controlling cement hydration with nanoparticles." *Cement and Concrete Composites,* 57, 64-67

Lazaro, A., Quercia, G. And Brouwers, H. J. H. (2014). "Synthesis of nano-silica at low temperatures and its application in concrete." *Proceedings of the International Conference Non-Traditional Cement & Concrete V, Brno, Czech Republic.*

Lecompte, T., Le Bideau, P., Glouannec, P., Nortershauser, D. and Le Masson, S. (2015). "Mechanical and thermo-physical behaviour of concretes and mortars containing Phase Change Material." *Energy and Buildings*, 94, 52-60.

Lee, K.O., Medina, M.A., Raith, E. and Sun, X.Q. (2015). "Assessing the Integration of a Thin Phase Change Material (PCM) Layer in a Residential Building Wall for Heat Transfer Reduction and Management." *Applied Energy*, 137, 699-706.

Li, G. (2004). "Properties of high-volume fly ash concrete incorporating nano-SiO$_2$." *Cement and Concrete Research*, 34 (6), 1043-1049.

Li, G. and Wu, X. (2005). "Influence of fly ash and its mean particle size on certain engineering properties of cement composite mortars." *Cement and Concrete Res*earch 35 (6), 1128-1134.

Li, P. P., Yu Q. L. and Brouwers H. J. H. (2018). "Effect of coarse basalt aggregates on the properties of Ultra-high-Performance Concrete (UHPC)." *Construction and Building Materials*, 170, 649–659.

Li, S., Roy, D. M. and Kumer, A. (1985). "Quantitative determination of pozzolanas in hydrated system of cement or Ca(OH)$_2$ with fly ash or silica fume." *Cement and Concrete Research*, 15(6), 1079– 1086.

Lim, S. and Mondal, P. (2015). "Effects of nanosilica addition on increased thermal stability of cement-based composite." *Materials Journal ACI*, 112 (2), 305-316.

Lin, W. T. (2020). "Reactive ultrafine fly ash as an additive for cement-based materials." *Materials Today Commun*ication, 25, 10146.

Ling, T. C. and Poon, C.S. (2013). "Use of phase change materials for thermal energy storage in concrete: an overview." *Construction and building materials*, 46, 55-62.

Ltifi, M., Guefrech, A., Mounanga, P. and Khelidj, A. (2011). "Experimental study of the effect of addition of nano-silica on the behaviour of cement mortars." *Mounir Procedia Engineering*, 900–905.

Lucas, S., Senff, L., Ferreira, V.M., Aguiar J. L. B. and Labrincha, J. A. (2010). "Fresh State characterization of lime mortars with pcm additions." *Applied Rheology*, 20(6), 63166 (1-7).

Ma, Q and Zhu, Y. (2017). "Experimental research on the microstructure and compressive and tensile properties of nano-SiO_2 concrete containing basalt fibers." *Underground space*, 2 (3), 175-181.

Marshall, A. L. (1972). "Thermal properties of concrete", *Building Science,* 7, 167-174.

Maynard, G. A., Hodge, D. M. and Bowman, A. D. (2010). "Tracing and disputing the story of nanotechnology." *International Handbook on Regulating nanotechnologies*. ISBN 9781849808125.

Mohammed, B. S., Adamu, M. and Liew, M. S. (2018). "Evaluating the effect of crumb rubber and nano-silica on the properties of high volume fly ash roller compacted concrete pavement using non-destructive techniques." *Case Studies in Construction Materials,* 8, 380-391.

Monteny, J., Vincke, E., Beeldeens, A., De Belie, N., Taerwe, L., Gemert, D. and Verstraete, W. (2000). "Chemical, microbiological, and in situ test methods for biogenic sulfuric acid corrosion of concrete." *Cement and Concrete Research,* 30(4), 623–634.

Narmluk, M., Toyoharu, N (2011) "Effect of fly ash on the kinetics of Portland cement hydration at different curing temperatures" *Cement and Concrete Research,* 41(6), 579-589.

Nazari, A., Riahi, S., Riahi, S., Shamekhi, S. F. and Khademno, A. (2010). "Benefits of Fe_2O_3 nanoparticles in concrete mixing matrix." *Journal of American Science,* 6(4), 102-106.

Nehdi, M. L. (2001). "Ternary and quaternary cements for sustainable development." *Article in Concrete International*, 23(4), 35-42.

Neville, A. M. (2008). "Properties of Concrete." *fourth edition, Pearson Education*.

Niall, D., West, R., McCormack, S. and Kinnane, O. (2016). "Thermal Mass Behaviour of Concrete Panels Incorporating Phase Change Materials." *Sustainable Built Environment Conference*, Hamburg, German.

Norhasri, M. S. M., Hamidah, M. S. and Fadzil, A. M. (2017). "Applications of using nano material in concrete: A review." *Construction and Building Materials,* 133, 91–97.

Norvell, C., Sailor, D. J. and Dusicka, P. (2013). "The effect of microencapsulated phase-change material on the compressive strength of structural concrete." *Journal of Green Buildings*, 8 (3), 116-124.

Obla, K., Hill, R. L., Thomas, M. D. A. and Shashiprakash, S. G. (2003). "Properties of concrete containing ultra-fine fly ash." *ACI. Materials Journal*, 100(5), 426-433.

Pasupathy, A., Velraj, R. and Seeniraj, R. V. (2008). "Phase change material-based building architecture for thermal management in residential and commercial establishments." *Renewable Sustainable Energy Revolution*. 12 (1), 39–64.

Pisello, A. L., D'Alessandroc, A., Fabianib, C., Fiorellic, A. P., Ubertinic, F, Cabezad, L. F., Materazzic, A. L. and Cotana, F. (2016). "Multifunctional analysis of innovative PCM-filled concretes." *Sustainability in Energy and Buildings Procedia,* 111, 81 – 90.

Powers, T.C. "The properties of fresh concrete." John Wiley & Sons, Inc. New York, 1968

Prasada Rao, D. V. and Navaneethamma, V. (2016). "Influence of nano-silica on strength properties of concrete containing rice husk ash." *International Journal of Advanced Research in Education & Technology*, 3 (1), 39-43.

Qiao, Q. and Fang, C. (1955). "Compressive and flexural strength of high strength phase change mortar." *Advances in Materials Machinery Electronics II AIP Conference Proceedings*, 020024-1–020024-4.

Qiao, C., Suraneni, P. and Weiss, J. (2018). "Damage in cement pastes exposed to NaCl solutions." *Construction and Building Materials,* 171, 120-127.

Qing, Y., Zenan, Z., Deyu, K. and Rongshen, C. (2007). "Influence of nano-SiO_2 addition on properties of hardened cement paste as compared with silica fume." *Construction and Building Materials,* 21, 539–545.

Quercia, G., Husken, G. and Brouwers, H. J. H. (2012). "Water demand of amorphous nano-silica and its impact on the workability of cement paste." *Cement and Concrete Research,* 42, 344–357.

Quercia. G. and Brouwers. H. J. H. (2010). "Application of nano-silica (nS) in concrete mixtures." *In: 8th fib PhD symposium in Kgs. Lyngsby*, Denmark.

Raki, L., Beaudoin, J., Alizadeh, R., Makar, J., Sato, T. (2010). "Cement and concrete nanoscience and nanotechnology." *Materials*, 3, 918-942.

Rashad, A. M. (2014). "A comprehensive overview about the effect of nano-SiO_2 on some properties of traditional cementitious materials and alkali-activated fly ash." *Construction and Building Materials*, *52*, 437- 468.

Richardson, I. G. (2008). "The calcium silicate hydrates." *Cement and Concrete Research,* 18 (2), 137-158.

Ricklefs, A., Thiele, A. M., Falzone, G., Sant, G. and Pilon, L. (2017). "Thermal conductivity of cementitious composites containing microencapsulated phase change materials." *International Journal of Heat and Mass Transfer*, 104, 71–82.

Roychand, R., Silva, S. D., Law, D. and Setunge, S. (2016). "Micro and nano engineered high volume ultrafine fly ash cement composite with and without additives." *International Journal of Concrete Structure Materials*, 10(1), 113-124.

Ruybal, S. S. (2007). "Comparison of ultrafine fly ash and silica fume in concrete mixes." *Thesis*, University of Colorado at Denver and Health Science Center, Boulder.

Sabry, Z. M. (2013). "Performance of concrete incorporating colloidal nano-silica." *UNLV Theses*, Dissertations, Professional Papers, and Capstones. 2628.

Sadrmomtazi, A. and Barzegar, A. (2010). "Assessment of the effect of nano-SiO_2 on physical and mechanical properties of self-compacting concrete containing rice husk ash." *2nd International conference on sustainable construction and technologies*, universita politecnica delle marche anchona Italy.

Safiuddin, M. and Hearn, N. (2005). "Comparison of ASTM saturation techniques for measuring the permeable porosity of concrete." *Cement Concrete Research*, 35(5), 1008-1013.

Safiuddin, M., Gonzalez, M., Cao, J. and Tighe S. L. (2014). "State-of-the-art report on use of nano-materials in concrete". *International Journal of Pavement Engineering*, 15 (10), 940-949

Saha, A. K. (2018). "Effect of class F fly ash on the durability properties of concrete." *Sustainable Environment Research*, 28(1), 25-31.

Sahoo, S., Das, B. B. and Musta S. (2017). "Acid, alkali and chloride resistance of concrete composed of low carbonated fly ash." *Journal of Materials Civil Engineering*, 29 (3), 04016242, 1-12.

Sahu, L. K., Mondloe, D. and Garhewal, A. (2017). "A review on thermal and mechanical properties of concrete containing phase change material." *Inernational. Research Journal Engineering Technol*ogy, 4(5), 2154-2165.

Said, A. M., Zeidan, M. S., Bassuoni, M. T. and Tian, Y. (2012). "Properties of concrete incorporating nano-silica." *Construction and Building Materials*, 36, 838-844.

Sakulich, A. R. and Bentz, D. (2012). "Incorporation of phase change materials in cementitious systems via fine lightweight aggregate." *Construction and Building Materials*, 35, 483–490.

Sanchez, F. and Sobolev, K. (2010). "Nanotechnology in concrete: a review". *Construction and Building Materials,* 24 (11), 2060–2071.

Sattawa, H., Pulngern, T. and Chucheepsakul, S. (2017). "Effect of nanosilica particle size on the water permeability, abrasion resistance, drying shrinkage, and repair work properties of cement mortar containing nano-SiO_2." *Advances in Materials Science and Engineering,* Article ID 4213690.

Savija, B. (2018). "Smart crack control in concrete through use of phase change materials (PCMs): A Review." *Materials*, 11, 654.

Scheffler, G. A. and Plagge, R. (2017). "Introduction of a drying coefficient for building materials." *ASHRAE Transactions*, 116.

Schossig, P., Henning, H. M., Gschwander, S. and Haussmann, T. (2005). "Micro-encapsulated phase change materials integrated into construction materials." *Solar Energy Materials*, 89, 297–306.

Sebok, T., Simonık, J. and Kuli, K. (2001). "The compressive strength of samples containing fly ash with high content of calcium sulfate and calcium oxide." *Cement and Concrete Research*, 31, 1101–1107.

Senff, L., Labrincha J. A., Ferreira, V M., Hotza, D. and Repette, W. L. (2009). "Effect of nano-silica on rheology and fresh properties of cement pastes and mortars." *Construction Building Material,* 23 (7), 2487-2491.

Sensale, G.R. (2006). "Strength development of concrete with rice husk ash". *Cement and Concrete Composites,* 28(2), 158-160.

Senthil, K.V. and Santhanam, M. (2003). "Particle packing theories and their application in concrete mixture proportioning: A review." *Indian Concrete Journal*, 77(9), 1324-1331.

Shafiq, N. and Cabrera, J. G. (2004). "Effects of Initial Curing Condition on the Fluid Transport Properties in OPC and Fly Ash Blended." *Cement and Concrete Composites* 26, 381-387.

Shaikh, F. U. A., Supit, S.W. M. and Sarker, P. K. (2014). "A study on the effect of nano silica on compressive strength of high volume fly ash mortars and concretes." *Materials and Design*, 60, 433–442.

Sharma B. (2013). "Incorporation of phase change material into cementitious system." *Thesis*, Arizona State University, USA.

Shekari, A. H. and Razzaghi, M. S. (2011). "Influence of nanoparticles on durability and mechanical properties of high performance concrete." *Proceedia Engineering,* 14, 3036-3041.

Sikoraa, P., Horszczaruka, E., Skoczylasa, K. and Rucinskaa, T. (2017). "Thermal properties of cement mortars containing waste glass aggregate and nanosilica." *Science direct Procedia Engineering*, 196, 159 – 166.

Singh, L. P., Ali, D. and Sharma, U. (2016). "Studies on optimization of silica nanoparticles dosage in cementitious system." *Cement and Concrete Composites, 70*, 60-68.

Singh, L. P., Goel, A., Sriraman, K., Bhattacharya, S. K., Sharma, U. and Mishra, G. (2015). "Hydration studies of cementitious material using silica nanoparticles." *Journal of advanced concrete technology, 13,* 345-354.

Singh, L. P., Karade, S. R., Bhattacharyya, S. K., Yousuf, M. M. and Ahalawat, S. (2013). "Beneficial role of nanosilica in cement based materials – a review." *Construction Building Materials, 47,* 1069–1077.

Singh, L. P., Sriraman, K., Bhattacharya, S. K and Sourabh, A. (2012a). "Preperation of size controlled silica nano particles and its functional role in cementitious system." *Journal of advanced concrete technology, 10,* 345-352.

Singh, L.P., Bhattacharyya, S.K., Mishra, G. and Ahalawat, S. (2012b). "Reduction of calcium leaching in cement hydration process using nanomaterials." *Materials Technology*, 27(3), 233–238.

Snehal, K, and Das, B. B. (2022). "Acid, alkali and chloride resistance of binary, ternary and quaternary blended cementitious mortar integrated with nano-silica particles." *Cement and Concrete Composite, Elsevier publications,* 233, 104214.

Snoeck, D, and Belie, N. D. (2017). "Reducing the risk of thermal cracking in cementitious materials by means of encapsulated phase-change materials." *Proceedings of the 1st International Conference on Construction Materials for Sustainable Future-* Zadar Croatia, 170-176.

Sobolev, K. (2009). "The development of a new method for the proportioning of high-performance concrete mixtures." *Cement Concrete Composites*, 26 (7), 901-907.

Sobolev, K. and Ferrada, M. (2005). "How nanotechnology can change the concrete world; Part one." *American Ceramic Society Bulletin,* 84 (11), 16–19.

Sobolev, K., Flores, I. and Hermosillo, R. (2006). "Nanomaterials and nanotechnology for high-performance cement composites." *Proceedings of ACI Session on Nanotechnology of Concrete: Recent Developments and Future Perspectives. American Concrete Institute*, Denver, U.S.A., 91-118.

Sonebi, M., Taengua, E.G., Hossain, K.M.A., Khatib, J. and Lachemi, M. (2015). "Effect of nanosilica addition on the fresh properties and shrinkage of mortars with fly ash and superplasticizer." *Construction and Building Materials, 84*, 269-276.

Soriano, L., Monzo, J., Bonilla, M., Tashima, M.M., Paya, J. and Borrachero, M.V. (2013). "Effect of pozzolans on the hydration process of Portland cement cured at low temperatures." *Cement Concrete Composite*, 42, 41–48.

SP 23, (1982). "Hand book on concrete mixes (based on Indian Standars)." *Bureau of Indian Standards.*

Stovall T., De Larrard F., Buil, M. "Linear Packing Density Model of Grain Mixtures." *Powder Technology*, 48, 1-12, 1986.

Stritih, U. (2003). "Heat transfer enhancement in latent heat thermal storage system for buildings." *Energy Buildings*, 35, 1097–1104.

Subramaniam, K. V., Gromotka, R., Shah, S. P, Obla, K. and Hill, R. (2005). "Influence of ultrafine fly ash on the early age response and the shrinkage cracking potential of concrete." *Journal of Materials in Civil Eng*ineering 17(1).

Supit, S. W. M., Shaikh, F. U. A. and Sarker, P. K. (2013). "Effect of nano-silica and Ultrafine Fly Ash on compressive Strength of high volume fly ash mortar." *Applied Mechanics and Materials*, 368-370, 1061-1065.

Suryavanshi, A. K. Scantlebury, J. D. and Lyon, S. B. (1996). "Mechanism of Friedel's salt formation in cements rich in tri-calcium aluminate." *Cement and Concrete Research,* 26(5), 717-727.

Taniguchi, N. (1974). "On basics concept of nano-technology." *Proceedings of International Conference on Production Engineering,* Tokyo, Part II. Japan Society of Precision Engineering.

Thomas, J. J., Jennings, H. M. and Chen J. J. (2009). "Influence of nucleation seeding on the hydration mechanisms of tricalcium silicate and cement." *Journal of Physical Chemistry*, 113 (11), 4327–4334.

Turkel, S., Felekoglu, B. and Dulluc, S. (2007). "Influence of various acids on the physico–mechanical properties of pozzolanic cement mortars." *Sadhana*, 32(6), 683–691.

Turner, L. K. and Collins, F. G. (2013). "Carbon dioxide equivalent (CO2-e) emissions: A comparison between geopolymer and OPC cement concrete." *Construction Building Material,* 43, 125–130.

User Manual of Software EMMA - www.silicafume.net, Elkem AS.

Wang, D., Yang, P., Hou, P., Zhang, Zhou, Z. and Cheng, X. (2016a). "Effect of SiO_2 oligomers on water absorption of cementitious materials." *Cement Concrete Research*. 87, 22-30.

Wang, G. and Ma, Y. (2018). "Drying shrinkage of alkali-activated fly ash/slag blended system." *Journal of Sustainable Cement Based Mater*ial, 7 (4), 203-213.

Wang, L., Zheng, D., Zhang, S., Cui, H., and Dongxu Li., (2016b). "Effect of nano-SiO_2 on the hydration and microstructure of portland cement." *MDPI. Journal nanomaterials*, 6(12), 241.

Wei, Z., Falzone, G., Das, S., Saklani, N., Pape, Y. L., Plone, L., Neithalath, N and Sant G. (2017). "Restrained shrinkage cracking of cementitious composites containing soft PCM inclusions: A paste (matrix) controlled response." *Materials and Design*, 132, 367–374.

Wescott, R. F., Martha, M. W. M. and Gajda, G. V. G. J. (2010). "Prospects for expanding the use of supplementary cementitious materials in california." *Keybridge Research LLC*.

Wongkeo, W., Thongsanitgarn, P. and Chaipanich, A. (2012). "Compressive strength and drying shrinkage of fly ash-bottom ash-silica fume multi-blended cement mortars." *Material Design,* 36, 655-662.

Yang, H. B., Liu, T. C., Chern, J. C and Lee M. H. (2016). "Mechanical properties of concrete containing phase-change material." *Journal of the Chinese Institute of Engineers,* 39(5), 521-530.

Yijin, L., Shiqiong, Z., Jian, Y. and Yingli, G. (2004). "Effect of fly ash on the fluidity of cement paste, mortar and concrete." *Proceedings of International Workshop on Sustainable Development and Concrete Technology*, Beijing, China, 339-345.

Yu, R., Spiesz, P. and Brouwers, H. J. H. (2014). "Effect of nano-silica on the hydration and microstructure development of ultra-high performance concrete (UHPC) with a low binder amount." *Construction and Building Materials*, 65, 140–150.

Zapata, L. E., Portela, G., Suárez, O. M. and Carrasquillo, O. (2013). "Rheological performance and compressive strength of superplasticized cementitious mixtures with micro/nano-SiO$_2$ additions." *Construction Building Materials,* 4, 708-716.

Zhang, J. and Scherer, G.W. (2011). "Comparison of methods for arresting hydration of cement." *Cement Concrete Research*, 41, 1024- 1036.

Zhang, M. H. and Li, H. (2011). "Pore structure and chloride permeability of concrete containing nano particles for pavement." *Construction and Building Materials,* Vol. 25, 608–616.

Zhang, M.H., Islam, J. and Peethamparan, S. (2012). "Use of nano-silica to increase early strength and reduce setting time of concretes with high volumes of slag." *Cement and Concrete Composites*, 34, 650–662.

Zhang, Z., Shi, G., Wang, S., Fang, X. and Liu, X. (2013). "Thermal energy storage cement mortar containing n-octadecane/expanded graphite composite phase change material." *Renewable Energy*, 50, 670-675.

Zhao, S. and Sun, W. (2014). "Nano-mechanical behavior of a green ultra-high performance concrete." *Construction Building Material*, 63, 150–160.

Zhou, X. M., Slater, J. R., Wavell, S. E and Oladiran, O. (2012). "Effect of PFA and GGBS on early ages engineering properties of Portland cement system." *Journal of Advanced Concrete Technology,* 10, 74-85.

PUBLICATIONS BASED ON PRESENT RESEARCH WORK

International Journals (SCI/ SCOPUS)

- **Snehal K** and B. B. Das, "Influence of Aggressive Exposure on the Degradation of Nano-Silica Admixed Cementitious Mortar Integrated with Phase Change Materials", *Construction and building materials, Elsevier publications,* 335, 2022, 127467. https://doi.org/10.1016/j.conbuildmat.2022.127467 *(I.F: 6.1411)*

- **Snehal K,** B B Das and Archana Sudi, "Pozzolanic Reactivity, Hydration and Microstructural Characteristics of Blended Cementitious Composites Containing Ultrafine particles", *Iranian Journal of Science and Technology-Transaction of Civil Engineering, Springer Publications, 2022.* https://doi.org/10.1007/s40996-022-00859-0 *(I.F: 0.32)*

- **Snehal K** and B. B. Das, "Pozzolanic reactivity and drying shrinkage characteristics of optimized blended cementitious composites comprising of nano-silica particles", *Construction and Building Materials, Elsevier publications*, 316, 2021, 125796. https://doi.org/10.1016/j.conbuildmat.2021.125796 *(I.F: 6.1411)*

- **Snehal K** and B B Das "Acid, alkali and chloride resistance of binary, ternary and quaternary blended cementitious mortar integrated with nano-silica particles", *Cement and Concrete Composite, Elsevier publications,* 233, 2021, 104214. https://doi.org/10.1016/j.cemconcomp.2021.104214 *(I.F: 7.586)*

- **Snehal K**, B. B. Das, "Effect of phase-change materials on the hydration and mineralogy of cement mortar", *Proceedings of Institute of Civil Engineers-Construction Materials, ICE publication*, 2020, ISSN 1747-650X, https://doi.org/10.1680/jcoma.20.00045 *(I.F: 0.96)*

- **Snehal K**, B. B. Das and Sumit K, "Influence of integration of phase change materials on hydration and microstructure properties of nano-silica admixed cementitious mortar", *Journal of Materials in Civil Engineering, ASCE publications*, 32(6), 2020, 04020108. https://doi.org/10.1061/(ASCE)MT.1943-5533.0003178 *(I.F: 3.266)*

- **Snehal K**, B. B. Das and Akanksha M **"**Early age, hydration, mechanical and microstructure properties of nano-silica blended cementitious composites", *Construction and Building Materials, Elsevier publications*, 233, 2020, 117212. https://doi.org/10.1016/j.conbuildmat.2019.117212 *(I.F: 6.1411)*

Book Chapters (SCOPUS)

Scopus:

- **Snehal K** and B. B. Das, "Influence of incorporating phase change materials on cementitious system – A review", *Recent Trends in Civil Engineering, Lecture Notes in Civil Engineering,* vol 105, 2020, pp. 33-63, *Springer nature, Singapore,* ISBN 978-981-15-8293-6. https://doi.org/10.1007/978-981-15-8293-6_4*. (I.F: 0.27)*

- **Snehal K** and B. B. Das, "Experimental set-up for thermal performance study of phase change material admixed cement composites -a review", Smart technologies for Sustainable development, Lecture notes in civil engineering, vol 78, 2020, pp. 137-149, *Springer nature, Singapore*. ISBN 978-981-15-5001-0. 10.1007/978-981-15-5001-0_13 *(I.F: 0.27)*

- **Snehal K** and B. B. Das, "Application of Andreassen and Modified- Andreassen model on cementitious mixture design-A review", Recent Developments in Sustainable Infrastructure. Lecture Notes in Civil Engineering, vol 75, 2020, pp. 397-408, *Springer nature, Singapore*, ISBN 978-981-15-4577-1. https://doi.org/10.1007/978-981-15-4577-1_63. *(I.F: 0.27)*

- **Snehal K** and B. B. Das, "Techniques for preparation and dispersion of nano-sio$_2$ in cementitious system - A review", Sustainable Construction and Building Materials, Lecture notes in civil engineering, vol 25, 2018, pp. 397-408, *Springer nature, Singapore*. ISBN 978-981-13-3317-0. https://doi.org/10.1007/978-981-13-3317-0_36. *(I.F: 0.27)*

Non-Scopus:

- B. B. Das and **Snehal K**, "Engineering properties of nanoparticles admixed concrete-A review", Advances in Concrete, Structural and Geotechnical Engineering, *Bloomsbury Publishing* Plc, 2018, pp. 190-195.

252

International/National conferences:

- **Snehal K** and B. B. Das, "Performance of binary and ternary blended cement mortar integrated with fly ash, ultra-fine fly ash and nano-silica", *16th NCB seminar on Cement, Concrete and Building Materials*, 03-06 Dec 2019, New Delhi, India. - *(Special Merit award)*

- **Snehal K**, Archana Dinesh T and B B Das "Experimental investigation on the influence of phase change material (PCM) on the properties of cement mortar", *4th UKIERI Concrete Congress- Concrete: The Global Builder,* March 5th – 8th, 2019, Dr B R Ambedkar National Institute of Technology Jalandhar, India.

- **Snehal K**, Ammu Menon and B. B. Das "Early Age and microstructure properties of cement mortar incorporated with fly ash, ultrafine fly ash and nano-SiO_2 particles Authored by", *Proceedings 3rd R. N. Raikar Memorial International Conference on Advances in Science and Technology of Concrete, Indian chapter of American concrete institute (ICACI),* Dec 14th -15th , 2018, St Regis, Mumbai, India.

OTHER PUBLICATIONS

Journals (SCOPUS)

- **Snehal K** and B. B. Das, "Mechanical and permeability properties of hybrid fibre reinforced porous concrete", *Indian Concrete Journal*, 2019, Vol. 93 (1), pp. 54-59. *(I.F: 0.243)*

Book Chapter (SCOPUS)

- Farsana C, **Snehal K** and B B Das, "Influence of fineness of mineral admixtures on the degree of atmospheric mineral carbonation", Smart technologies for Sustainable development, Lecture notes in civil engineering, vol 78, 2020, pp. 117-136, *Springer nature, Singapore*. ISBN 978-981-15-5001-0. 10.1007/978-981-15-5001-0_12 *(I.F: 0.27)*

International Conference

- Vismaya K, **Snehal K** and B. B. Das, "Impact of phase change materials on the durability properties of cementitious composites- A Review", International Conference on Advances in Construction and Management,11th – 12th March 2021, College of Engineering Pune, India. *(Accepted: Springer publication)*

- Archana Sudi, **Snehal K** and B. B. Das, "Durability properties of nano-silica- A review", International Conference on Advances in Construction and Management,11th – 12th March 2021, College of Engineering Pune, India.

- B. B. Das and **Snehal K**, "Engineering properties of opc and ppc based concretes prepared with minimum and maximum water-cement ratio", 1st International Conference on Durability of Building and Infrastructure, Jan 10th -12th 2018, Miri, Sarawak, Malaysia.

Google Scholar Profile: https://scholar.google.com/citations?user=B3t4AvEAAAAJ&hl=en

CURRICULUM VITAE

PERSONAL DETAILS

Name : **SNEHAL K**

Father's Name : Kusumadhar K V

Mother's Name : Usha Kusumadhar

Date of Birth : 08-08-1990

Email ID : snehalshine090@gmail.com

Contact Number : +91-9901893761

EDUCATION QUALIFICATION:

Course	Institution/University	Year of Passing	Class Obtained	Percentage Of Marks
BE (Civil Engineering)	KVG college of Engineering, Sullia	2012	First Class with Distinction	77.46%
M Tech (Structural Engineering)	M S Ramaiah Institute of technology, Bangalore	2014	First Class with Distinction	9.27 CGPA

WORK EXPERIENCE:

Organization	Post held	Duration
Nitte Meenakshi Institute of Technology, Bangalore	Assistant Professor	August 2014-June 2017
National Institute of Technology Karnataka, Surathkal	Research Scholar	July 2017-January 2022

RESEARCH PUBLICATIONS:

Type of Publication	No. of Publications (Under Review)
International/ National Journal Papers	8 (1)
Book Chapters	6
International Conferences	8